Tanta University
Faculty of Engineering
Structural Engineering Department

Influence of Construction Processes induced Vibrations on Soil and Adjacent Structures

A THESIS

Submitted for the Degree of Master of Science

In Engineering (Structural Engineering)

By

Mohammed Massoud Ramadan

B.Sc. Civil Engineering, Tanta University, 2013

Under the Supervision of

Prof. Marawan Shahien
Professor of Geotechnical Engineering
Faculty of Engineering - Tanta University

Assoc. Prof. Ahmed Farouk
Assoc. Professor of Geotechnical Engineering
Faculty of Engineering - Tanta University

(2019)

Tanta University
Faculty of Engineering
Structural Engineering Department

Researcher Name

Mohamed Massoud Abdel Maksoud Ramadan

Thesis Title

"Influence of Construction Processes induced Vibrations on Soil and Adjacent Structures"

No	Name	Position	Signature
1	Prof. Mohamed Hisham Hamdi Abdel Mohsen (committee chair and Examiner)	Professor of Geotechnical Engineering, Alexandria University	
2	Prof. Suzan Saad Mahmoud Salem (Examiner)	Professor of Geotechnical Engineering, National Research Center	
3	Prof. Marawan Maghawri Shahien (Supervisor and Examiner)	Professor of Geotechnical Engineering, Tanta University	
4	Assoc. Prof. Ahmed Farouk Abdel Kader (Supervisor and Examiner)	Assoc. Professor of Geotechnical Engineering, Tanta University	

Abstract

Abstract

The development in construction field has increased with high rate in the last decades; many modern ways are started to be used to make the construction process easier than before. This thesis is focusing on two methods of construction in geotechnical field and they are pile driving and dynamic compaction. Both techniques produce high magnitude of vibration through soil due to the large amount of energy which is used in driving or compaction. Vibrations are generated in large values and propagate quite fast and affect many wide areas around the vibration source.

Those vibrations may have a very destructive effect on the adjacent structures and the heritage buildings or even the underground facilities. The damage occurs due to two reasons, soil settlement beneath foundation or the directly vibrations on the building. PPV (peak particle velocity) is considered the main indicator for the possible damage which may happens to the structures, therefore, a lot of parameters and their effect on PPV are studied in this thesis.

Soil settlement is a very dangerous problem facing engineers when they have a vibration source such as pile driving or dynamic compaction , the available models for evaluating settlement values due to vibrations are also investigated.

In addition different of wave barriers as a way of preventing wave's propagation and protecting the adjacent structures close to the vibration source are investigated in details.

Key Word:-

PPV, Finite element, Construction vibration, Pile Driving, Soil Stiffness, Plaxis, SAP, Dynamic compaction, Vibration limits, Damage criteria, Dynamic settlement, Wave barriers.

Acknowledgement

ACKNOWLEDGEMENT

I would like to express sincere appreciation to ***Prof. Dr. M. Shahein***, professor of soil Mechanics and Foundation, Tanta University who has managed, regardless of his great responsibility, to provide me with extremely valuable comments and encouragement during this research.

I am greatly obliged to ***Assoc. Prof .Dr. A. Farouk,*** Associated professor of soil Mechanics and Foundation, Tanta University for his valuable assistance, persistent inspiration, and positive criticism during the research work and perpetration of the thesis.

I want to thank ***my father and my uncle*** for encourage me during my study and give me the enough positive support to complete my thesis.

I would like also, to extend my thanks to all my family specially my ***mother, brothers and sister*** for their encouragement, as well as thanks to all my friends and my partners in my place of work for their help and support.

I am also grateful to ***Soil Mechanic Research Laboratory staff*** of the Faculty of Engineering, Tanta University for their support and helping me in all the problems I had.

Summary

SUMMARY

Construction and industrial of dynamic sources produce environmental vibration problems for the surrounding soils and the adjacent structures. High vibrations and vibration-induced settlements could cause disturbance to sensitive devices inside buildings and even be the cause of structural damage and foundation failure. The main objectives of this thesis are to study the effect of construction born vibration through both pile driving and dynamic compaction techniques on the response of surrounding soil and the adjacent structure response. In this thesis all the available data for construction vibration limits and standards are provided to help the design engineer to take all precautions to avoid any possible damage that may occur to adjacent facilities.

Pile driving or dynamic compaction process-induced high values of PPV (peak particle velocity) through the surrounding soil, therefore the construction vibration due to those both techniques were investigated in details. PPV is considered as the most concern parameter to express the vibration hazard, therefore PPV is investigated at different (soil stiffness, rammer masses, drop heights, pile material and pile embedment lengths in case of pile driving). All these parameters can help researchers or design engineers to predict PPV values to avoid any possible damage in the construction site.

A series of Axisymmetric finite element analysis using Plaxis 8.2 dynamic module were run on single piles installed using driving technique (hammer type). The peak particle velocity (PPV) was calculated for pile installations by various hydraulic hammers weights considering both clay and sand deposits with various stiffnesses. The PPV of the propagated waves in the ground with distance from the source of vibration was analyzed. It is found that by increasing soil stiffness the PPV increases and then reduces by getting far from the vibration source for both pile driving and dynamic compaction. Increasing hammer mass and the dropping height increase the energy which leads to higher values of PPV. It is noticed that by increasing the pile embedment length the PPV decreases at the ground surface. It can be seen that

wooden piles produce higher values of PPV due to their low impedance and the values of energy loss is low as well. For steel and reinforced concrete, both have a close trend in PPV values.

Comparison between Finite Element results by Plaxis model and other prediction models for Pile Driving and dynamic compaction PPV values were set up to show which more suitable prediction model can express the PPV results in the site.

A comparison between PPV values due to pile driving and dynamic compaction is investigated to figure out which process produces higher values and thus higher damage. It can be concluded that dynamic compaction has a large values of PPV due to the higher magnitude of energy which increases PPV values at the ground surface.

The acceleration versus time history of the pile driving vibration obtained by the Finite element model (Plaxis) were used as input in another module using SAP2000 V.14 to simulate the structure model that is affected by such dynamic effect. Using SAP model shows the direct effect of vibration on the adjacent structures.

By investigating the available models for PPV values prediction through a comparison with many infield measurements, it was found that most of the prediction models only depend on the scaled energy or scaled distance but neglecting many other important parameters such as soil stiffness, length of pile, method of driving and etc.

Settlement of soil due to construction vibration is became a serious problem facing engineers when pile driving or dynamic compaction are being processed. A lot of equations and models are set to estimate the values of soil settlement due to vibration. In this thesis the available models are investigated.

Previous researchers developed different ways to reduce the hazard of vibration waves through the soil and tried to prevent its propagation. It is very important to insure the safety of the structures against vibration waves, and hence the wave barriers as a method of protection are studied in this thesis to know the optimum procurement to achieve and construct an effective barrier.

Goals and Objectives:

This thesis has the following main objectives:

1-Collectiing of the available data for vibration limits and internationals standards for both human response and structure response, as well as damage criteria, investigating the most widely used prediction models of PPV (engineering models, numerical models, theoretical models… etc).

2- Investigating the effect of pile driving on the soil by calculating PPV using Plaxis 8.2 and studying the destructive effect on the adjacent structures by using SAP 2000.

3- Comparing between infield measurements of PPV records and the available PPV prediction models, to cognition the most realistic model to be used for evaluating the PPV.

4- Studying the effect of dynamic compaction on the surrounding soil using Plaxis 8.2 to calculate PPV values.

5- Discussing the soil settlement beneath foundation and at different distances from the vibration source through the available models of calculating settlement.

6- Investigating of the effect of wave barriers on the wave propagation through soil for preventing the possible hazard on the adjacent structures.

Thesis Structure:

This thesis consists of seven chapters, as follows:-

Chapter 1 Introduction:

This chapter presents an introduction to identify the context and motivation of this thesis, and gives a summary of main thesis objectives and contents. Besides some recorded damages due to construction vibration.

Chapter 2 Damage Criteria:

This chapter reviews the available vibration limits and standards for PPV values to expect the possible damage to the structures.

Chapter 3 Effect of Piles driving on Soil and Structures:

This chapter discusses the hazard of the construction vibration on soil and structures as well as illustrating the mechanism of the propagated waves through soil and also reviewing the different types of models for PPV prediction. This chapter also explains in details the numerical modeling, and describes the finite element analysis and its applications. It also contains the verification example for the Plaxis model used in this study presents the variable parameters that have been used to study the behavior of PPV through soil due to pile driving. A comparison between infield measurements and the most used models for PPV prediction is set to verify the reasonable model for PPV prediction.

Chapter 4 Effect of Dynamic Compaction on Soil and Structures:

This chapter presents variable parameters that have been used to study the behavior of PPV due to dynamic compaction process.

Chapter 5 Soil Settlement due to Construction Vibration:

This chapter presents different models that can be used for evaluating settlement values due to construction vibration.

Chapter 6 Wave Barriers:

This chapter presents the different types of wave barriers and their effect on PPV path in soil through the investigation of the barrier dimensions, infill material, and the barrier distance from the vibration source.

Chapter 7 Conclusion

In the conclusion chapter the main ideas and the results are highlighted and briefed.

Table of Contents

TABLE OF CONTETS

LIST OF CONTETS

Chapter (1) - Introduction

Chapter (2) –Vibration Criteria

Chapter (3) – Effect of Pile Driving on Soil and Structure

Chapter (6) – Wave barriers

Chapter (7)-Conclusions

References

Appendixes

PUBLISHED PAPERS

LIST OF FIGURES

Chapter (1) – Damage Criteria

Chapter (2) – Vibration Criteria

Chapter (3) – Effect of Pile Driving on Soil and Structure

Chapter (4) – Dynamic Compaction

The effect of dynamic compaction earthborn vibration on soil and adjacent structures.

Chapter (5) – Settlement

Soil settlement due to construction vibration

Chapter (6) – Wave Barriers

LIST OF TABLES

Chapter (2) – Vibration Criteria

Chapter (3) –Pile driving – Effect of Pile Driving on Soil and Structure

Chapter (4) – Dynamic Compaction –The effect of dynamic compaction earthborn vibration on soil and adjacent structures.

Chapter (5) – Settlement – Soil settlement due to construction vibration

SYMBOLS AND NOTATIONS

PPV Peak particle velocity [mm/s]

Φ Internal angel of friction [^{o}]

N Number of stories

γ_{dry} Dry density[kN/m^3]

γ_{wet} Wet density[kN/m^3]

v Poisson ratio

ψ Delitancy angle[^{o}]

Uy Vertical displacement[m]

E Modulus of elasticity [kN/m^2]

A Area [m^2]

D.L Dead load [kN/m^2]

L.L Live load [kN/m^2]

W Weight [kN/m^2]

d Depth[m]

H Dropping height [m]

f Frequency [Hz]

α , β Rayleigh waves

C_{ref} Soil cohesion [kN/m^2]

ax Horizontal acceleration [m/s^2]

ay Vertical acceleration [m/s^2]

E.pp Excess porewater pressure [kN/m^2]

Vx Horizontal velocity [m/s]

Vy	*Vertical velocity [m/s]*
Eoed	*Oedometer modulus [kN/m^2]*
M	*power*
Eur	*Unloading modulus [kN/m^2]*
R_{inter}	*Interface strength reduction*
A_{max}	*Maximum displacement amplitude [m]*
A_p	*Cross sectional area of the pile [m^2]*
a	*Acceleration [m/s2]*
c	*Wave propagation velocity [m/s]*
C_B	*Wave propagation velocity in the pile [m/s]*
C_H	*Stress wave velocity in hammer [m/s]*
C_p	*Wave propagation velocity of P-wave [m/s]*
C_R	*Wave propagation velocity of R-wave[m/s]*
C_s	*Wave propagation velocity of S-wave [m/s]*
D	*Material damping*
G_{max}	*Initial shear modulus[MPa]*
G_s	*Secant shear modulus [MPa]*
g	*Acceleration of earth's gravity* [m/s^2]

Chapter 1
Introduction

Chapter 1

INTRODUCTION

1.1 General:

Construction and mining processes using modern techniques can produce environmental vibration problems for the surrounding soils and adjacent structures. Human activities can generate soil vibration with variation in intensity, which mainly depends upon the source of vibration. The waves induced by vibration source may cause a potential damage to existing buildings. More specifically, these vibrations can cause ground settlements and deformations that may lead to a differential settlement of foundations and deformations or cracking in the structures.

The aim of this study is to know the effect of construction vibration on soil and adjacent structures by the following steps; 1) collection of sufficient data about the nature of the wave propagation through the soil. 2) Evaluating the value of PPV (peak particle velocity) by gathering the available models for estimating PPV. 3) Review for the vibration limits and the vibration criteria which set by the different codes and standards. 4) Assembling enough data for piles driving process and the available driving machines (vibratory or hammer impact) and their range of energy, piles material, investigation of different parameters in pile driving mechanism on the PPV values, 5) Highlight the dynamic compaction process and the effect of different parameters on the PPV values. 6) Dissection of the most famous models and methods for estimating soil settlement due to construction vibration. 7) Quest the optimum methods to prevent the waves propagation through soil by creating wave barriers.

1.2 Damage caused by vibrations

Damage of structures may be caused by the vibration induced differential settlement as well as by vibrations transmitted directly to structures as shown in Figure 1.1 and Figure 1.2 which illustrate the hazard associated with different

sources of vibration and the damage depend on the energy of the source which is responsible of vibration.

The complexity of these vibrations related problems makes it difficult to identify the causes of damages as shown in Figures. 1.3 and 1.4. Vibration could be a reason to enlarge old cracks or even create new ones as shown in Figure 1.5. Construction vibration activities are very harmful to adjacent structures as shown in Figure 1.6.

Figure.1.1: Collapsing of Minard Hall facade along the northwest wall of the building due to excavation and near the excavation site, piles been driven (after Nowatzki 2009)

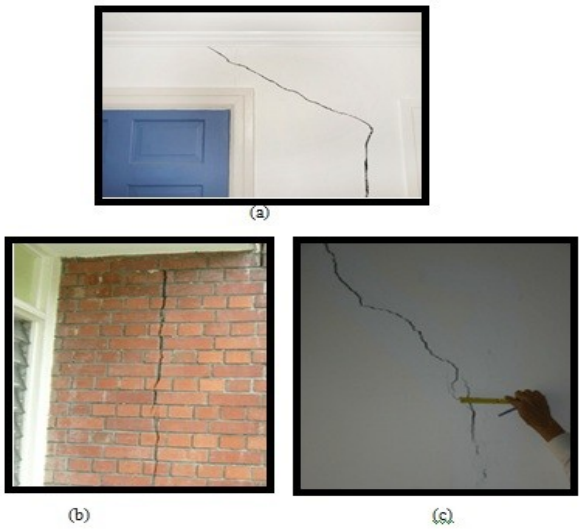

Figure 1.2: Damage from adjacent construction vibration (www.p-consurvey.com)

Figure1.3: Damage due to construction vibration (www.exponent.com)

Figure1.4: Observing building vibration damage caused by an 18t pad foot roller (www.youtube.com/watch?v=acBaXbMHNfE)

Figure 1.5: Subway Train Derails in Brooklyn Bench walls and concrete tunnel linings are susceptible to age, water damage and vibration from construction above.

a. Vibration damage inside the house

b. Pile driving next to the house

Figure 1.6: Documented infield measurements due to pile driving for construction foundation for a new transmission line in South Carolina coastal plain , (after Forbes and Camp 2013)

1.3 Sources of construction vibration:

There are a lot of sources of construction vibration which is considered as a serious problem to the adjacent structures and it can be classified as follow:

- Dynamic compaction (Figure 1.7).
- Pile driving technique (Figure 1.8).
- Pile vibratory technique (Figure 1.9).
- Blasting (mining and excavation), (Figure 1.10).
- Roads construction (Figure 1.11).
- Demolition of buildings (Figure 1.12).

Figure 1.7: Dynamic compaction technique. King Abdullah University, Saudi Arabia. (www.swissboring.com)

Figure 1.8: Pile driving technique hammer weight, ABI MOBILRAM, Lockhart Enterprises in Los Angeles, California.

(www.hammersteel.com/10-22-10-abi-mobilram-pile-driving-saved-lockhart.html

Figure 1.9: Pile vibratory technique. (http://piling-equipment.com)

Figure 1.10: Blasting for securing roads, Evans Pass Rd, Sumner, Christchurch Date: July & August 2012, (www.abseilaccess.co.nz)

Figure 1.11: Pad foot roller for roads construction. **(**www.shutterstock.com**)**

Figure 1.12: Demolition for a building, Frankfurt, Germany.
(www.rt.com/news/demolition-explosion-frankfurt-skyscraper-541)

1.4 Conclusion

In the last few decades the construction technology has developed very fast, that technology can be seen in the modern ways of construction including new devices such as pile driving machines, dynamic compaction, blasting, demolition and etc. These modern techniques of construction also have a side effect on humans and structures by producing waves through soil and noise which could lead to damage to structures.

Damage due to construction vibration is considered to be a serious problem for structures. Many types of damage in adjacent structures are illustrated due to wave propagation in soil.

Chapter 2
Vibration Criteria

Chapter 2

Vibration Criteria

2.1 Introduction

The propagated waves in the soil mainly expressed by the PPV (Peak Particle Velocity) and became an indicator for structures damage, so it becomes necessary for the design engineer to be aware of these international standards of PPV limits before starting a new project includes born vibration.

The information is used in this chapter to develop a synthesis of these criteria that can be used to evaluate the potential for damage and annoyance from vibration-generating activities. Through the past decades, huge numbers of vibration criteria and standards have been suggested by organizations, codes, government agencies and by researchers. In this chapter most of vibration limits are collected and reviewed.

2.2 Vibration Criteria

Peak particle velocity is often used as the measure of vibration intensity and it is considered as a threshold of damage, Therefore, PPV values are an important indicator for the degree of damage due to sources of vibration.

The different sources of construction vibration define and control the type of the generated wave, the wave type is concluded as the following main types depending on the source of vibration after Zekkos et al (2013):

- Transient or Impact Vibration (blasting impact, pile driving, and demolition).
- Steady-state or Continuous (vibratory pile drivers, compressors and large pumps).
- Pseudo-steady-state vibrations (jackhammers, trucks, cranes, and scrapers).

The variation between vibration criteria from country to another is very different in values. The following discussion provides a brief of vibration limits that is reported by various researchers, organizations, and etc. The effect of vibration on Human response and structures will be studied.

1. Human response:

- **Wiss (1974)** defined limits for PPV values and its effect on human response as shown in Table 2.1.

Table 2.1: The human response to transient vibration is summarized after (Wiss1974).

Peak particle Velocity (mm/s)	Human Response
51	Severe
23	Strongly perceptible
6	Distinctly perceptible
0.9	Barely perceptible

- **Reiher (1931)** in Table 2.2 summarized the results of PPV values on human response to steady-state (continuous) vibration.

Table 2.2: The human response to continuous vibration, Reiher (1931)

PPV (in/sec)	Human Response
3.6 (at 2 Hz)–0.4 (at 20 Hz)	Very disturbing
0.7 (at 2 Hz)–0.17 (at 20 Hz)	Disturbing
0.10	Strongly perceptible
0.035	Distinctly perceptible
0.012	Slightly perceptible

- **Whiffen (1971)** summarized the results of another study for PPV values due to traffic (continuous vibrations) on the human response as shown in Table 2.3.

Table 2.3: Human Response to Continuous Vibration from Traffic, Whiffen (1971)

PPV (in/sec)	Human Response
0.4–0.6	Unpleasant
0.2	Annoying
0.1	Unpleasant Begins to annoy
0.08	Readily perceptible
0.006–0.019	Threshold of perception

- **ISO 2631(Mechanical vibration and shock** summarizes the vibration criteria for vibration sources in Table 2.4 with predominant frequencies in the range of 8–80 Hz.

Table 2.4: ISO 2631 Vibration Criteria

Building Use	Vibration Velocity Level (VdB)	Vibration Velocity rms Amplitude (in/sec)
Workshop	90	0.032
Office	84	0.016
Residence	78 day/75 night	0.008
Hospital operating room	72	0.004

- **FTA (2006)** (Federal Transit Administration) has developed vibration criteria based on building use. These criteria, shown in Table 2.5, are based on overall rms vibration levels expressed in VdB.

Table 2.5: Federal Transit Administration vibration criteria

Land Use Category	Vibration Impact Level for Frequent Events (VdB)	Vibration Impact Level for Infrequent Events (VdB)
Category 1: Buildings where low ambient vibration is essential for interior operations	65	65
Category 2: Residences and buildings where people normally sleep	72	80
Category 3: Institutional land uses with primarily daytime use	75	83

Note: “Frequent events” is defined as more than 70 events per day. “Infrequent events” is defined as fewer than 70 events per day.

Table 2.6 shows an indication of the average human response to vibration and air overpressures due to blasting that may be anticipated when the person is at rest, situated in a quiet surrounding according to Transportation and

Construction Vibration Guidance Manual (California Department of Transportation 2013).

Table 2.6: Human Response to Blasting Ground Vibration and Air Overpressure

Average Human Response	PPV (in/sec)	Airblast (dB)
Barely to distinctly perceptible	0.02–0.10	50–70
Distinctly to strongly perceptible	0.10–0.50	70–90
Strongly perceptible to mildly unpleasant	0.50–1.00	90–120
Mildly to distinctly unpleasant	1.00–2.00	120–140
Distinctly unpleasant to intolerable	2.00–10.00	140–170

Note: VdB: velocity level in decibels

2. Structures

Hendriks (2004) (Caltrans Experiences), Technical Advisory, Vibration TAV-04-01-R0201 stated that considerable amount of researches have been done to correlate vibrations from single events such as dynamite blasts with architectural and structural damage. The Transport and Road Research Laboratory in England has researched continuous vibrations to some extent and developed a summary of vibration amplitudes and reactions of people and the effects on buildings as shown in Table 2.7. These are the criteria used by Caltrans to evaluate the severity of vibration problems. Traffic, train, and most construction vibrations (with the exception of pile driving, blasting, and some other types of construction (demolition) are considered continuous.

Table 2.7: A Survey of Traffic-induced Vibrations after Whiffen and Leonard (1971)

Vibration Amplitude (Peak Particle Velocity)		**Human Reaction**	**Effect on Buildings**
mm/s	in/sec		
0.15-0.30	0.006-0.019	The threshold of perception; possibility of intrusion	Vibrations unlikely to cause damage of any type
2.0	0.08	Vibrations readily Perceptible	Recommended upper amplitude of the vibration to which ruins and ancient monuments should be subjected
2.5	0.10	An amplitude at which continuous vibrations begin to annoy people	Virtually no risk of "architectural" damage to normal buildings
5.0	0.20	Vibrations annoying to people in buildings (this agrees with the amplitudes established for people standing on bridges and subjected to relative short periods of vibrations)	Threshold at which there is a risk of "architectural" damage to normal dwelling - houses with plastered walls and ceilings Special types of finish such As a lining of walls, flexible ceiling treatment, etc., would minimize "architectural" damage
10-15	0.4-0.6	Vibrations considered unpleasant by people subjected to continuous vibrations and unacceptable to some people walking on bridges	Vibrations at a greater amplitude than normally expected from traffic, but would cause "architectural" damage and possibly minor structural damage

Types of damage to construction vibration:

1. Structural damage is any type of change which could compromise the stability of the structure.
2. Cosmetic damage is basically everything else which affects the appearance of the house.

- **Chae (1978)** classifies buildings in one of four categories based on age and condition showing the vibration criteria for different conditions of different structures types is illustrated for PPV limits which could be harmful to the structures as shown in Table 2.8.

Table 2.8: Building vibration criteria for the residential Structures based on age and condition Chae (1978)

Category	PPV (Single Blast)		PPV (Repeated Blast)	
	mm/s	in/sec	mm/s	in/sec
Buildings of Substantial Construction	100	4	50	2
Residential, New construction	50	2	25	1
Residential, Poor Condition	25	1	12.5	0.5
Residential, Very Poor Condition	12.5	0.5	-	-

- **Dowding (1996)** illustrated the maximum allowable PPV values for various structure types and conditions as shown in Table 2.9. It is important to make clear define the type of building damage that is considered.

Table 2.9: The impact of construction vibrations induced by the different type of sources is also assessed by Dowding (1996).

Structure and condition	Limiting Peak Particle Velocity	
	mm/s	in/sec
Industrial Buildings	50	2
Residential	12.5	0.5
Residential, New construction	25	1
Historic Buildings	12.5	0.5
Bridges	50	2

- **The Swiss Association of Standardization** has explained a series of vibration damage criteria that show the difference between single-event sources (blasting) and continuous sources (machines and traffic), (after Wiss 1981). The criteria are also differentiated by frequency. Assuming that the frequency range of interest for construction and traffic sources is 10–30 Hz, Table 2.10 shows criteria for 10–30 Hz. PPV vs structure class is illustrated in Table 2.10.

- **Konan (1985)** reviewed numerous vibration criteria relating to historic and sensitive buildings and purposed a recommendation to the set of vibration criteria for transient (single-event) and steady-state (continuous) sources. Konan recommended that criteria for continuous vibration be about half the amplitude of criteria for transient sources as shown in Table 2.11.

Table 2.10: Swiss Association of Standardization Vibration Damage Criteria (after Wiss 1981).

Structure Class	Continuous Source PPV (in/sec)	Single-Event Source PPV (in/sec)
Class I: buildings in steel or reinforced concrete, such as factories, retaining walls, bridges, steel towers, open channels, underground chambers and tunnels with and without concrete alignment	0.5	1.2
Class II: buildings with foundation walls and floors in concrete, walls in concrete or masonry, stone masonry retaining walls, underground chambers and tunnels with masonry alignments, conduits in loose material	0.30	0.7
Class III: buildings as mentioned above but with wooden ceilings and walls in Masonry	0.2	0.5
Class IV: construction very sensitive to vibration; objects of historic interest	0.12	0.3

Table 2.11: Konan Vibration Criteria for Historic and Sensitive Buildings

Frequency Range (Hz)	Transient Vibration PPV (in/sec)	Steady-State Vibration PPV (in/sec)
1–10	0.25	0.12
10–40	0.25–0.5	0.12-0.25
40–100	0.5	0.25

- **Siskind et al. (1980)** illustrated probabilistic methods to vibration damage thresholds for blasting. Three damage thresholds have been identified and are shown in Table 2. 12 in terms of PPV for probabilities of 5, 10, 50, and 90%.

Table 2.12: Siskind et al (1980) Vibration Damage Thresholds

Damage Type	PPV (in/sec)			
	5% Probability	10% Probability	50% Probability	90% Probability
Threshold damage: loosening of paint, small plaster cracks at joints between construction elements	0.5	0.7	2.5	9
Minor damage: loosening and falling of plaster, cracks in masonry around openings near partitions, hairline to 3-mm (0–1/8-in.) cracks, fall of loose mortar	1.8	2.2	5	16
Major damage: cracks of several mm in walls, rupture of opening vaults, structural weakening, fall of masonry, load support ability affected	2.5	3	6	17

- **The American Association of State Highway and Transportation Officials 11**(AASHTO, 1990) also specify the maximum vibration levels for preventing damage to structures from construction or maintenance activities. Table 2.13 summarizes the AASHTO maximum levels.

Table 2.13: AASHTO Maximum Vibration Levels for Preventing Damage

Category	Peak Particle Velocity	
	(mm/s)	(in/sec)
Historic sites or other critical locations	2.5	0.1
Residential buildings, plastered walls	5.0-7.5	0.2–0.3
Residential buildings in good repair with gypsum board walls	10-12.5	0.4–0.5
Engineered structures, without plaster	25-37.5	1.0–1.5

2.3 Vibration Limits

- **USBM RI8507 limits**

The frequency of construction vibration based safe limits for cosmetic cracking threshold was originated for one to two-story residential structures by the U.S. Bureau of Mines (Siskind et al., 1980). The limits illustrated in Figure 2.1 have the following displacement and velocity values for the four ranges of the dominant frequency: 0.76 mm (0.03 in) for 1 to 4 Hz, 19 mm/s (0.75 in/s) for 4 to 15 Hz, 0.2 mm (0.008 in) for 15 to 40 Hz, and 50.8 mm/s (2.0 in/s) for 40 to 100 Hz. The limit of 19 mm/s (0.75 in/s) for 4 to 15 Hz is used for drywall while the limit of 13 mm/s (0.5 in/s) for 2.5 to 10 Hz is applied for plaster.

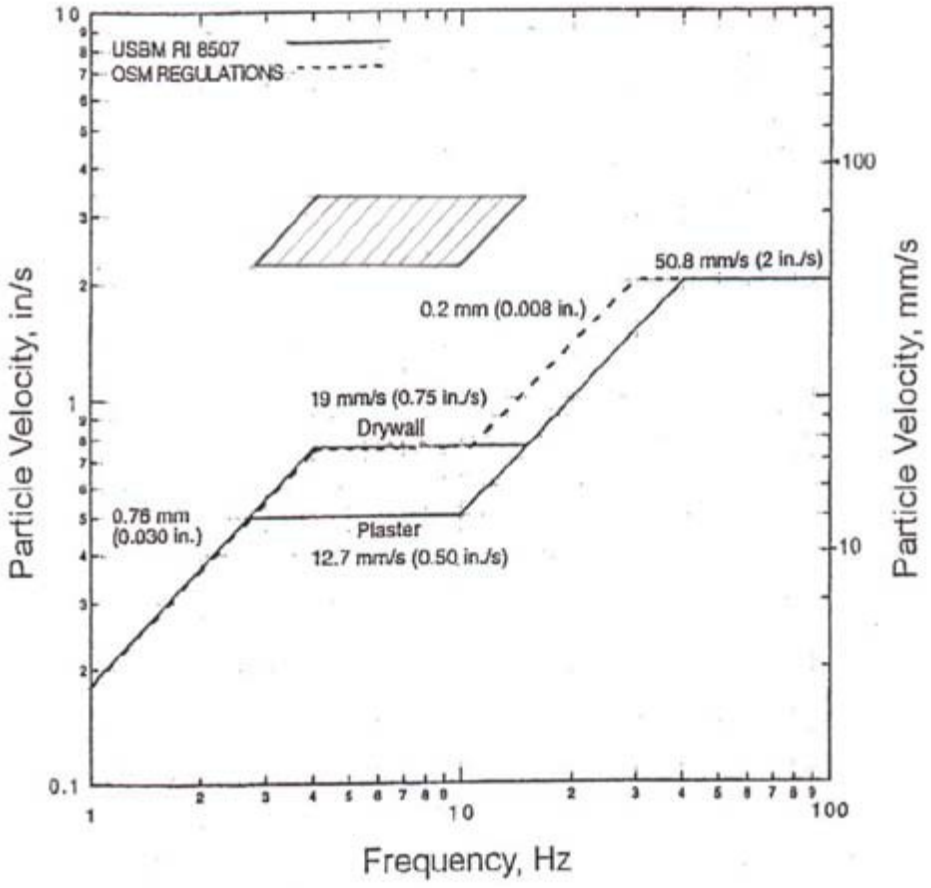

Figure 2.1: Safe level blasting criteria from USBM RI 8507 and the derivative version (dashed line), the Chart Option from OSM surface coal mine regulations. The Shaded area shows maximum velocities of structural vibrations with amplification of 4.5 at resonance. Data were modified from Siskind (2000) and the plot was adapted from Svinkin (2008).

Damage probability as reported in USBM RI 8507 and reproduced in C. Dowding (1996) explained three different categories to illustrate damage level due to PPV as shown in Figure 2.2.

1. Threshold damage," defined as an opening of old cracks and formation of a new hairline crack.
2. Minor damage," such as broken windows, loosened or fallen plaster, and hairline cracking of masonry
3. Major structural damage," such as wide cracking or shifting of foundations or bearing walls

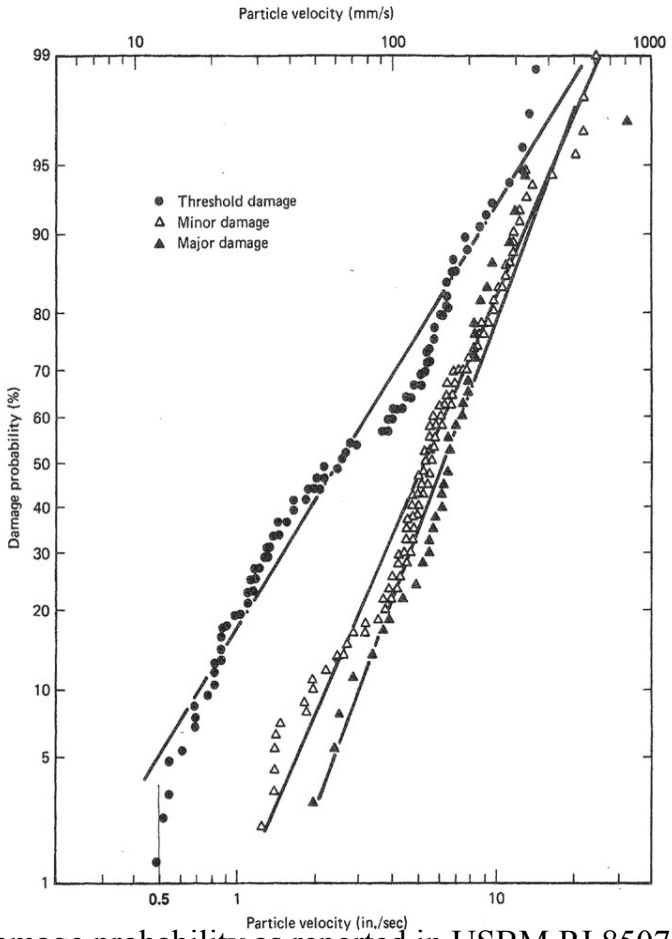

Figure 2.2: Damage probability as reported in USBM RI 8507 and reproduced in C.H. Dowding, 1996.

- **OSMRE Limits** (Office of Surface Mining and Reclamation Enforcement)

The derivative version of the USBM safe limits shown in Figure 2.2 was included as the Chart Option in the surface coal mine regulations by the Office of Surface Mining (OSM, 1983). The comments above on the USBM limits can also be addressed to the Chart Option. Nevertheless, Siskind (2000) pointed out simple and workable OSM distance dependent PPV criteria for blasting: 31.8 mm/s (1.25 in/s) for 0 to 92 m (300 ft), 25.4 mm/s (1 in/s) for 92 m (301 ft) to 1525 m (5000 ft), and 19 mm/s (0.75 in/s) for distances greater than 1525 m (5000 ft). These vibration limits were found for low-rise residential houses.

OSMRE also addressed air overpressure limits in its 1983 regulations. It considered the characteristics of the recording systems and established the following limits as shown in Table 2.14.

Table 2.14: OSMRE (1983) Overpressure Limits.

Recording Device Characteristics	Limits
Lower Limit of 0.1 Hz	134 dB
Lower Limit of 2.0 Hz	133 dB
Lower Limit of 6.0 Hz	129 dB
slow response	105 dBc

For several years, an air overpressure limit of 140 dB was used primarily to prevent injury to workmen's' hearing; it also successfully prevented damage to structures. In recent times, lower limits have been used, mostly in attempts to reduce annoyance.

- **Florida DOT Limits**

Currently, 0.5 in/s is the general PPV limit in FDOT projects, while 0.2 in/s is used by some districts on entire projects. The limit of 0.2 in/s tends to reduce complaints but does not eliminate them. Vibratory rollers, tandem rollers, and sheet pile installation, in particular, are a major source of vibration-related complaints in FDOT projects.

- **Russian Limits**

The Russian limits of 30 to 50 mm/s (1.18 to 1.97 in/s) for the vibrations of sound structures were found by the Moscow Institute of Physics of the Earth to assess the safety of structures from the explosive effects of various blasts in the air, on the ground, and under the ground at the time of the Second World War (Sadovskii, 1946). These vibration limits work well for building vibrations excited by different dynamic sources. It is necessary to accompany the direct measurement of structural vibrations with an observation of the results of dynamic effects.

- **The Swedish limits**

The Swedish Standard SS 02 52 11 was established in 1999 and is the most elaborate standard currently available (SIS 1999). It deals with vibrations caused by piling, sheet piling, excavation, and soil compaction. Guidance levels of acceptable vibrations, as well as instructions for measurement of vibrations in buildings, are given based on more than 30 years of practical experience in a wide range of soils. The proposed vibration values do not take into consideration psychological effects (noise or comfort) on the occupants of buildings. Neither do they consider the effects of vibrations on sensitive machinery or equipment in buildings, Massarch (2004).

The vibration levels in the standard are based on experience from measured ground vibrations (vertical component of particle velocity) and observed damage to buildings, with comparable foundation conditions. The vibration level V is expressed as the peak value of the vertical vibration velocity. It is measured on the bearing elements of the building foundation and is determined from Eq.2.1.

$$V = V_0 F_b F_m F_g \qquad \text{(Eq.2.1)}$$

Where: V_0 = vertical component of the uncorrected vibration velocity in mm/s, F_b = building factor, F_m = material factor and F_g = foundation factor. Values for V_0 are given in Table 2.15 for different ground conditions and construction activities and are maximum allowable values at the base of the building.

Table 2.15: Uncorrected vibration velocity (V_0), after Massarch (2004)

Foundation Condition	Piling, Sheet piling or Excavation	Soil Compaction
Clay, silt, sand or Gravel	9 mm/s	6 mm/s
Moraine (till)	12 mm/s	9 mm/s
Rock	15 mm/s	12mm/s

Buildings are divided into five classes with respect to their vibration sensitivity after Massarch (2004) as shown in Table 2.16. Classes 1 to 4 are applied to

structures in good condition. If they are in a poor state, a lower building factor should be used.

Table 2.16: Building Factor (F_b) after Massarch (2004)

Class	Type of Structure Building	Factor, Fb
1	Heavy structures such as bridges, quay walls, defense structures etc.	1.70
2	Industrial or office buildings	1.20
3	Normal residential buildings	1.00
4	Especially sensitive buildings and buildings with high value or structural elements with wide spans, e.g. church or museum buildings	0.65
5	Historic buildings in a sensitive state as well as certain sensitive ruins	0.5

The structural material is divided into four classes with respect to their vibration sensitivity as shown in Table 2.17. The most sensitive material component of the structure determines the class to be applied. Table 2.18 defines a foundation factor. Lower factors are applied to buildings on shallow foundations, whereas buildings on piled foundations are accorded higher factors due to their reduced sensitivity to ground vibrations.

Table 2.17: Material Factor (Fm), after Massarch (2004)

Class	Type of Building Material	Factor, Fm
1	Reinforced concrete, steel or timber	1.20
2	Unreinforced concrete, bricks, concrete blocks with voids, lightweight concrete elements	1.00
3	Light concrete blocks and plaster	0.75
4	Limestone, lime-sandstone	0.65

Table 2.18: Foundation Factor (F_g), after Massarch (2004)

Class	Type of foundation	Factor, Fg
1	Slab, raft foundation	0.60
2	Buildings founded on friction piles	0.80
3	Buildings founded on end-bearing piles	1.00

- **British Limits**

Vibration damage limits on structures in the United Kingdom are illustrated by the British Standard BS 7385. Part 2 :(1993), "Evaluation and measurement for vibration in buildings - Part 2: Guide to damage levels from ground-borne vibration". This part of British Standard 7385 provides guidance on the assessment of the possibility of vibration-induced damage in buildings due to a variety of sources and sets guide values for building vibration based on the lowest vibration levels above which damage has been credibly demonstrated. Sources of vibration which are considered include blasting (carried out during mineral extraction or construction excavation), demolition, piling, ground treatments (e.g. compaction), construction equipment, tunnelling, road and rail traffic, and industrial machinery.

Table 2.19 gives vibration limits for cosmetic damage expressed as the maximum value of anyone of three orthogonal component particle velocities measured during a given time interval.

The values in Table 2.19 relate to transient vibrations, which do not give rise to resonant responses in structures, and to low-rise buildings.

Table 2.19: Transient vibration guide values for cosmetic damage, measured at the base of the building. BS 5228-2:2009. From Massarch & Fellenius (2014).

Type of building	Peak velocity in a frequency range of predominant pulse	
	4 to 15 Hz	15 Hz and above
Reinforced or framed structures Industrial and heavy commercial buildings	50 mm/s at 4 Hz and above	50 mm/s at 4 Hz and above
Unreinforced or light framed structures Residential or light commercial type buildings	15 mm/s at 4 Hz increasing to 20 mm/s at 15 Hz	20 mm/s at 15 Hz increasing to 50 mm/s at 40 Hz and above

- **German Standard**

The German standard, DIN 4150, Part 3 (1999), "Vibration in buildings - Part 3: Effects on structures" addresses the effects of construction-induced vibrations on buildings for short term and continuous vibrations. The code is applied to problems where vibrations affect buildings and structures, located on or below the ground surface. Table 2.20 gives frequency-dependent guidance values of peak particle velocity for different types of structures or buildings. After Massarch & Fellenius (2014).

DIN 4150-3 also gives guidelines regarding the execution of vibration measurements in buildings. If resonance can be expected in the structure, vibration measurements shall be performed on several floor levels (not only on the top floor).

- **Swiss Standard**

Swiss standard SN 640 312 has been introduced in 1979 and considers the effect of vibrations from transient (shock) and continuous vibrations. Buildings are divided into four categories as illustrated in Table 2.21

Table 2.20: Guidance values of vibration velocity for the evaluation building damage for short-term and long-term impact, DIN 4150, Part 3. from Massarch & Fellenius (2014).

Structure/Object Type	Frequency Hz	Peak Velocity		Location of Measurement
		mm/s Short-term:	mm/s Long –term	
Offices and industrial premises	1	20	-	
	10	20	-	
	10	20	-	
	50	40	-	Foundation
	50	40	-	
	100	50	-	
	1	-	10	Top floor
	100	-	10	Horizontal
Domestic houses and similar construction	1	5	-	
	10	5	-	
	10	5	-	
	50	15	-	Foundation
	50	15	-	
	100	20	-	
	1	-	5	Top floor
	100	-	5	Horizontal
Other buildings sensitive to vibrations	1	3	-	
	10	3	-	
	10	3	-	
	50	8	-	Foundation
	50	8	-	
	100	10	-	
	1	-	2.5	Top floor
	100	-	2.5	Horizontal

Table 2.21: Building categories, SN 640312. From Massarch &Fellenius 2014.

Building Category	**Building Type**
I	Reinforced concrete structures for industrial purposes, bridges, towers etc. Subsurface structures such as caverns, tunnels with or without concrete lining
II	Buildings with concrete foundations and concrete floors, buildings made of stone and concrete masonry blocks Subsurface structures, water mains, tubes and caverns in soft rock
III	Buildings with concrete foundations and concrete basement, timber floors, masonry walls
IV	Especially vibration-sensitive structures and buildings requiring protection

For vibration limits for the continuous disturbance are presented in Table 2.22. Two different frequency ranges have been chosen, 10 - 30 and 30 - 60 Hz, respectively. The Swiss limits are also briefed after Wiss (1981) in Table 2.10

Table 2.22: Swiss recommendation of maximum vibration levels for continuous vibrations, SN 640312.

Building Category	Frequency Range Hz	Recommended vibration velocity mm/s
I	10 -30	12
I	30 -60	12 – 18
II	10 -30	8
II	30 -60	8 -12
III	10 -30	5
III	30 -60	5-8
IV	10 -30	3
IV	30 -60	3 – 5

- **Hong Kong Government Regulations**

The Hong Kong Buildings Department has issued a Practice Note, APP-137 "Ground-borne Vibrations and Ground Settlements Arising from Pile Driving and Similar Operations" which provides guidelines on the control of ground-borne vibrations and ground settlements generated from pile driving or similar operations with a view to minimizing possible damage to adjacent properties and streets. The effect of ground-borne vibration from piling works on adjacent structures is assessed by the maximum peak particle velocity (PPV). The maximum PPV shall be evaluated from the peak particle velocities at three orthogonal axes measured at ground levels of the structures in question. The guide values of maximum PPV presented in Table 2.23 are suggested to give minimal risks of vibration-induced damage. After Massarch and Fellenius 2014.

Table 2.23: Empirical guidelines according to HK Practice Note, APP-137, Massarch and Fellenius 2014

Type of building	Guide values of maximum PPV (mm/s)	
	Transient vibration (e.g. drop hammer)	Continuous vibration (e.g. vibratory hammer)
Robust and stable buildings in general	15	7.5
Vibration sensitive/ dilapidated buildings	7.5	3

- **Australian Standard 2187.2**

Australian Standard (AS) 2187.2 provides even more conservative vibration criteria compared to the British Standard 7385. The recommended PPV of the AS 2187.2 are that the houses and low-rise residential buildings and commercial and industrial buildings are 10mm and 25.4 mm in PPV [mm/sec] (0.39 and 1.0 in PPV [in/sec]), respectively.

- **Egyptian code 202 - 2001**

The Egyptian code set limits of 50 mm/s as a safety limit for structures adjacent to vibrations for frequency more than 40 Hz (in case of blasting) and 20 mm/s for frequency less than 40 Hz (in case of pile driving). The safety limits are shown in Table 2.24.

Table 2.24: Egyptian code for soil mechanics and foundations

Effect	PPV (mm/s)
Slightly perceptible	0 – 50
Influential	51 - 110
A bit destructive	111 - 160
Very destructive	161 – 250

2.4 Conclusion

Vibration limits and damage criteria are different from one place to another, every standard of these limits depend on a wide number of parameters to control the damage due to PPV on soil and adjacent structures and also the human response. The Swedish limits consider the most effective limits because it doesn't give constant values, it gives suitable parameters depend on soil condition, building material, foundation type. All that data make it easily to predict the PPV with high accuracy. Massarch and Fellenius 2014 illustrated that the Swedish standard SS 02 52 11 was specifically developed for pile-driving induced ground vibrations. It is the only known standard specifically addressing vibrations due to pile driving. It is based on the vertical vibration velocity and chosen independently of vibration frequency and takes into consideration ground conditions, building material, and type of the building foundation.

Chapter 3
Effect of Pile Driving on Soil and Structures

Chapter 3

Effect of Pile Driving on Soil and Structure

3.1 Introduction:

Pile driving currently becomes one of the main sources of vibration due to human activities in the field of construction. The construction and retrofit of bridges and retaining walls often include driving of piles or sheet piles for foundation support or earth retention. Pile-driving is performed typically by use of an impact or vibratory hammers. This process induces vibrations into the ground which can be transmitted to nearby structures. The vibration waves may cause a potential damage to buildings. More specifically, these vibrations can cause ground settlements and deformations that may lead to differential settlements of foundations and deformations or cracking in the structures.

3.2 Wave generation:

The driving process creates vibrations, which radiate from the shaft and the toe of the pile into the soil. The larger the intensity of the stress wave, the larger the dynamic force and the intensity of ground vibrations. In addition to the vibration intensity, which often is expressed in terms of peak particle velocity (PPV), also the vibration frequency is important parameter represents the possible damage to adjacent structures, when the dominant frequencies of the generated vibrations harmonize with the resonance frequency of buildings or building elements, the risk of building damage increases, Massarch and Fellenius (2014).

3.3 The component of pile installation:

The mechanism of the energy transfer includes the following steps:

- Energy is transmitted from the hammer to the pile.
- The interaction between the pile and the soil, (wave generation).
- Propagation of the waves in the surrounding soil.
- Soil to structure interaction, (damage formation).

Figure 3.1shows the process of energy transfer from the driven pile to the soil and then to the adjacent building.

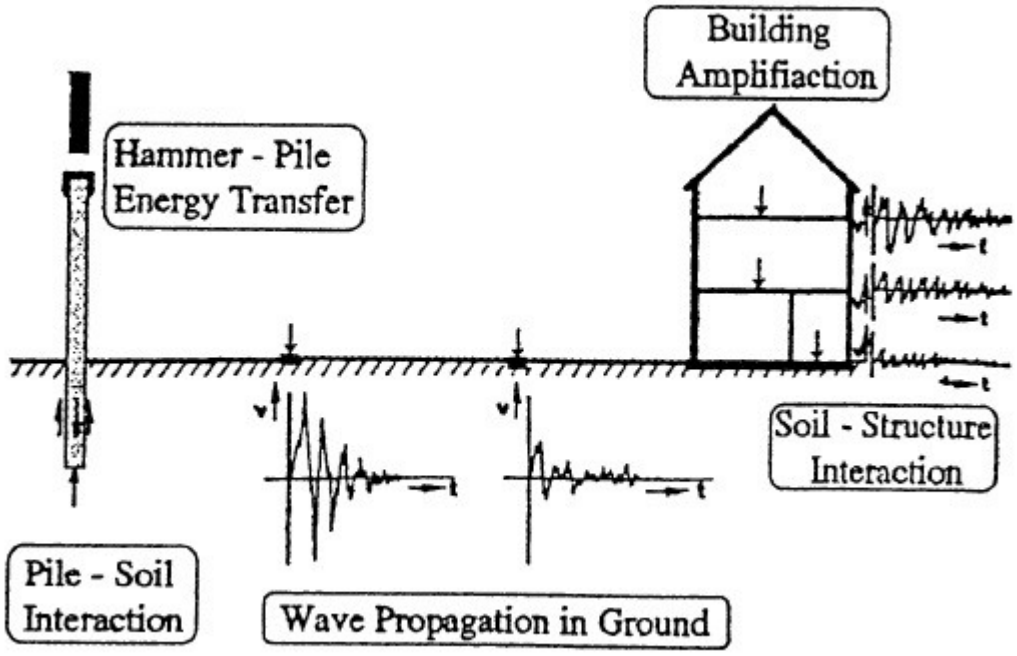

Figure 3.1: wave propagation in ground (Massarsch 1993)

The level of structural vibrations caused by construction and industrial sources depends mostly on the following factors 1) dynamic loads transmitted on the ground, 2) the medium of soil where wave propagate from the dynamic sources, 3) soil conditions, 4) soil-structure interaction, and 5) susceptibility of structures. Each factor can affect structural vibrations, after Svinkin (2008).

3.3.1 The hammer:

There are two main techniques for pile installation, by driving or by vibratory hammers as it mention in the introduction. In the case of impact hammer, the pile is installed into the ground by repeated blows from a hammer raised by rope and fall back by gravity (single acting) or could be accelerated downwards (double acting), after (Svinkin 1996).

Another case, the vibratory hammers is attached to the pile and acting with the pile as the same object, continuously moves upward and downward rapidly with no any loss in the energy.

Component of hammering system for pile driving

The simple component of the hammering system are summarized in the following points, also are shown in Figure 3.2.

1. Driving Rigs
2. The Hammer
3. Cushion Material
4. The Pile

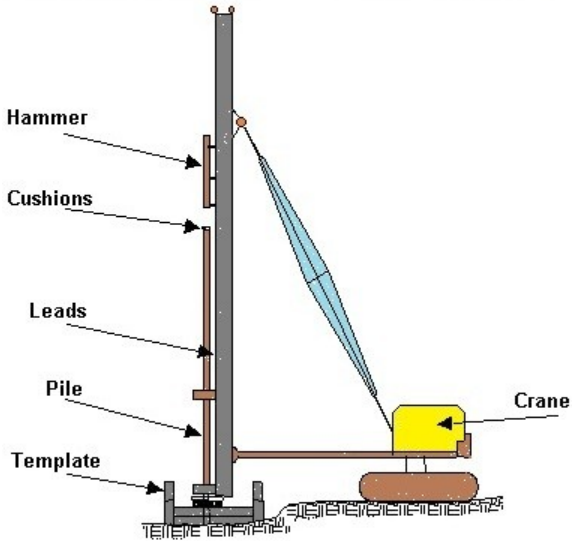

Figure 3.2: Pile driving system (www.aboutcivil.org)

Impact Hammers:

There are famous four types of impact hammers, Drop hammers, Air/steam hammers, Diesel hammers, and Hydraulic Hammers.

1. **Drop hammers:**

The drop hammer is the oldest type of hammers was ever used. It is usually raised by a crane and released to impact the pile top, it is considered as a very simple hammer, however how slow it is and also its efficiency is inconsistent. Drop hammers consist of a mass that is lifted to a certain height (drop height)

and then released (dropped) onto the pile. The mass may be enclosed in a cylinder (Martin, 1980). The dropping mass is shown in Figure 3.3.

Figure: 3.3: An Example for the typical mass of the dropping hammers.

2. Air/Steam Hammers

Widely used since the 19th century, it is considered to have more advantages than impact hammer because of requiring little maintenance and long duration. The advantages and the disadvantages of the air/steam hammer are shown in Table 3.1. A double acting Steam hammer is shown in Figure 3.4.

Table 3.1: The advantages and the disadvantages of the air/steam hammer

Air/Steam Hammer	
Advantages of single acting air/steam hammer	**Disadvantages of single acting air/steam hammer**
Same stroke each impact	Additional support equipment required
Consistent operation rate	Heavy hammer
Low impact velocity	Not as dependable as diesel
Cleaner exhaust	Thick hammer cushion stack required

Figure 3.4: Double acting Steam hammer (http://www.pilebuck.com)

3. Diesel hammers:

The diesel hammer is a very large two-stroke diesel engine. The mass is the piston, and the apparatus which connects to the top of the pile is the cylinder. Pile driving is started by having the mass raised by auxiliary means usually a cable from the crane holding the pile driver which draws air into the cylinder. Diesel fuel is added/injected into the cylinder. The mass is dropped, using a quick-release. There are two types of Diesel hammer, the first one is the open end hammers and it can reach about 40-55 blows per minute. The other type is the closed end diesel hammer and it can reach about 75- 85 blows per minute. The advantages and the disadvantages of diesel hammer for both single and double acting are shown in Table 3.2.

Table 3.2: Advantages and disadvantages of diesel hammer

Diesel Hammer	
Advantages of open-end diesel hammer	**Disadvantages of open-end diesel hammer**
Very Simple; dependable	Delivered energy variable
No additional support equipment required	Less efficient energy transfer
Lightest net mass of energy	Produces higher pile stresses
Readily available	Dirty exhaust spray
	Difficult to spot operation problems
Advantages of closed-end diesel hammer (double acting)	**Disadvantages of closed-end diesel hammer** (double acting)
No additional support equipment required	Lowest efficiency
Drives piles faster	Most difficult to spot operation problems
Lightmass	

4. Hydraulic hammers:

Hydraulic hammer is the newest kind of impact hammers. The main concept of its operation is using a fluid to move the ram up and down. The Advantages and disadvantages of the hydraulic hammer are shown in Table 3.3. The hydraulic hammer is shown in Figure 3.5. For more understanding, the components of the hydraulic hammers see Figure 3.6. There are also different types of hydraulic hammers depend on the type of pile material and its diameter see Figure 3.7

A hydraulic hammer is a modern type of piling hammer used in place of diesel and air hammers for driving steel pipe, precast concrete, and timber piles. The first successful hydraulic hammers were developed in Scandinavia 1960s.

Figure 3.5: Hydraulic hammer (http://www.hammersteel.com/)

Table 3.3: The advantages and the disadvantages of hydraulic hammers

Hydraulic hammers	
Advantages	**Disadvantages**
Controllable variable stroke	Need hydraulic power pack and hoses
High efficiency blow	Need dedicated person for hydraulic controls
Low impact velocity	Reparability / high tech
Light mass	
Clean running, quiet	

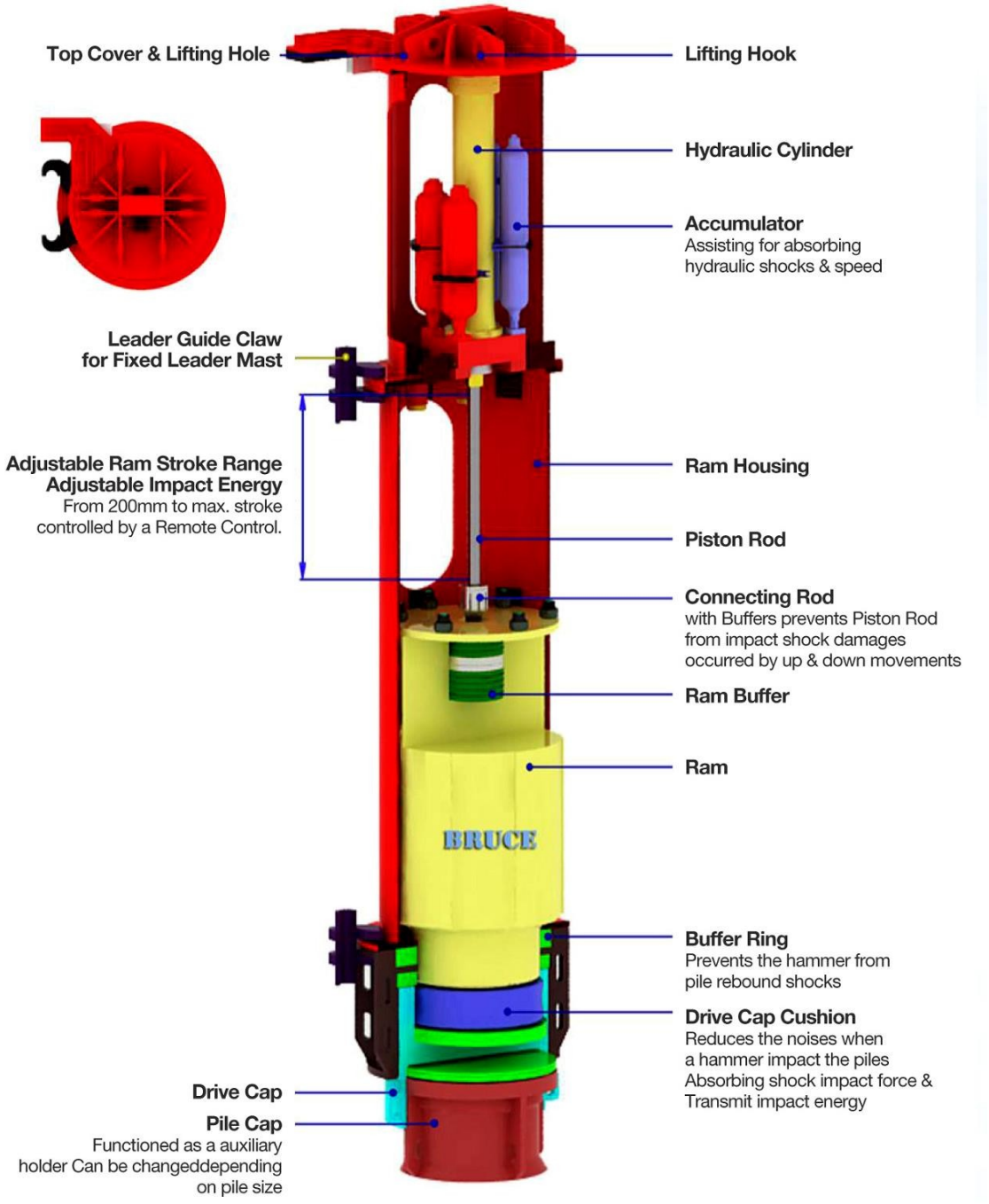

Figure 3.6: Hydraulic hammer component (http://en.koper.pro)

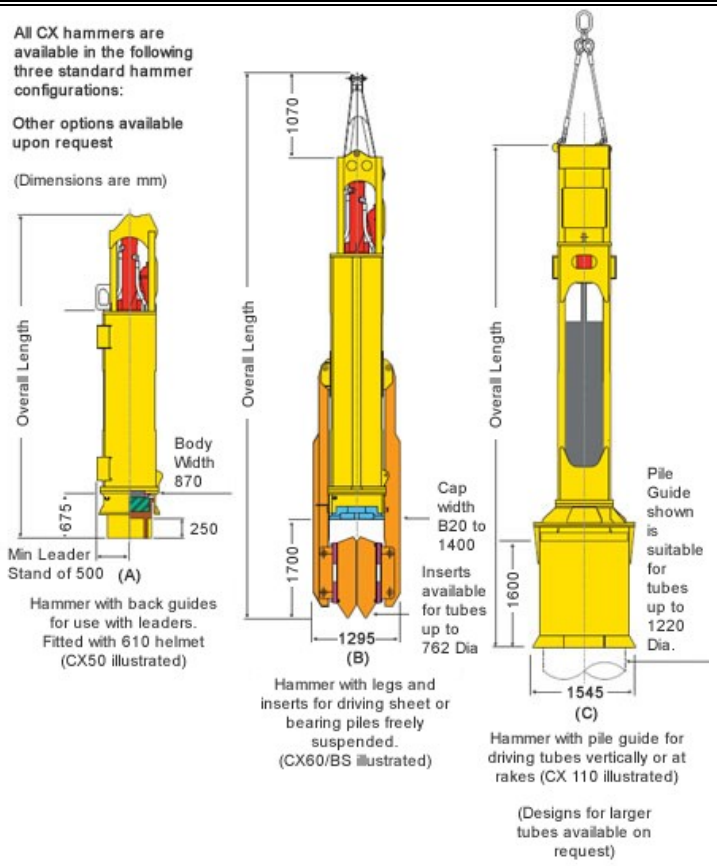

Figure 3.7: Different types of hydraulic hammers.

Vibratory Hammers:

Vibratory driving is used throughout the world mainly for driving and extracting sheet piles. The common explanation for the working principle of vibrating is the generation of excess pore pressure around the sheet pile. This excess pore pressure reduces the friction and tip resistance. Sinking of the sheet pile results from the mass of the sheet pile and vibrator,(Meijers 2007)

The hammer is run by a power generator and a control panel is usually mounted on the power generator. The whole vibrator is mounted on a piling frame (Holeyman, 2002) (Rausche, 2002) (Viking, 2006) (Whenham, 2011) (Whenham & Holeyman, 2012). A free hanging model is illustrated in Figure 3.8.

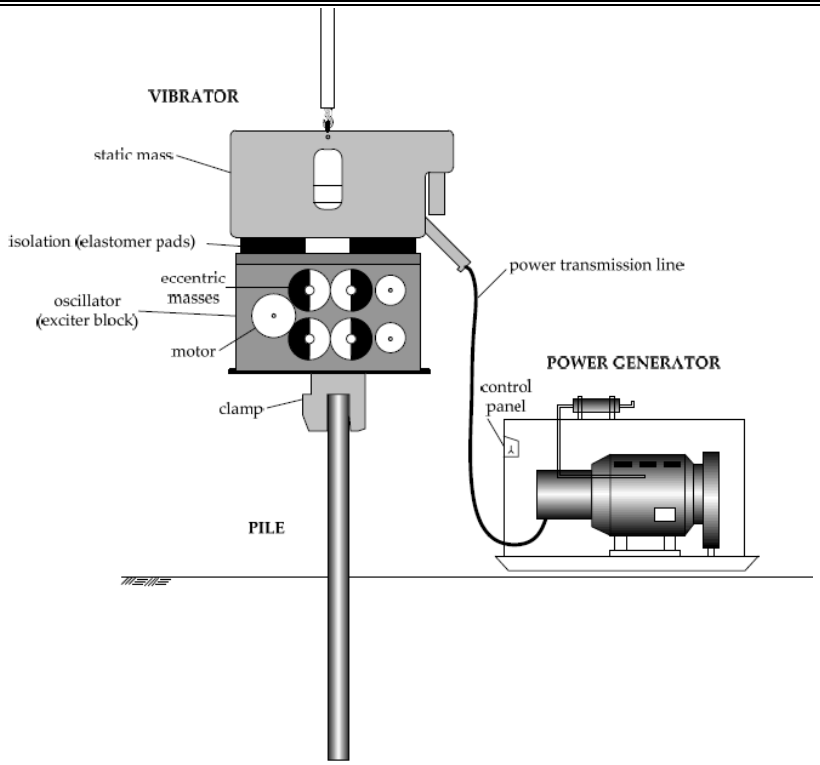

Figure 3.8: Equipment for vibratory driving of piles (free hanging model), modified after Massarsch (2000b) and Holeyman (2002) adapted from Deckner (2013).

A vibratory driver drives the pile into the soil with two mechanical actions; a vibratory action and a stationary action (Deckner 2013). The vibratory action is produced by the counter-rotating masses and the stationary action by the mass of the pile and hammer (the static mass) (Holeyman, 2002).

Hammer mass and its driving energy should be chosen wisely depends on soil type and the adjacent structures conditions to prevent any possible damage. Appendix (C) contains some of hammers data adapted from GRLWEAP Hammer Database (2015), these data is to help design engineers to choose the suitable hammer for the field of work.

3.3.2 The Pile.

Driven piles are deep foundation elements driven to a design depth or resistance. Types include timber, pre-cast concrete, steel H-piles, and pipe

piles. The technique has been used to support buildings, tanks, towers and bridges. Driven piles can also be used to provide lateral support for earth retention walls, steel sheet piles and soldier piles are the most common type of driven piles for this application.

- **Steel piles**

Many different sections are available for steel pile, H-piles, and pipe piles (being driven by impact hammer), their common use is in the foundation objects, on the other hand flat sheet steel piling and Z- sheet steel piling (being driven by vibratory hammer), their common use is in shoring the deep excavation.

- **Concrete pile**

Is considered as the most famous types of piles and also widely used in Egypt rather than any other kind of piles. Concrete piles have a variation of use but the focus will be on precast piles which can be driven. Lately composite piles become used as well.

- **Wooden pile**

The timber pile is probably the oldest types of piles for foundation and it has been used for many centuries. In some countries, and for particular applications, timber piles are still a cost-effective solution.

3.3.3: Soil-pile interaction

The energy transmitted from the pile to the soil depends mainly on the type , the efficiency of the hammer and the pile material. Heckman and Hagerty (1978) showed the significant of the pile impedance in the driving process (pile impedance is relying on pile material). The values of different piles impedance are shown in Table 3.4. The relation between the impedance of the pile and the amplification effect is shown in Figure 3.9**.**

Table 3.4: Impedance of different pile types (after peck et al 1974)

Material	Area (cm^2)	Impedance (kNs/m)
Wood		
Klin dry	506	137
Southern pipe	506	160
Concrete		
10 inch (25.4 cm)	506	421
20 inch (50.8 cm)	2027	1680
Steel		
HP 10×57	108	446
HP 12×53	100	434
HP 14×117	222	959
Pipe 103/4×0.188	40	166
Pipe 103/4×0.279	59	257
Pipe 103/4×0.365	77	316
Pipe 103/4×0.188 (mandrel)	344	1416
Steel concrete pile		
103/4 × 0.279	576	634

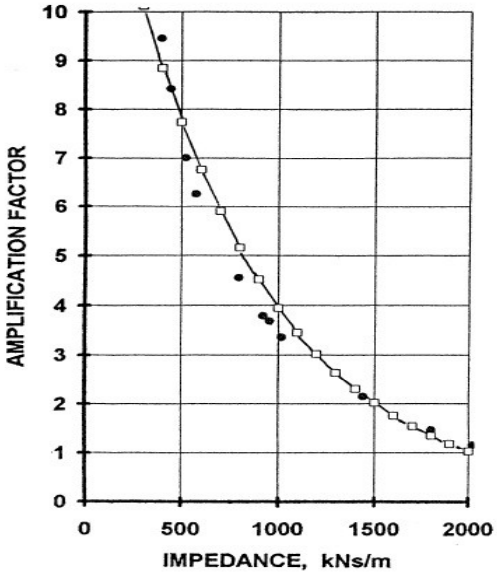

Figure 3.9: vibration amplification factor as a function of pile impedance, the vibration amplification effect has been set at unity for an impedance of 2000kN//m. (Massarsch 1993).

The penetration of the pile into the ground during the driving process generates both elastic and plastic deformations. At a short distance from the pile (one pile radius) most of the energy propagate as elastic waves, Massarsch (1993), as it shown in Figure 3.10.

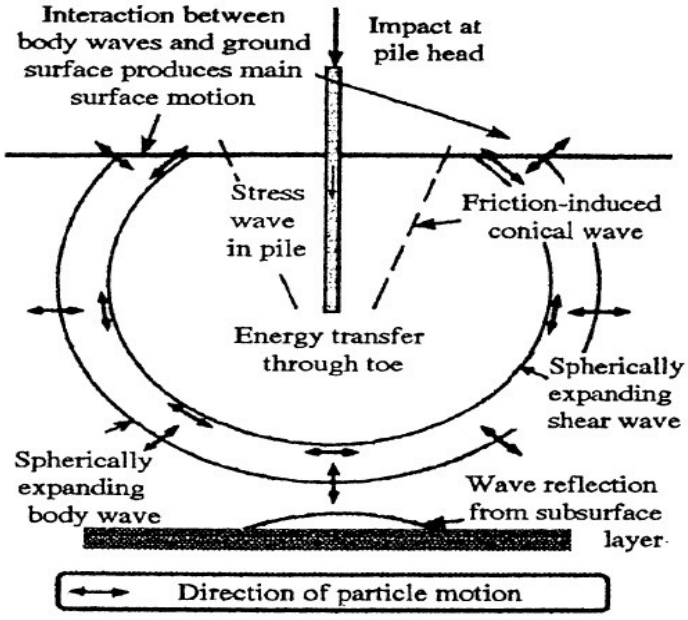

Figure 3.10**:** Schematic representation of wave field in the ground generated by impact on a pile after (Martin 1980)

3.4 Types of generated waves:

Propagation of ground-borne vibrations due to a vibratory excitation source, such as a pile driver or vibratory roller impacts the ground, energy is transferred from the construction equipment to the ground.

The principal wave types that transmit vibratory energy away from a source on or near the ground to a distant receiver are as follows:

- Rayleigh (R- waves).
- Shear (S- waves).
- Compression (P- waves).

The three wave types produce different patterns of motion in soil particles as they pass through soil. Therefore, structures will be deformed differently by

each type of wave. Figure 3.11, shows schematically the variation in soil particle motion with S & P waves away from the vibration source.

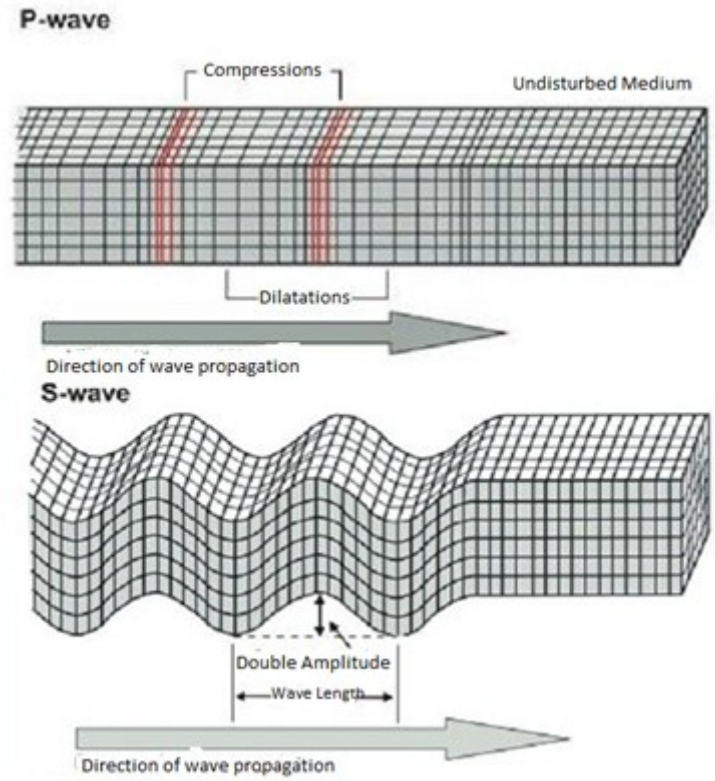

Figure 3.11: Deformation characteristics of P-, S- and R-waves (SOS-LIFE Earthquake Early Warning System 2004–2005: www.lamit.ro/earthquake-early-warning-system.htm).

3.4.1 Vibration propagation through soils:

At small distances from the vibration source, all three wave types will arrive together and greatly complicate wave identification; whereas at large distances, the more slowly moving S- and R-waves begin to separate from the P-wave and allow identification.

Rayleigh waves propagate at surface, which travel in a cylindrical form. This means that most of the Rayleigh wave's energy is confined to a volume below the surface that is one wave length deep

3.4.2 Vibration waves energy:

The P-wave is the fastest, followed by the S-wave, then the R-wave. Along the surface of the ground, the P- and S- waves decay more rapidly than the R-wave. Therefore, the R-wave is the most significant disturbance along the surface of the ground and may be the only clearly distinguishable wave at large distances from the source. R-waves account for 67% of the total energy, S-waves for 26% and P-waves for 7% when the exciting force is applied vertically to the propagation direction (Richart et al 1970).

The characteristic wave system for a short-duration ground disturbance, when the vibration source and the receiving point are a few metres to a few hundred metres apart, is shown in Figure 3.12. It can be seen that the P-wave arrives first at the receiver, followed by the S- wave and finally the R- wave. Figure 3.13, shows Generation mechanism of waves.

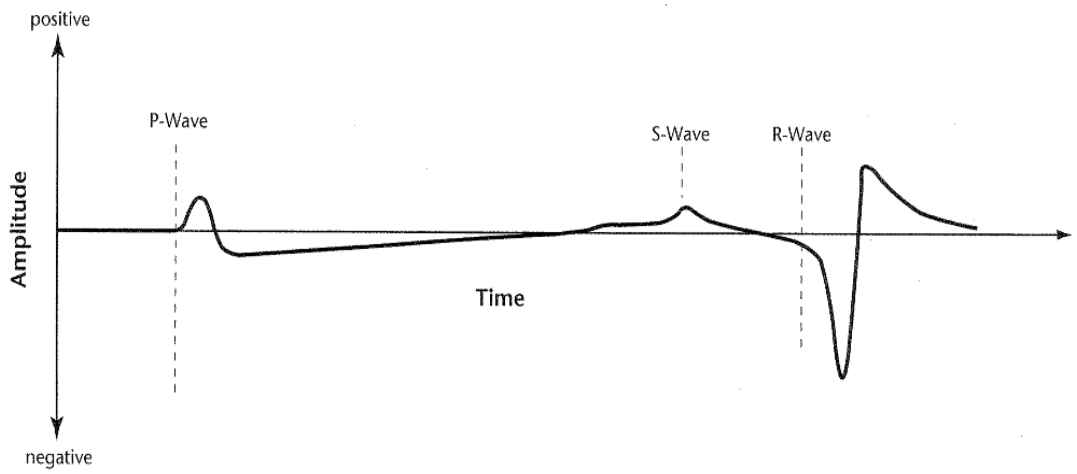

Figure 3.12 Characteristic wave systems from a surface point source (after Jones & Stokes Associates 2004)

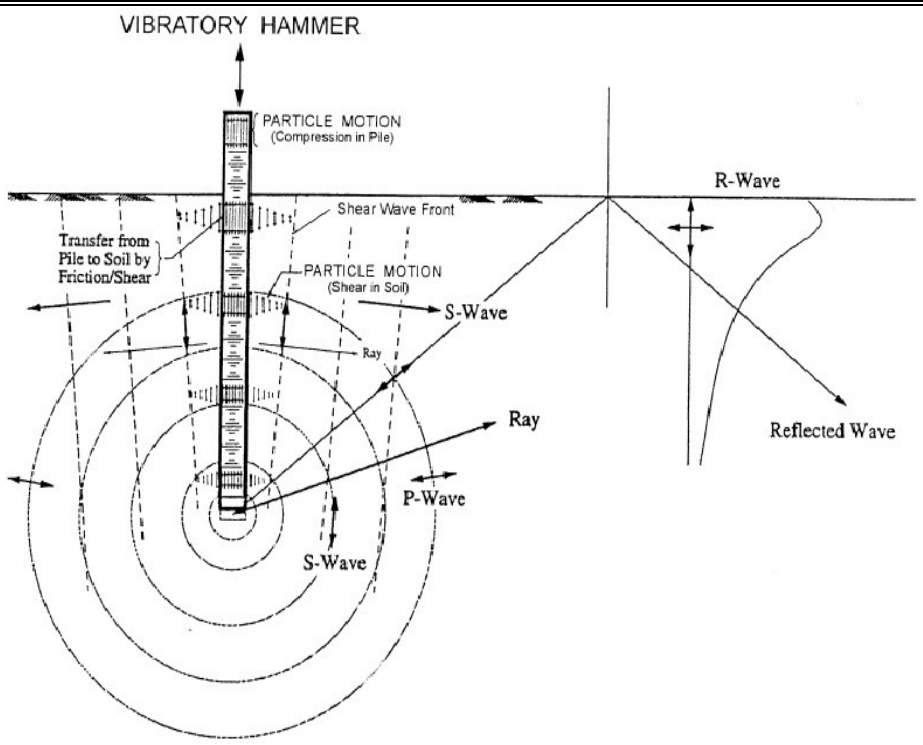

Figure 3.13: Generation mechanism of seismic waves during vibratory (or impact) driving of piles in homogeneous soil (adapted from Woods 1997)

3.4.3 The three propagated wave's properties

Properties of these three wave types are summarized in Table 3.5. This difference in geometric attenuation between surface and body waves translates to the lower geometric attenuation coefficient (0.5 to 2) as listed in Table 3.5.

The elastic waves keep attenuate through the soil. Wave attenuations are caused by two different effects as shown below (after Massarsch (1993) ,Wood and Jedele (1985)) :

- Enlargement of the wave front as the distance from the source increased (geometric damping).
- Internal damping of the wave energy by the soil.

The geometric damping depends on the type and the location of vibration source and the material damping is related with ground properties and vibration amplitude.

Wave velocity depends on soil type, by increasing the stiffness of the soil the velocity increased. For example velocity in rock layer is greater than clay layer as shown in Figure 3.14 and in Table 3.6.

Table 3.5: Properties of vibration waves (after Jackson et al 2007)

Wave type	Other name for wave type	Transmission through the ground	Wave front	Particle motion	Geometric attenuation coefficient (m^{-1})
Rayleigh	R-wave	Confined to surface	Cylindrical	Particles move in circular motion in the vertical plane resulting in motion both along and perpendicular to the direction of wave propagation	0.5
Shear	Secondary or S-wave	Body	Spherical	Particles move in the direction of the wave propagation and also perpendicular (either horizontal or vertical) causing a twisting deformation in small areas	2
Compression	Primary or P-wave	Body	Spherical	Particles move in the direction of the wave propagation, small areas contracting and expanding in response	2

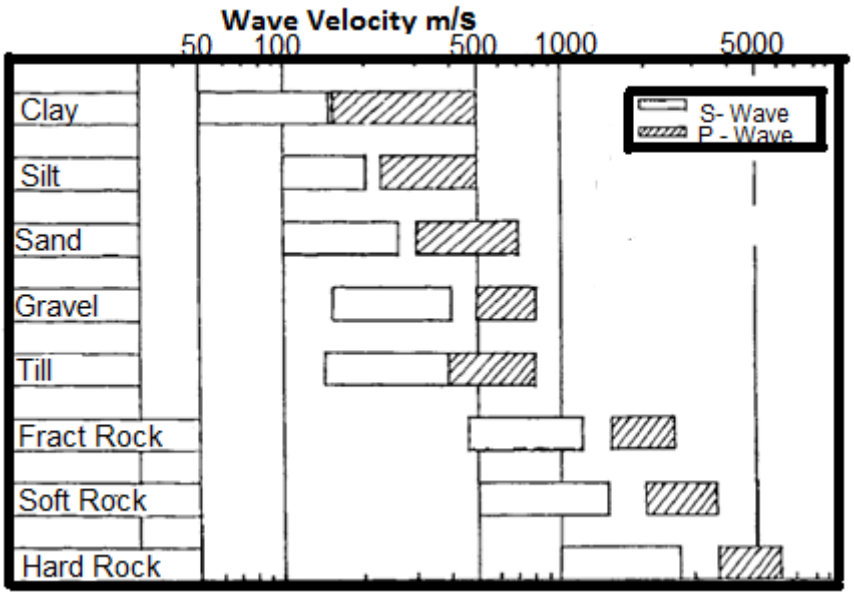

Figure 3.14: Range of P-, and s-wave velocity for different geologic materials, (modified after Massarsch 1983)

Table 3.6: Estimated propagation velocities for different materials (after Dowding 2000)

Material	Wave velocity (m/s)	
	Compression (p-wave)	Shear (s-wave)
Limestone	2000-5900	1000-3100
Metamorphic rocks	2100-3500	1000-1700
Basalt	2300-4500	1100-2200
Granite	2400-5000	1200-2500
Sand	500-2000	250-850
Clay	400-1700	200-800

3.4.4 Rayleigh waves

Rayleigh waves are considered as a type of surface wave that travel close to the surface of soil. Rayleigh waves include both longitudinal and transverse motions that decrease exponentially in amplitude as distance from the surface increases. The existence of Rayleigh waves was predicted in 1885 by Lord Rayleigh, after whom they were named. In isotropic solids these waves cause the surface particles to move in ellipses in planes normal to the surface and

parallel to the direction of propagation as shown in Figure 3.15.When P&S waves reaching the surface a part of them converted to R-waves.

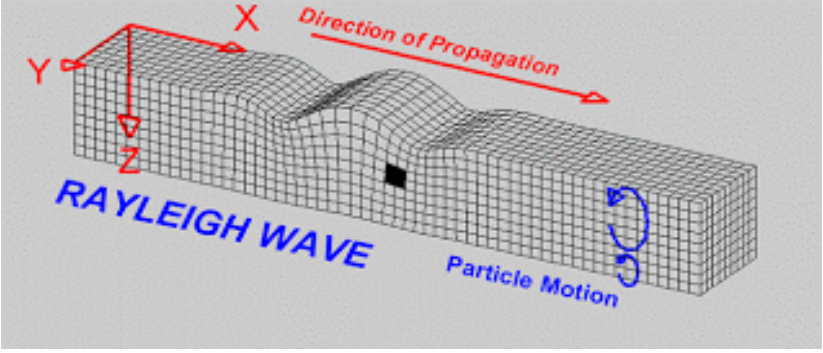

Figure 3.15 Soil particle motion of Rayleigh waves (seismicwaveanalysisgroup /seismic-waves)

R-waves involve both vertical and horizontal particle motion (Kramer, 1996). At a depth of around $0.2\lambda_R$ (where λ is the wave length) the motion changes direction to rotate in a prograde direction (Bodare, 1996), see Figure 3.16

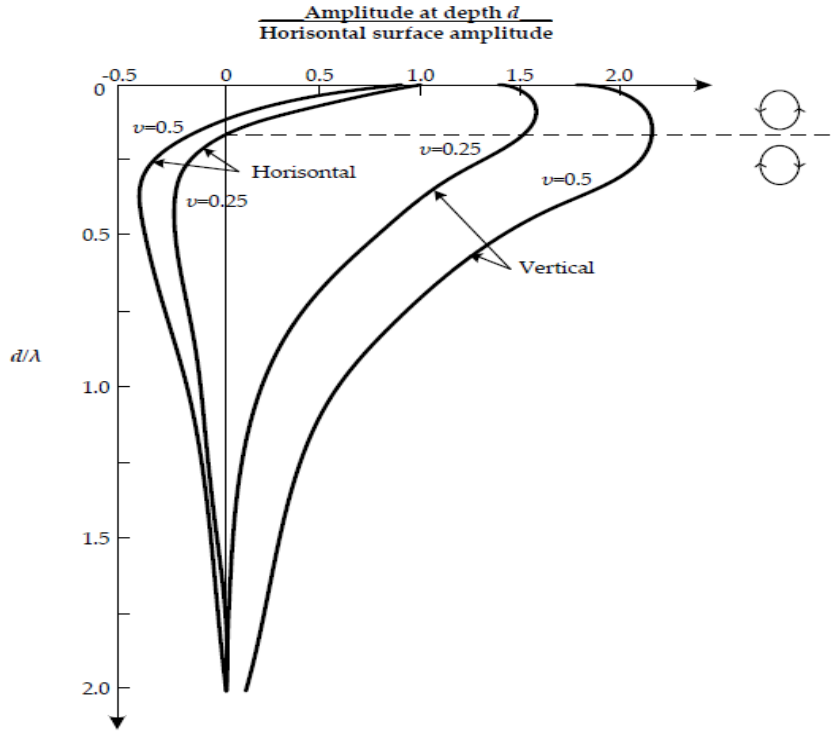

Figure 3.16: Horizontal and vertical vibration amplitude of the Rayleigh wave as a function of depth, Poisson's ratio and wave length (modified after Richart et al. 1970).

It can be seen that the vertical amplitude component is larger than the horizontal amplitude, also the horizontal amplitude decreased rapidly with depth, that conclusion by Deckner (2013) is confirmed by finite element model.

3.5 Damage due to pile driving

Structure damage occurs in the result of combined influence of structure vibration, displacement, velocity, acceleration, and frequency.

Vibration effects on structures depend on a number of factors such as dynamic sources, the soil medium where waves propagate, soil conditions at location of structures, soil-structure interaction, and susceptibility of structures to vibrations.

There are two fundamental mechanisms for vibration damage which are 1) distortion from inertial loads, and 2) settlement of the soils supporting the foundation. If the soil settlement is not uniform, distortion and damage can occur.

3.5.1 Damage evaluation

For evaluate the risk for damage to a building due to pile-driving induced vibrations, it is necessary to define the type of building damage. There are two different types of effect on building damage, the directly vibration and settlement of the soil which the building resting on

Damage to buildings and their foundations can be related to four different damage categories as shown in Figure 3.17. Massarch (2000),

- Damage Category I consists of static ground movements, which can occur in the vicinity of deep excavations. The installation of displacement piles can also give rise to heave and lateral displacements, which can damage buildings.
- Damage Category II is caused by ground distortion. When the waves propagate along the ground surface, foundations of adjacent buildings can

be subjected to a large number of upward (hogging) and downward (sagging) movements.

- Damage Category III is due to settlement caused by ground vibrations. Settlement due to vibrations is largest in loose, granular soils, such as sand and silt.
- Damage Category IV comprises building damage caused by dynamic effects in the building itself, which is the only damage category typically considered in vibration standards.

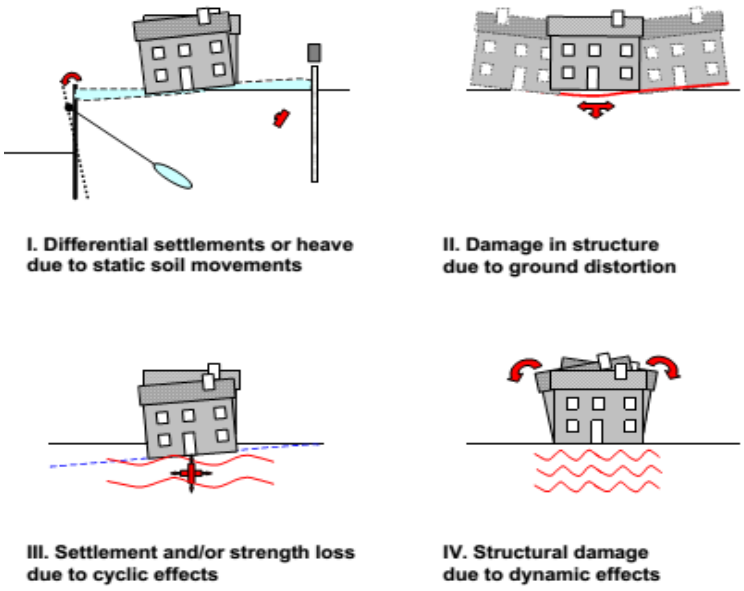

Figure 3.17: Damage mechanism due to pile driving of piles or sheet piles after (Massasrch 2000).

3.5.2 Behavior of damage

There are a considerable diversity of buildings and underground facilities, these structures and their parts, for instance, floors, internal walls etc., have different responses to the same ground vibrations. Besides, subjects of concerns such as glass in residential houses, computerized systems, instrument cabinets, medical apparatuses and other sensitive devices in offices that also have their own responses to ground vibrations.

Propagating waves expose buildings or installations in the ground to repeat distortion cycles (sagging as well as hogging).as shown in Figure 3.18 which

illustrate the effect of wave propagation below a brick wall. It will be noticed that the soil could be distorted by sagging or hogging, continuously upward and down word, this effect is fundamentally a cyclic loading problem and not a dynamic effect.

Burland and Wroth (1974) have shown that "static damage" can occur in load-bearing walls as a result of hogging at a relative deflection $d/B > 1.5 10^{-4}$, where d is the vertical deflection (displacement amplitude) and B is the building length. In the case of ground vibration propagation, distortion is critical when the wave length L becomes shorter than the building length B. This is the case when the surface wave length of the propagated velocity is low, which is typical for soft clays and silts below the ground water level.

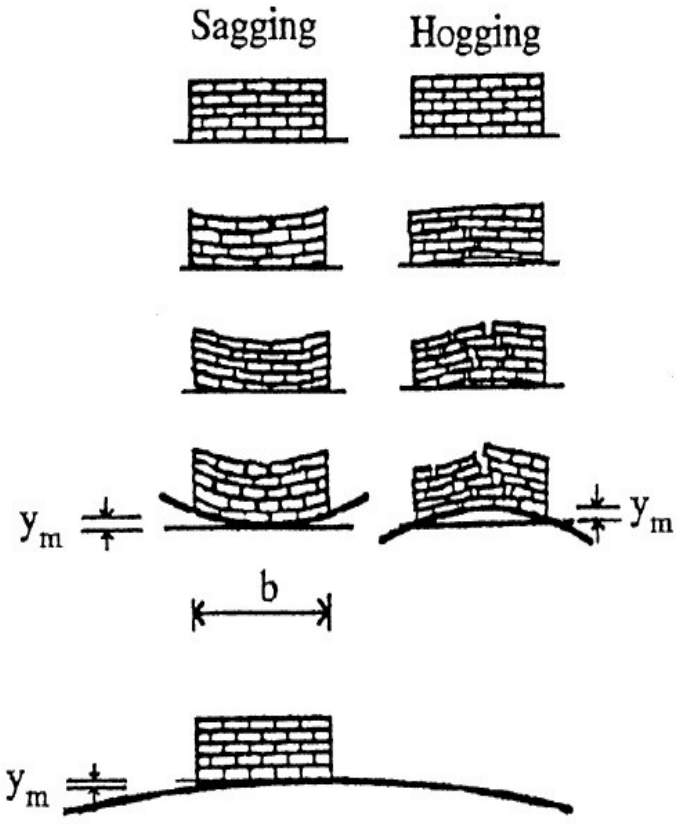

Figure 3.18: Influence of wave length on cracking of a brick wall due to hogging and sagging of the ground (after Massarsch and Broms 1991).

3.5.3 Buildings conditions

In Figure 3.19, three examples for building damage due to vibration are illustrated after Massarsch and Fellenius, (2014).

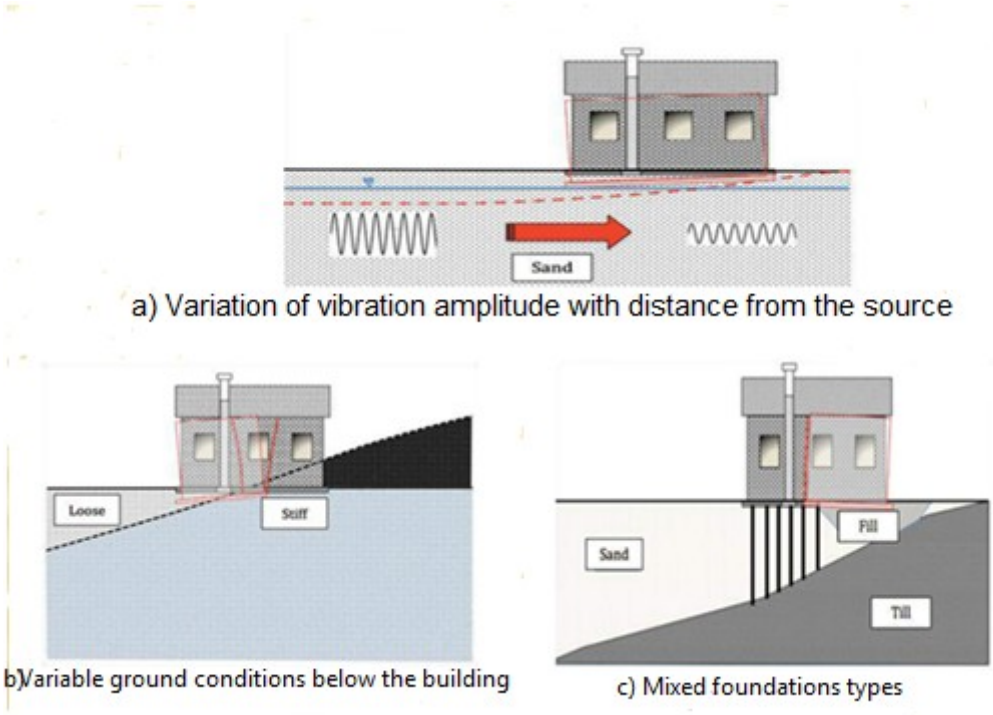

Figure 3.19: Importance of foundation conditions on total and differential settlement caused by ground vibrations (after Massarsch and Fellenius, 2014)

- First example (a) is a building on loose sand or silt (any type of soft or loose soil). If the building is founded on un compacted granular soil and the area has not previously been exposed to strong ground vibrations (such as pile driving, dynamic compaction or blasting), the building is more prone to suffer vibration damage due to soil densification with varies amounts depends on the distance from the source and building width, which leads to differential settlement.
- Second example (b) shows a building, which is founded in a slope, where material, had been excavated from the slope and placed to create a level foundation. Unless the placed fill is well-compacted, the risk of differential settlement between the fill and the excavated area below the building will be high.

- Third example (c) shows a building, which is partly founded, on natural or filled soil, and partly on piles. Differences in stiffness of the foundation can lead to differential movements between different parts of the building.

3.5.4 Structure response due to vibration

The damage potential of pile-driving vibrations depends on the displacement and the frequency of the vibration. Neither of these two characteristics alone will damage a structure. Concerning displacement, it is common knowledge that a structure can be uniformly jacked through several feet without causing damage. Likewise, with regard to frequency, normal sound, in passing through a wall, can vibrate the wall at high frequencies (several thousand cycles per second) without causing damage. It is a combination of displacement (amount of motion) and frequency which causes damage. The particle velocity of earthborn vibration is the best measure of damage potential because it combines displacement and frequency in the most significant manner (after Wiss 1981)

Svinkin (2008) illustrated different three ways to show the structure response due to construction vibration as following:

1. **Direct Vibration Effects on Structures**

vibration effects on structures can be considered within a distance equal to the final excavation depth in rock (close-in blasting) or one pile length from a driven pile. These distances can be substantially larger for susceptible structures. Intensity of structural vibrations depends on soil-structure interaction. Direct minor and major structural damage without resonant structural responses were observed in the velocity 33-191 mm/s range for frequencies of 2 to 5 Hz and in the velocity 102-254 mm/s range for frequencies of 60 to 450 Hz as shown in Figure 3.20.

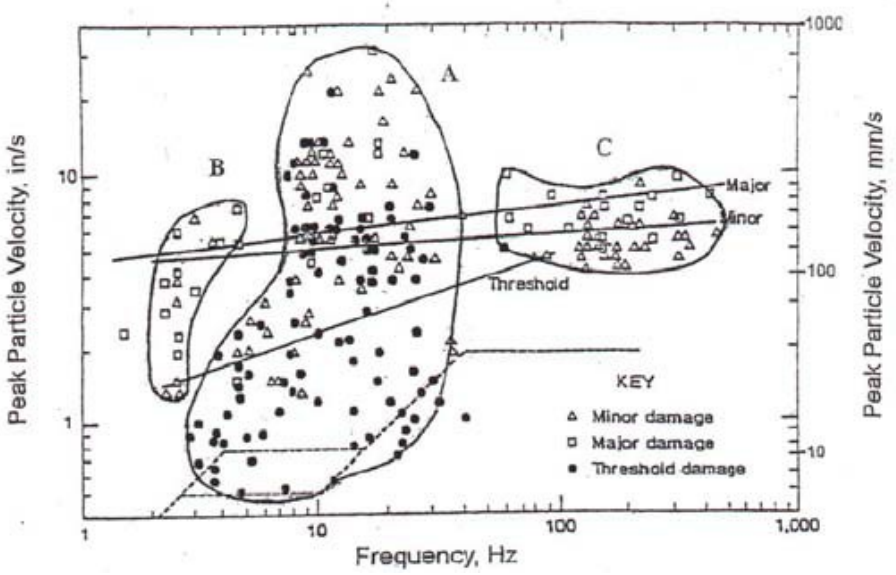

Figure 3.20: Ground vibrations from blasting and structure damage summary grouped in three zones. Dashed lines define USBM safe limits. (Data were modified after Siskind 2000).

2. Resonant Structural Vibrations

The proximity of the dominant frequency of ground vibrations to one of building's natural frequency can amplify structural vibrations and even generate the condition of resonance. Records of ground and structure vibrations with close dominant frequencies are shown in Figure 42.21. It can be seen that the PPV of structural vibrations increased up to 2.7 times in comparison with that of ground vibrations and structural vibrations began to increase after the first cycle of ground vibrations.

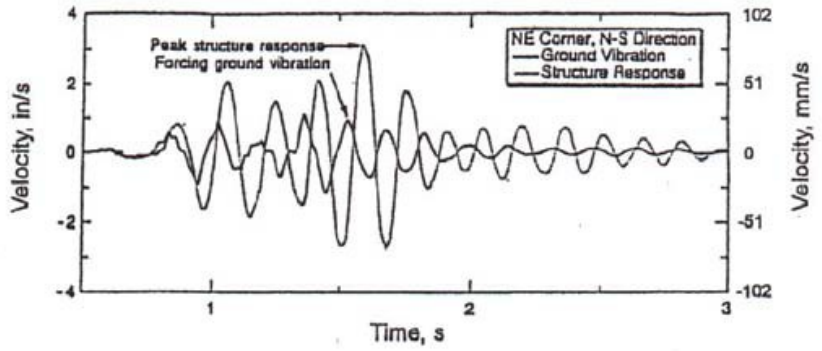

Figure 3.21: Ground and structure vibrations with frequency of 5.8 Hz near structure resonance (Siskind 2000). Plot was originally from Crum (1997).

3. Resonance of Soil Layers

Matching the dominant frequency of propagated waves to the frequency of a soil layer can create the condition of resonance and generate large soil vibrations. Such amplification of soil vibrations may happen during vibratory pile driving. Woods (1997) noted that layers between about 1-5 m thick may produce a potential hazard for increasing vibrations when vibrators with operating frequencies between 20-30 Hz install piles in soils with shear wave velocities of 120 to 600 m/s. The use of vibratory drivers with variable frequency and force amplitude may minimize damage due to accidental augmentation of ground vibrations.

3.6 Ground Heave Due to Pile Driving:

One of the possible damage due to pile driving is ground heave. Hagerty and Peck (1971) conclude that heave effects are most pronounced within saturated insensitive clay soils. Based on the results of several case studies, they further state that the volume of surface heave outside the area of pile foundations is equivalent to the Volume of approximately 50 % of the displaced soil. Depending on the proximity of adjacent buildings or surface features, the heave may cause distress and possibly structural damage, therefore it becomes important to estimate the magnitude and patterns of heave outside the construction site in order to preserve the integrity of the abutting features. Previous studies, including those by Cummings et al. (1950) and numerous discussion papers, Lo and Stermac (1965), Soderberg (1967), D'Appolonia and Lambe (1971), and Vesic (1972), have attempted to explain the factors which contribute to heave. Several of these papers present field data which substantiate that heave effects are related to build-up of excess pore pressure, volume of displaced soil, sequence of driving, and clay sensitivity. The effect of soil heave on buildings and facilities is shown in Figures 3.22 and 3.23 respectively.

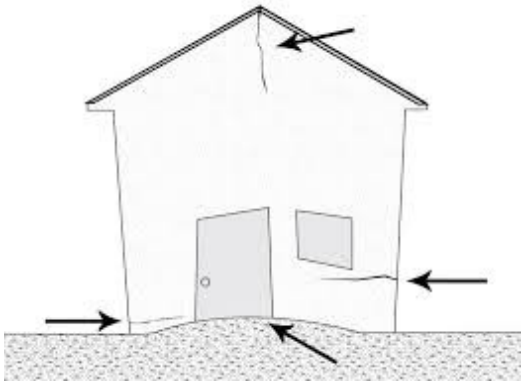

Figure 3.22: The effect o soil heave on the structures.
(www.foundationrepairsaz.com).

Figure 3.23: The effect o soil heave on the facilities (railway lines) after Reddy et al (2008).

3.7 Models for Prediction of PPV due to pile driving

It is important to accurately predict the peak particle velocity (PPV) of the vibrations because it is considered a very important parameter to predict the level of structural damage expected due to vibration, (Dowding (1996))

Deckner (2013): reviewed the prediction expressions available in literature to predict PPV due to vibration born from pile driving. Deckner (2013); divided models used for prediction of vibrations from pile driving into three categories: 1) Empirical models that models are based on empirical knowledge from previous measurements and experience.

2) Theoretical models such as finite element models or analytical models.

3) Engineering models (sometimes are called mixed approach models) these are a mix of empirical models, theoretical models and engineering knowledge.

Golitsin (1912) derived a simple equation for surface waves generated by earthquakes to calculate a reduction of the maximum displacement of ground vibrations between two points at distances r_1 and r_2 from the source as shown in Eq.3.1

$$A2 = A2\sqrt{r1/r2}\, e^{-\gamma(r2-r1)} \qquad \text{(Eq.3.1)}$$

Where A_1 = amplitude of vibrations at a distance r_1 from the source, A_2 = amplitude of vibrations at a distance r_2 from the source γ = attenuation coefficient. The term $(r_1/r_2)^{0.5}$ indicates the radiation or geometric damping, and the term exp $[-\gamma\ (r_2-r_1)]$ indicates the material or hysteretic damping of wave attenuation between two points.

Wiss (1967) discovered that the vibration magnitude due to pile driving varied by the amount of energy transmitted to the soil, the soil properties and the distance from the source and concluded that the particle velocity varied with the square root of the energy of the hammer. Since then many prediction models have taken the form of a power law (or energy based prediction model) in which the ground vibration magnitude is assumed to be dependent on the hammer energy.

Attewell & Farmer (1973) purposed a model considered from the early empirical prediction models of PPV as shown in Eq.3.2

$$V(mm/s) = K\frac{\sqrt{W0}(\mathbf{joules})}{r(m)} \qquad \text{(Eq.3.2)}$$

Where K is a constant varies from 0.25 to 1.50, when k 1.5 the output of PPV is a vertical component. Eq.3.2 usually used calculating PPV values in case of pile driving.

Heckman & Hagerty (1978) presented a formula to predict PPV values through pile driving case as following in Eq.3.3.

$$V(mm/s) = K\frac{\sqrt{W0}(joules)}{r(m)} \quad \text{(Eq.3.3)}$$

Where, K value varies for material type of driven pile. The variation explained reduction of K value as the energy distribution capacity which is measured from impedance value rise.

J. M. Ko, et al. (1990) drove an experimental study for quantifying PPV magnitude at distance from vibration source. From every measurement, PPV values were plotted Vs distance from vibration source. J. M. Ko et al. used data from study location and obtained α and V parameters at distance of 1.0 m from driven pile on alluvial silty sand soil. The reference values are $\alpha = 0.04\ m^{-1}$ and V = 70 mm/sec, so the empirical equation from J. M. Ko et al. is shown in Eq.3.4. where are is the distance from the vibration source.

$$PPV(mm/s) = 70\sqrt{\frac{1}{r(m)}}e^{-0.04(r-1)} \quad \text{(Eq.3.4)}$$

Attewell et al. model (1992a and 1992b) assumed that a quadratic regression curve is the best fit to field measurements of ground vibrations due to pile driving than the previously used linear regression curve, (Attewell & Farmer, 1973). The advanced model proposed the following equation for the prediction of PPV due to pile driving in Eq.3.5.

$$\log V = X1 + X2\log\left(\sqrt{\frac{Wo}{r}}\right) + X3\log\left(\frac{\sqrt{Wo}}{r}\right)^2 \quad \text{(Eq.3.5)}$$

Where v (PPV) = vibration velocity (mm/s), x_1, x_2 and x_3 = constants of proportionality, W_0 = input energy (J), r = distance between source and point of interest (m). Constants x_1, x_2 and x_3 are functions of the soil conditions at the site of pile driving. Proposed values of the constants of proportionality are given according to Deckner (2013) as shown in Tdbles 4.6. and 4.7.

Table 3.6: Values of x1, x2 and x3 for impact pile driving, from Attewell et al. (1992b).

Curve fit	X_1	X_2	X_3
Best fit	-0.519	1.38	-0.234
Half a standard deviation	-0.296	1.38	-0.234
One standard deviation	- 0.073	1.38	-0.234

Table 3.7: Values of x1, x2 and x3 for vibratory pile driving, from Attewell et al. (1992b).

Curve fit	X_1	X_2	X_3
Best fit	-0.464	1.64	-0.334
Half a standard deviation	-0.213	1.64	-0.334
One standard deviation	0.038	1.64	-0.334

Attewell et al. (1992b) proposed that the values for half a standard deviation should be used for normal construction work while one standard deviation should be used where high security against vibration is needed. For the best fit line there is a risk of exceeding the estimated values of 50%, for half a standard deviation the risk is 31% and for one standard deviation the risk is reduced to 16% (Attewell et al., 1992b).

Lewis and Daive (1993), drove a simple equation for PPV prediction due to pile driving as shown in Eq.3.6. Where "a" is the acceleration and "f" is the frequency of the propagated wave.

$$\mathrm{PPV} = \frac{\mathrm{a}}{2\pi \mathrm{f}} \qquad \text{(Eq.3.6)}$$

Robinson (2006), performed more extensive study to estimate ground motions from total resistance. The author combined ground motion measurements of peak particle velocities (PPV) for consecutive hammer impacts measured at a large construction site in Wisconsin with PDA pile velocity measurements. The PDA monitoring was primarily utilized to determine bearing capacity of the

300 mm (12 inch) to 400 mm (16 inch) diameter, closed ended pipe piles, both at the end of driving and during restrike testing. Using these measurement results, Robinson showed that this information can also be used to develop a wave equation based prediction of PPV at some distance from the pile driving site, based on the GRLWEAP (Pile Dynamics, 2005) hammer-pile-soil model and wave propagation theory as illustrated in Eq.3.7.

$$PPV = k \cdot V_{RTL} \left(\frac{D}{Do}\right)^{-n} \qquad \text{(Eq.3.7)}$$

Where k is a dimensionless constant represents impedance and total resistance, n is a dimensionless exponent, Do is pile radius, D is the seismic distance. The total resistance, V_{RTL}, is force acting on the pile. As an initial model, n was set to 1.

Svinkin (2008) developed a relationship for the prediction of PPV due to pile driving. Svinkin's model is based on determination of the vibration velocity on the pile head, and from that computes PPV. The following relationship is proposed for the ground vibration due to pile driving as shown in Eqs.3.8 and 3.9.

$$Vg = Vp \frac{\sqrt{Wo}}{r} \qquad \text{(Eq.3.8)}$$

Where V_g = ground vibration (mm/s) (PPV) and V_p = pile vibration at the pile head

$$Vp = \sqrt{\frac{2C_B.Wo}{Zp\ Lp}} \qquad \text{(Eq.3.9)}$$

Where C_B = wave propagation velocity in the pile (m/s), Z_p = pile impedance (kNs/m), L_p = pile length (m), W_0 = energy transferred to the pile (J), r = distance from the pile to the point of interest.

3.7.1 Theoretical models

Theoretical models use a different approach for the prediction of vibrations due to pile driving than empirical models. Deckner (2013). Theoretical models are usually built up of numerical or analytical modeling in different computer

programs. Davis (2010) has listed several numerical methods which can be used for prediction of ground vibrations, the most common that are present in existing prediction models are:

- Finite Difference Time-Domain Method (FDTD or FDM)
- Finite Element Method (FEM)
- Boundary Element Method (BEM)

Waarts & Bielefeld (1994) presented a model to predict vibrations due to pile driving. The only necessary input data for the prediction is the type of pile and hammer and the results of a CPT test. Deckner (2013).

The Waarts & Bielefeld model is actually divided into two different models. The model for the pile driving, described by the stress wave simulation program Tnowave, and the model for the wave transmission in soils described by the finite element package Diana. The Tnowave program is based on the one dimensional stress wave theory and it simulates the pile driving process for many combinations of pile driving hammers (both impact and vibratory hammers), pile types and soil conditions. From Tnowave the load applied to the soil is computed. The load, consisting of the force at the pile toe and the outside friction on the pile, is thereafter put into Diana. With Diana displacements, velocities and accelerations can be computed as a function of time in every point in the soil. Deckner (2013).

Holeyman (1993) set a model for calculating vertical shear waves propagating away from the pile and is based on a radial discrete model. The cylindrical model is illustrated in Figure 3.24 and consists of disks or concentric rings with increasing distances the further from the pile they are located. The rings have their own individual masses and transmit forces to their neighboring rings. This method of soil modelling is meant to simulate geometric damping. Deckner (2013)

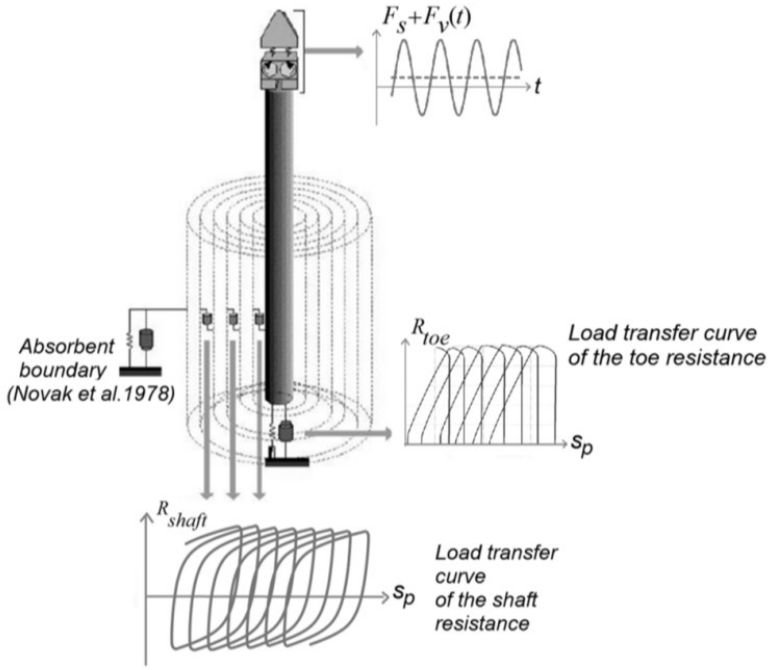

Figure 3.24: Vibratory driving model developed by Holeyman (1993) (Whenham, 2011 from Holeyman, 1993b).

Whenham (2011) using Finite Element Method (Plaxis), where he modelled vibratory pile driving in the commercial FEM software Plaxis. The problem set up is an axisymmetric geometry extending 40 m in the radial direction and 25 m in the vertical direction, see Figure 3.25. The boundaries are chosen as absorbent boundaries at the bottom and right hand side, and have the function that compression waves that hit the boundary perpendicularly will be absorbed while shear waves will still give a small boundary effect. Deckner, (2013).

The load is added as point loads distributed between 0 and 2.25 m at the centre of symmetry. This load model assumes that the force applied to the soil by the pile is equally distributed along the pile shaft, Deckner (2013). The soil is considered to be linear elastic, and material damping is represented by a damping parameter proportional to the mass and stiffness of the system. Deckner, (2013).

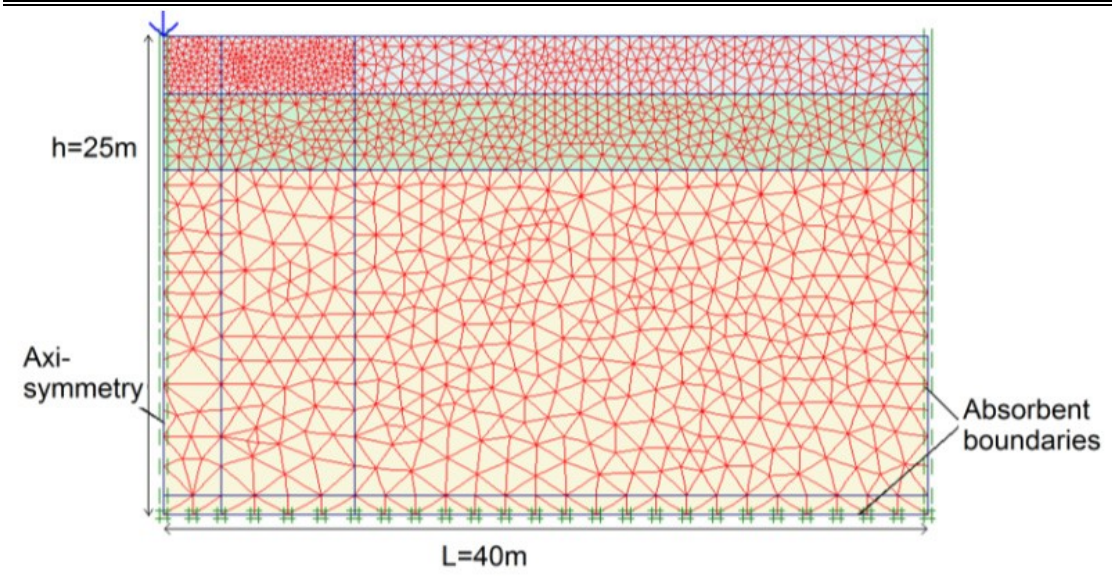

Figure 3.25: Plaxis model (after Whenham, 2011). (adapted From Deckner, 2013).

Masoumi et al. (2006, 2007, and 2008) presented a numerical prediction model made up of a coupled finite element boundary element model in order to predict free field vibrations due to impact and vibratory pile driving as shown in Figure 3.26. The pile is modeled as linear elastic material using the finite element technique and the soil is modeled as a horizontally layered elastic half space using the boundary element technique. The pile-soil interaction is modeled using a sub domain formulation. As their focus is on vibrations in the far field, Masoumi et al. (2006 and 2007) assumed a linear elastic constitutive behavior of the soil as the deformations are believed to be relatively small. The damping is assumed to be independent of frequency and no separation is allowed between pile and soil. The soil is assumed to be horizontally layered.

To solve the system, the Structural Dynamics Toolbox in Matlab is first used to make the finite element model of the pile. Then the soil impedance and the modal responses of the soil are computed using the program MISS 6.3.

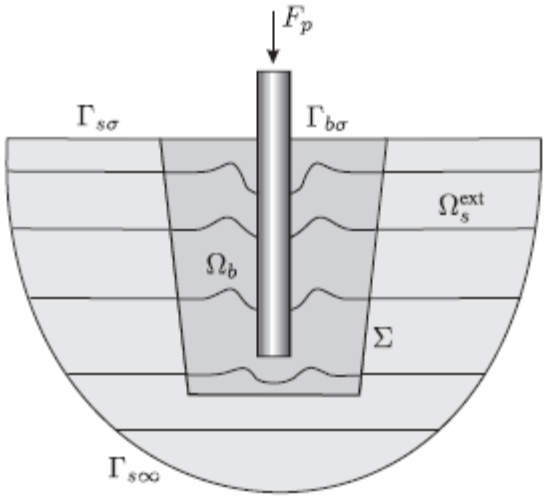

Figure 3.26: Geometry and outline of the problem (after Masoumi et al., 2009).

Masoumi et al. (2009) developed a numerical model to predict the maximum impact velocity during pile driving process and verified the numerical model by the field data presented by Wiss (1981). Rezaei et al. (2016) compared FEM results of PPV with exprimental results after Wiss (1981) and the numerial model of Masoumi et al. (2009) the comparison is shown in Figure 3.27.

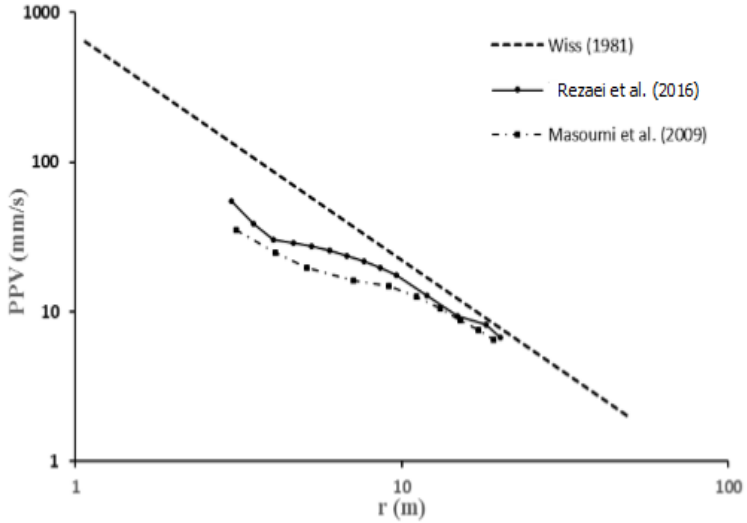

Figure 3.27: Comparison of PPV values of Rezaei et al (2016) study with experimental results of Wiss (1981) and numerical results of Masoumi et al. (2009)

Mahutka & Grabe (2006) presented a model in which vibratory pile driving is modelled by non linear dynamic finite element analysis with an explicit time integration scheme. The installation process of the vibratory pile driving is modelled using FEM and computations are done in the computer program Abaqus. The pile is modelled as a laterally supported rigid axisymmetric surface while the soil is discretised with axisymmetric continuum elements.

Mahutka & Grabe (2006) performed field tests to validate their model. They measured the acceleration at the pile as well as the vertical and horizontal velocities at four points located 1m, 2 m, 4 m and 8 m from the vibratory driven pile. Deckner, (2013). The measured results show a good agreement with the modelled results, see Figure 3.28.

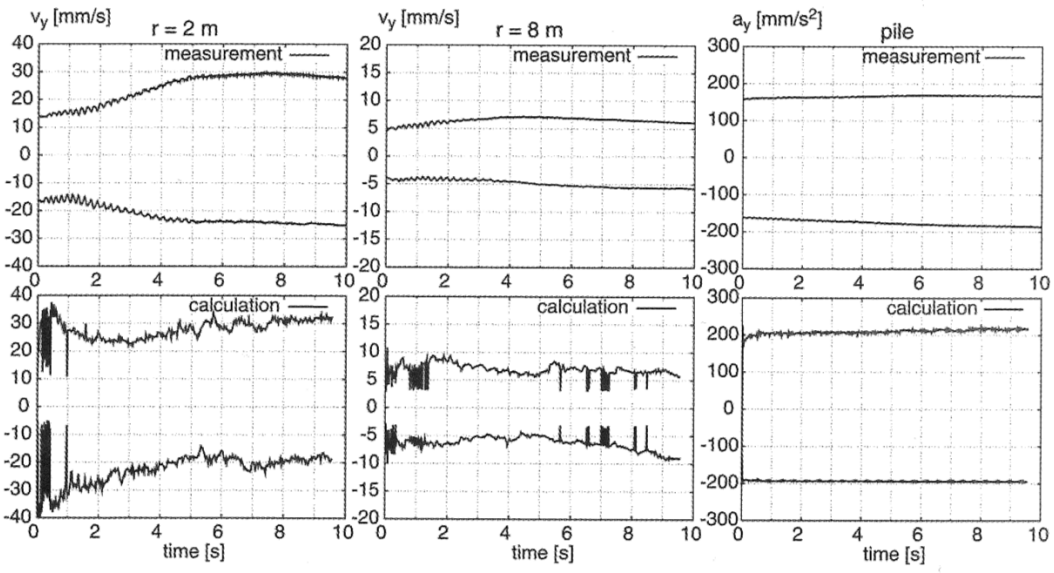

Figure 3.28: Measured and calculated vibration velocity at the ground surface and acceleration at the pile (after Mahutka & Grabe, 2006).

Khoubani & Ahmadi (2012) have created an axisymmetric finite-element model using Abaqus to predict vibrations in the form of PPV from impact driven piles in homogenous soil. In the model the entire penetration process, from the ground surface to the desired depth, is included. Plastic deformations in the soil next to the pile as well as a slip frictional contact between pile and soil are accounted for in the model.

The modeled results were compared with the results measured by Wiss (1981) and showed good agreement. They also compared their results with the numerical results presented by Masoumi et al. (2009). Khoubani & Ahmadi (2012) reported higher values than Masoumi et al. (2009) for a distance of 5-9 m and vice versa for distances of 9-23 m Deckner 2013.

Rezaei, M. et al. (2016), have created a finite element model, using ABAQUS, for simulating continuous pile driving process from the ground surface and measured PPV values due to different parameters such as elastic modulus, shear strength parameters, impact force and pile diameter. Rezaei, M. et al. (2016), have verified their model by comparing the results with experimental results of Wiss (1981) and numerical results of Masoumi et al. (2009). The comparison of the field and numerical data showed good consistency between PPV values as shown in Figure 3.27. The predictions of this study were even closer to the field data of Wiss (1981) than that of Masoumi et al (2009).

Rezaei, M. et al. (2016) concluded the following:

- The increase in shear strength (cohesion or friction angle) of the soil increased the peak particle velocity.
- The maximum particle velocity decreased with increase in elastic modulus of soil. (That point is discussed later and illustrated that by increasing soil stiffness the PPV increased and proved by the Plaxis model, Massarch & Fellenius (2008), Srbulov (2011) and Crabb (2000).
- The maximum particle velocity increased with increase in pile diameter.
- According to the numerical results, the mentioned parameters affected PPV in closer distances from the pile and their impacts can be neglected in greater distances.
- Peak particle velocity on the ground surface did not reach its maximum value at full penetration. In general, the maximum PPV occurred in a lower depth known as the critical depth of vibration.

Setiawan and Fad (2012) present modeling of vibrations using finite element method (Plaxis model), to obtain the Peak Particle Velocity (PPV) as managed value in associating vibration risk due to pile driving by comparing the output values of PPV with the different vibration limits (database of standards, ie; U.S. of Surface Mining (OSM), German Institute of Standards (DIN), British Standards Institution (BSI) and the Swiss Association of Highway Engineers (SN). Mohr Coloumb was used for clay, Hardening soil was used for sand and Linier Elastic model for pile with axisymmetric analysis. The PPV values vs distance are shown in Figure 3.29.

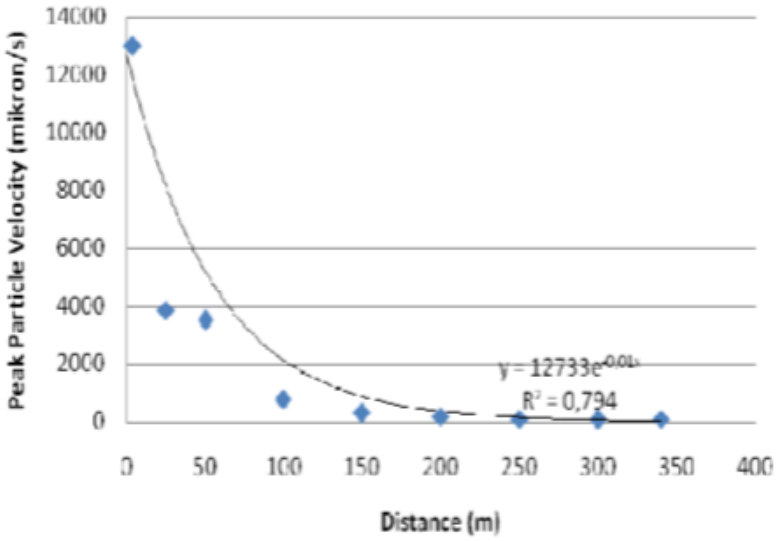

Figure 3.29: Curve of peak particle velocity (PPV), (after Setiawan and Fad 2012).

Setiawan and Fad (2012) concluded the following:

- Axisymmetric 2D finite element method could simply predict the ground vibrations of driven pile.
- The allowable distance for the pile constructions to prevent damage of adjacent structures must be larger than 100 m.

Olivecrona and Ulander (2016) reported that the vibrations of a single hammer blow at different pile depths are studied and compared with a field test. The object is to investigate the possibility to make a satisfactory finite

element simulation of the vibrations due to pile driving. Two soil plasticity models are used along with a linear elastic model. The plastic models are the Mohr-Coulomb yield criterion and the Drucker-Prager yield criterion.

The models are based on a field test in Skövde made by Nilsson (1989) and with his results used in a paper by Massarsch and Fellenius in (2008). When the models are compared, the particle velocities at different distances and depths in the soil are studied. For every simulation a corresponding particle velocity graph is presented. The graphs show the extracted values of particle velocity during a time interval of 0.7 seconds. This interval represents the time for a single hammer impact with additional time for the waves to propagate. as shown in Figure 3.30.

Olivecrona and Ulander (2016) investigated the following parameters:

- Vibrations at surface with horizontal distance of 10, 20 and 40 meters from the pile at different pile depths.
- Differences in results with material models such as Mohr-Coulomb, Drucker-Prager.
- Alteration in Young's modulus.

Olivecrona and Ulander (2016) model is a 2D geometry of the soil and pile is built up with the geometry tool in COMSOL Multiphysics. Since the surroundings of the test site are considered to be homogenous, a symmetry line is created in the middle of the pile.

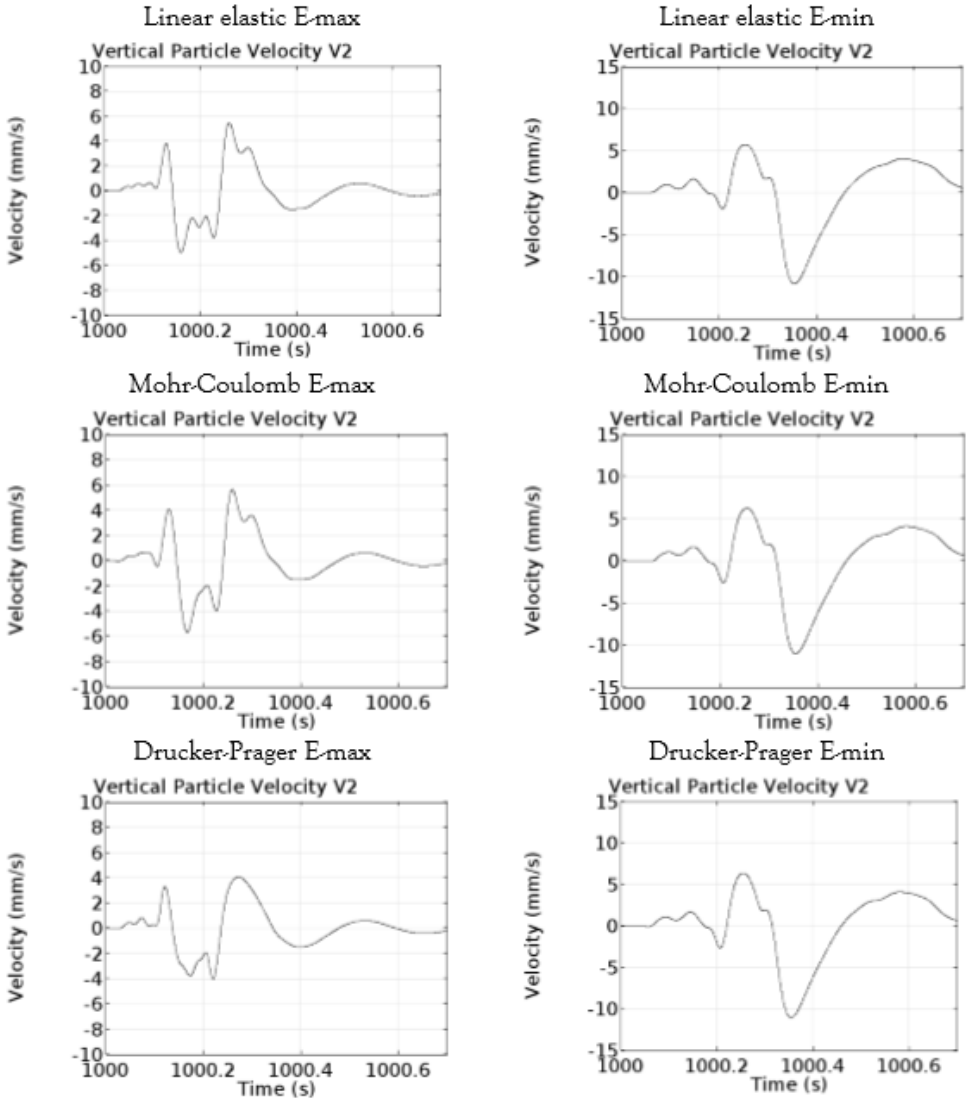

Figure 3.30: Velocity vs time graphs (Pile depth 3 meters) at probe point V_1. E_{max} in the left column, E_{min} in the right column. Elastic, Mohr-Coulomb and Drucker-Prager are presented, (after Olivecrona and Ulander 2016).

Olivecrona and Ulander (2016) concluded the following:

- With accurate material properties and parameters for a given situation, the vibrations and wave propagations due to pile driving can be computed in a realistic way using a finite element software.
- Some differences were found in the Drucker-Prager yield criterion and the Mohr-Coulomb yield criterion simulations in comparison with the elastic model.

- The possibility to make vibration- and wave computations with a FE-model can be an efficient tool for predicting vibrations and wave propagation. Hence, this makes the FE-model to be a complement to field tests if accurate soil properties and piling conditions are at hand

Serdaroglu (2010), implement a numerical method using ABAQUS to simulate dynamic loading of a single pile, and study the factors influencing the stress wave propagation in the soil surrounding the pile like soil properties, pile embedment length and hammer energy.

Serdaroglu (2010), In the dynamic analysis, investigated the following parameters to illustrate their effect on PPV: (1) the soil type, (2) the pile embedment length and (3) the released hammer energy.

Serdaroglu (2010), concluded the following:

- For the first analysis, the PPVs are higher in stiff clay in the near field, which is 9 m or less away from the pile; (2) the PPVs are higher in soft clay in the far field, which is more than 9 m away from the pile; (3) the shear waves dominate in the soft clay whereas the primary waves dominate in the stiff clay.
- For the second analysis, is performed for three cases consisting of fully, half, and quarterly embedded piles. The peak particle velocities at different distances from the pile on the ground surface are plotted. The quarterly embedded pile yields greater vibration amplitudes with respect to the half and fully embedded piles. Although the applied energy from the pile hammer remains constant, the magnitude stress waves encountering the ground surface are greater for the less embedded piles.
- In the last case, the effect of hammer energy is studied for three cases. In these cases, peak forces of 2,000 kN (F), 6,000 kN (3F) and 10,000 kN (5F) are considered to be applied on top of the pile. The time histories of the peak particle velocities at different depths are plotted. It is concluded

that increase in hammer energy causes increase in the peak particle velocities.

Serdaroglu (2010) presented PPV values against distance from the pile being driven for at different parameters to illustrate the effect of difeerent soil properties, pile embedment length and hammer masss on the wave propagation through soil. Figures 4.30, 4.31 and 4.32 show the effect of the mentioned parameters.

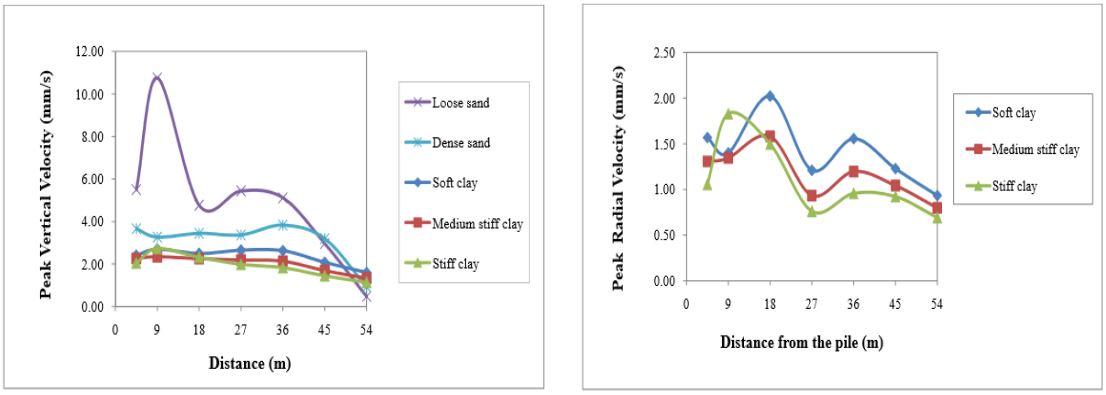

a) Sand soils b) Clay soils

Figure 3.31: Effect of different soil properties on PPV values (after Serdaroglu 2010)

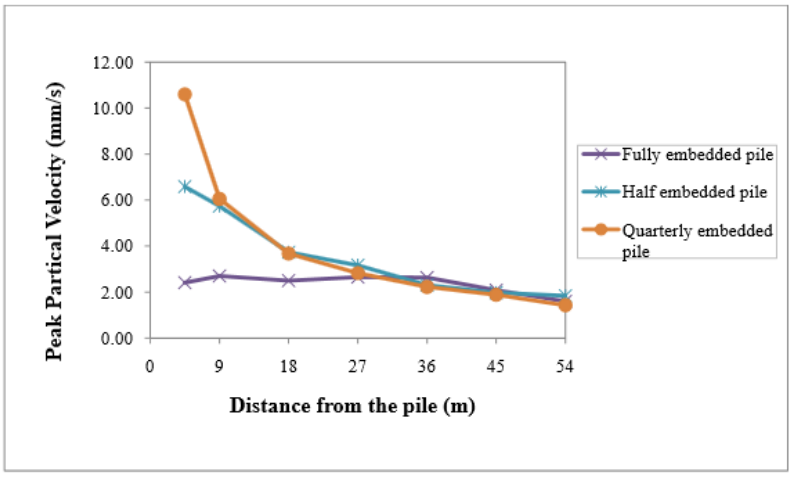

Figure 3.32: Effect of different embedment pile length on PPV values (after Serdaroglu 2010)

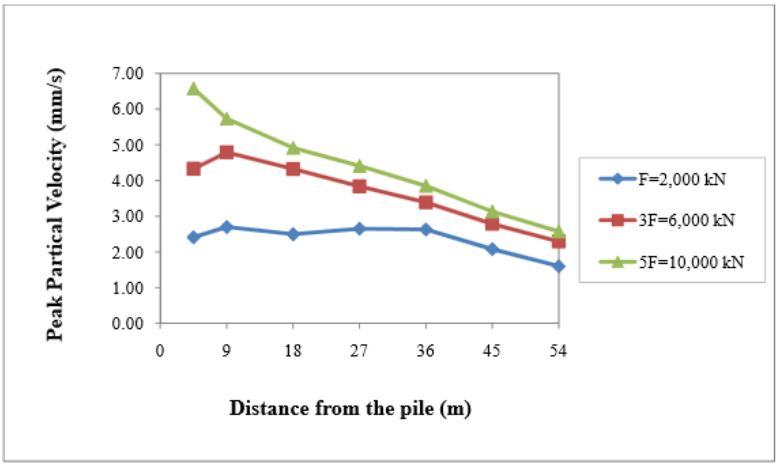

Figure 3.33: Effect of different hammer masss on PPV values (after Serdaroglu 2010)

Reuver (2016), tried to evaluate the vibratory pile installation effects on adjacent buried pipe structures through a coupled analytic approach through a finite element model using ABAQUS.

A parameter sensitivity study is applied to test all individual model components on their behavior with respect to condition changes. From the study can be concluded that the coupled modified vibration estimation method of Massarsch and Fellenius (2008) (named Wave Propagation Model in this research) to the proposed pipe structure representation (named Pipe Structure Model in this research). The most important research goal achieved is the possibility to predict the oscillatory behavior of the pipe to enforced vibration waves from vibratory sheet pile installation. Although the comparison between the Wave Propagation Model and the ABAQUS model show complementary results, due to the the lack of observation regarding field measurement data the authenticity of the model is not yet confirmed.

The axi-symmetric ABAQUS model, applied for his Master Thesis research project, represents a 2D axisymmetric situation of a round pile installed in the subsurface. Round piles have complementary stiffness behavior with respect to the axi-symmetric axis. PPV values adapted from Abacus according to Reuver

(2016) vs WPM values for different types of soil are plotted against pile depth as shown in Figure 3.33.

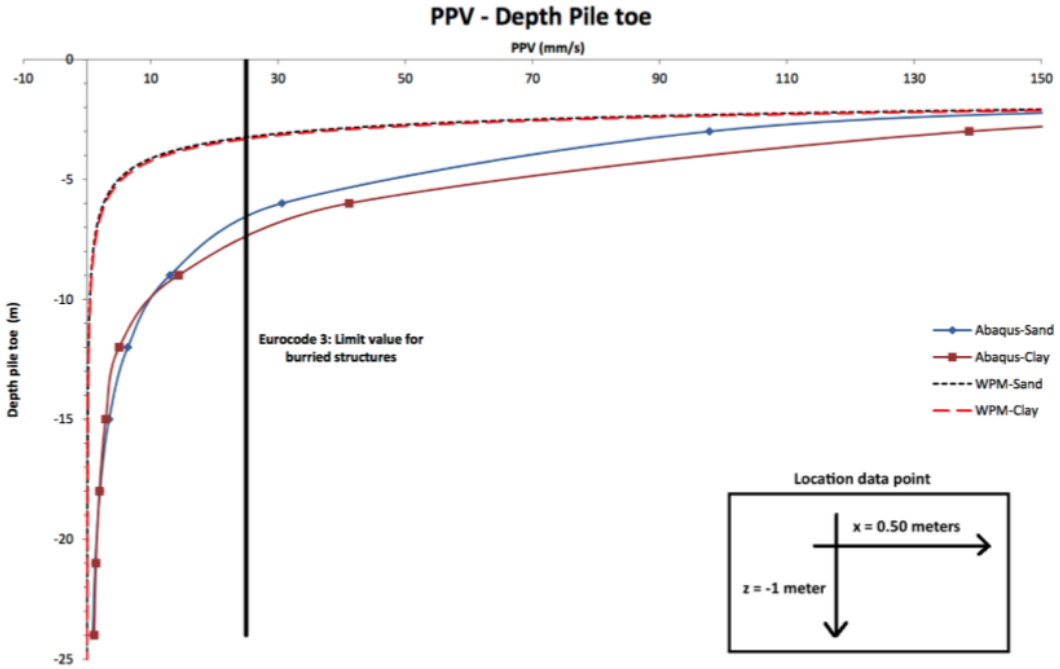

Figure 3.34: ABAQUS and WPM calculation, Peak Particle Velocity (PPV) as a result of different pile toe depths. Data positioning point is 0.50 meter from center pile at1meter below surface level

Lo, et al. (2012) presented a calculation methodology called SBFEM, it stands for Scaled Boundary Finite Element Method, to simulate the vibratory driving of a pile. In this simulation the near-field (pile-soil) is modeled by FEM and the far-field (unbounded soil) by SBFEM. The soil is assumed to be linear elastic. The pile depth is predefined and the model is simulated in a time-domain analysis. From their result they conclude that vibration amplitude do not get affected in a significance way by the different subsoil properties even if the penetration depth is varied. Another conclusion from Lo, et al. (2012) is that the soil stiffness affect the surface vibration, when penetrating a softer layer between two stiffer layers an amplification of the wave amplitude have been noticed.

Ekanayake, et al. (2013) presented an axisymmetric FEM-model to investigate the effect of vibratory and resonant vibratory pile driving in cohesive soil. They used an elastic-perfectly plastic soil model with an adaptive mesh to simulate the pile driving to a depth of ~4 m. In this study the software Abaqus is used with a time-domain approach. The pile was assumed to be a rigid body as it penetrated the soil.

Jastrzebska, et al. (2014) produced a constitutive model developed by the authors, called RU+MCC, based on the Modified Cam Clay model is used. In the analysis a time domain approach with a New mark scheme are used as well as a plain-strain and axisymmetric model of vibratory driven pile. They conclude that the ground surface acceleration has a decreasing tendency with increasing toe depth.

Lupiezowiec, et al. (2014) made a linear elastic axisymmetric model, with time-domain approach, of an impact driven pile. The damping effect was modelled according to Rayleigh and the numerical calculations were carried out with a New mark scheme. They conclude that a more complex model for damping must be adopted to get a more accurate result, but they highlighted the fact that input parameters of the soil is of high importance for the result in the range of small strains.

Olsson (2014) made two 3D FEM-models in Comsol Multiphysics to find an optimal piling depth regarding the spreading of ground vibrations via the piles from a piled structure, one is a site specific model of Gamla Ullevi, Gothenburg, Sweden and the other an idealized isotropic model. Both of the models are linear elastic and both use a frequency and a time domain approach. In both models material damping is applied and both models are computed for one depth at the time. Olsson (2014) concluded that piles shorter than 20 m seems to excite Rayleigh waves and piles longer than 20 m do not excite Rayleigh waves over a frequency of 4 Hz.

Susila, et al. (2014) performed a 2D axisymmetric study in the FEM-software Plaxis Dynamic. The vibration occurs from an impact driven pile. Susila, et al.

(2014) concludes from their parametric study that PPV value is proportional to the soil stiffness and inversely proportional to the pile driving depth.

Larsson (2016) set a FEM – model using COSMOL for simulating sheet piles installation using vibratory. The model was verified after field measurement for Guillent (2013) and Deckner, et al. (2015b). From his study he concluded the following, the sheet pile bends and deflects during vibratory driving, the shear modulus of the surrounding soil affects mostly the vertical acceleration of the sheet pile, the driving force affected acceleration and deflection of the sheet pile. The increasing of driving force increases the acceleration. The penetration depth has an influence on the behavior of the sheet pile. The accelerations of the sheet pile decrease with deeper penetration depth.

3.8 Engineering Models for Prediction of PPV due to pile driving

Deckner 2013 illustrated some of engineering models for estimating vibration values as follow:

Massarsch & Fellenius (2008) (engineering model) introduced a model for estimating vibrations from impact pile driving. The method includes the force applied to the pile head, the dynamic stresses in the pile and the dynamic resistance along the pile toe and pile shaft. This approach is promising and allows for proper estimation of energy transmission from the hammer to the soil, and thus allows for more accurate estimation of vibrations induced and their attenuation characteristics.

Massarsch & Fellenius (2008) suggested that the calculation of ground vibrations induced by pile driving with impact hammers be based on the following approach:

- Determine the dynamic pile hammer properties
- Determine the dynamic pile properties
- Estimate the peak particle velocity of the stress wave

- Assess the vibration transmission efficacy along the pile shaft and at the pile toe
- Calculate the propagation of spherical wave energy from the pile toe to the ground surface, taking into account wave reflection
- At the critical distance from the pile on the ground surface, calculate the vibration attenuation of surface waves
- Calculate the cylindrical waves from the pile shaft

Svinkin (1996) presented a prediction model based on the concept of the impulse response function. The impulse response function models behaviour of the soil. As, Svinkin (1996) puts it "the impulse response function is an output signal of the system based on a single instantaneous impulse input". In this prediction model, the output is a location of interest, the dynamic system is the soil and the input is the ground at the place for pile driving.

By setting up an experiment of applying known magnitudes of impact on the site of interest, for example by dropping a mass and recording the oscillation at impact, the impulse response function is determined. Once the impulse response function is known the dynamic loads for pile driving are computed by wave equation analysis. Finally Duhamel's integral (Smith & Downy, 1968) is used to find the predicted vibrations. The prediction model is based on the assumption that the soil behaves as a linear material, Deckner (2013).

Table 3.8 summarizes the prediction models of estimating vibrations due to pile driving.

Only the common models for PPV prediction which is used by design engineers are highlighted in this Table 3.8.

Particle velocity should be observed in three mutually perpendicular directions. While damage criteria developed by USBM (US Bureau of Mines) and other organizations have been based on the maximum single value of the three directional components, since real waves are three dimensional and the transducer axes may not be exactly in line with the source of vibrations.

Table 3.8: Prediction of PPV for pile driving

Prediction method /model	Reference
K value varies for material type of driven pile. The variation explained reduction of K value as the energy distribution capacity which is measured from impedance value rise.	Heckman & Hagerty method (1978)
V is Vertical PPV, Where K is a constant varies from 0.25 to 1.50	Attewell & Farmer (1973)
Where v = vibration velocity (mm/s), x1, x2 and x3 = constants of proportionality, W_0 = input energy (J), r = distance between source and point of interest (m). Constants x1, x2 and x3 are functions of the soil conditions at the site of pile driving Proposed values of the constants of proportionality are given according to Deckner(2013) see Tables 2.3 and 2.4.	Attewell et al. model (1992a and 1992b)
V_g = ground vibration (mm/s) (PPV) V_p = pile vibration at the pile head c_B = wave propagation velocity in the pile (m/s), Z_p = pile impedance (kNs/m), L_p = pile length (m), W_0 = energy transferred to the pile (J), r = distance from the pile to the point of interest	Svinkin (2008)
The research yielded attenuation curve which accommodates energy, distance, and damping (geometric and material damping).	J.M. Ko,et. al. method (1990)

NUMERICAL MODELING

3.9 Analysis

This chapter presents the analysis of the results of the effect of construction vibration such as pile driving or pile vibratory on soil and the adjacent structures. A series of models were run for different soil types to show the effect and the hazard of construction vibration on soil and the nearby structures.

3.9.1 Finite Element Models

Finite element analyses of pile driving are carried out using Plaxis 8.2 2D dynamic version. A set of general fixities of the boundary conditions of the problem are considered automatically by the Plaxis program. The Rayleigh damping is considered at vertical boundaries with α, $\beta = 0.01$, the plastic properties of soil are defined by using material damping, which is defined in Plaxis by Rayleigh (α and β), where The Rayleigh damping is considered to be object-dependent in material data set to consider the plastic properties of soil during the dynamic analysis in Plaxis. Plaxis model for pile driving is shown in Figure 3.35. The mesh was generated and refined twice around the pile to improve the accuracy of the results as shown in Figure 3.36. For impact hummers, the analysis was based on three phase's plastic (staged construction) and two phases for dynamic analysis (total multipliers). The dimensions of the soil model for pile driving are taken around 50 m in depth and 150 m in width after some mesh experiments.

The Finite Element Analysis (FEA) is a numerical method for solving problems of Geotechnical engineering. Useful for problems with complicated geometries, loadings and material properties where analytical solutions cannot be obtained and not accurate. The details of FEA are briefed in Appendix-A.

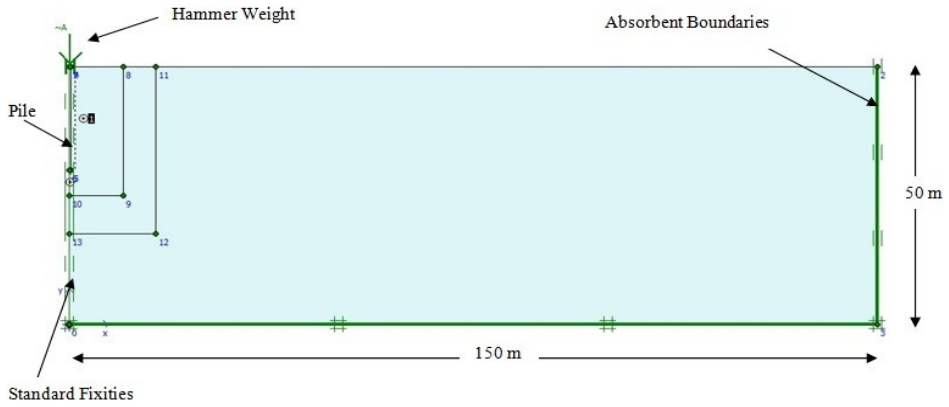

Figure 3.35: Plaxis model for pile driving simulation

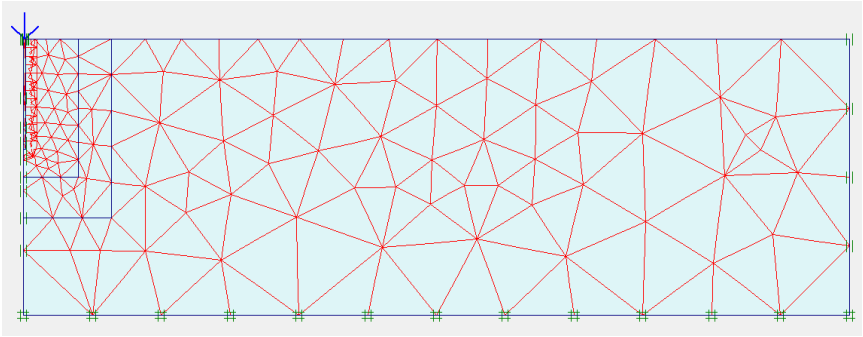

Figure 3.36: Mesh generation for Plaxis model

Different parameters used in the Plaxis model are illustrated as shown in Table 3.9. "Mohr Columb" undrained model is used for modeling clay, while "hardening soil" for modeling sand because of the fast loading process, (adapted from Plaxis dynamic manual) and it gives reasonable values also agreed with the verification model. The pile in Plaxis is modeled as a linear elastic non porous. The pile has a circular cross section with a diameter of 0.4m with varied length (Lpile) of (10, 15 and 20m). To simulate the behavior of reinforced concrete in Plaxis model, the Poisson's ratio is taken "ν" of 0.1, unit mass "γc" of 25 kN/m^3 and modulus of elasticity of 22E6 kN/m^2.

Table 3.9: The different parameters used in the models in this chapter

Parameter	symbol	Clay1	Clay2	Clay3	Sand1	Sand2	Sand3	Pile	Units
Unit mass above pheratic line	γ_{unsat}	14	16	18	17	18	20	25	kN/m^3
Unit mass below pheratic line	γ_{sat}	16	18	20	19	20	22	—	kN/m^3
Elastic modulus	E_{ref}	5000	8000	16000	25000	33000	40000	22×10^6	kN/m^2
Oedometer modulus	E_{oed}	—	—	—	25000	33000	40000	—	kN/m^2
Power	M	—	—	—	0.5	0.5	0.5	—	—
Unloading modulus	E_{ur}	—	—	—	75000	99000	120000	—	kN/m^2
Poisson's ratio	ν	0.2	0.32	0.35	0.3	0.33	0.35	0.15	—
Cohesion	C_u	25	40	80	1	1	1	—	kN/m^2
Friction angle	ϕ	1	1	1	30	35	40	—	°
Dilatancy angle	ψ	0.0	0.0	0.0	0.0	5	10	—	°
Interface strength reduction	R_{inter}	0.6	0.6	0.6	1	1	1	—	—

3.9.2 Model verification

This part describes an example that has been used to verify the dynamic response of soil using PLAXIS 2D -Dynamic Module Version 8.2. In that example the results from Plaxis 2D dynamic version is compared with the field measurement of ground vibrations caused by sheet pile driving as stated by Petřík et al, (2012).

The selected parameters of soil layers after Petřík et al (2012) are given in Table 3.10.

Table 3.10: Soil parameters after Petřík et al, 2012

Parameter	Soil / Units	1 CSI	2 SM	3 CS2	4 S-F	5 Slate
Thickness H	M	0-4.5	4.5-7	7-12.5	12.5-20	20-x
Bulk density γ	kN/m^3	18.5	18	18.5	17.5	24
Modulus of elasticity E	MN/m^2	4	15	4	25	60
Poisson number ν	-	0.35	0.3	0.35	0.3	0.25
Cohesion c	kN/m^2	14	5	14	1	100
Internal friction angle φ	^{o}	24.5	29	24.5	31.5	28

The planar version of the Plaxis V8.2 calculation developed for creation of mathematical models. Plaxis V8.2 2D has a calculation, dynamic module that makes it possible to solve dynamic problems using the FEM. The dynamic analysis results from Newton's law of motion.

The mathematical models were selected as axisymmetric ones within the range of 150 x 50 m (length x width) (see Figure 3.37), Conventional geometrical boundary conditions are set up in the models The rock environment was made up of five layers with a simple horizontal interface. Physical and mechanical properties of the soils were set up according to Table 3.10. The effect of water on the models was neglected due to simplification. The transversal and longitudinal velocities of propagation of seismic waves are automatically determined in the calculation software.

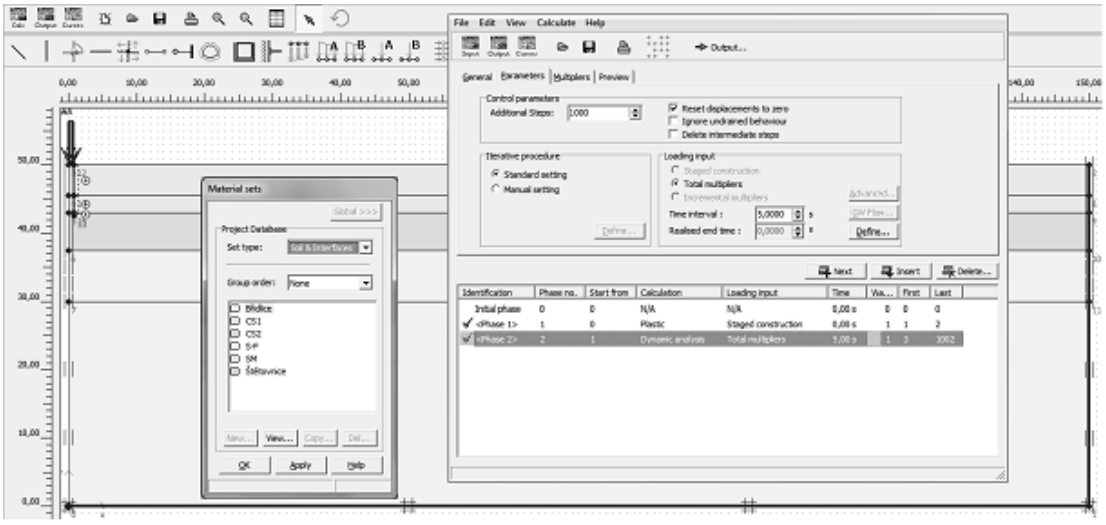

Figure 3.37: Example of numerical model in Plaxis 2D (after Petřík et al 2012).

The primary state of stress was generated by the software system automatically pursuant to the properties of soils under consideration and the depth. The steel sheet piles in the models reached the depth of approx 8 m. The dynamic force of the vibratory hammer was defined for the manufacturer's data (see Table 3. 11), from the centrifugal force of 1015 kN at various frequencies of the vibrating action (up to 38 Hz). The calculation and the model-based analysis

were carried out in two stages. The simulated model from Plaxis is shown in Figure 3.38

Table 3.11: Parameters of ICE type 18 RF-ts vibratory hammer (www.ice-holland.com).

18 RF-ts specifications		
Eccentric moment	`0-18	Kgm
Max. centrifugal force	1015	kN
Max. centrifugal force	2300	Rpm
Max. amplitude including clamp	11.6	Mm
Total mass including clamp	4120	Kg

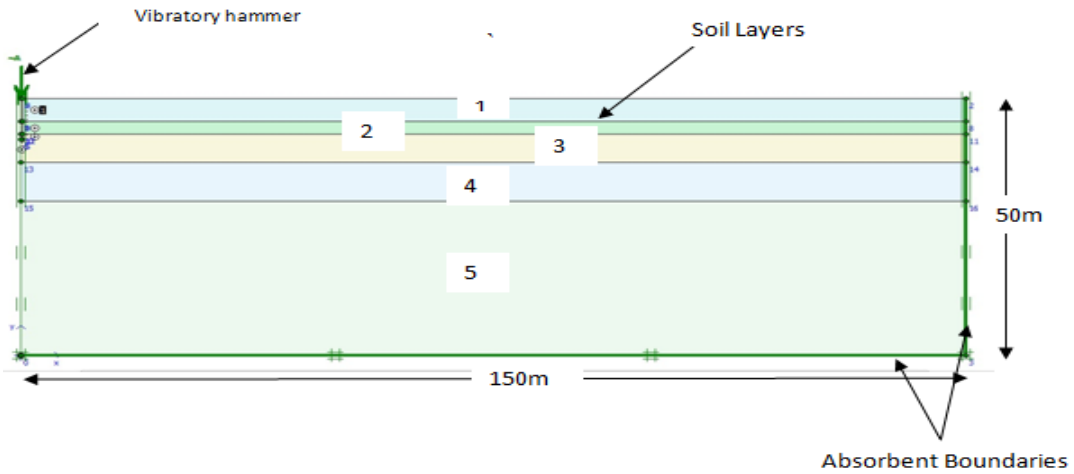

Figure 3.38: The verification model from Plaxis

The numerical model and measurements in the site after Petřík et al (2012) are shown in (Figure 3.39). It is a comparison of the model-based damping curves with the data measured in the field at different frequencies. The oscillation velocity was measured at different distances from the vibratory hammer.

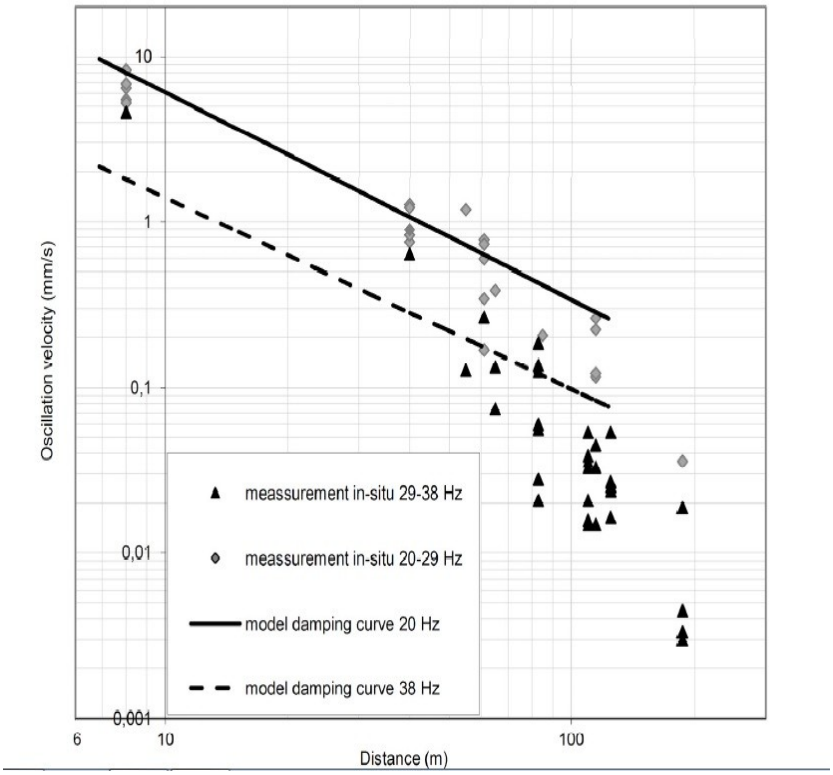

Figure 3.39: Comparison of the numerical model-based on damping curves with the data measured in the field (after Petřík et al 2012)

The results of the numerical model from Plaxis for f=38 Hz follow the trend of Petřík et al (2012) results and a good agreement is achieved as it shown in (Figure 3.40). A comparison between field measurements, numerical results from Petřík et al (2012) and Plaxis model is carried out and proved the validity of using Plaxis 2D dynamic V.8.2. The results of the numerical model from Plaxis follow the trend of Petřík et al (2012) results and a good agreement is achieved as shown in Figure 3.40.

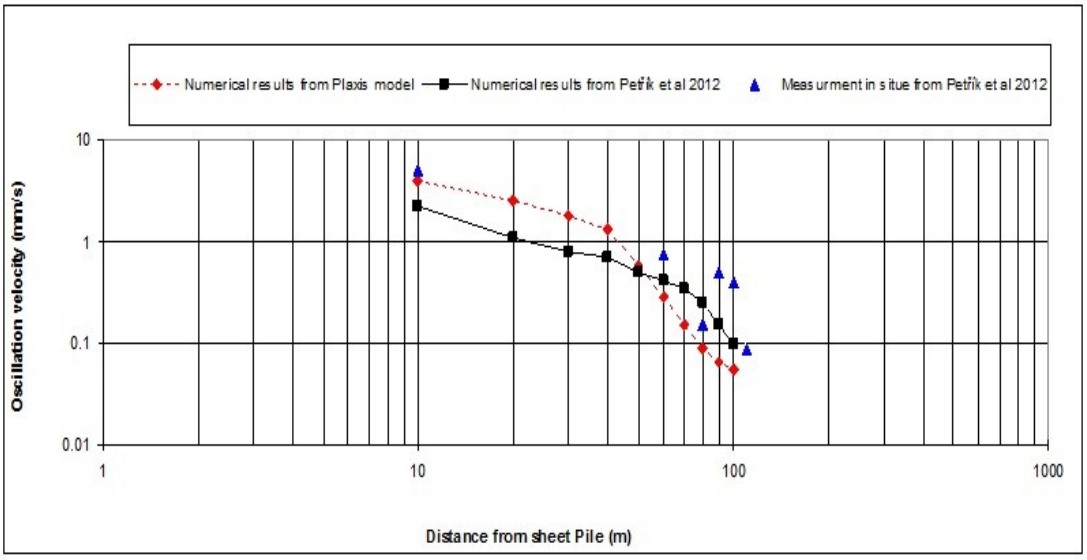

Figure 3.40: The Comparison of the numerical results from plaxis model, the numerical results and the measurement in situe from Petřík et al (2012).

3.10 The effect of pile driving on the soil:

3.10.1 Effect of different soil stiffness on the peak particle velocity (PPV):

The propagation velocity is the speed with which the wave passes the cork, while the particle velocity is the speed with which the cork moves up and down.

Only vertical component shows higher values of velocity, therefore, focus will be on the vertical component of PPV, since previous researchers have shown that the horizontal components in the radial and tangential directions are usually small, i.e. 30% and never exceeded 80% of vertical component. (Brenner and Viranuvut 1977).

Problem under investigation is simulated using Plaxis dynamic 2 D. V.8.2. The effect of soil stiffness on PPV is studied using sand and clay deposits. For the first trial pure layer of clay is studied with different stiffness of clay vary from soft clay to hard clay, the same condition also is used for sand and vary from loose to dense sand. PPV measured at the ground surface at different points from the driving source by Plaxis model. Figures 3.41 and 4.42 show the

maximum velocity of Plaxis model in clay. Figure 3.43 shows the variation of PPV with distance from driving source in clay at different stiffness. As expected, the velocity decreases with the increase of the distance from driving source because of wave attenuation depending on the soil damping coefficient. It shows that the PPV increase with the increase in the stiffness of the clay. Distance from Sources. The waves travel in all directions from the source of vibrations forming a series of fairly harmonic waves with the dominant frequency equal or close to the frequency of the source.

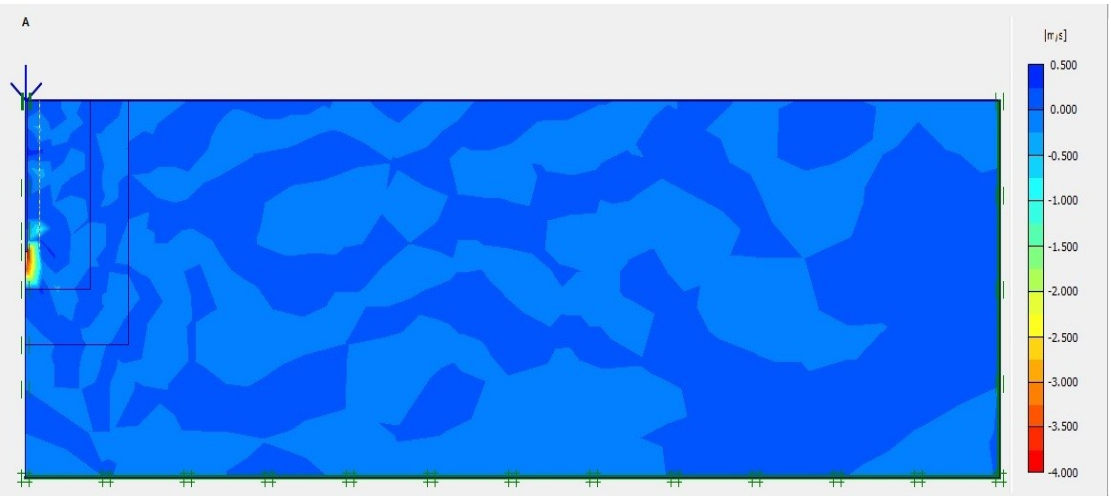

Figure 3.41: Maximum velocity in clay at E 5000 kPa adapted from Plaxis model.

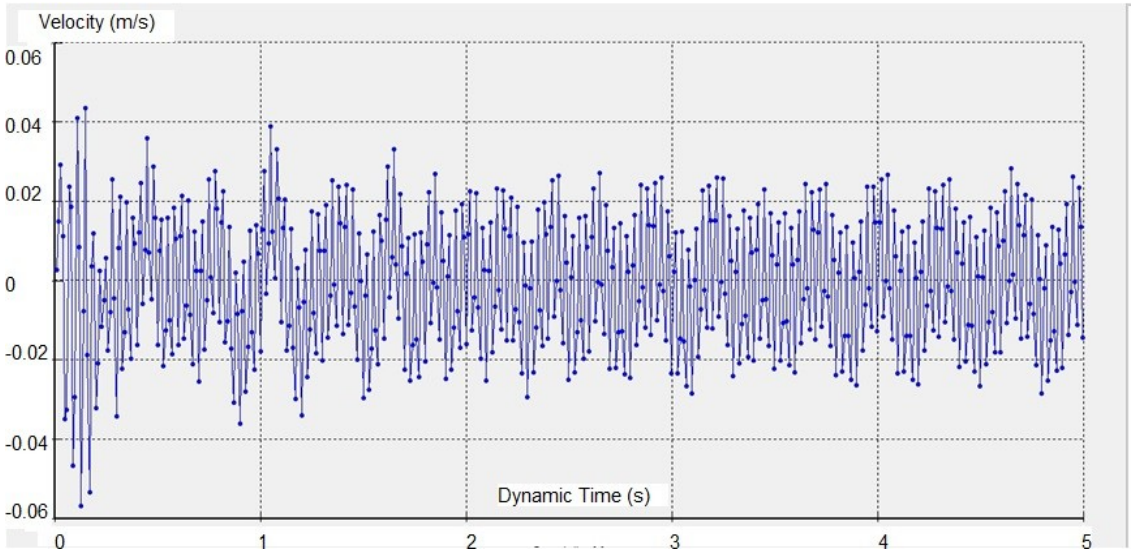

Figure 3.42: Velocity in clay with dynamic time at E 5000 at 6m from the driving source.

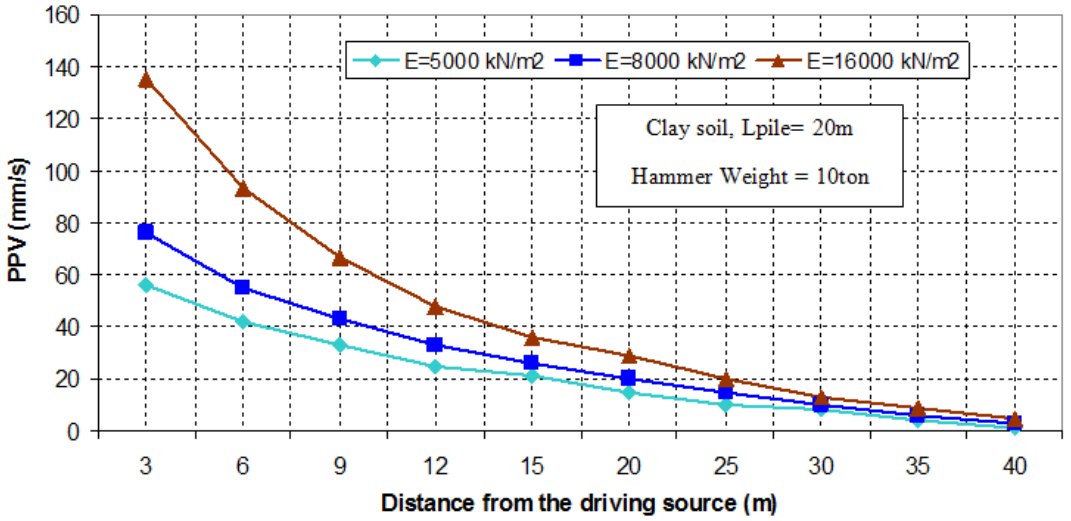

Figure 3.43: PPV in clay at different soil stiffness with distance from the driving source.

The decrease in PPV with distance from the pile driving source is confirmed by the analysis. The PPV of the born vibrations increases with the increase of the stiffness of the surrounding soils. By calculating the PPV at different points from the driving source the dangerous effect can be illustrated and become easier to avoid that influence. The methodology presented in this thesis can be used to evaluate the limiting vibration induced PPV in the Egyptian Code of Practice and/or in the international standards as mentioned in chapter 2.

For sandy soil, the effect of different stiffness's on the PPV is studied. The maximum velocity from Plaxis 8.2 is illustrated in Figure 3.44 to represent the propagation of waves through the surrounding soil. At the ground surface and at 3m from pile driving, PPV is measured with dynamic time as output from Plaxis model as shown in Figure 3.45. Figure 3.46 shows the variation of PPV with distance from driving source in sand at different stiffness.

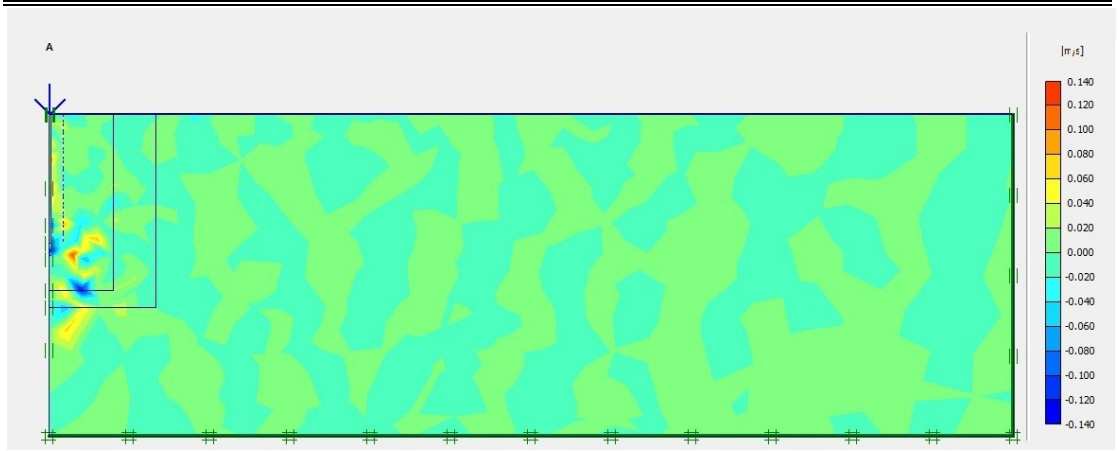

Figure 3.44: Maximum velocity in sand at E 33000 kPa from Plaxis model.

The elastic waves keep attenuate through the soil. Wave attenuations are caused by two different effects (after Massarsch 1993), Enlargement of the wave front as the distance from the source increased (geometric damping) and internal damping of the wave energy by the soil.

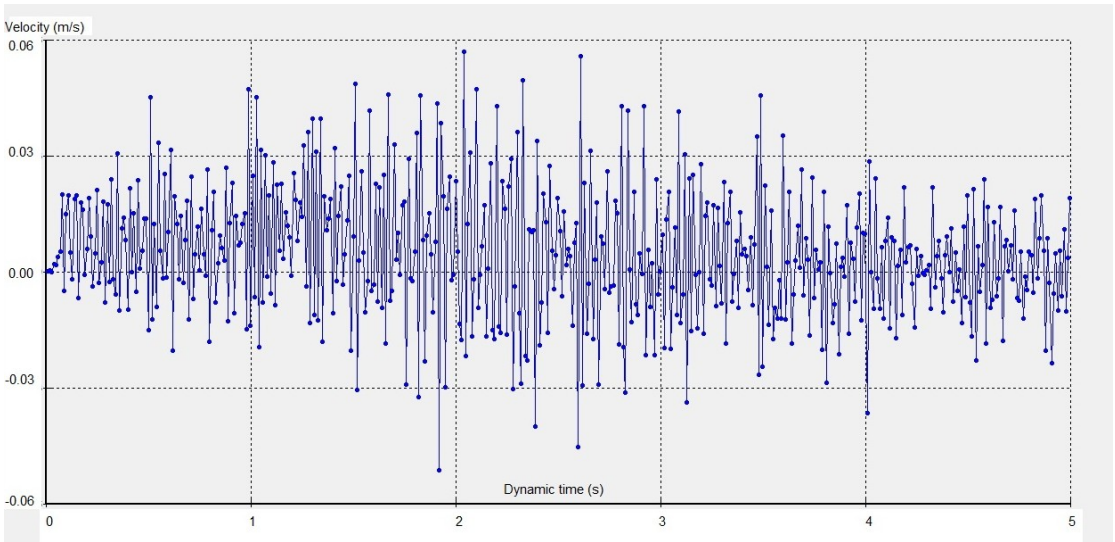

Figure 3.45: Velocity in sand at E 33000 kPa with dynamic time at 3m from pile driving.

It is noticed that PPV decreased with the increase of distance from the driving source. PPV values in the sand are larger than PPV values in clay due to the difference between soil stiffness from clay to sand.

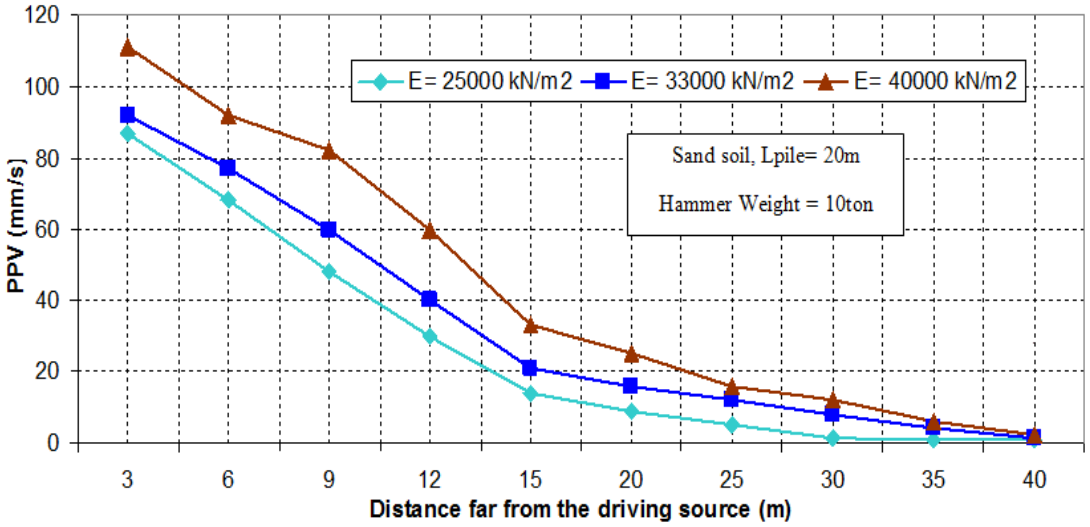

Figure 3.46: PPV in sand at different soil stiffness with the distance from the driving source.

It can be defined that in clay soil the relation between PPV values and distance from the driving source is a linear relation at distance equals to 0.45 L (where L is pile length) from the driving source. On the other hand the same trend is in sandy soil but the relation between PPV and the distance from the driving source is linear at distance equals to 0.75 L (where L is pile length)from the driving source. The values of geometric and material damping are higher in soft soils than those in denser, firmer soils. Moreover, the PPV of ground vibrations tends to increase as soil materials become denser with the number of blows. Propagation velocity is an important factor because it is an indirect measure of rock/soil properties that affect the decay of PPVs as well as wavelengths. Generally, propagation velocity increases with increasing soil stiffness. A wave propagates more quickly through a hard, dense material than through a soft, pliable material. Jointing and weathering of rock masses greatly affect propagation velocities through changing rock stiffness. Hope and Hiller

(2000) also noted (in line with the observations of many others) that vibrations tended to increase as the stiffness of the soil increased.

3.10.2 Effect of different hammers mass of pile driving on the peak particle velocity

Different hammer masses are investigated in 10, 15, and 20 ton respectively, for pile driving and its effect on PPV is studied. Extreme PPV is measured at the ground surface for clay soil as shown in Figures 3.47 and 3.48. At the pile toe is where the maximum PPV. The effect of driving hammer mass on PPV on both clay and sand is also investigated as shown in Figures 3.49 and 3.50 In general, the increase in hammer mass increases PPV in both clay and sand. The observed trend could be explained by the fact that the increase in hammer mass increases the input energy to the pile ground system thus higher born vibration levels as reflected in PPV. The difference in stiffness between clay and sand influences the magnitudes of PPV. Such difference could be partly explained by the level of damping in clay as compared to sand. Therefore, the PPV values in the sand are higher than those developed in the clay. It is further noticed that the increase in PPV with the increase in hammer mass is more pronounced in sand as compared in clay.

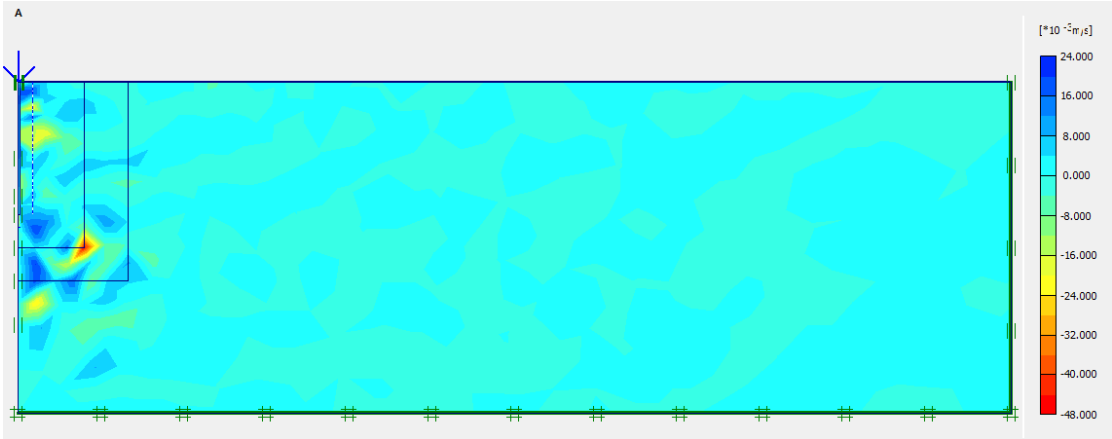

Figure 3.47: Extreme velocity in clay at hammer mass 15 ton output from Plaxis model.

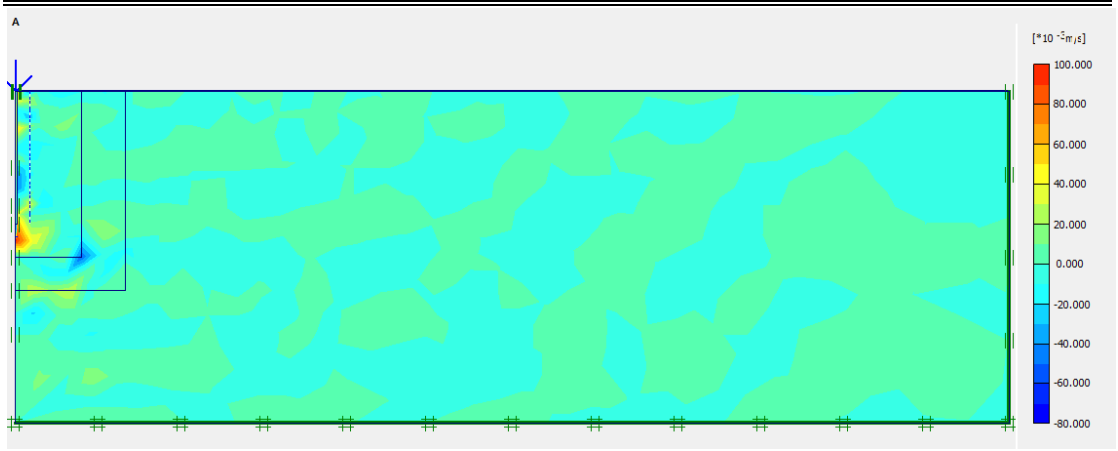

Figure 3.48: Extreme velocity in clay at hammer mass 20 ton output from Plaxis model.

Driving hammer mass increases the levels of PPV in the surrounding soil due to the increase in the energy level of the vibration source as shown in Figures 3.49 and 3.450. Selecting the proper equipment for pile installation can make and break a project technical and economic success. Underpowered equipment may cause excessive numbers of hammer blows and pile fatigue and installation may not be even possible. Selecting very powerful equipment also may cause damage and/or require unnecessary capital expense. It is very important to choose the suitable equipment of pile installation. Massarsch and Fellenius (2014) noted that the driving process creates vibrations, which radiate from the shaft and/or the toe of the pile into the soil. The larger the intensity of the stress wave, the larger the dynamic force and the intensity of ground vibrations.

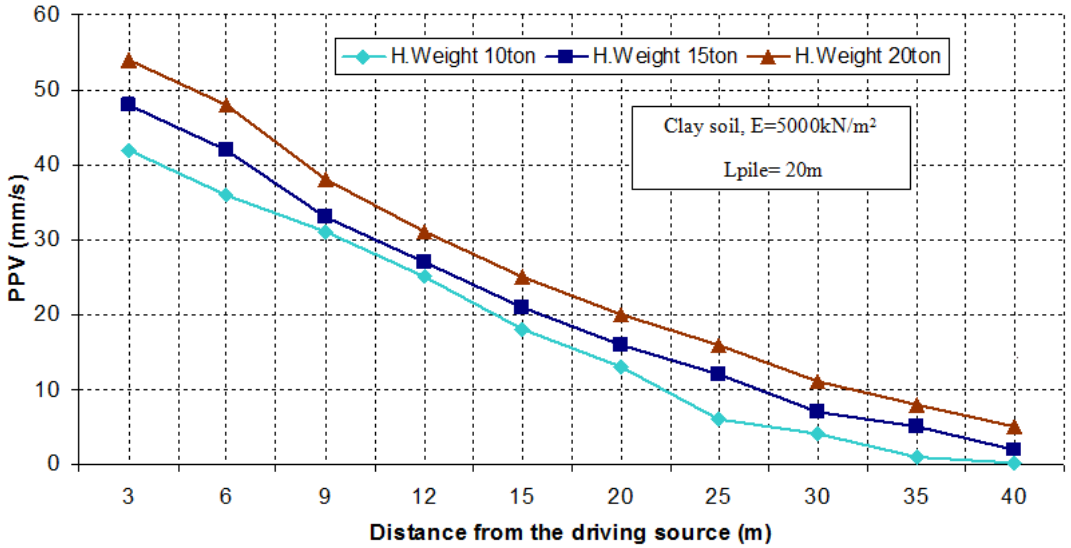

Figure 3.49: Velocity in clay at different masses of hammers with the distance from the driving source.

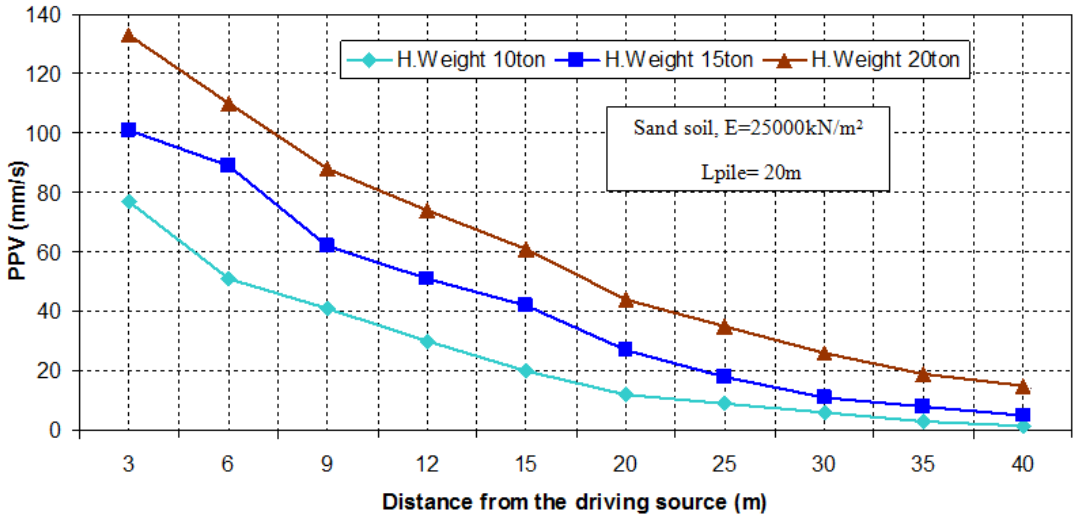

Figure 3.50: Velocity in sand at different masses of hammers with distance from the driving source.

3.10.3 Effect of ram drop height on PPV due to pile driving:

The effectiveness of pile driving depends basically on the proper choice of hammer size as shown in the previous paragraph 3.10.1. For constant ram mass, the dynamic behavior of the hammer, pile and soil relate to the ram drop height and ram impact velocity. The soil, in turn, has intrinsic properties and a dynamic behavior that is influenced by the nature of loading. The dynamic soil

behavior affects hammer performances while pile size and stiffness affect soil behavior Hussein (1992).

Therefore the effect of ram drop height on PPV is investigated to illustrate the importance of the difference of the drop height in both clay and sand deposits. It is noticed that by increasing the height of ram drop, the magnitude energy of the impact increased and normally increases the PPV. Figure 3.51 shows the variation of PPV values at different drop heights of the ram with distance from the driving source in the sand.

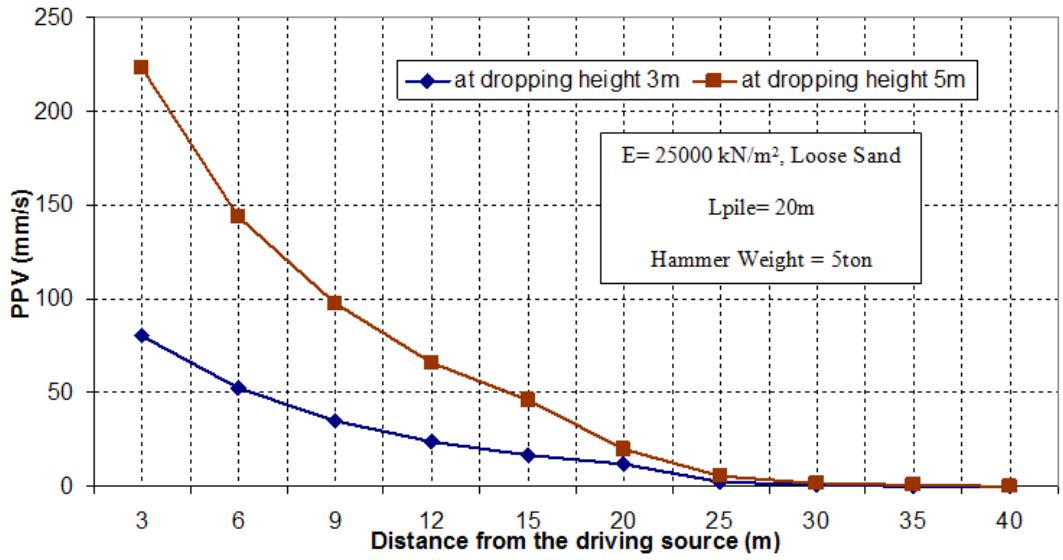

Figure 3.51: Velocity in sand at different dropping heights with distance from the driving source.

Figure 3.52 shows the effect of the ram drop height on PPV in clay soil. The same trend in the sand is the same in the case of clay soil, the difference only in the values of PPV due to the difference of soil stiffness. It is concluded that the dropping height of the mass is the very effective parameter controlling the magnitude of PPV, which could be a sign of possible damage and how can be avoided by reducing or choosing the suitable dropping height, for achieving the purpose of driving with minimum damage.

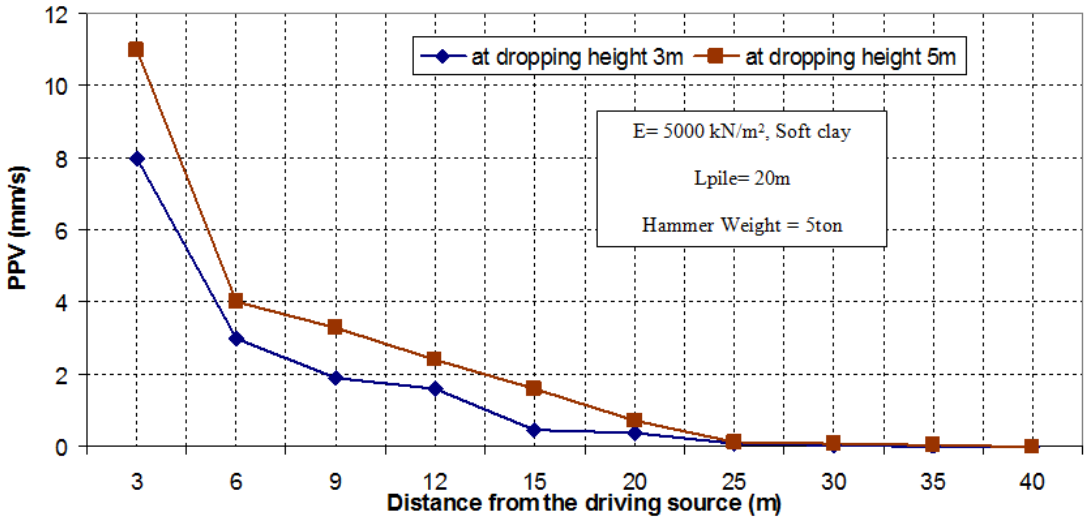

Figure 3.52: Velocity in clay at different dropping heights with distance from the driving source.

`3.10.4 Effect of different embedment lengths of pile on PPV:

Figure 3.53 shows the difference between the values of PPV measured at the ground surface for different embedded pile lengths. Because of the vibrations, waves that are generated at the pile toe and a partial amount of energy get lost along the pile shaft due to friction, the PPV decreased at the ground surface. It is also found that the maximum values of the PPV are observed at a pile length of 10m and kept reducing at pile lengths of 15 and 20 m respectively for the same distance from the pile driving. By getting far from the driving source, normally all the values decreased due to damping coefficient of soil and the attenuation of the waves through the soil.

Figure 3.54 shows the variation of PPV values at different pile lengths in clay soil with the distance from the driving source. It is illustrated that by increasing the pile embedment length the PPV decreased. As shown previously the source of vibration is the pile toe that is why by increasing the pile toe, the PPV decreased at the ground surface. The same trend in sand also happens in clay, but with lower values of PPV in clay deposits.

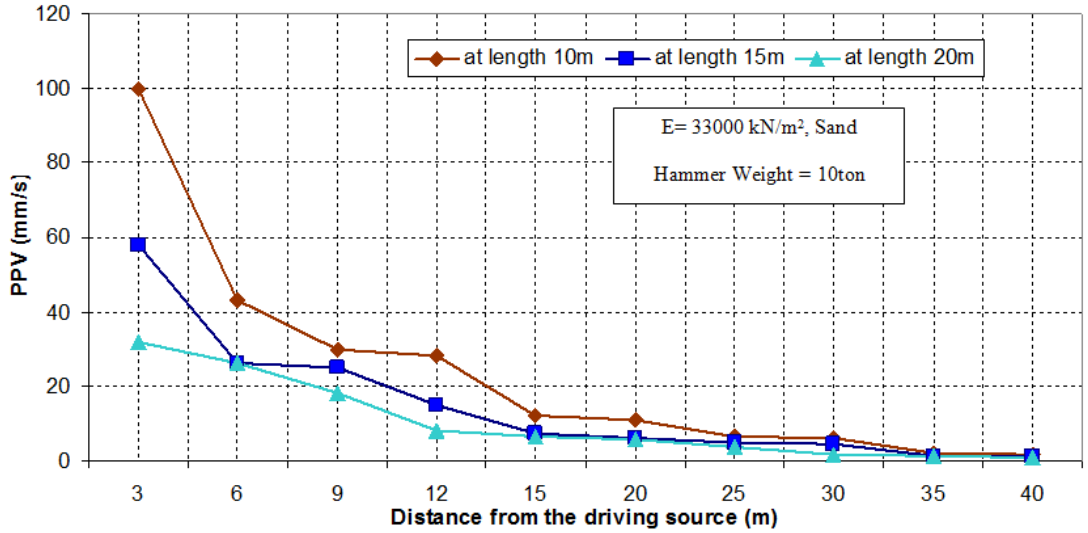

Figure 3.53: PPV in sand measured at ground surface for different pile embedment lengths with distance from the driving source.

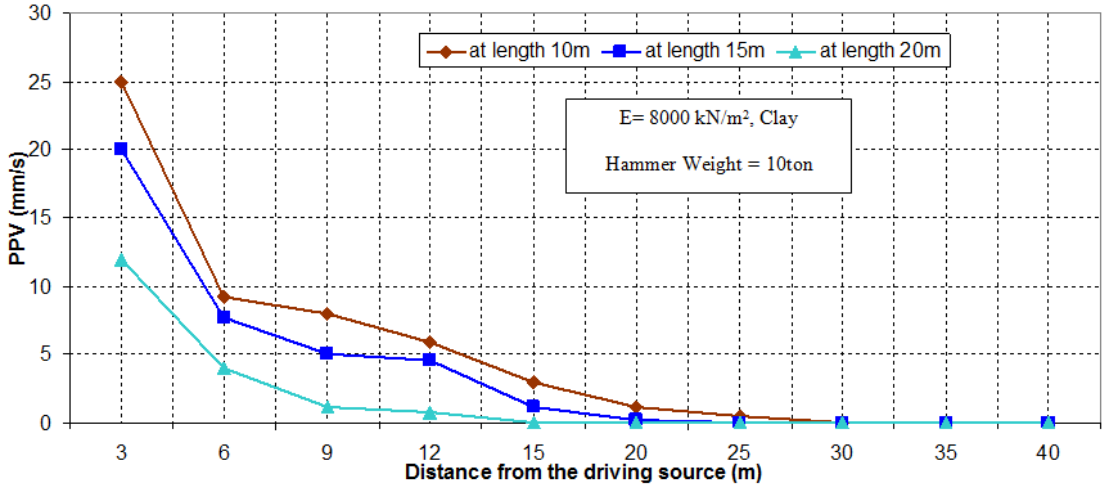

Figure 3.54: PPV in clay measured at ground surface for different pile embedment lengths with distance from the driving source.

The energy coupled to the ground at the tip of the pile during driving is a function of the ratio of impedances of the pile and ground at the level of the tip. GRL WEAP and PDA analysis demonstrate that about 50% of the rated hammer energy reaches the top of the pile. This energy is called ENTHRU. Although energy is lost to shaft friction as the pile is driven, these losses have

been neglected. It is conservatively assumed that all ENTHRU energy reaches the tip of the pile to maximize the predicted shear strain.

Particle velocity in the soil at the tip depends on the relative impendances of the pile and soil at the tip and the energy reaching the pile tip (Massarsch and Fellenius, 2008)

`3.10.5 Effect of different pile's material on PPV:

Many types of driving piles are widely used around the world according to its material type. Wooden, precast reinforced concrete and steel piles are the most main types of driving piles around the world. In Egypt the most common type is the precast piles due to its low cost comparing with steel piles and also for its durability and long term serviceability.

A comparison between the three types of piles is made to illustrate the effect of the pile material on PPV to choose the appropriate type of the driven pile in the site, However it is not available option to choose the pile type to reduce the PPV because every construction site has its design and the type of pile material is chosen already. Knowing the effect of pile material on PPV still important parameter in evaluating construction vibration damage limits.

For the comparison, a pitch pine wooden pile is used with E, 9×10^6 kN/m^2 and intensity 0.0067 kN/m^3. A 252 pilling steel pipe grade 3 is used with E, 310×10^6 kN/m^2. The concrete pile is typically the same as used in the previous calculation.

It is noticed that the wooden pile produce higher values of PPV due to its low stiffness and the values of energy loss in friction is low as well. For steel and reinforced concrete, the both have a close trend in PPV values. Figure 3.55 show the variation of PPV values due to different of piles material with the distance from the driving source. The pile impedance affect clearly on PPV as it illustrated by Heckman and Hagerty (1978). By increasing the pile impedance the PPV decreased, The reduction of pile impedance by say 30%

can increase the ground vibration amplitude by a factor of 10 after Massarsch (1993), Heckman and Hagerty (1978). Another important parameter which cannot be neglected is the effect of damping.

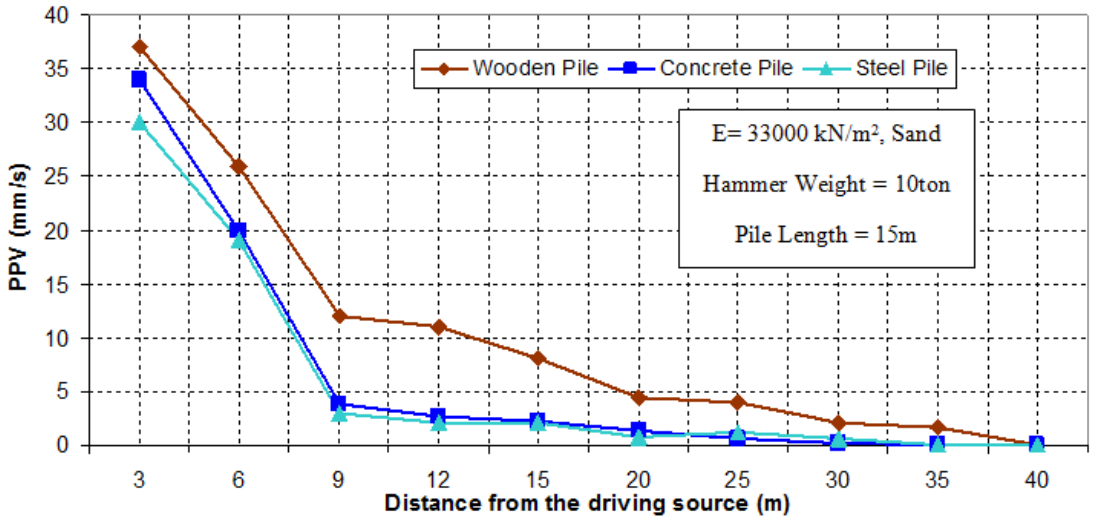

Figure 3.55: PPV in sand measured at ground surface for pile materials with the distance from the driving source.

`3.10.6 Effect of the mass of an adjacent structure on PPV:

This study generally aims to investigate the effect of construction vibration on soil and adjacent structures; however, there are another parameters can control the PPV values. It is found that by increasing soil stiffness, the PPV increases. Therefore existing of adjacent structure near to the driving source can help in increasing soil densification which can increase the PPV values. An equivalent load of the structure is used to simulate the structure mass in Plaxis model as shown in Figure 3.56. These calculations are based on three phases, and the first phase is for plastic analysis (staged construction), second face for the surcharge mass is consolidation phase and the third phase is for dynamic analysis (total multipliers).

As expected the PPV increased due to the structure mass and reached its maximum values exactly in the middle of the structure as shown in Figure 3.57.

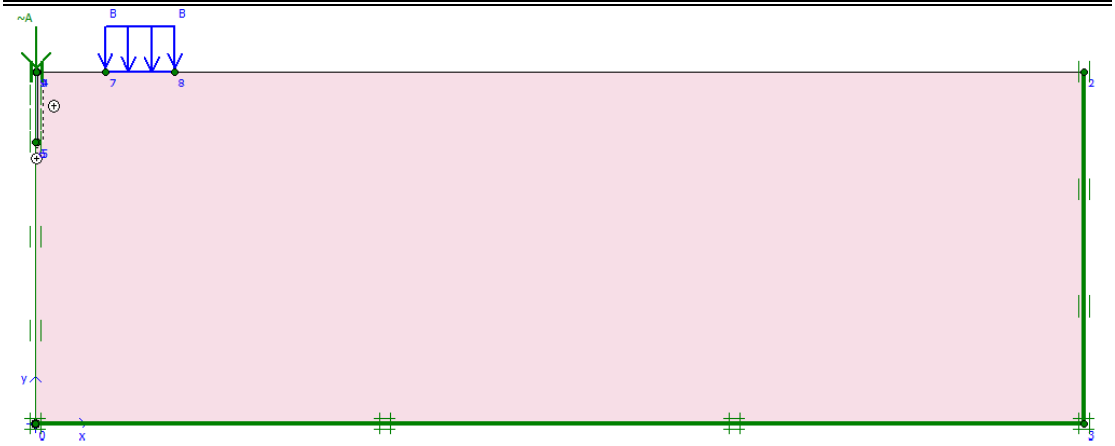

Figure 3.56: Plaxis model simulating the equivalent mass of an adjacent structure at 10m distance from the driving source.

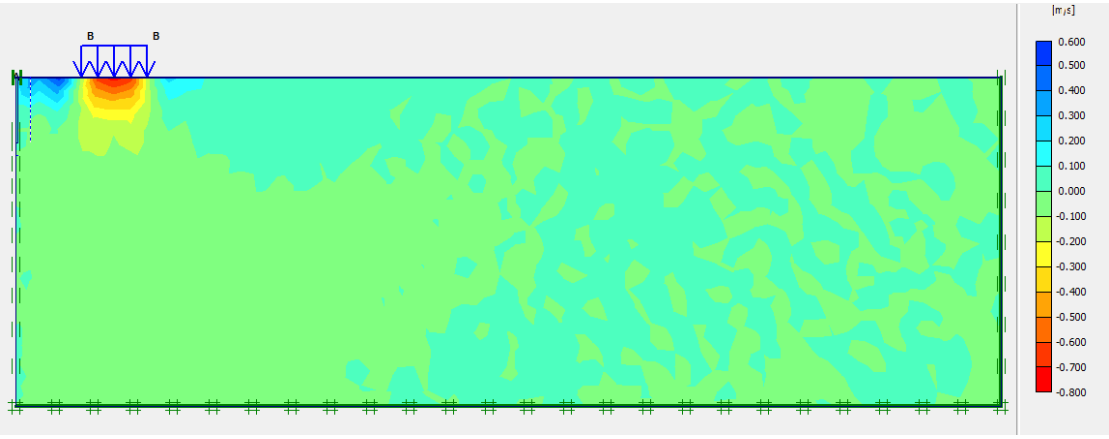

Figure 3.57: Extreme velocity in sand soil at E, 33000 kN/m^2 and equivalent load 200 kN/m^2 (ten floors building), from Plaxis model.

A comparison between two buildings, the first one consists of ten floors but the other one consists of five floors, both are made to simulate the effect of surcharge mass on PPV values. It is noticed that by increasing the mass of structures (equivalent load) the PPV increased and the maximum of the PPV at the middle of the structure length. By comparing the values of the PPV in case of the surcharge load and without the surcharge load, it found that there are a huge difference between the values reaches up to 60 % increasing of PPV by increasing the mass by 50 %. Figure 3.58 shows a comparison between three values of PPV at different cases of surcharge loads, the first case with an

equivalent load 200 kN/m^2 (ten floors building), the second case with an equivalent load 100 kN/m^2 (five floors building) and the third case is without any adjacent loads. It clearly can be seen that the wide difference between the values according to the loads. It can be concluded that driving piles or any other source of vibration near to an existing structure that leads to increase the PPV which leads to more damage and hazard on adjacent soil and structures.

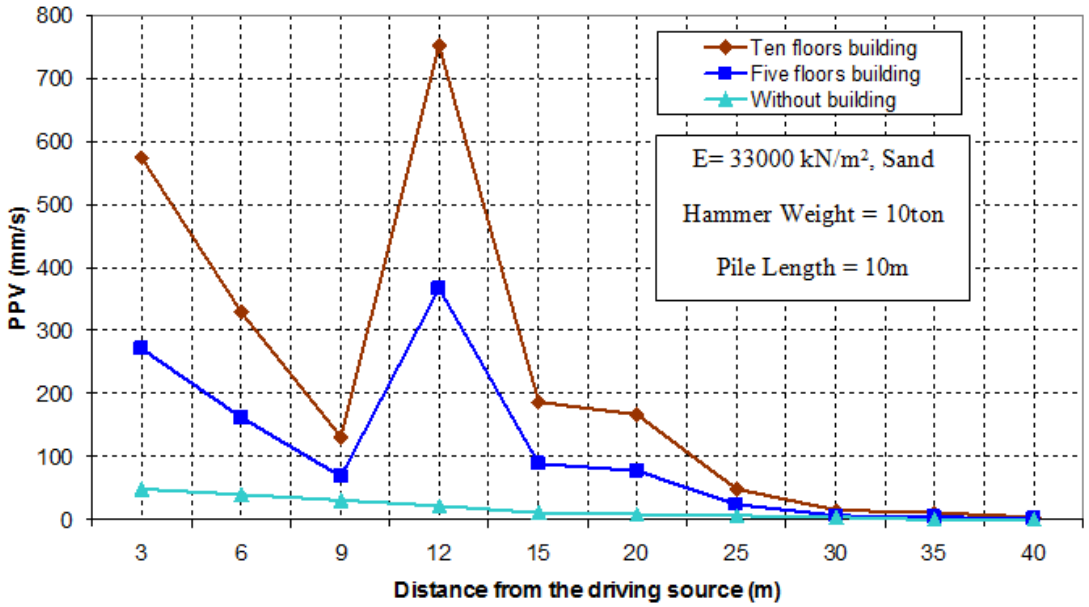

Figure 3.58: PPV in sand measured at ground surface for different masss and heights of buildings with the distance from the driving source.

3.10.7 Comparison between Finite Element results and other prediction models for Pile Driving PPV values:

Figure 3.59 shows the variation between the values of PPV from Plaxis at different soil stiffness, Svinkin (2008) and Atewell &Farmer (1973) models. It is noticed that a difference between the values of the three models especially in the zone close to the driving source, that difference between PPV values is backed to the different parameters in the formulas of the prediction models as shown in Table 3.12 . For Svinkin (2008) model, Vp (pile vibration at the head of the pile) is included in the model for estimating PPV which depends on CB (wave propagation velocity in the pile). On the other hand, Attewell & Farmer

(1973) model depends only on impact energy and the distance from the driving source, therefore Svinkin (2008) model can be considered more valid for calculating PPV for higher soil stiffness based on the reasonable parameters in his formula, also without neglecting the length of pile which considers an important parameter and affect directly on PPV values as illustrated in Figures 3.53 and 3.54.

It is confirmed by the analysis that by increasing soil stiffness the PPV increases. In Figure 3.59 the effect of soil stiffness on PPV for Plaxis model is also investigated and compared with the other predictions models of PPV values. For lower stiffness values of sand, the PPV is reduced. Attewell & Farmer (1973) model shows a close trend to the Plaxis model in case of loose sand.

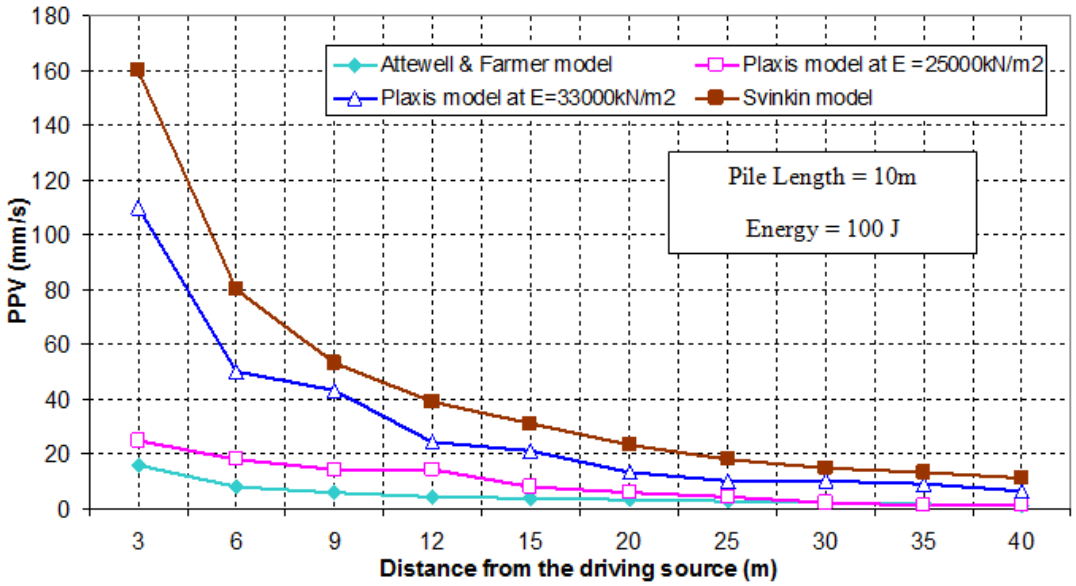

Figure 3.59: Comparison between PPV values from Finite Element and other prediction models for PPV values due to pile driving in sand soil.

3.11 Soil Structure Interaction:

3.11.1 The effect of PPV on the adjacent structure.

The wave propagates through soil as illustrated before that waves transfer in all the directions from the driving source. The wave energy in the ground depends on soil type and the source of vibration. The attenuation coefficient of the soil is controlling the energy of the wave and how far it will continue in the soil from the driving source. The hazard of vibration is proved by comparing PPV values from the analysis and vibration criteria (standard limits) on soil and adjacent structures and also in the human response. The effect of the direct damage of vibration on the structures was quite difficult to be shown by Plaxis model therefore another model using SAP 2000 is proposed to study the direct effect of vibration waves on the buildings. The acceleration versus time history of the pile driving vibration obtained by the Finite element models were used as input in another module using SAP2000 V.14 to simulate the structure model that is affected by such dynamic effect.

SAP model depends on the horizontal acceleration time history due to pile driving obtained from Plaxis dynamic analysis to simulate the vibration effect of the propagated waves. The structural model is used to investigate the influence of pile driving induced vibration on the adjacent structures in the form of displacement.

In order to study the effect of pile driving on adjacent structures. The numerical program SAP2000 V.14 was used to simulate an adjacent structure by modeling a skeleton structure consists of beams, columns, slabs and springs that represents the soil subgrade reactions as shown in Figure 3.60. The output of Plaxis in the form of acceleration induced time history was used as an input in the SAP model to study the effect of driving induced waves which affect not only on the soil underneath the structure but also directly to the structure.

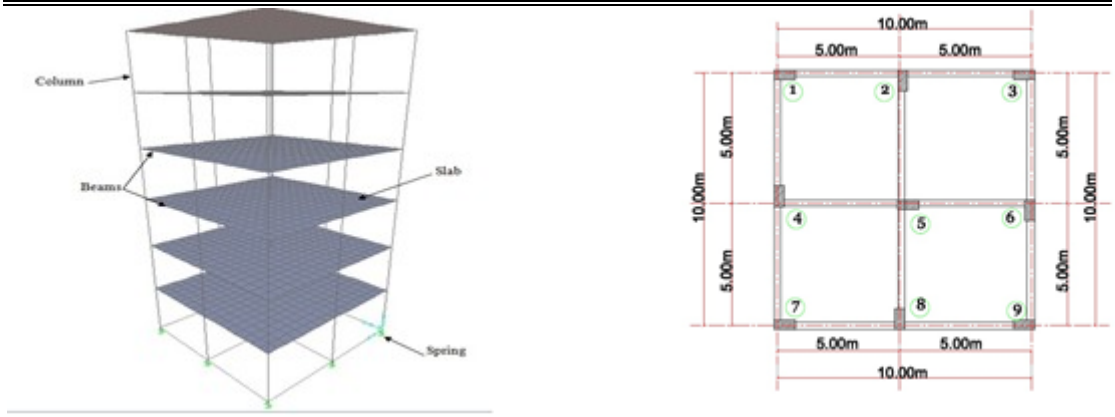

a) 3D skeleton of the 6 floor building b) Plan of the structure.

Figure 3.60: SAP 3D model for the structure adjacent to the driving source

The SAP model simulates a residential building (skeleton) consists of six floors and supported by isolated footings. The building had footprint of 10mx10m. The slabs were 0.12 m in thickness. The external columns had 0.3mx0.6m in cross section. The internal column had 0.3mx0.9m in cross section. The beams had dimensions of 0.25mx0.50 m in cross-section. The footings are rectangular in shape. The external footings were 2.5 m in width and 3.5m in length, while the internal footing was 3m in width and 4m in length as shown in Figure 3.61. A live load of 2kN/m2 was considered. The full details of SAP 2000 analysis see Appendix B.

The horizontal acceleration time history due to pile driving obtained from Plaxis dynamic analysis described above (see Figure 3.62) is used as an input for the 3D SAP structural analysis model. The 6 floor structure in the SAP model is vibrated using the acceleration time history of the vibration born from pile driving. The adopted maximum horizontal accelerations from Plaxis dynamic models at various distances from the driving source are plotted in Figure 3.63 for both cases of clay and sand surrounding soils.

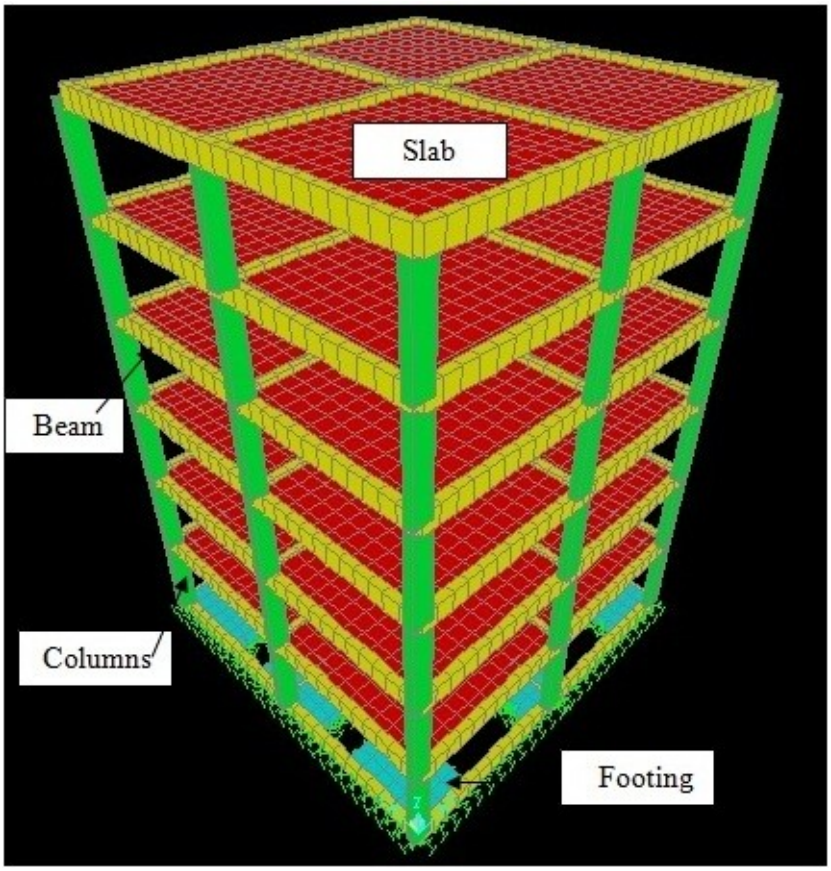

Figure 3.61: Structure model representing the 6 floors adjacent building adapted from SAP model.

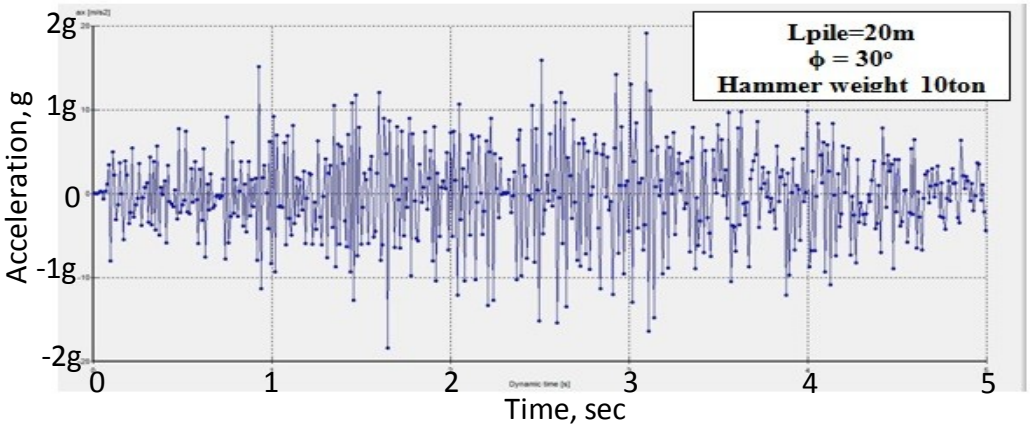

Figure 3.62: Horizontal acceleration time history of the born vibration due to pile driving 3m away from the source as obtained from the Finite Element model (g=9.81 m/s2)

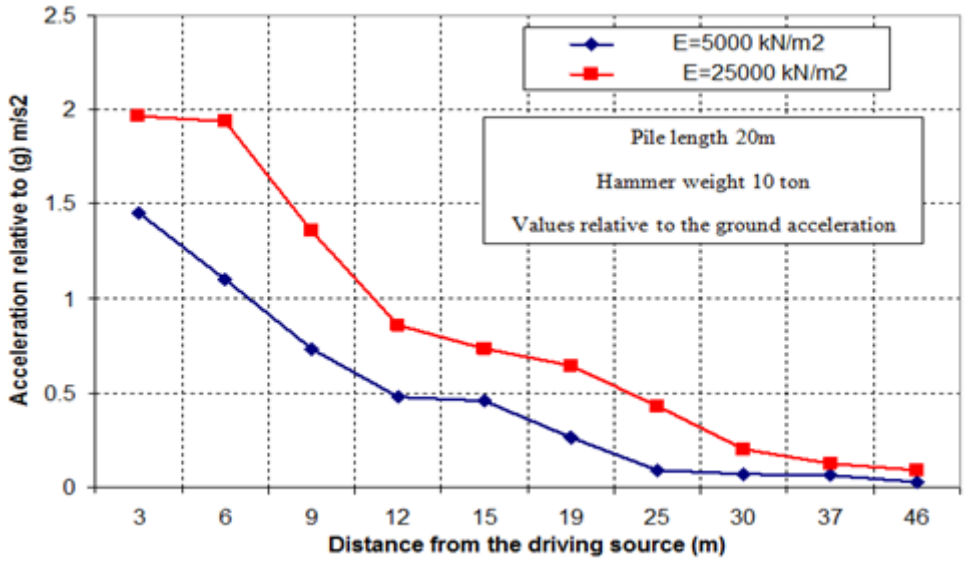

Figure 3.63: Maximum horizontal accelerations due to pile driving in clay and sand at different distances from the driving source, (g=9.81 m/s^2)

The output data of Plaxis represented in acceleration formula listed in Excel sheet to be used in feeding SAP.

The horizontal acceleration is defined as a case of loading in SAP. The load type is time history acting the same way of Earthquake load or any other horizontal loads. A load combination is set between the ultimate loads of the building (life load + dead load) and the function of pile driving as shown in Figure 3.64.

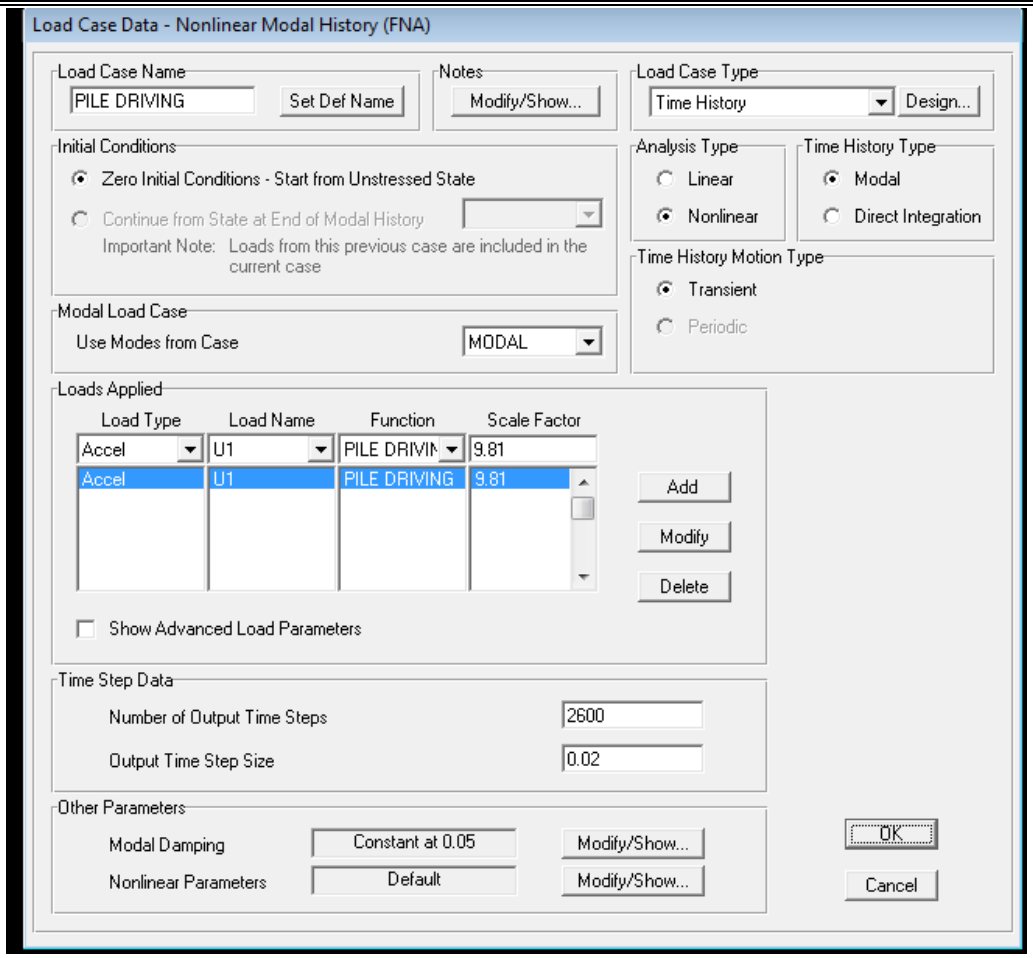

Figure 3.64: The input of pile driving acceleration time history data in SAP model.

The vertical displacement resulted from the structural vibration obtained from SAP model is used as a possible cause of damage that could occur to the structure. The vibration induced vertical displacements at the corner of a structure at point (1) (see Figure 3.43b) in the cases of clay (E=5 MPa) and sand (E=25 MPa) is shown in Figure 3.65. In general, the magnitudes of the vertical displacement in sand are higher than that in clay. The difference could be related to difference in stiffness and the values of horizontal acceleration. The maximum distances at which the vibration induced displacement becomes less than 5 mm are in the cases of clay and sand are 6 m and 10 m, respectively.

According to the data in Figure 3.65, the minimum distances at which such criteria is violated in the clay soil at E 5 mPa and sand soil for E 25 mPa cases are 0.55 L and 0.3 L (where L is the pile length) respectively.

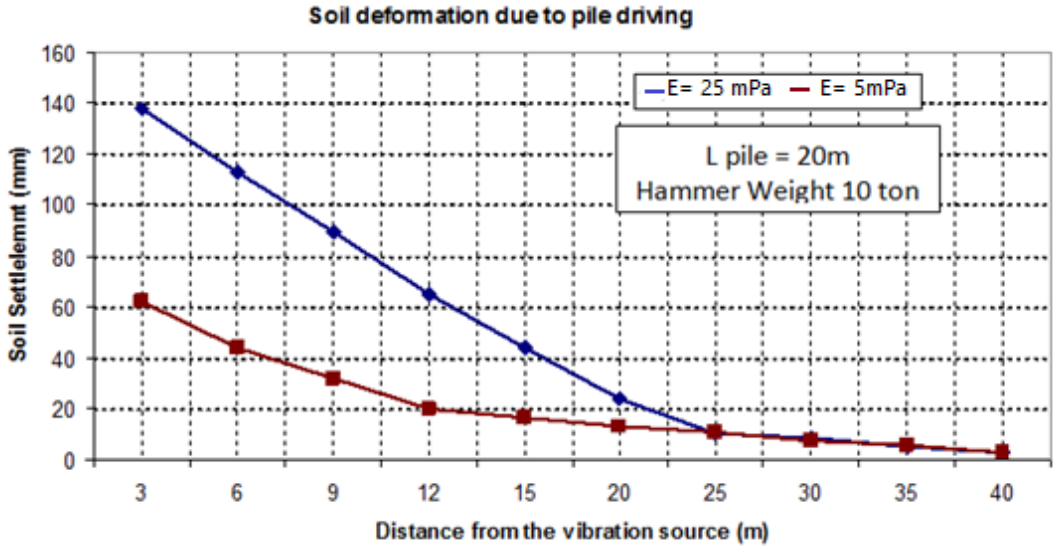

Figure 3.65: The vertical displacement at different distance from the source in clay and sand soils from SAP.

SAP model also can show the effect of direct vibration on the building members. While the building is subjected to vibration the straining action in members increased comparing by the case without vibration as shown in Figures 3.66 and 3.67. It can concluded that the effect of pile driving or any other source of vibration is avery significant and should be calculated to avoid any possible damage on the adjacent structures.

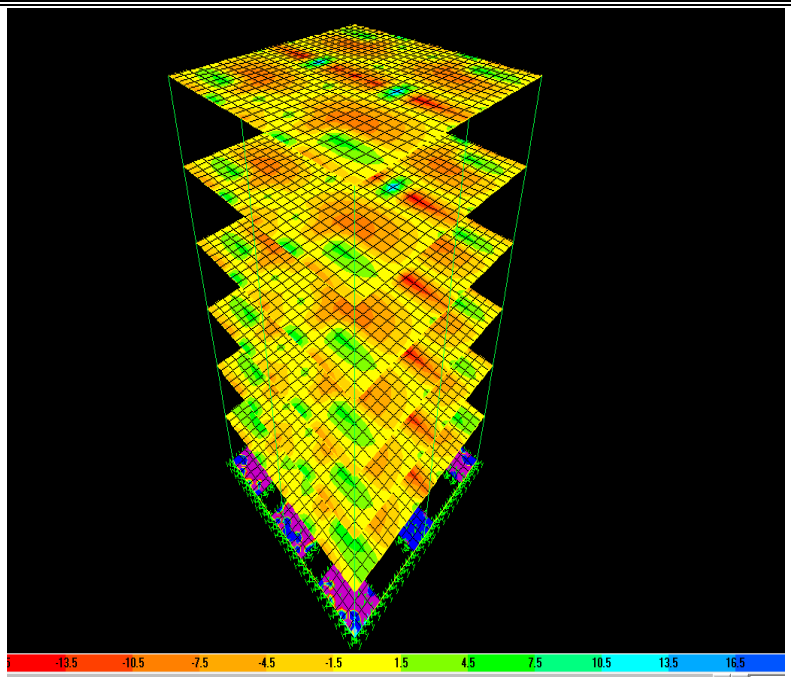

Figure 3.66: The straining action of shells (m), In the normal case of loading without pile driving effect.

It can obviously noticed that the increase of the values of moment on shells in the case of considering the effect of pile driving as extra loads on the structure. Beside the increase of straining actions in beams and columns which could leads to a significant structural damage.

That is why design engineers should be aware about that effect of pile driving earth born vibration on the adjacent structures.

In addition to the vibration intensity, which often is expressed in terms of particle velocity, also the vibration frequency is important. When the dominant frequencies of the generated vibrations harmonize with the resonance frequency of buildings or building elements, the risk of building damage increases, Massarsch and Fellenius (2014)

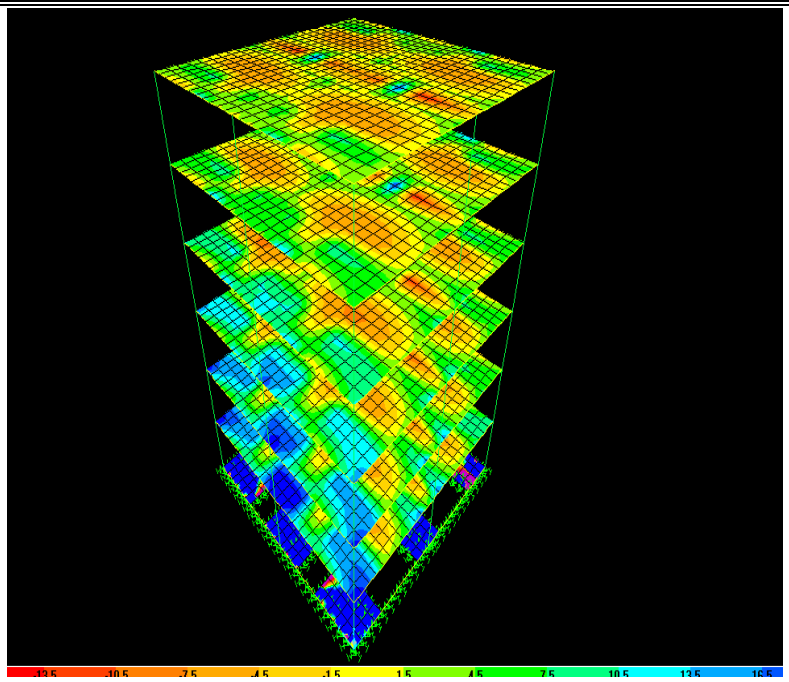

Figure 3.67: The effect of pile driving on the straining action on the shells (M)

The methodology presented in this part can be used to evaluate the limiting vibration induced PPV in the Egyptian Code of Practice and/or in the international standards.

The amplitudes of motion can be expressed in terms of acceleration, velocity and displacement. The first data reported from an earthquake record is generally the peak ground acceleration (PGA) which expresses the tip of the maximum spike of the acceleration ground motion as shown in Figure 3.68.

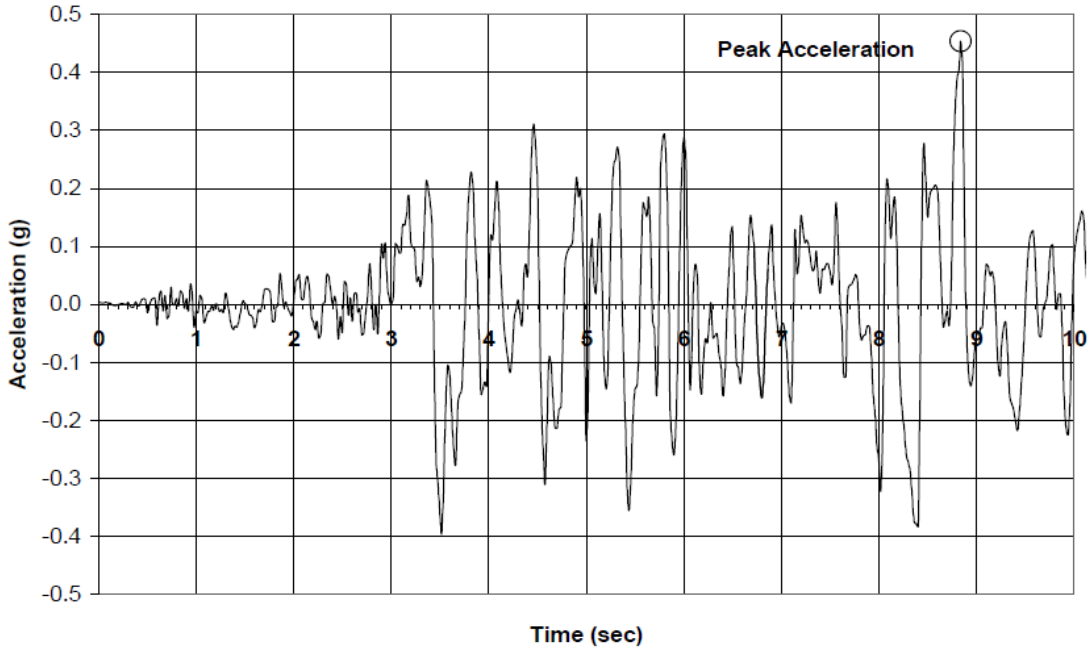

Figure 3.68: Recorded ground motion (Holiday Inn, Van Nuys 1994, 270 degrees: 0–10 sec)

3.12 Investigation and comparison between PPV values from insitu measurements and PPV values from prediction models.

Prediction models of PPV is investigated in chapter two of this thesis, in this section the validity of each model is investigated by being compared with infield measurements and different records, for reaching a conclusion to choose the suitable model for calculating PPV.

Many data for PPV values in different sites and with different conditions (pile length, pile diameter, pile material, soil type, hammer type, location of recording ...etc) is collected with the available parameters which given by the authors. Table 3.13 summarizes the available case studies about PPV measurements infield.

Table 3.13: Infield measurements of PPV for different sites.

Author	Soil type	Pile type and Dimensions (m)	Energy (joule)	Hammer type	Measurements depth (m)
Moor et al (1995)	Yellow fine sand	0.82m long Steel pile	980	Drop hammer	Surface source & impeded source
Moor et al (1995)	Soft to firm clay	0.82m long Steel pile	980	Drop hammer	Surface source & impeded source
Peter (1953)	1.8m hurnus 1.lm clayey sand followed by sandy loam	3m long cast in place concrete diameter 0.55m	21680	Single acting express steam	
			11615	Demag quick stroke steam	
	3.5m fill, 3.2m peat then gravel with silty sand	8m long cast in place concrete diameter 0.55m	21680	Single acting express steam	
			11615	Demag quick stroke steam	
	Gravel	10m long cast in place concrete diameter 0.55m	11615	Demag quick stroke steam	
Sior (1961)	Cohesive	Sheet pile	49050	steam	
	Cohesive	3.2m long cast in place pile	117720	steam	
Dulmatov (1967)	Sat sand	8m long sheet pile	9310	Drop hammer	2.4m
	0.2m buildings waste, >2m sat.loam	24m long hollow reinforced concrete diameter 0.6m	0.5m : 29430 >5m: 58860	Drop hammer	3.25m
Attewell & Farmere (1973)	Fine sand		1350/cycle	Wet vibrofloatation	
	Uncompacted fill		2700/cycle	dry vibroflotation	
	Stiff silty clay on firm laminated clay	Sheet pile	2400 to 60700		
	Coarse sand on stiff clay base		1050 to 10500	Shell boring	
	Layered medium sand & silt	H-Piles	9100 to 36500		
	Laminated clay			Diesel hammer	
	Layered dense sand and gravel		212000		

Author	Soil type	Pile type and Dimensions (m)	Energy (joule)	Hammer type	Measurements depth (m)
Brenner and Chittikuladi -lok (1975)	Clayey sand	25m prestressed concrete pile dimensions 0.43*0.43	68670	Drop hammer	
Wiss (1967)	Clay	Concrete pile	15, 000-ft-lb		
	Dry sand				
	Wet sand				
	Silty clay	13m concrete pile	39228	Drop hammer	12m
	Sandy silt	12m concrete pile	39228	Drop hammer	9.5m
	Soft marl	12m H-steel pile	39228	Drop hammer	9m
	Silty clay	12m H-steel pile	39228	Drop hammer	10m
	Glacial clay	32m H-steel pile	61000	Diesel hammer	25m
	Sand stone	27m H-steel pile	61000	Diesel hammer	23.5m
	Boulder clay	16m sheet pile	37200	Diesel hammer	12.5m
	Sandy clay	32m H-steel pile	31382	Diesel hammer	14.5m
Uromeihy (1990)	Silty clay	12m H-steel pile	37200	Diesel hammer	8.2m
	Glacial clay	21 H-steel pile	11900	Air hammer	15.3m
	Alluvial deposits	9m sheet pile	4100	Air hammer	7.2m
	Coastal deposits	10m sheet pile	4100	Air hammer	6.2m
	Silty clay	12m sheet pile	6400	Air hammer	5.6m
	Glacial stiff clay	23 H-steel Pile	39228	Hydraulic hammer	20.5m
	Glacial stiff clay	23 H-steel Pile	39228	Hydraulic hammer	21.5m
	Glacial sandy clay	35m H-steel pile	39228	Hydraulic hammer	19m
	Sandy silt	23m H-steel pile	39228	Hydraulic hammer	17m
	Silty clay	9m sheet pile	39228	Hydraulic hammer	8.2m
	Dense gravel	32m H-steel pile	23536.8	Hydraulic hammer	30.5m
	Silty clay	32m H-steel pile	23536.8	Hydraulic hammer	21.5m
	Dense sand	14m sheet pile	68649	Hydraulic hammer	10.75m
	Brown clay	12m sheet pile	39228	Hydraulic hammer	8m
	Dense sand	5m sheet pile	2000	Vibro driver	4.5m

Author	Soil type	Pile type and Dimensions (m)	Energy (joule)	Hammer type	Measurements depth (m)
	Alluvial clay	20m tube pile	10700	Vibro driver	2.7m
	Glacial clay	14m H-steel pile	10700	Vibro driver	11m
	Dense gravel	21m tube pile	5600	Vibro driver	14.7m
	Silty clay	9m sheet pile	10700	Vibro driver	6.5m
	Clayey silt	16m H-steel pile	10700	Vibro driver	11m
	Dense silt	9.5m sheet pile	3400	Vibro driver	4.7m
	Dense sand	16m sheet pile	10700	Vibro driver	7.5m
	Sand & Gravel	14m sheet pile	10700	Vibro driver	6m
	Sandy clay	16m sheet pile	10700	Vibro driver	4.8m

The previous records of PPV values for the above mentioned authors have plotted vs. scaled energy as shown in Appendix D.

The investigation is based on Uromeihy (1990) in-field measurements data, it provide a very detailed data for each case. Uromeihy(1990) measured the three component of PPV radial, transverse and vertical but for the comparison with the available models the resultant PPV is choosed.

By investigating each available prediction models and compared with PPV infield measurements, it illustrated that the different methods have special conditions should be adapted to get the correct values of PPV.

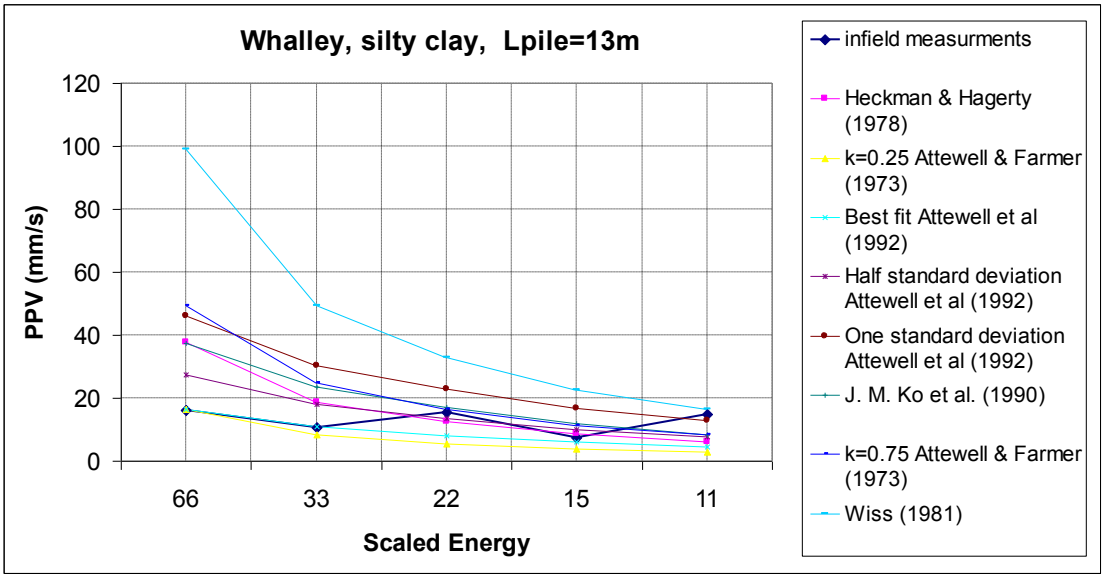

Figure 3.69: The comparison between prediction models and infield measurements, Lpile 13m, whalley site, silty clay soil

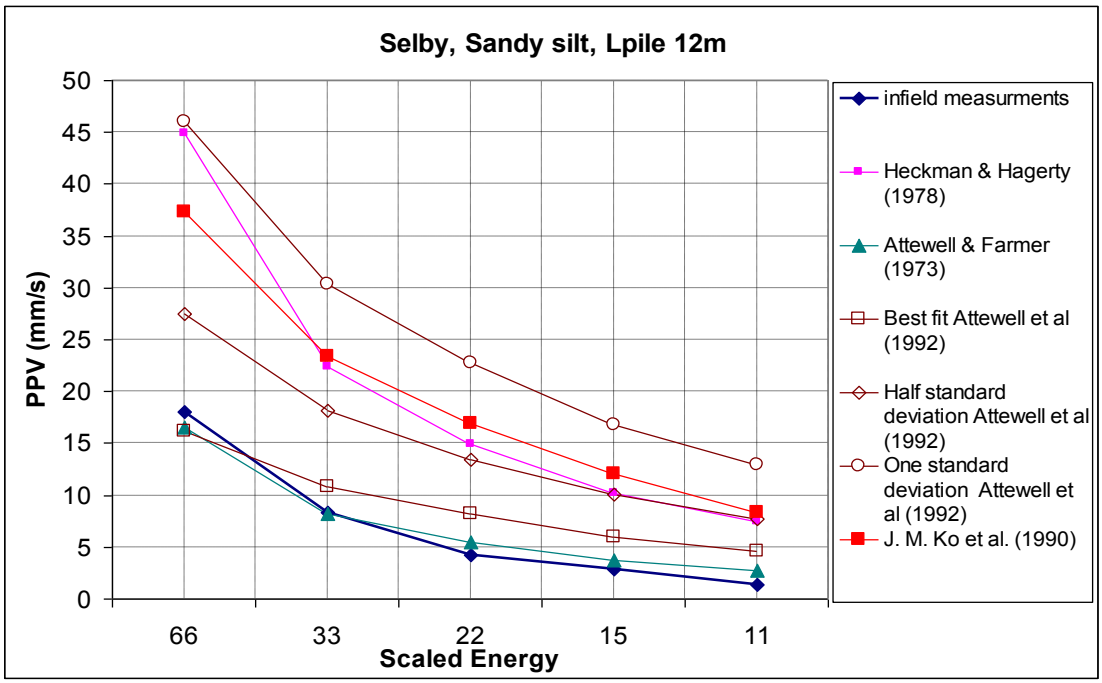

Figure 3.70: The comparison between prediction models and infield measurements at Lpile 12m in selby site, sandy silt soil.

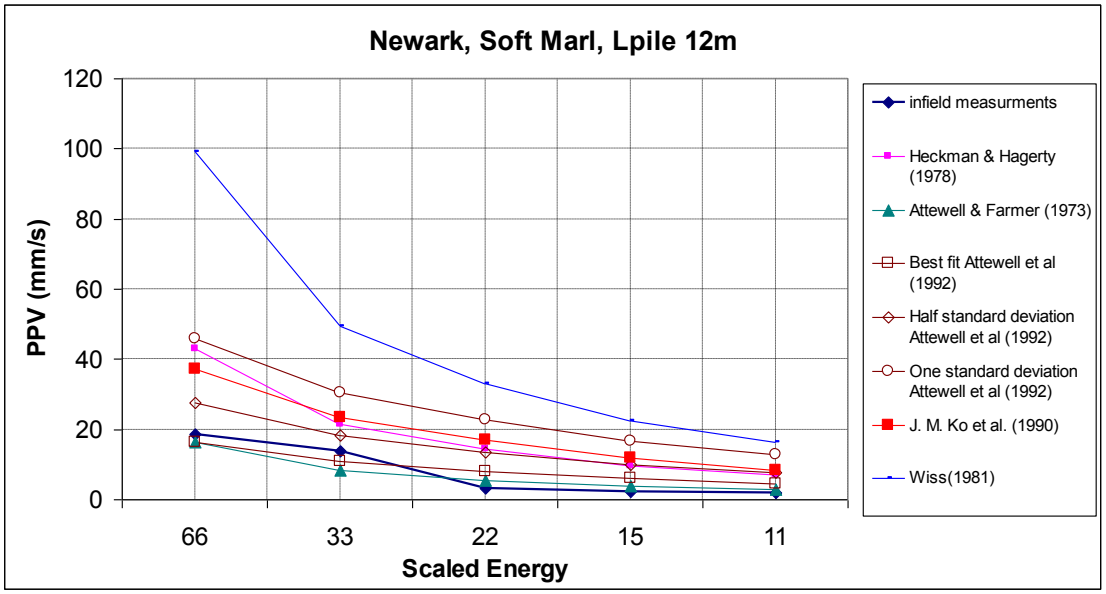

Figure 3.71: The comparison between prediction models and infield measurements at Lpile 12m in Newark site, soft marl soil.

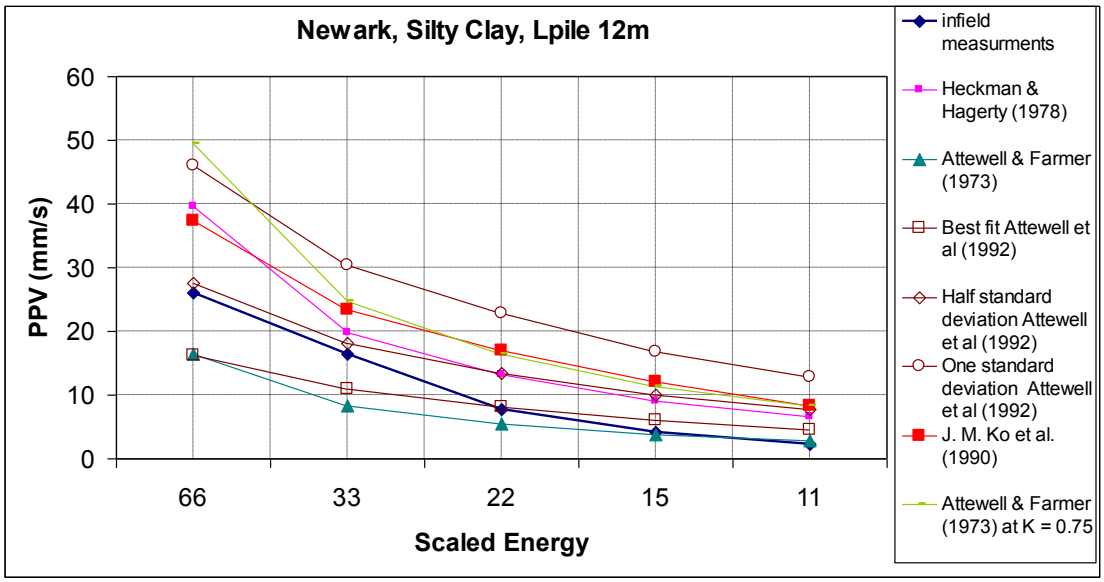

Figure 3.72: The comparison between prediction models and infield measurements at Lpile 12m in Newark site, silty clay soil.

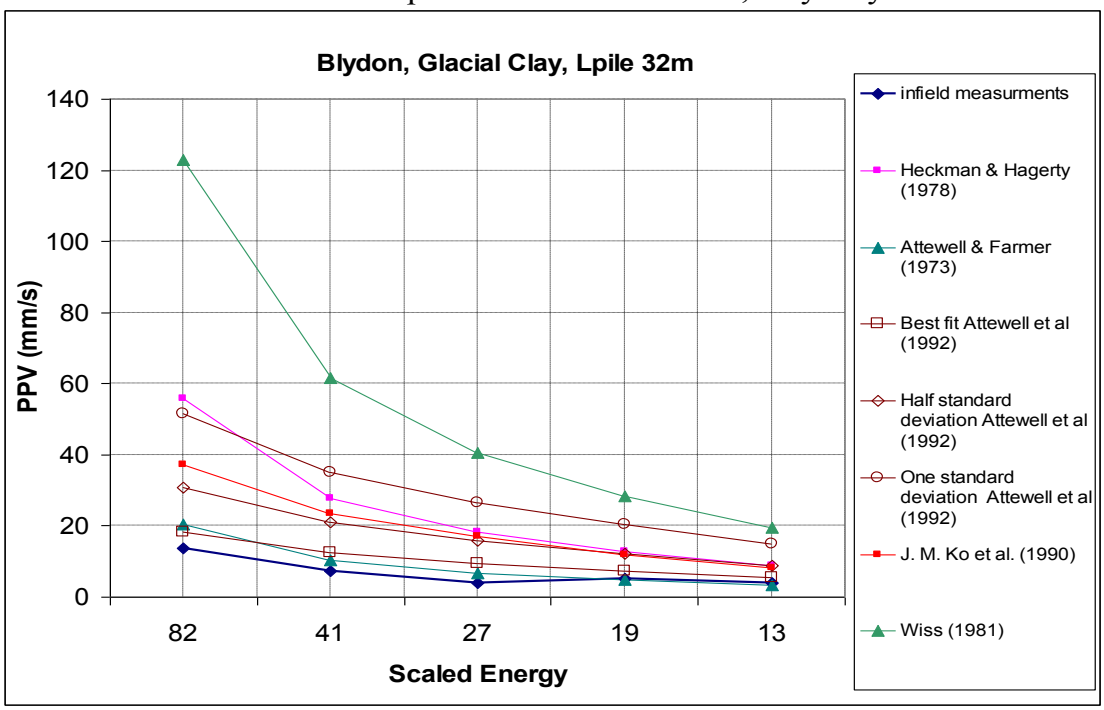

Figure 3.73: The comparison between prediction models and infield measurements at Lpile 32m in Blydon site, glacial clay soil.

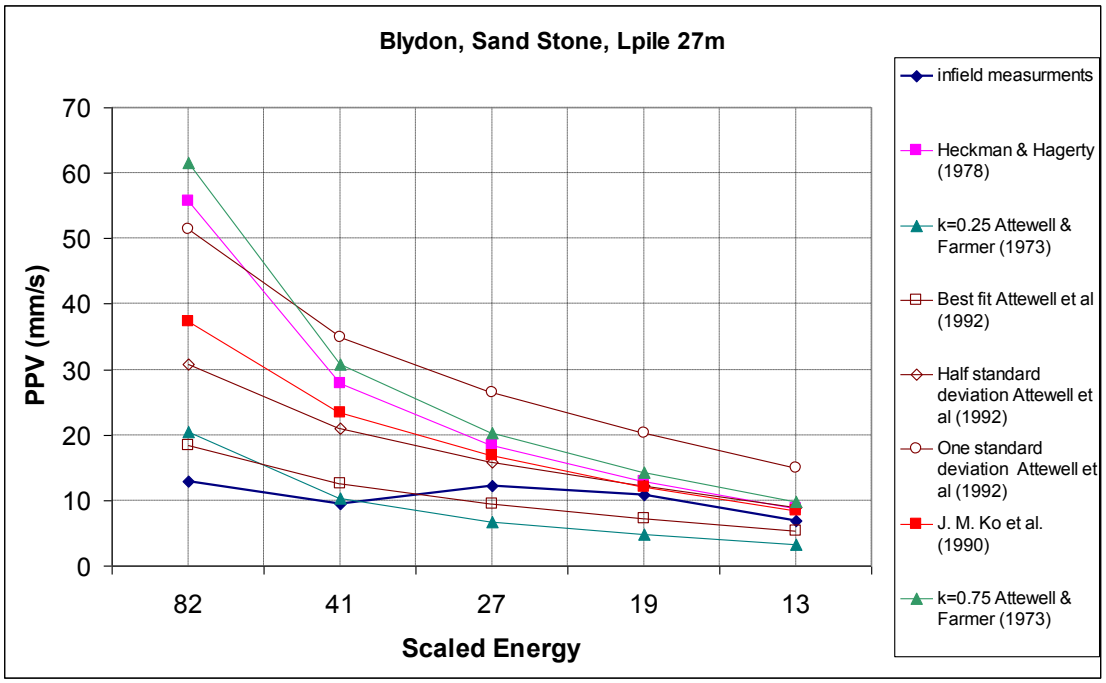

Figure 3.74: The comparison between prediction models and infield measurements at Lpile 27m in Blydon site, sand stone soil.

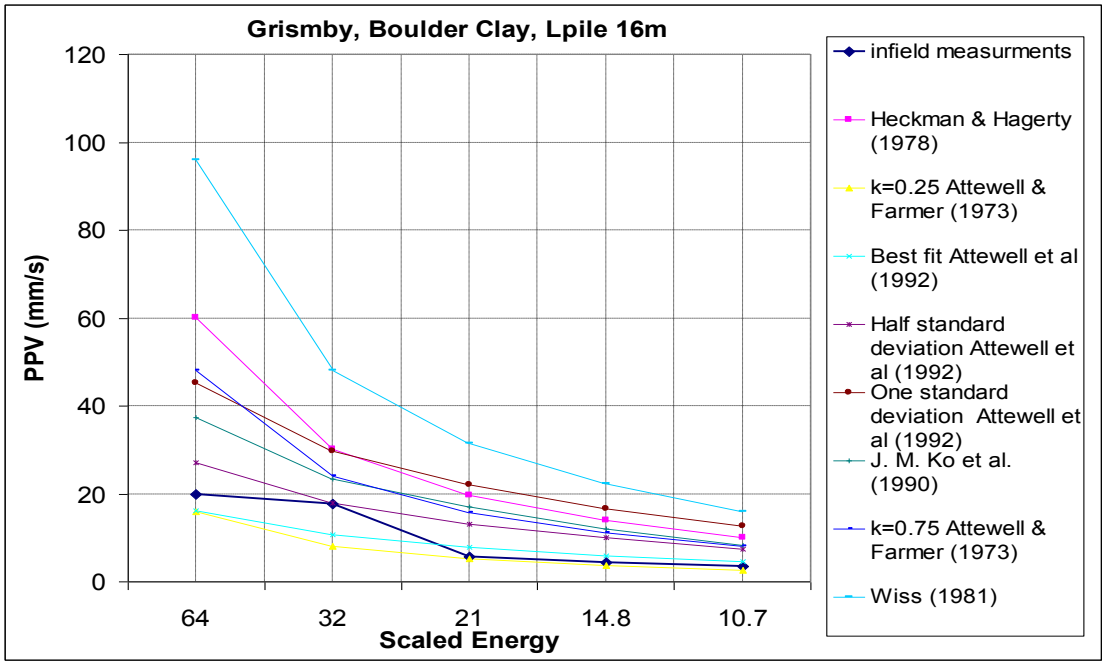

Figure 3.75: The comparison between prediction models and infield measurements at Lpile 16m in Grismby site, boulder clay soil.

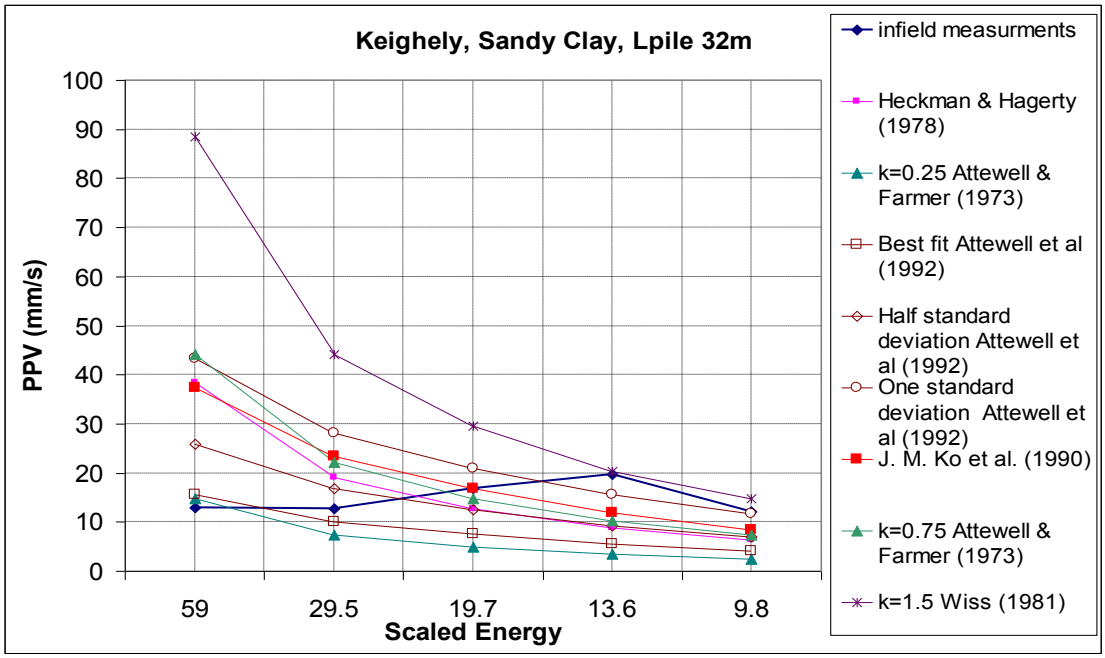

Figure 3.76: The comparison between prediction models and infield measurements at Lpile 32m in Keighely site, sandy clay soil.

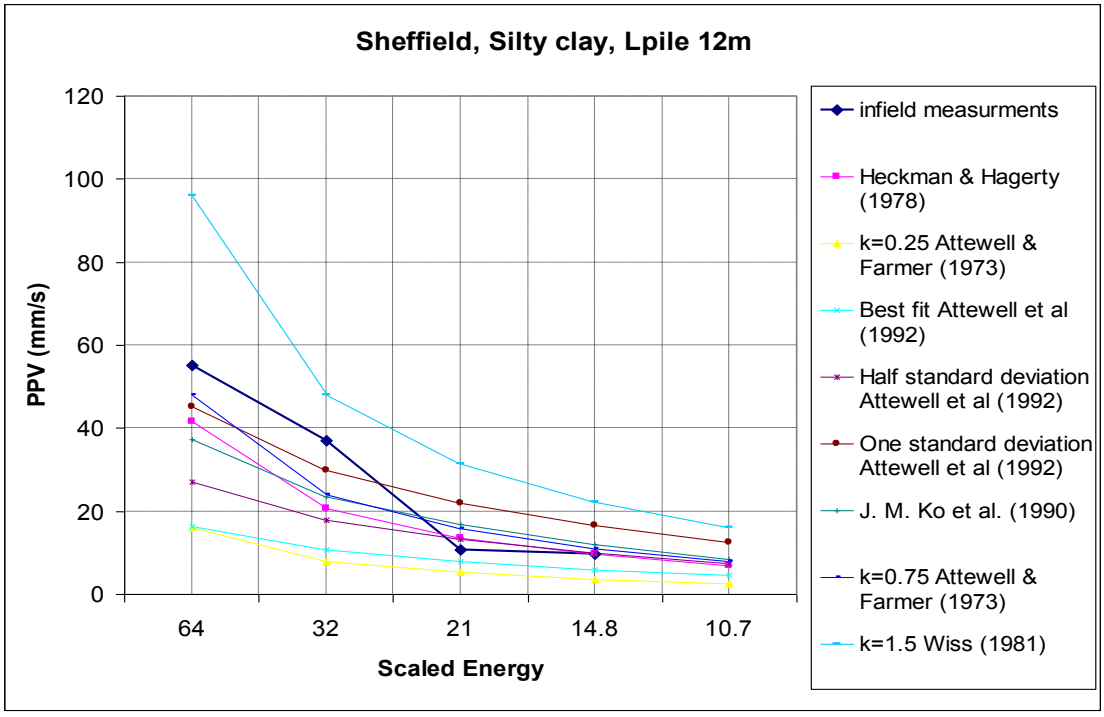

Figure 3.77: The comparison between prediction models and infield measurements at Lpile 12m in Sheffield site, silty clay soil.

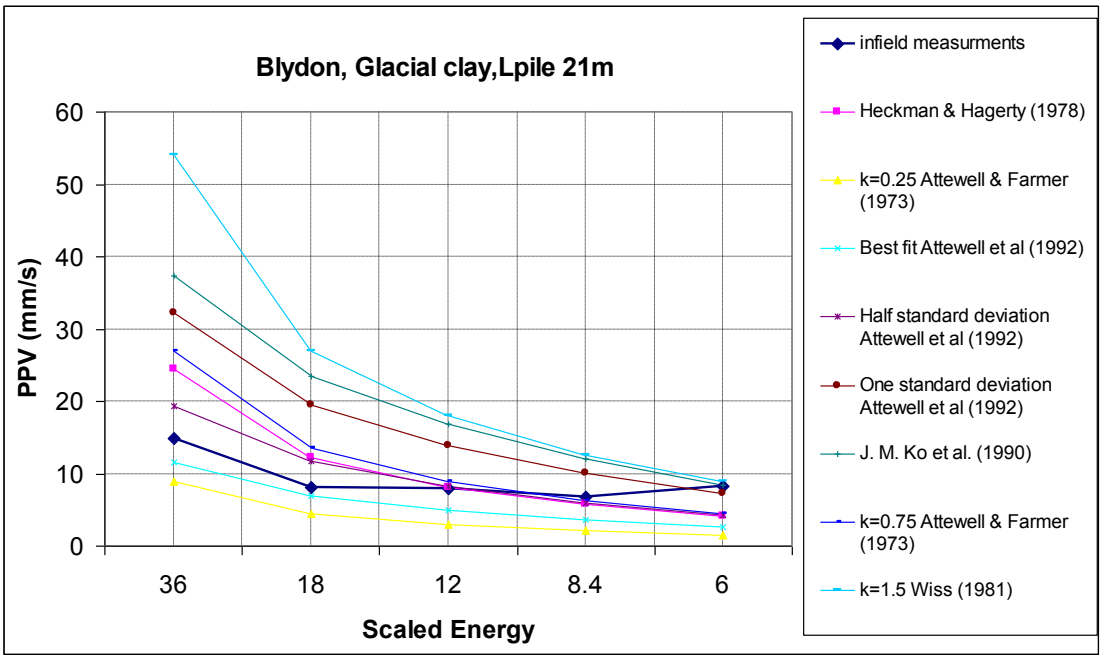

Figure 3.78: The comparison between prediction models and infield measurements at Lpile 21m in Blydon site, glacial clay soil.

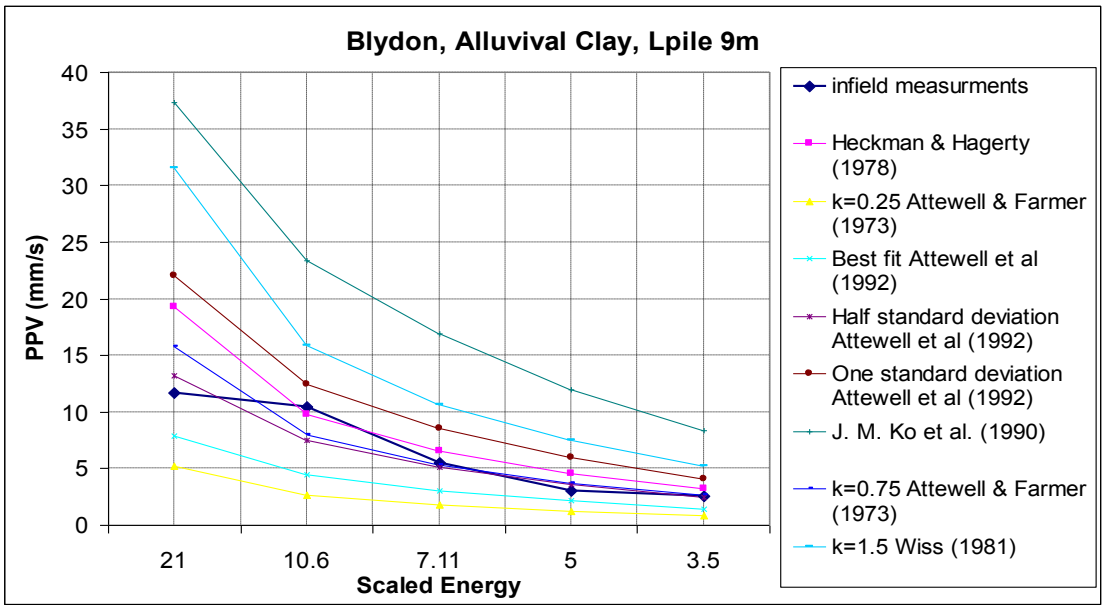

Figure 3.79: The comparison between prediction models and infield measurements at Lpile 9m in Blydon site, alluvial clay soil.

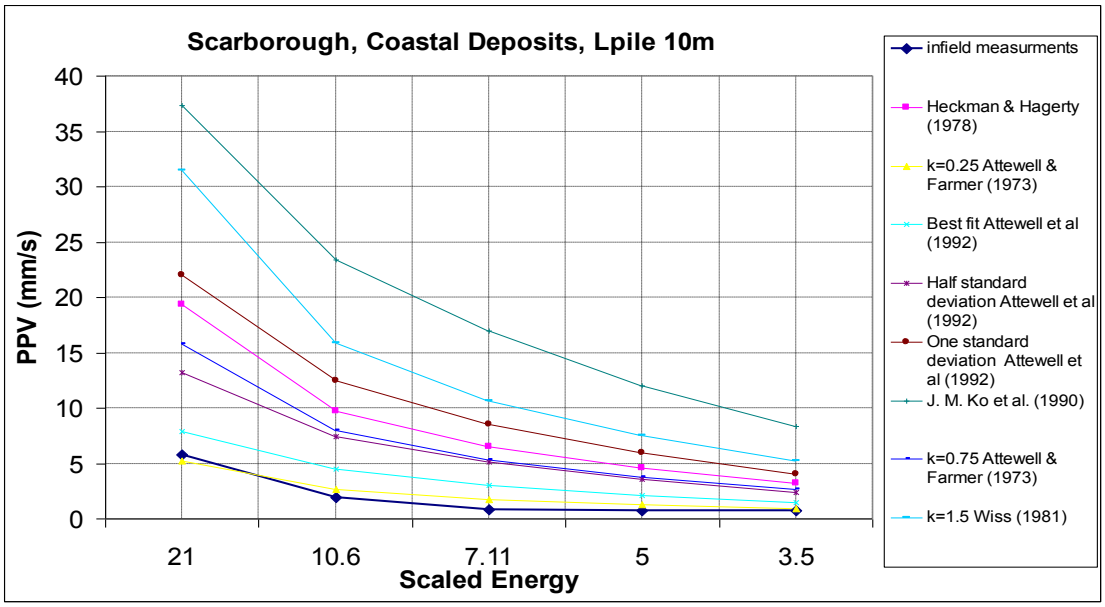

Figure 3.80: The comparison between prediction models and infield measurements at Lpile 10m in Scarborough site, coastal deposits soil.

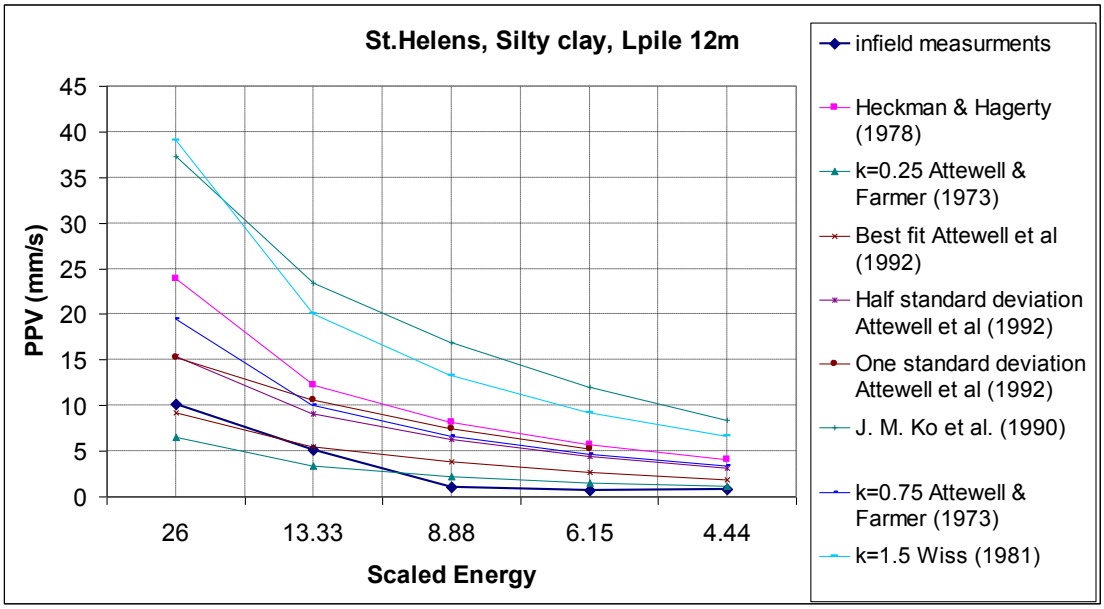

Figure 3.81: The comparison between prediction models and infield measurements at Lpile 12m in St.Helens site, silty caly soil.

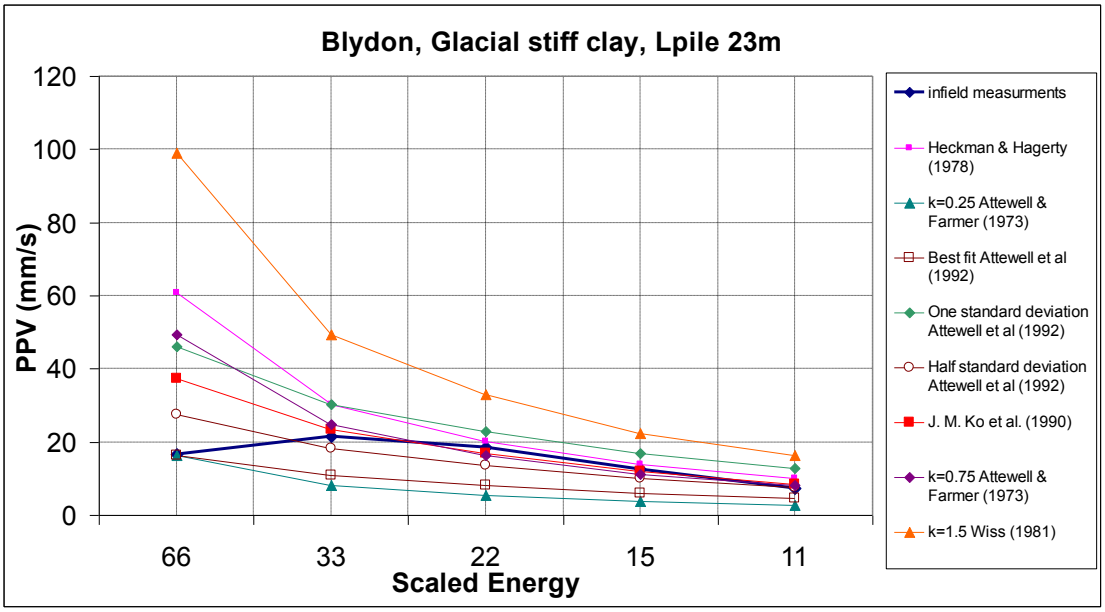

Figure 3.82: The comparison between prediction models and infield measurements at Lpile 23m in Blydon site, glacial stiff caly soil.

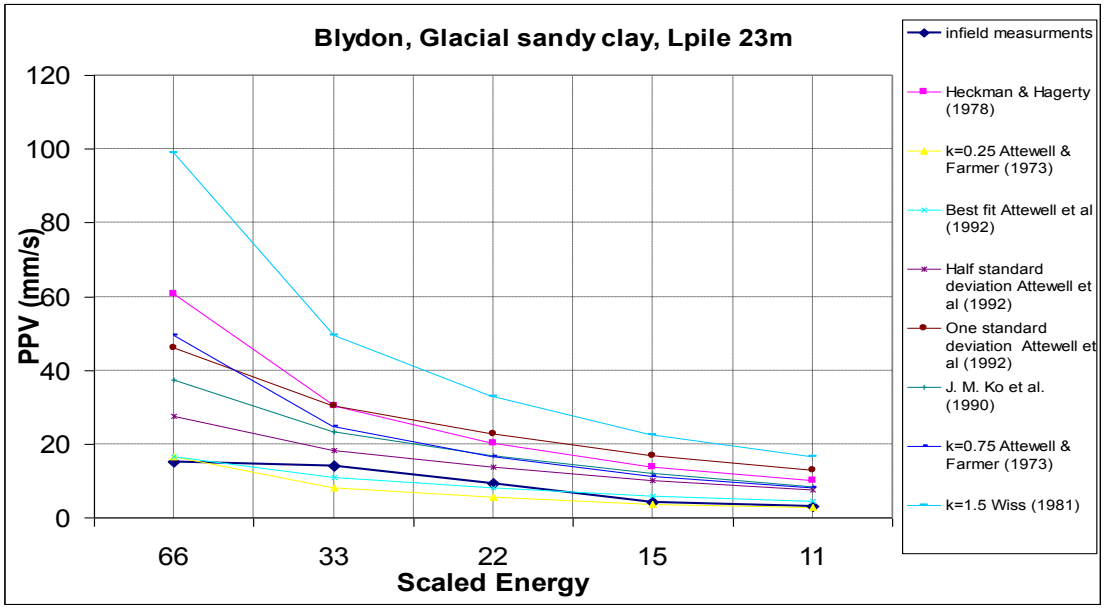

Figure 3.83: The comparison between prediction models and infield measurements at Lpile 23m in Blydon site, sandy caly soil.

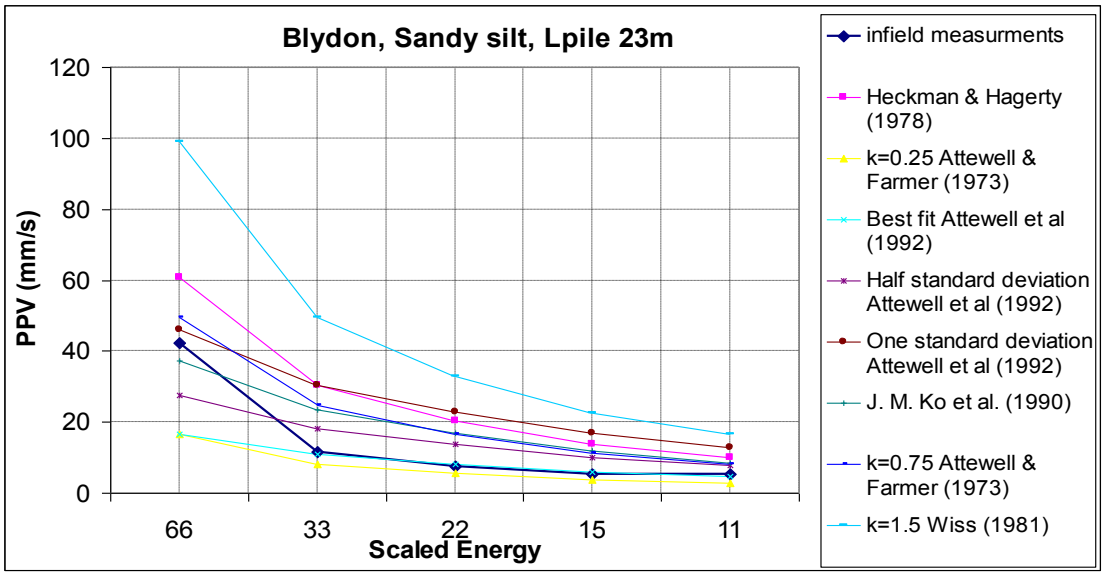

Figure 3.84: The comparison between prediction models and infield measurements at Lpile 23m in Blydon site, sandy silt soil.

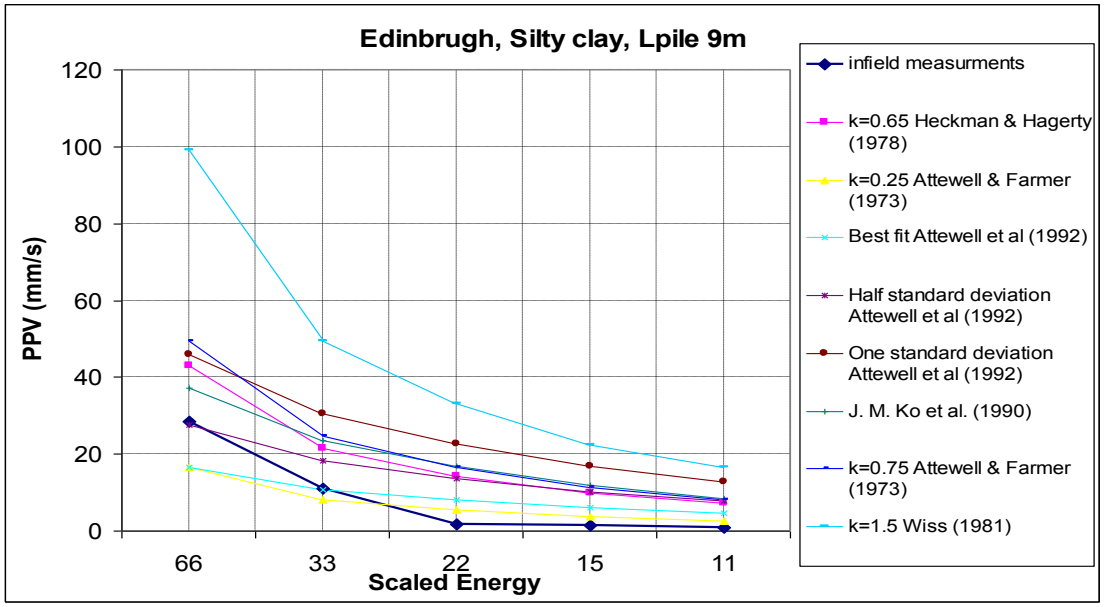

Figure 3.85: The comparison between prediction models and infield measurements at Lpile 23m in Blydon site, sandy silt soil.

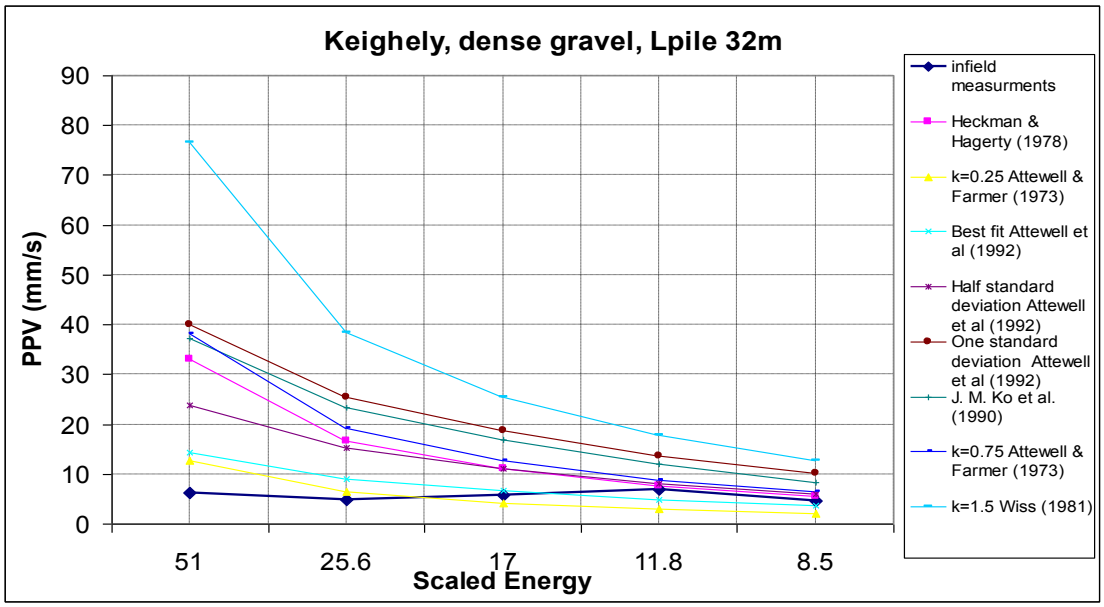

Figure 3.86: The comparison between prediction models and infield measurements at Lpile 32m in Keighely site, dense gravel soil.

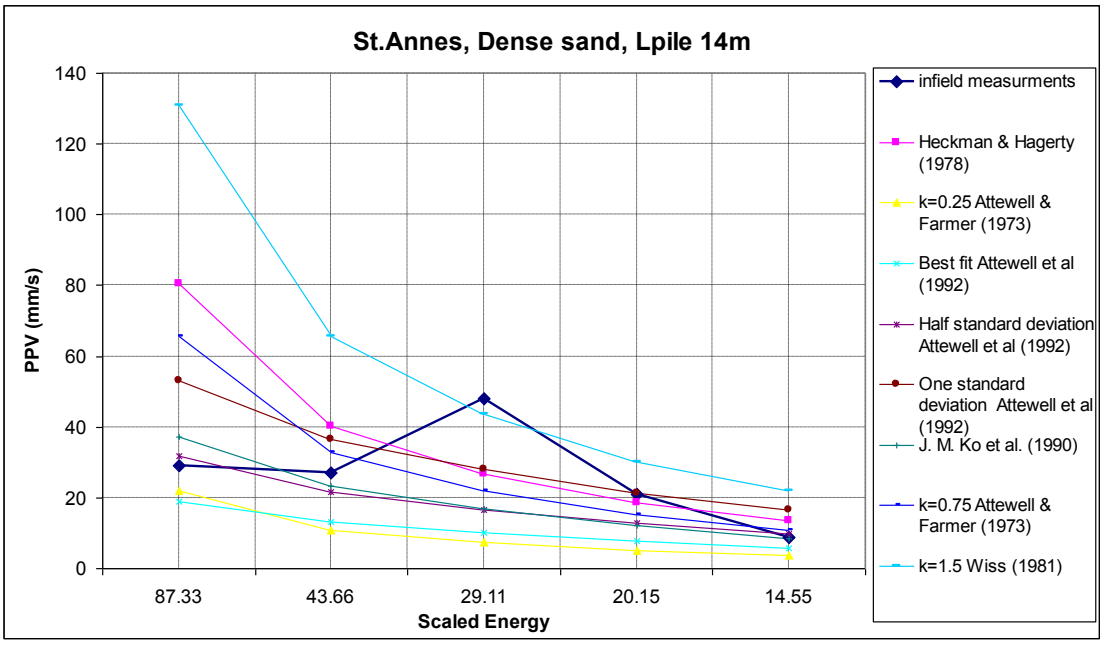

Figure 3.87: The comparison between prediction models and infield measurements at Lpile 14m in St.Annes site, dense sand soil.

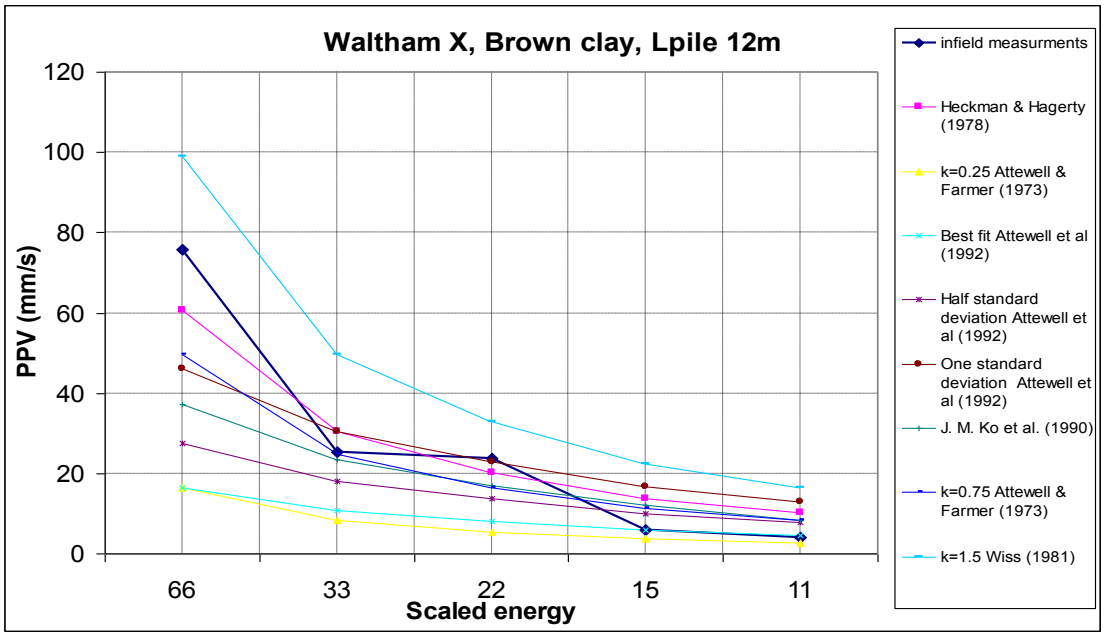

Figure 3.88: The comparison between prediction models and infield measurements at Lpile 12m in Waltham X. site, brown clay soil.

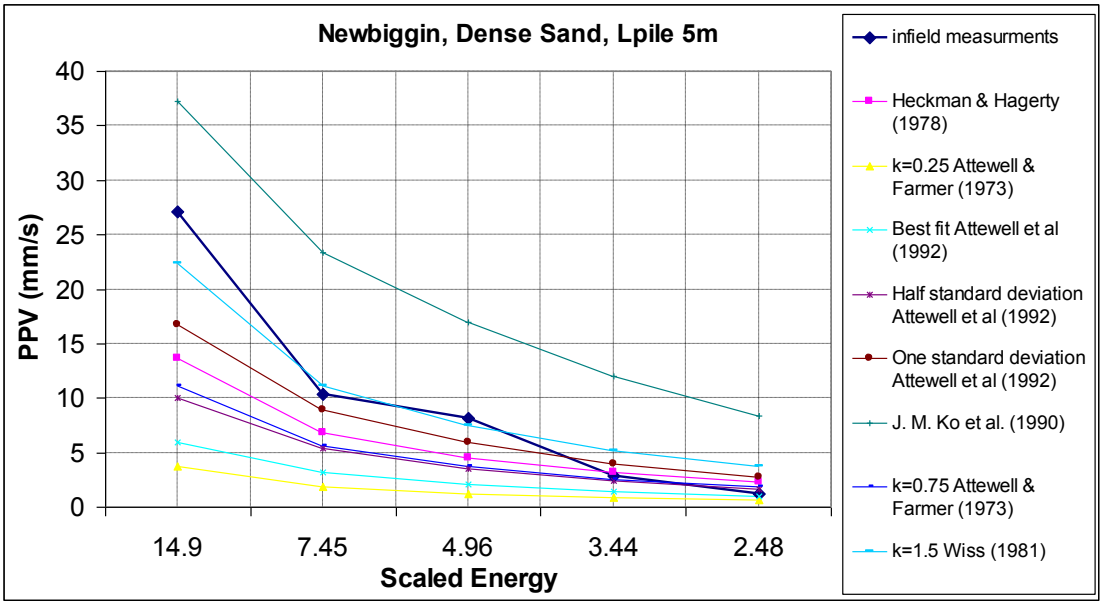

Figure 3.89: The comparison between prediction models and infield measurements at Lpile 5m in Newbiggin. site, dense sand soil.

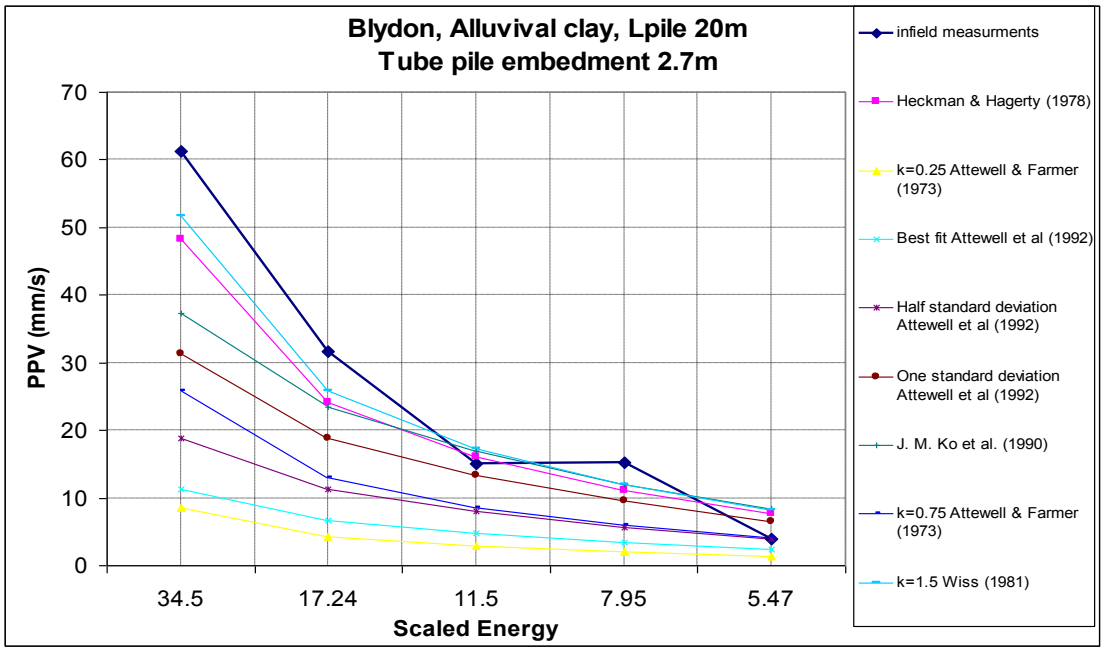

Figure 3.90: The comparison between prediction models and infield measurements at Lpile 20m, tube pile in Blydon site, alluvial clay soil.

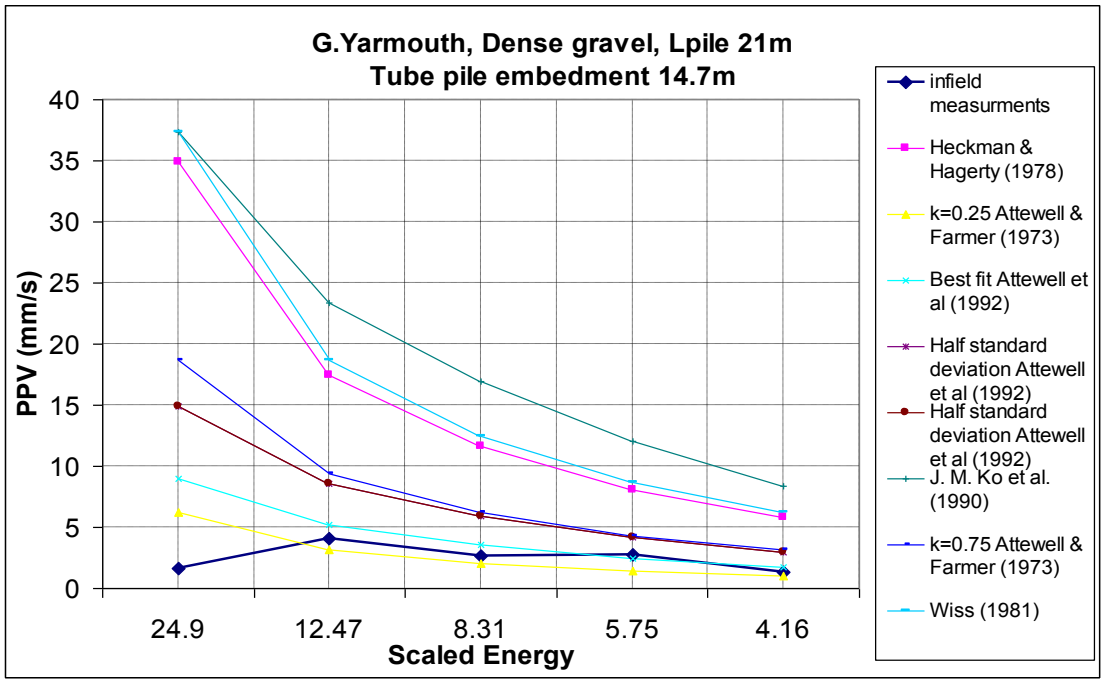

Figure 3.91: The comparison between prediction models and infield measurements at Lpile 21m, tube pile in G.Yarmouth site, dense gravel soil.

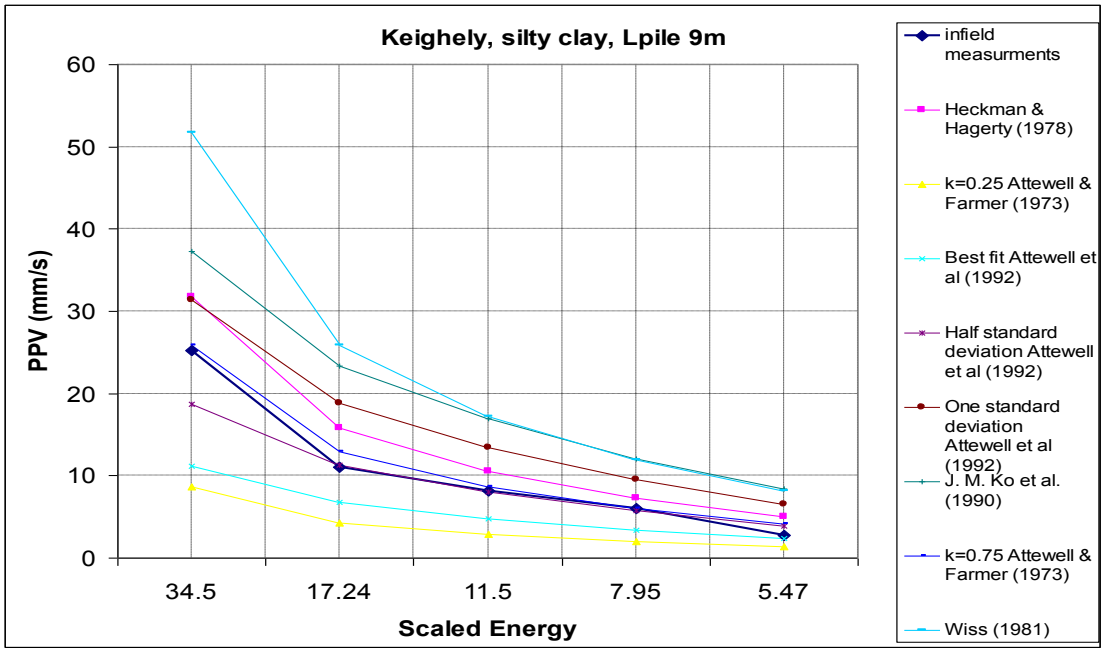

Figure 3.92: The comparison between prediction models and infield measurements at Lpile 9m in Keighely site, silty clay soil.

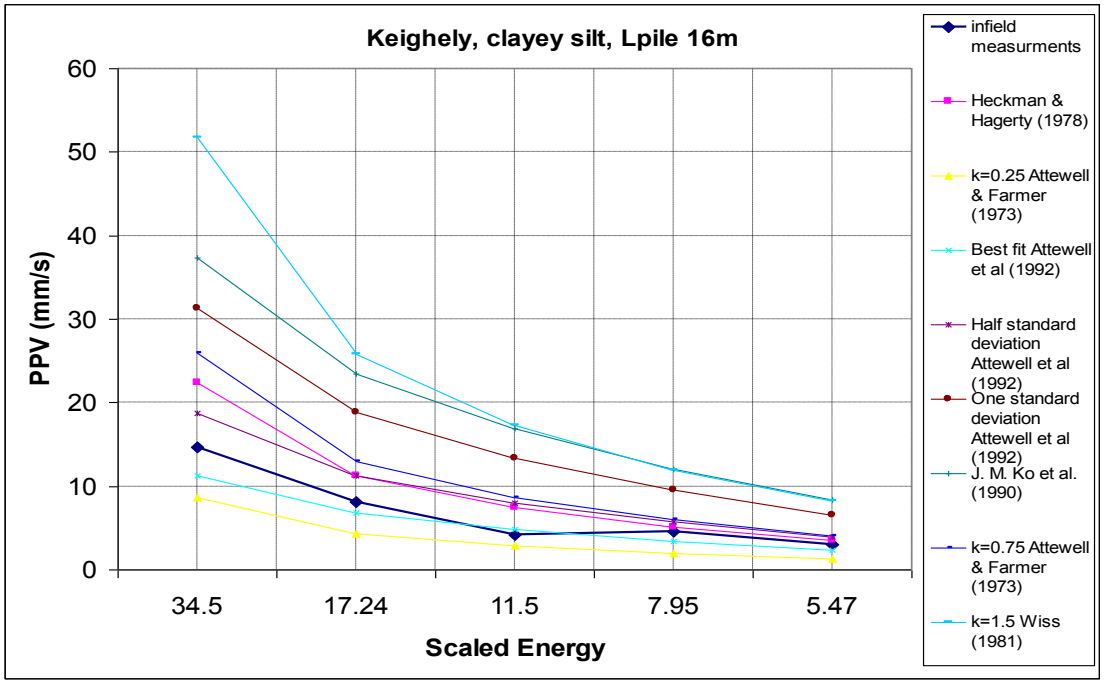

Figure 3.93: The comparison between prediction models and infield measurements at Lpile 16m in Keighely site, clayey silt soil.

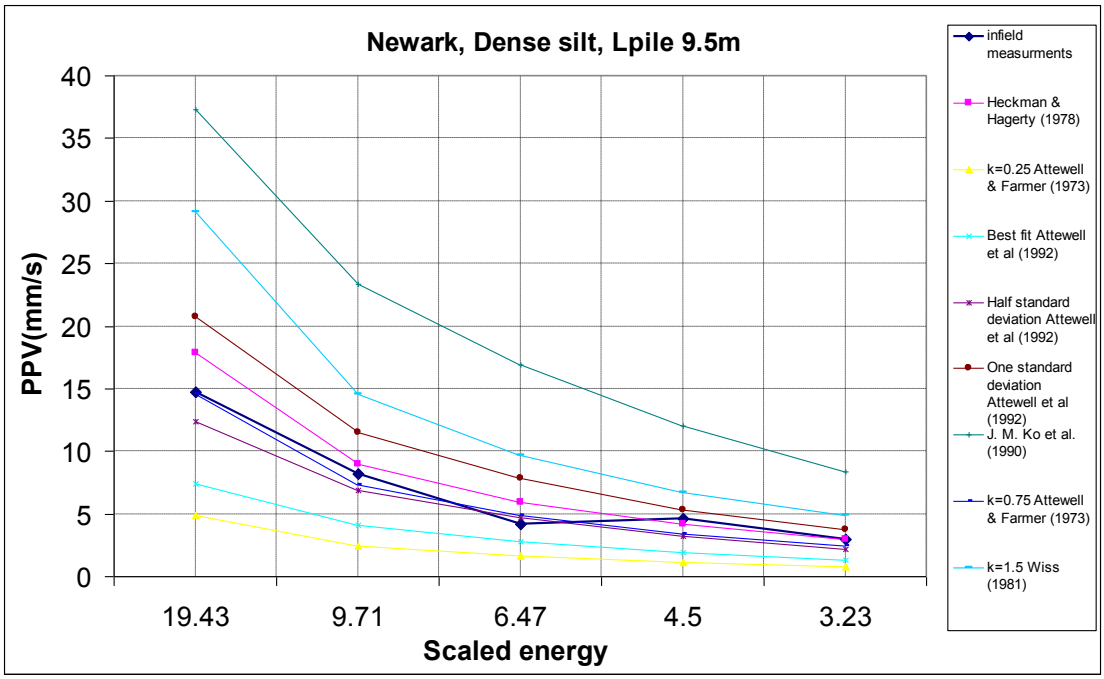

Figure 3.94: The comparison between prediction models and infield measurements at Lpile 9.5m in Newark site, dense silt soil.

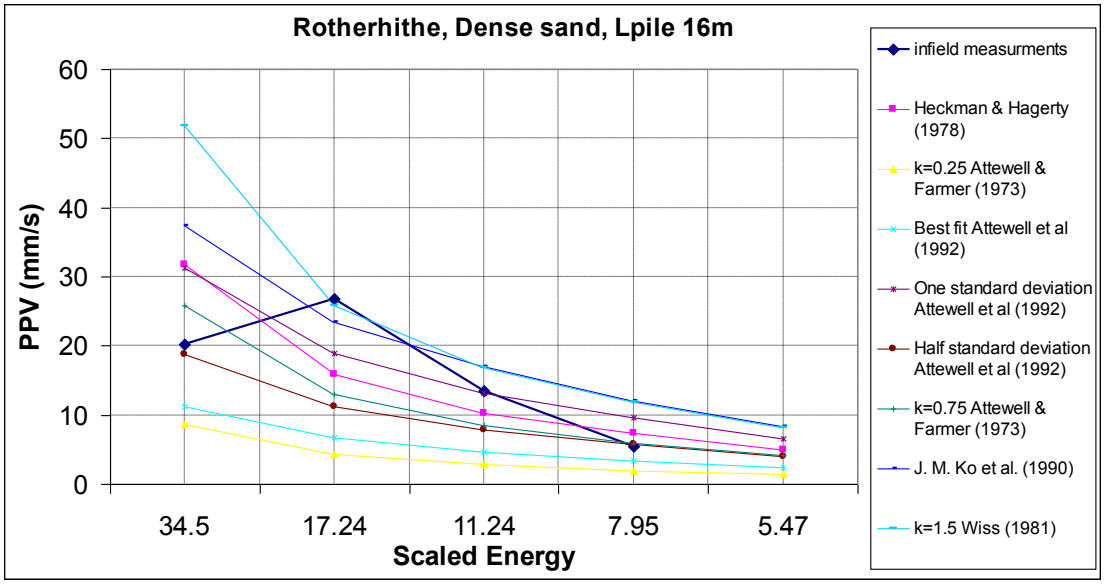

Figure 3.95: The comparison between prediction models and infield measurements at Lpile 16m in Rotherhithe site, dense sand soil.

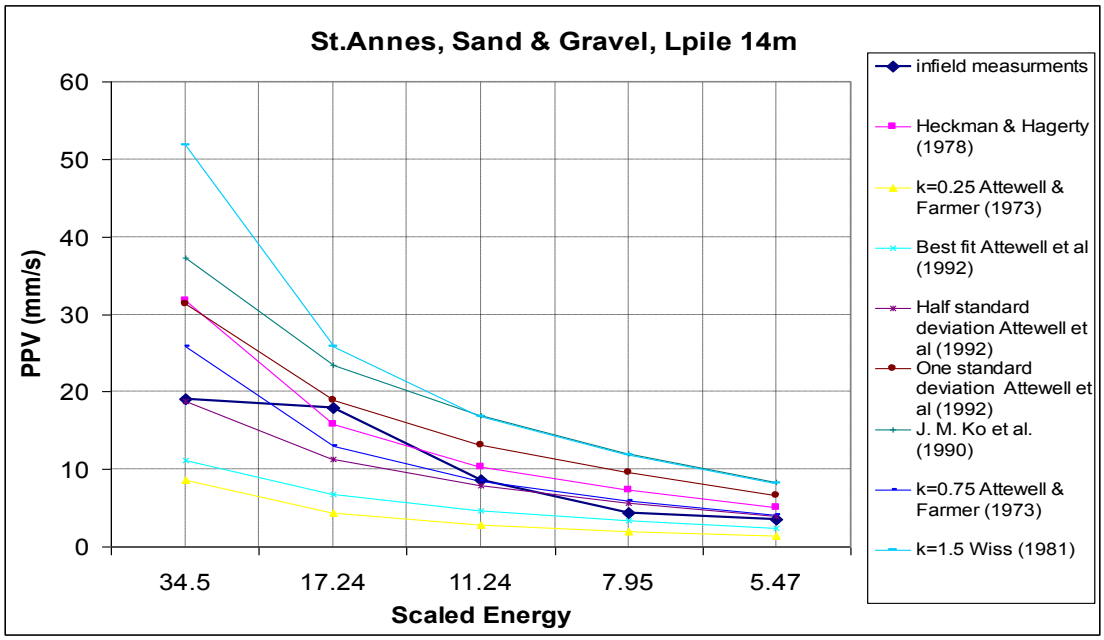

Figure 3.96: The comparison between prediction models and infield measurements at Lpile 14m in St.Annes site, sand & gravel soil.

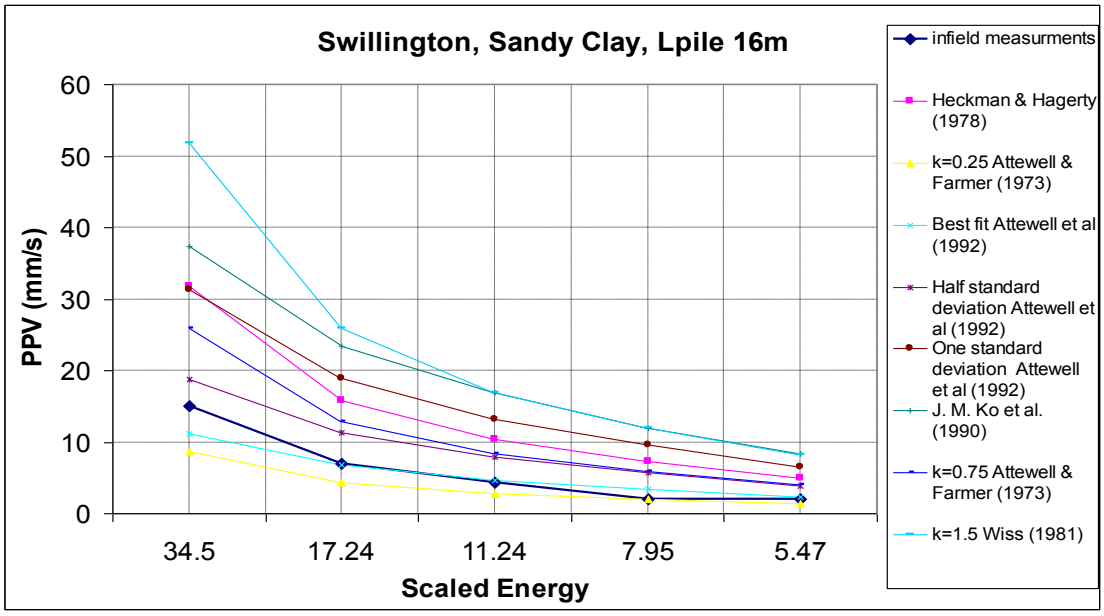

Figure 3.97: The comparison between prediction models and infield measurements at Lpile 16m in Swillington site, sand clay soil.

For a better comparison between predicted PPV (by different models) and measured PPV (from Uromeihy 1990) to show which model gives more reasonable values of PPV and closer to the measured PPV. The following

figures show the comparison between PPV (measured and predicted) for different groups of energies depending on hammers masss were which used in pile driving by Uromeihy (1990).

- **Heckman and Hagerty (1978) model at different energies:-**

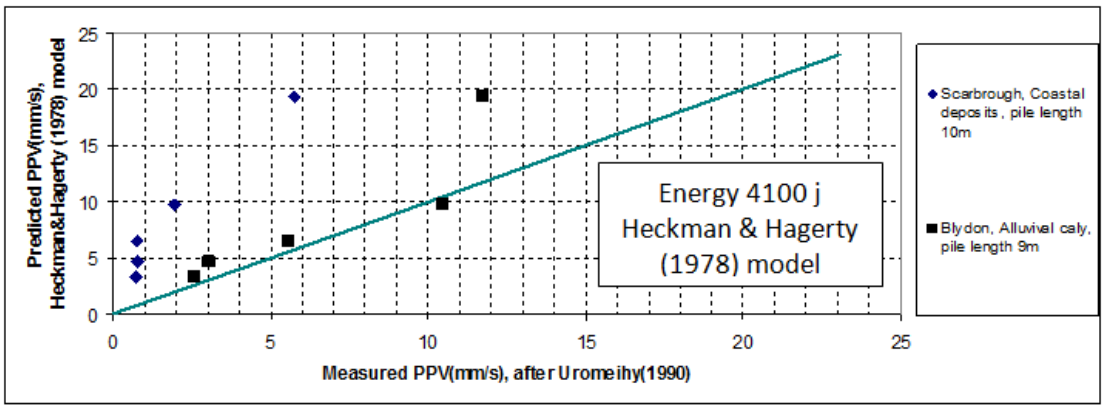

Figure 3.98: The comparison between predicted and measured PPV at energy of driving 4100 joule.

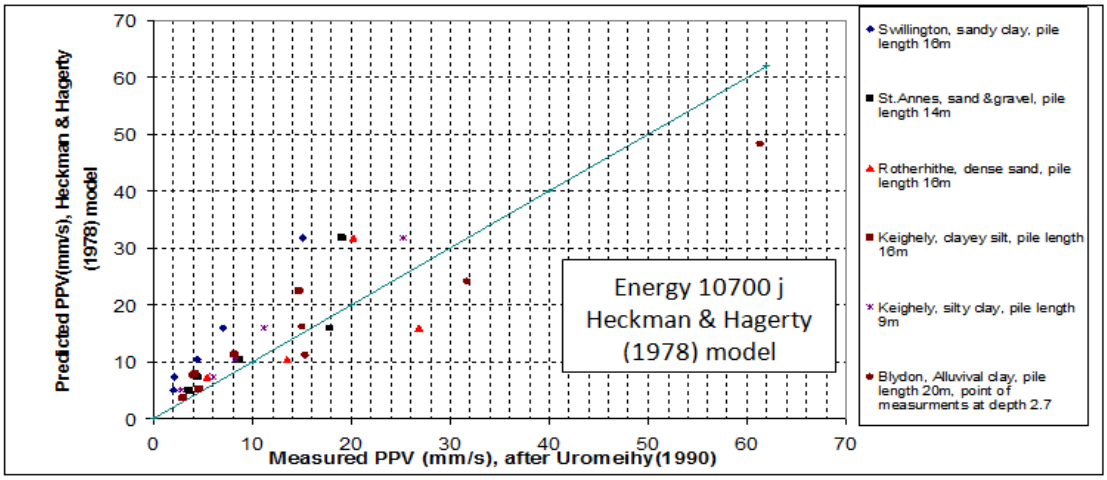

Figure 3.99: The comparison between predicted and measured PPV at energy of driving 10700 joule.

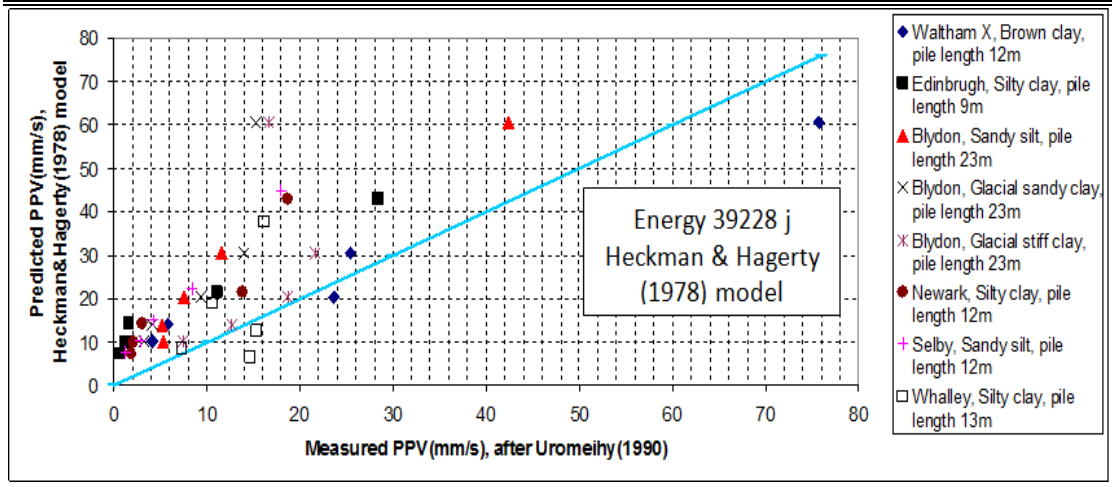

Figure 3.100: The comparison between predicted and measured PPV at energy of driving 39228 joule.

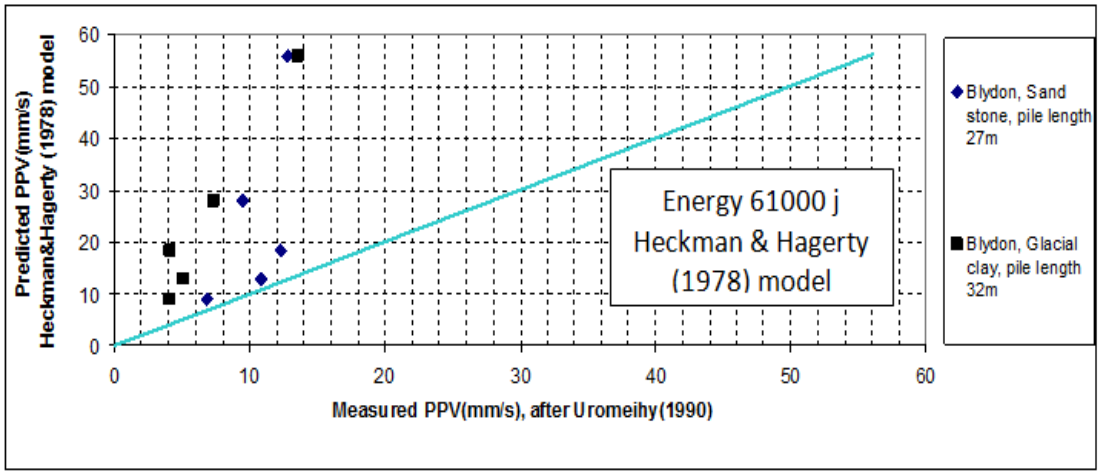

Figure 3.101: The comparison between predicted and measured PPV at energy of driving 61000 joule.

- **Attewell & Farmer (1973) model at k=0.25 for different energies:-**

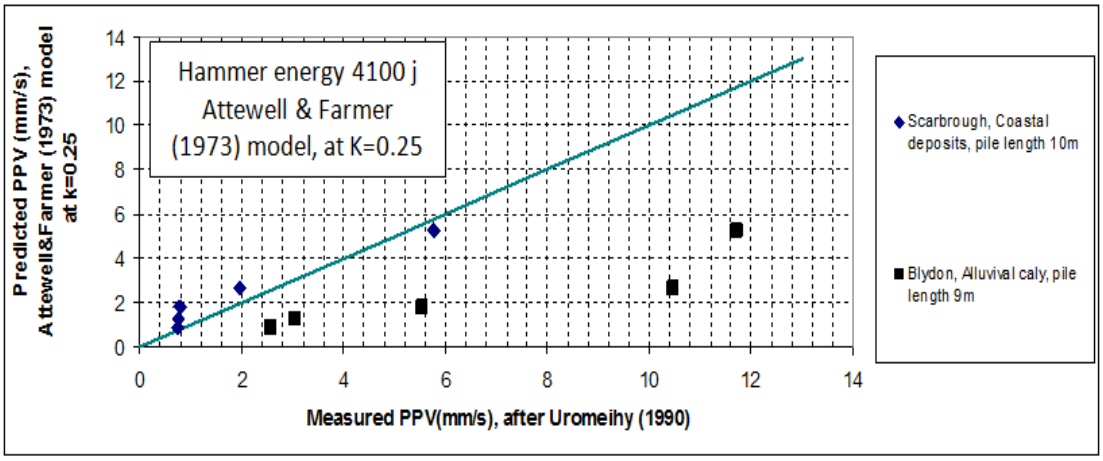

Figure 3.102: The comparison between predicted and measured PPV at energy of driving 4100 joule.

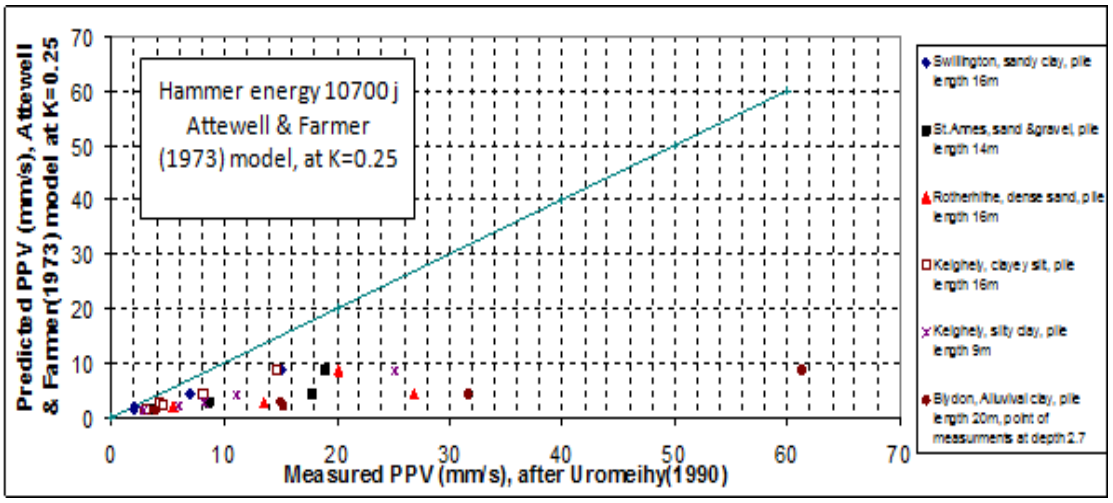

Figure 3.103: The comparison between predicted and measured PPV at energy of driving 10700 joule.

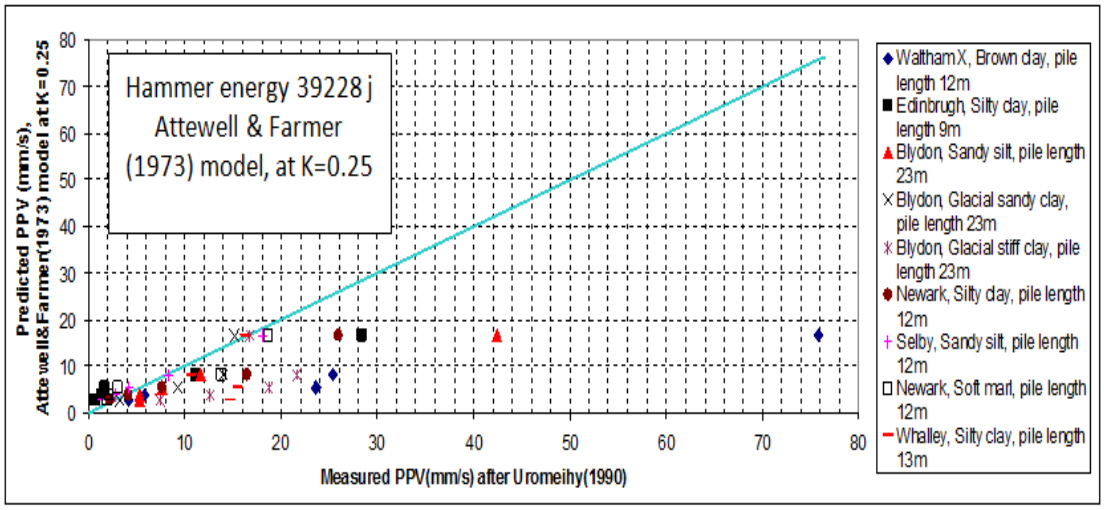

Figure 3.104: The comparison between predicted and measured PPV at energy of driving 39228 joule.

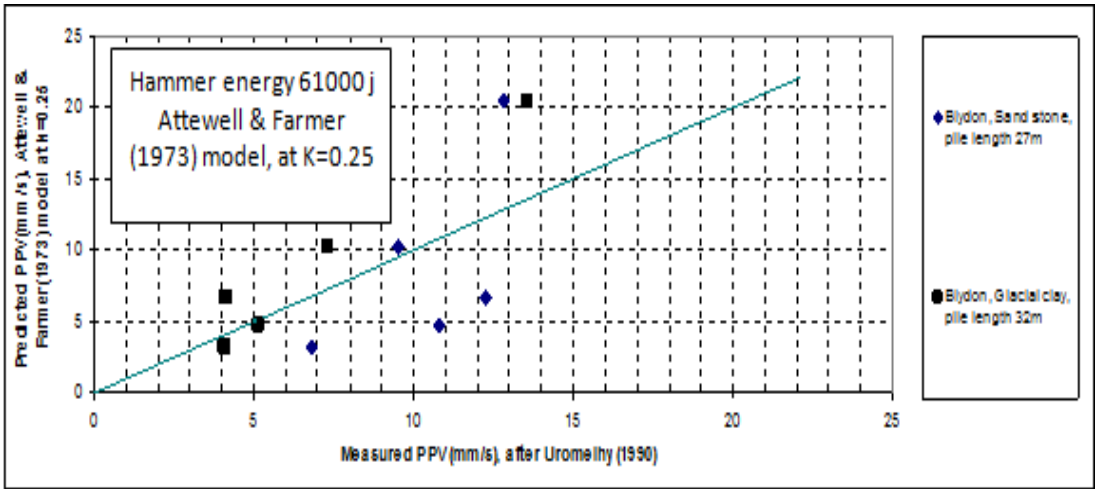

Figure 3.105: The comparison between predicted and measured PPV at energy of driving 61000 joule.

- **Attewell & Farmer (1973) model at k=0.75 for different energies:-**

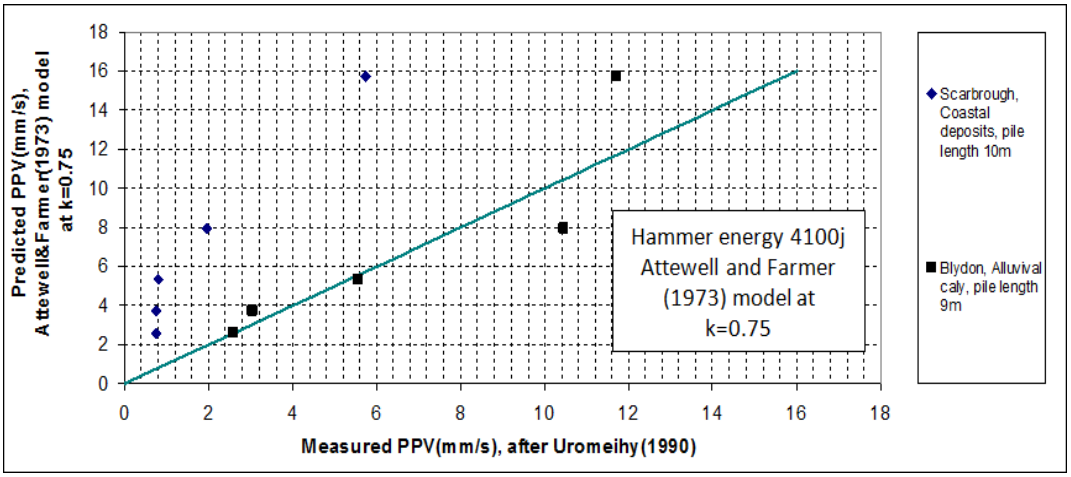

Figure 3.106: The comparison between predicted and measured PPV at energy of driving 4100 joule.

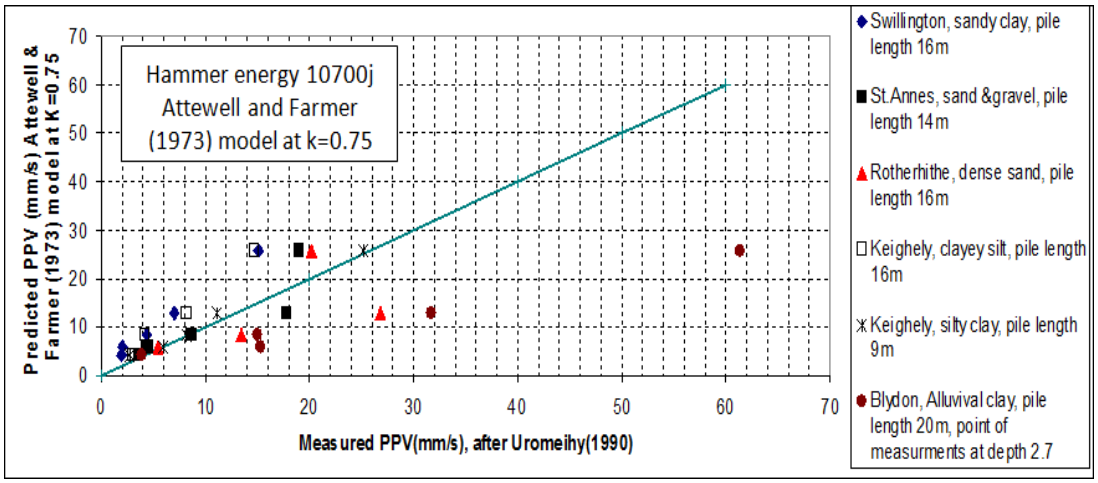

Figure 3.107: The comparison between predicted and measured PPV at energy of driving 10700 joule.

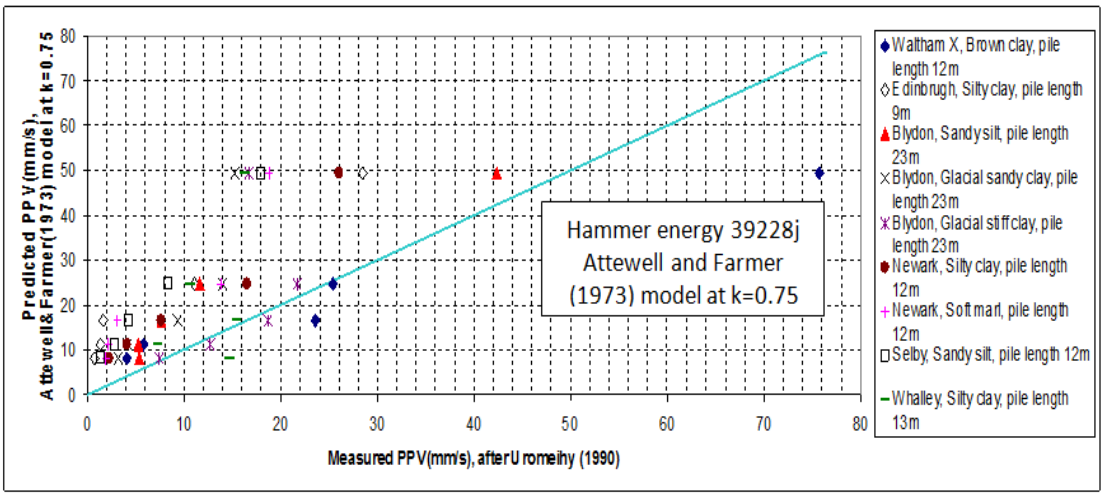

Figure 3.108: The comparison between predicted and measured PPV at energy of driving 39228 joule.

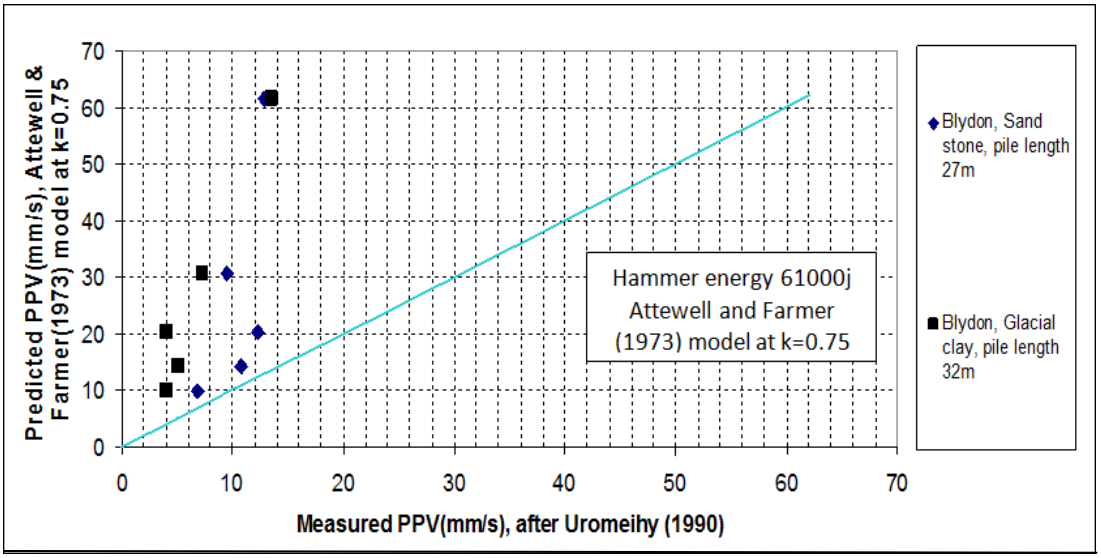

Figure 3.109: The comparison between predicted and measured PPV at energy of driving 61000 joule.

- **Attewell et al (1992) best fit model at different energies:-**

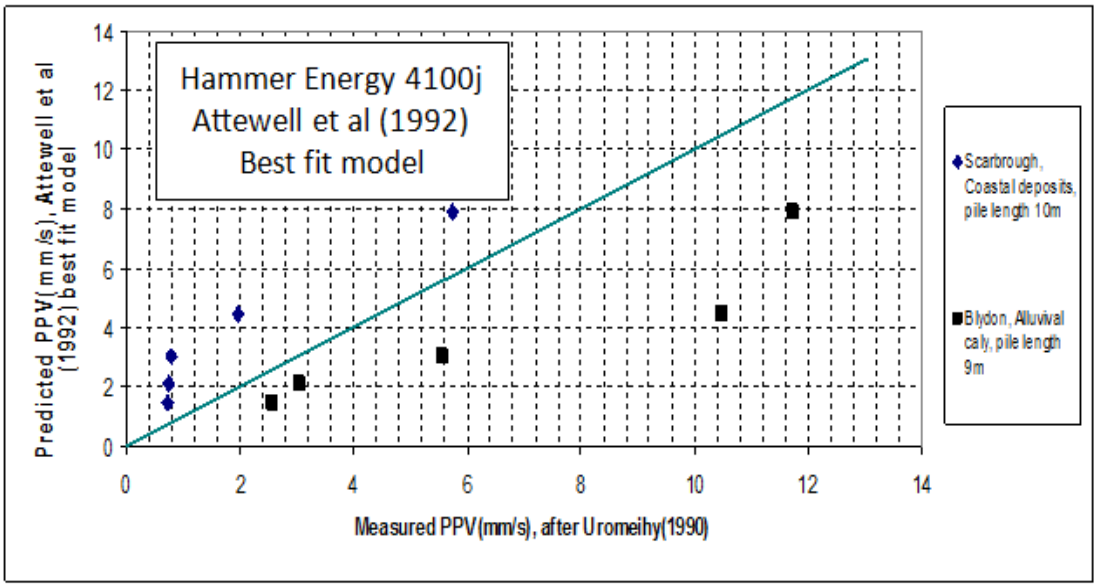

Figure 3.110: The comparison between predicted and measured PPV at energy of driving 4100 joule.

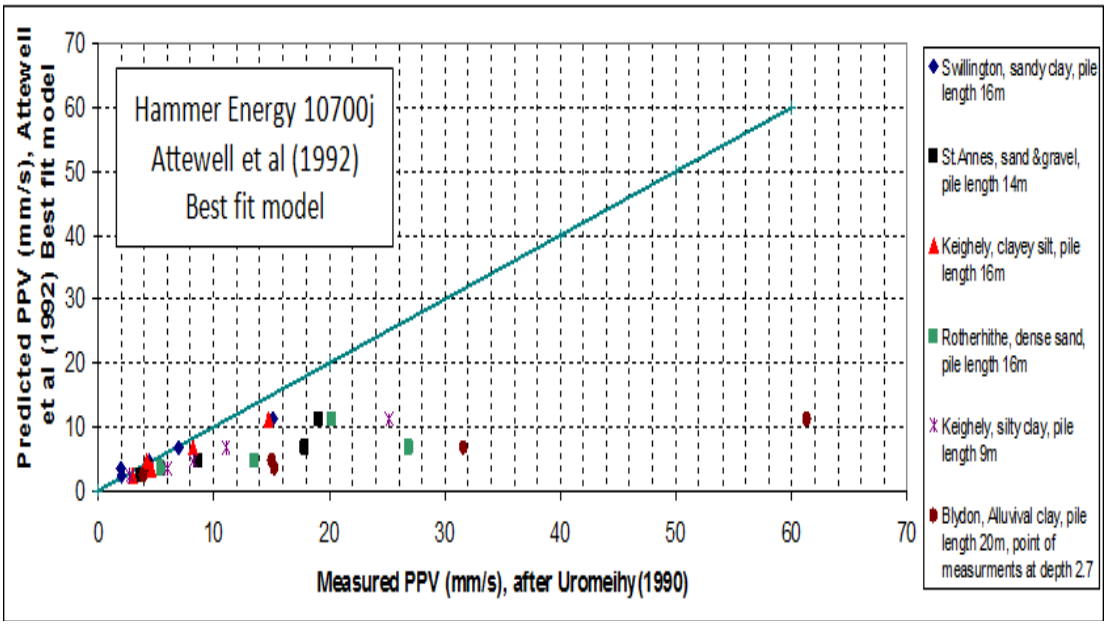

Figure 3.111: The comparison between predicted and measured PPV at energy of driving 10700 joule.

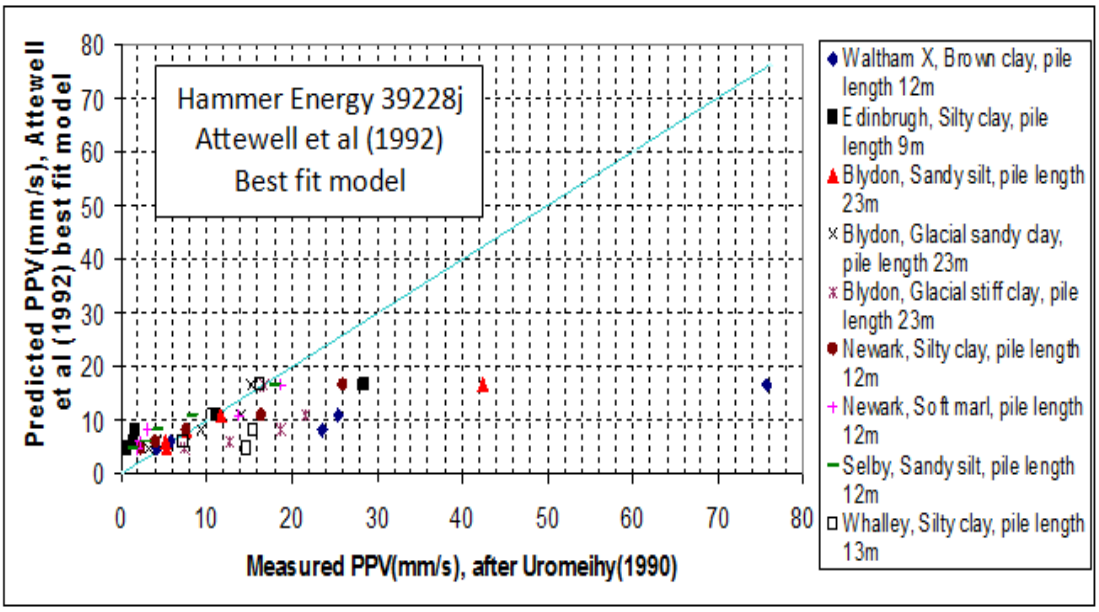

Figure 3.112: The comparison between predicted and measured PPV at energy of driving 39228 joule.

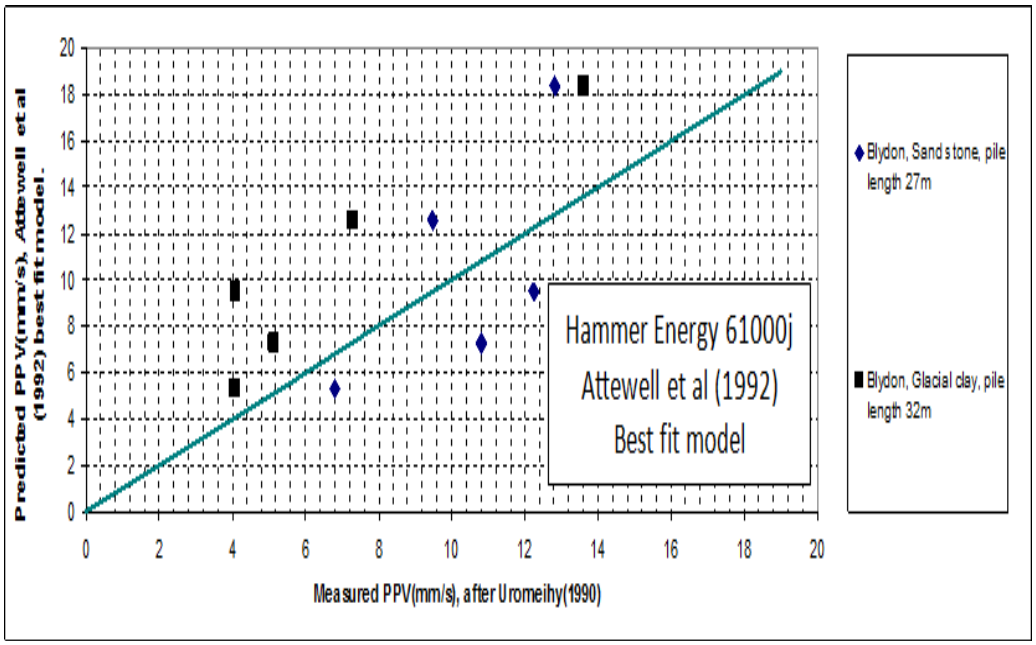

Figure 3.113: The comparison between predicted and measured PPV at energy of driving 61000 joule.

- **Attewell et al (1992) half standard deviation model at different energies:-**

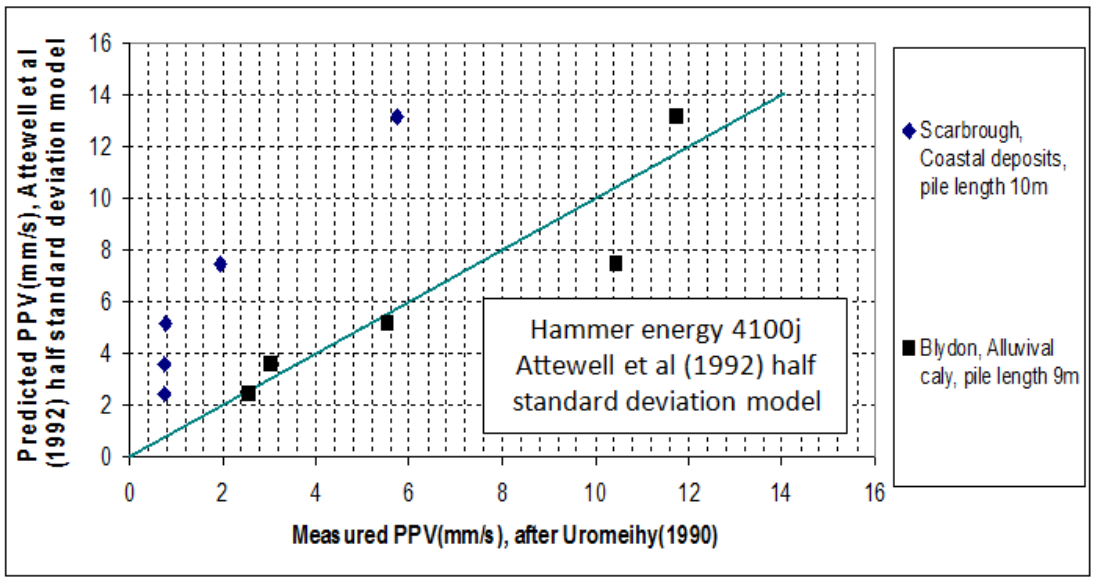

Figure 3.114: The comparison between predicted and measured PPV at energy of driving 4100 joule.

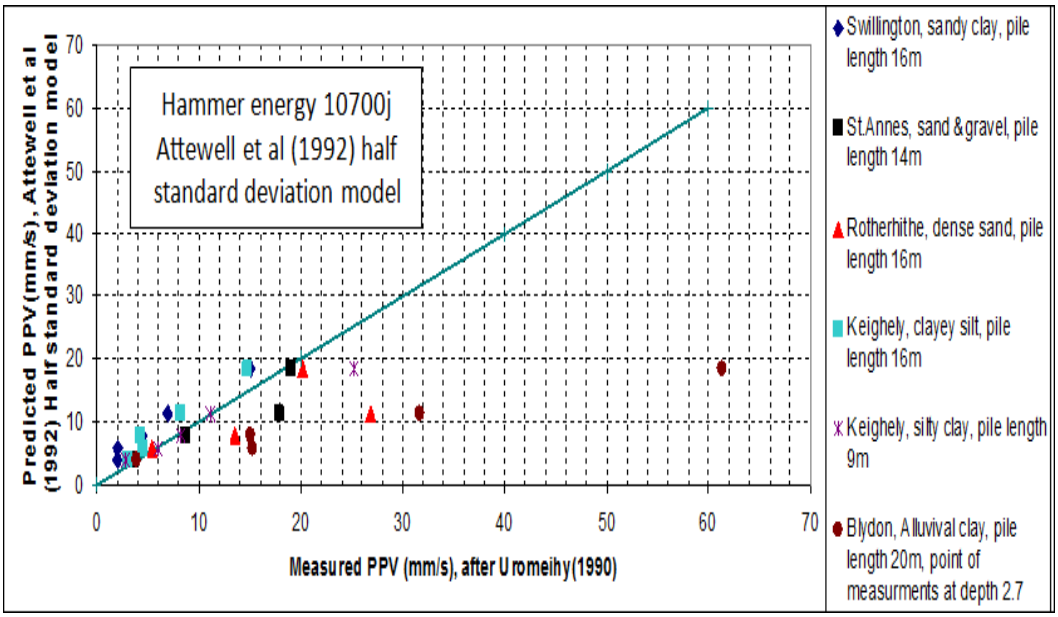

Figure 3.115: The comparison between predicted and measured PPV at energy of driving 10700 joule.

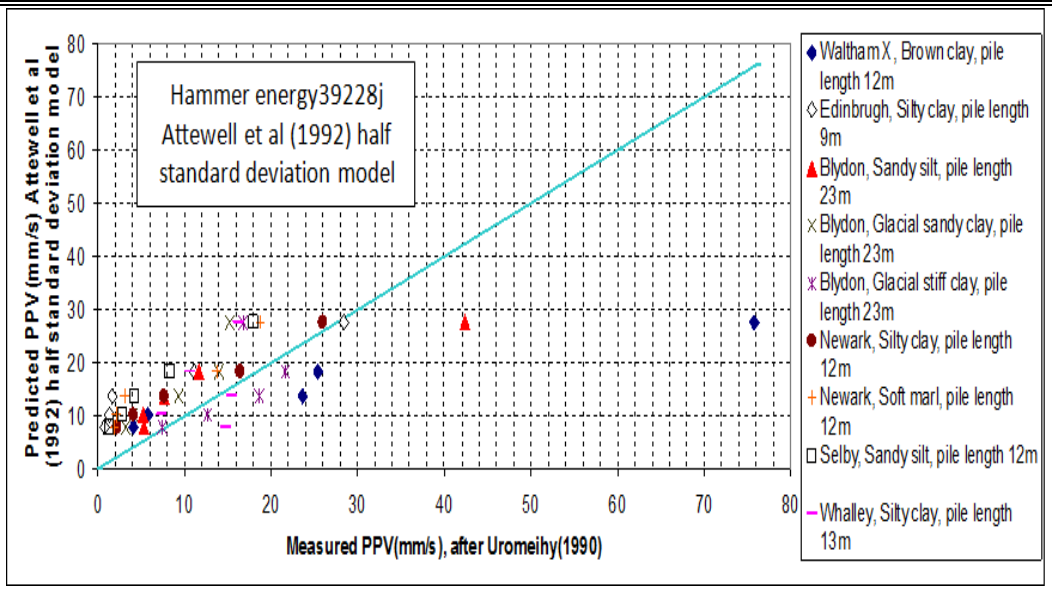

Figure 3.116: The comparison between predicted and measured PPV at energy of driving 39228 joule.

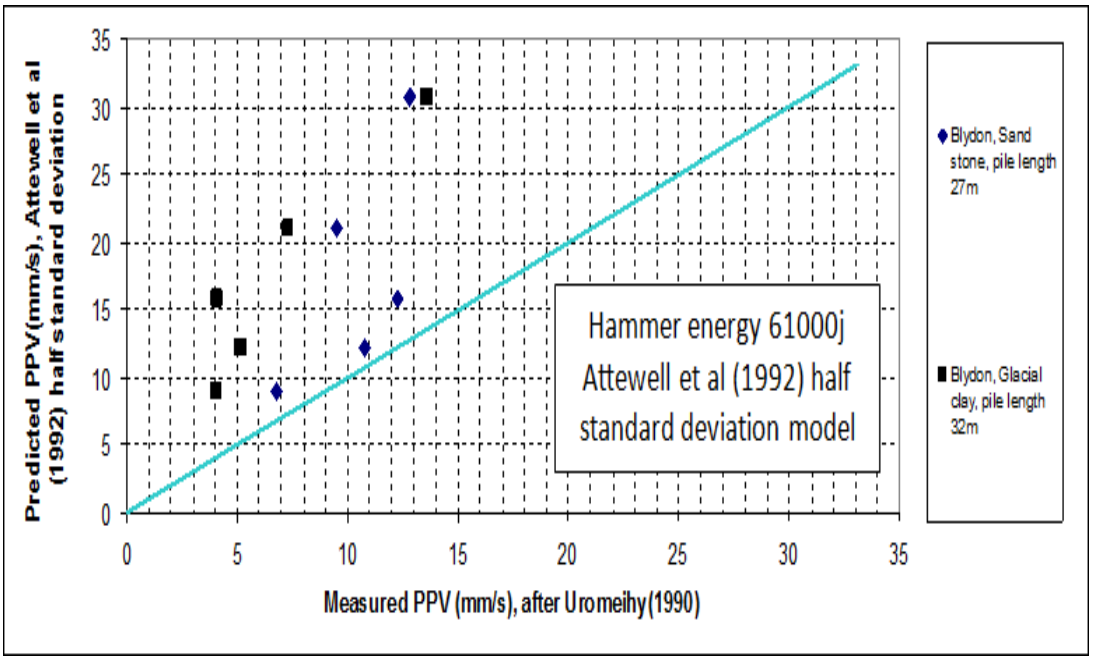

Figure 3.117: The comparison between predicted and measured PPV at energy of driving 61000 joule.

- **Attewell et al (1992) one standard deviation model at different energies:-**

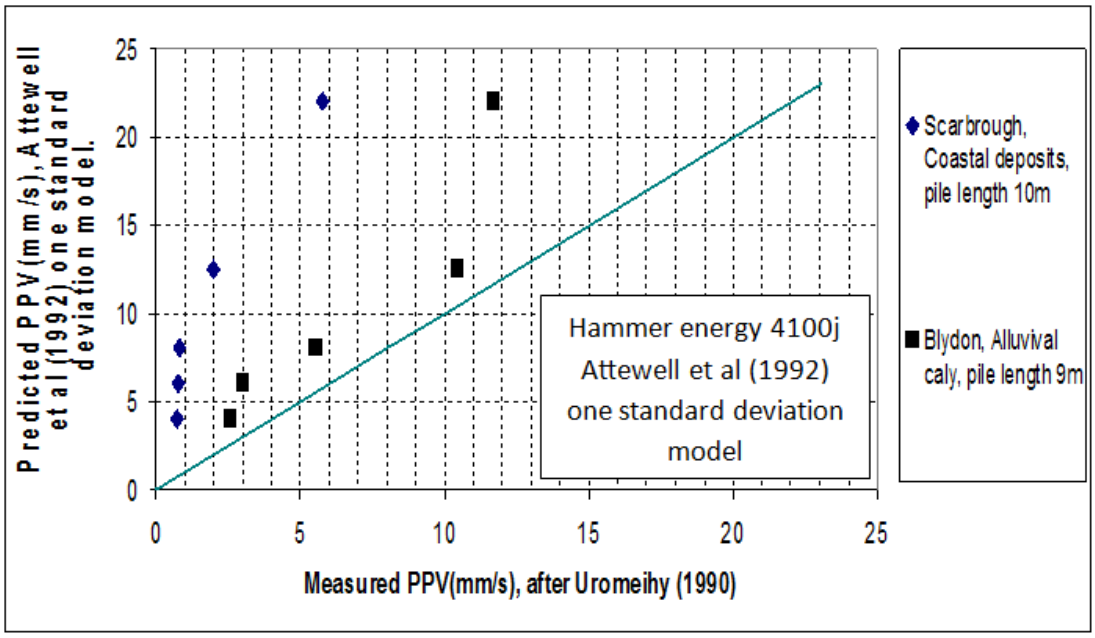

Figure 3.118: The comparison between predicted and measured PPV at energy of driving 4100 joule.

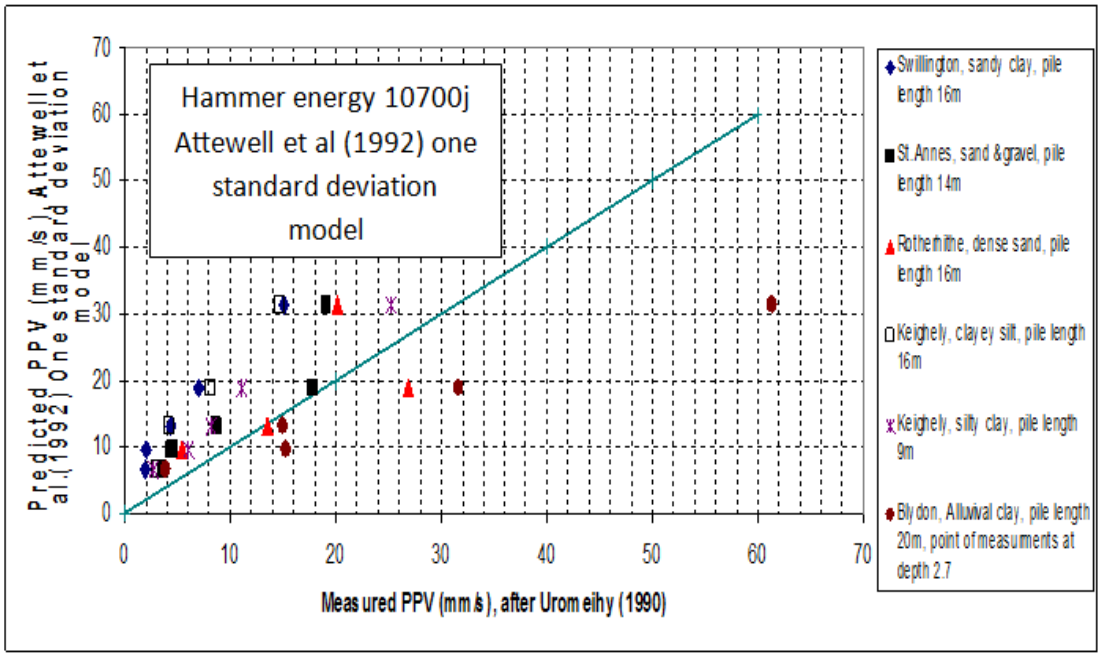

Figure 3.119: The comparison between predicted and measured PPV at energy of driving 10700 joule

.

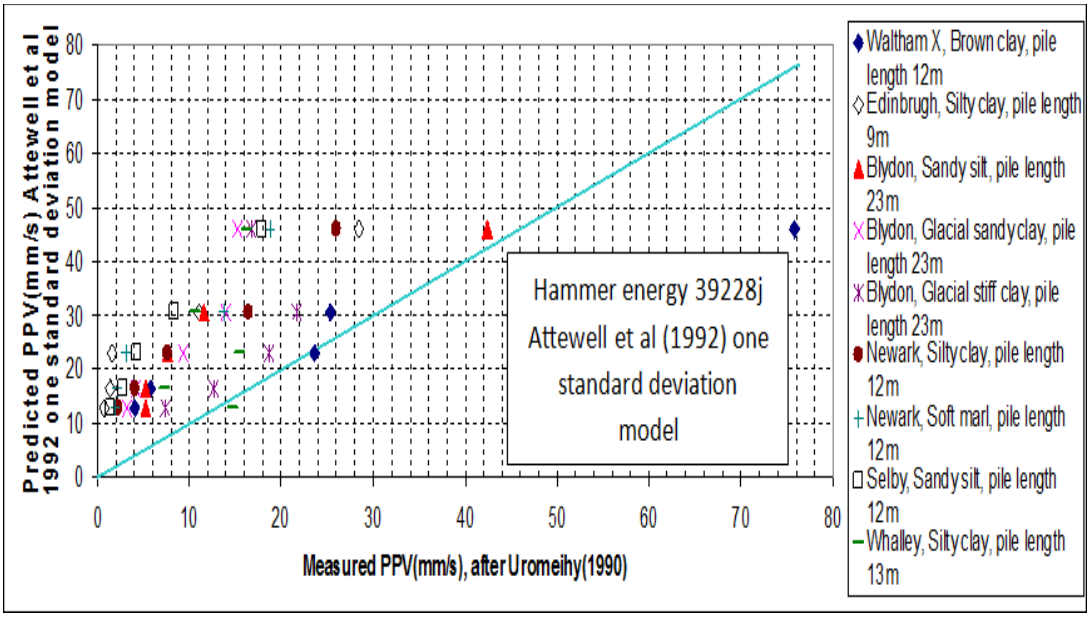

Figure 3.120: The comparison between predicted and measured PPV at energy of driving 39228 joule.

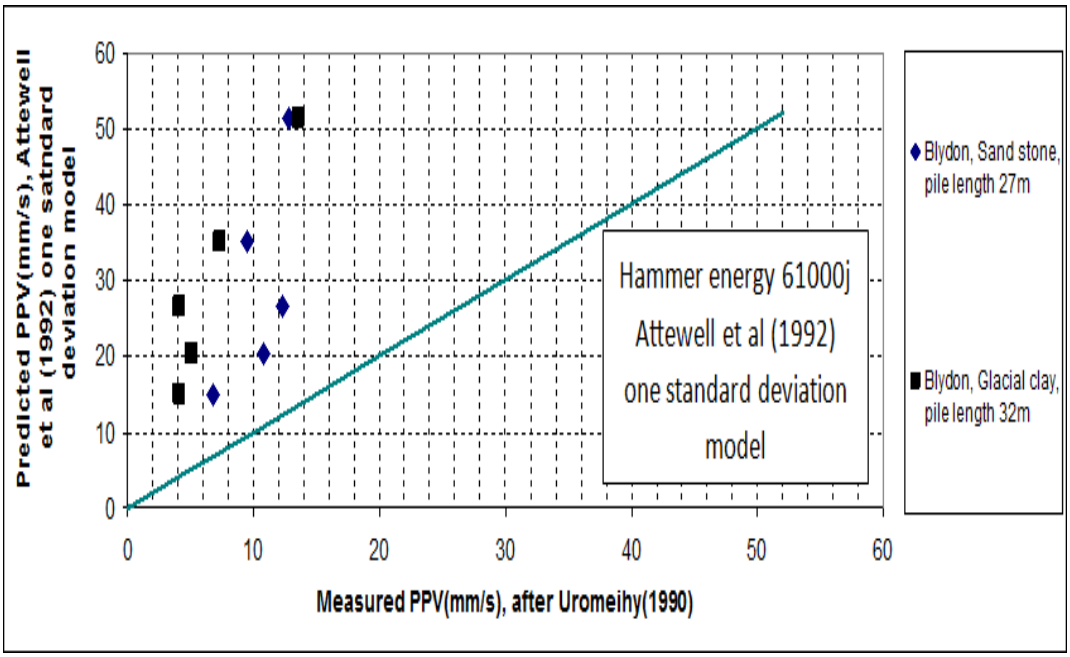

Figure 3.121: The comparison between predicted and measured PPV at energy of driving 61000 joule.

- **J.M.Ko (1990) model at different energies:-**

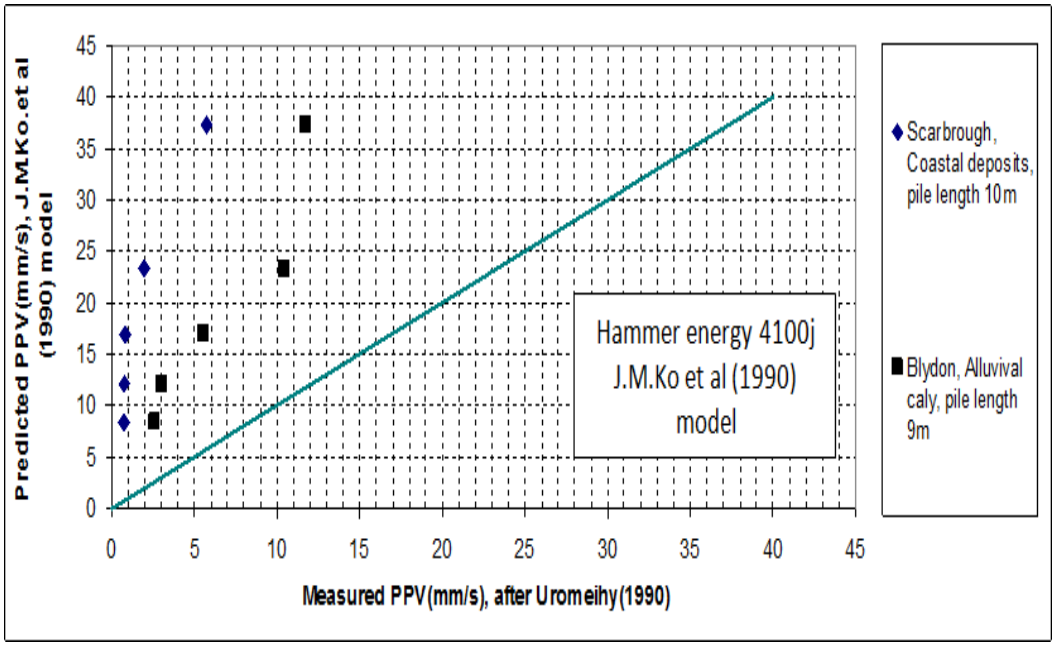

Figure 3.122: The comparison between predicted and measured PPV at energy of driving 61000 joule.

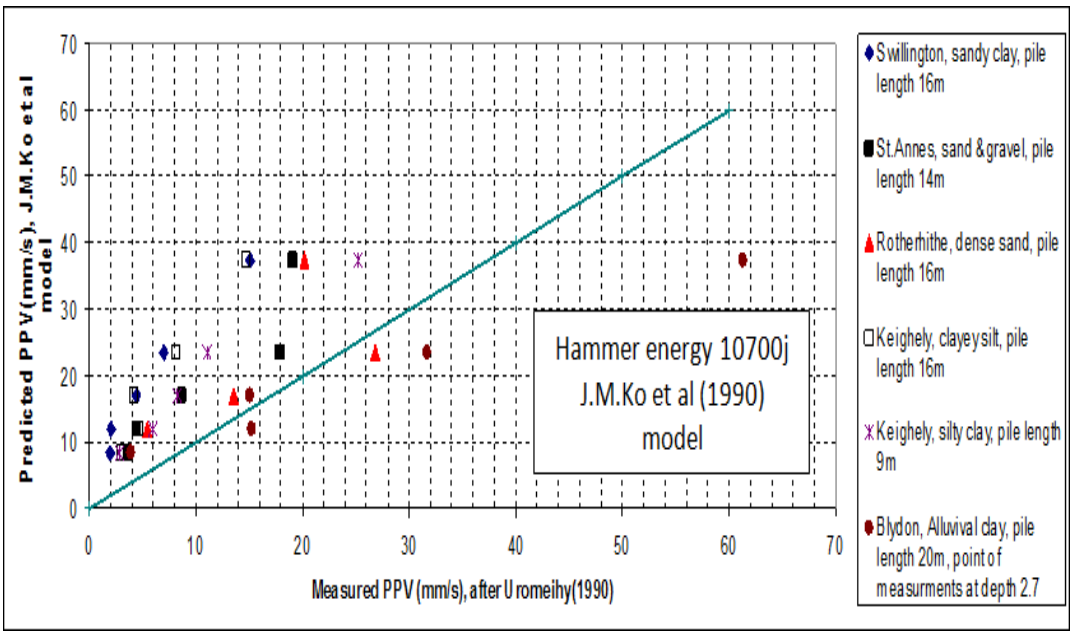

Figure 3.123: The comparison between predicted and measured PPV at energy of driving 10700 joule.

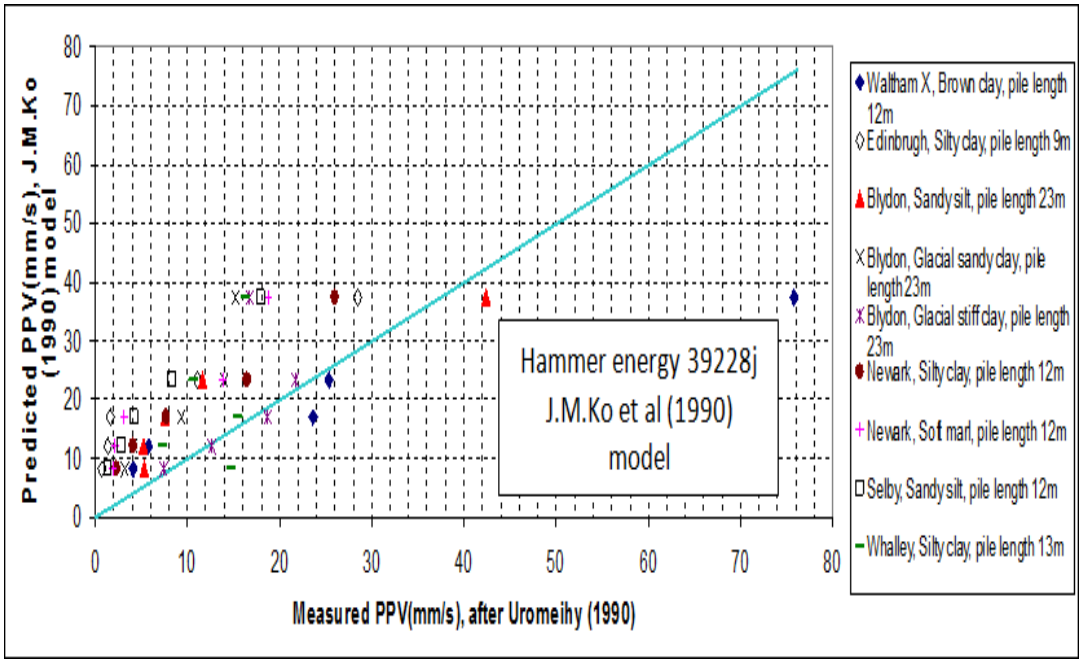

Figure 3.124: The comparison between predicted and measured PPV at energy of driving 39228 joule.

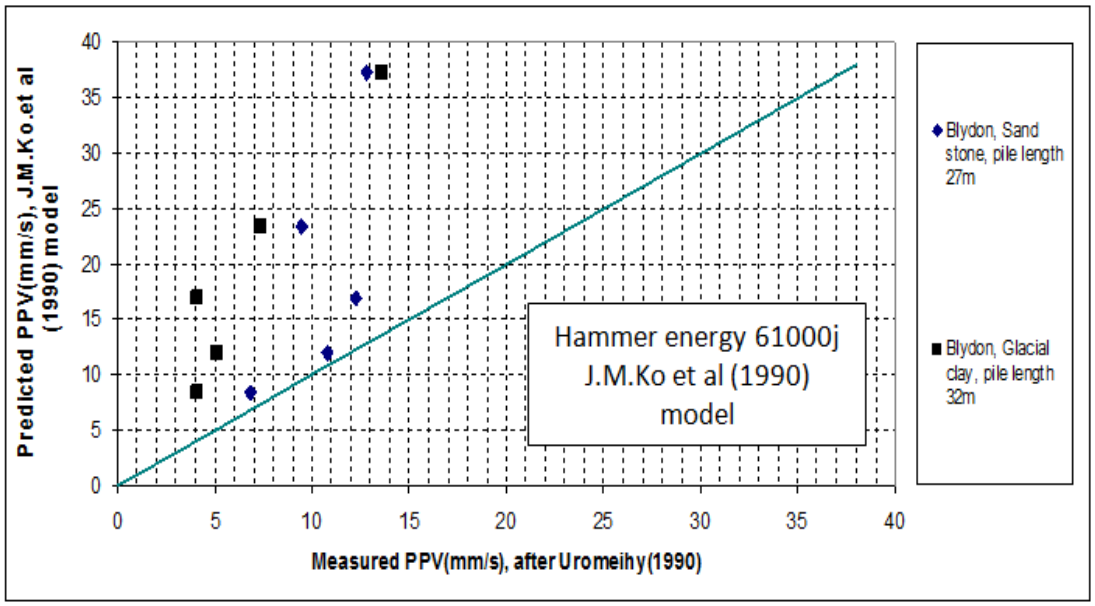

Figure 3.125: The comparison between predicted and measured PPV at energy of driving 61000 joule.

- **Wiss (1981) model at k=1.5 for different energies:-**

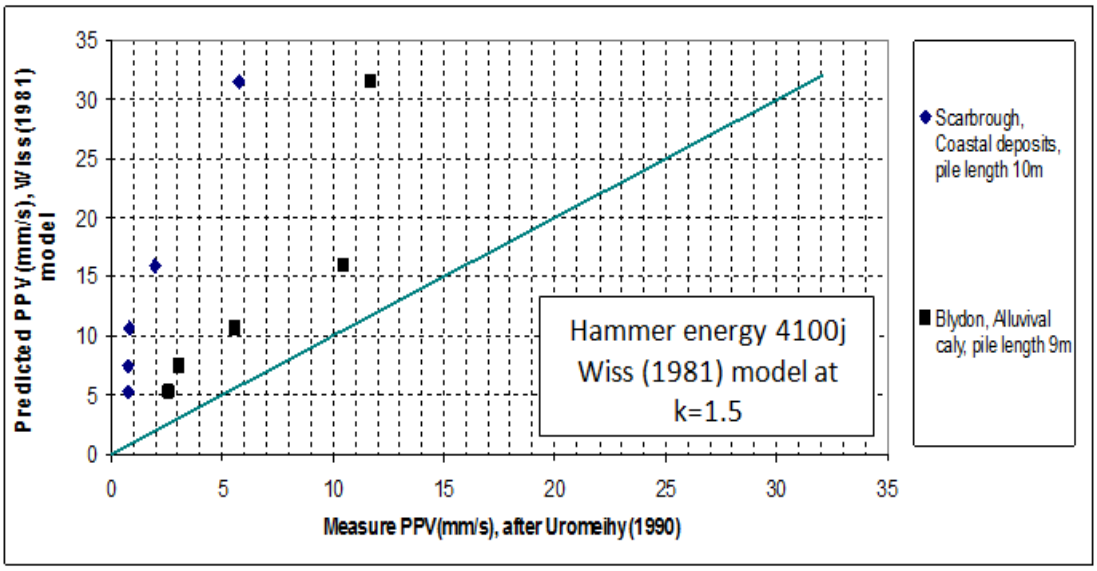

Figure 3.126: The comparison between predicted and measured PPV at energy of driving 4100 joule.

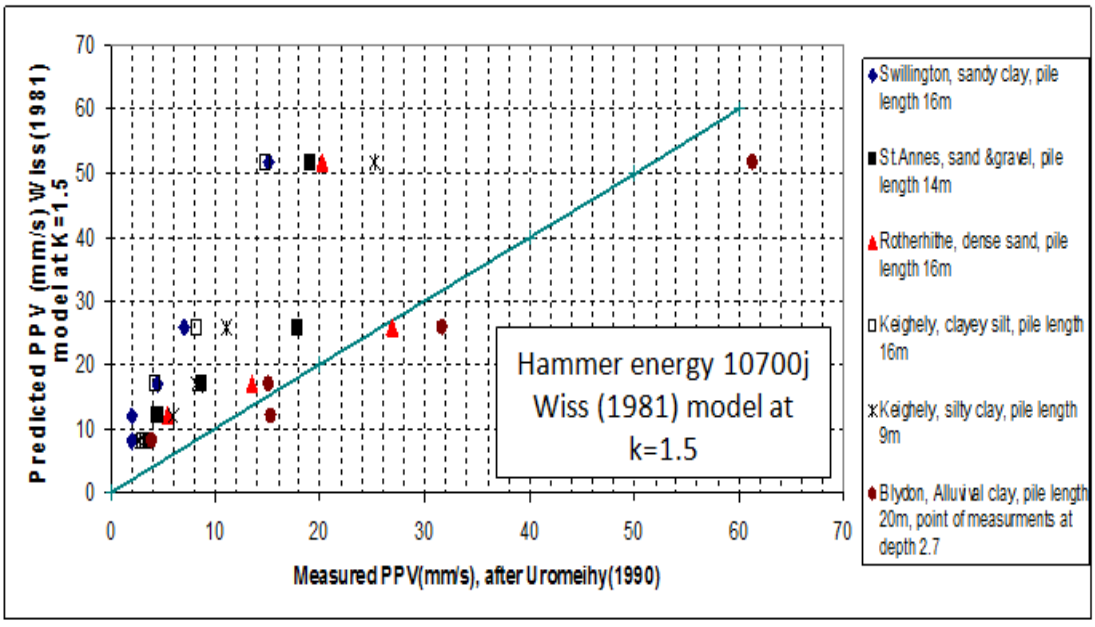

Figure 3.127: The comparison between predicted and measured PPV at energy of driving 10700 joule.

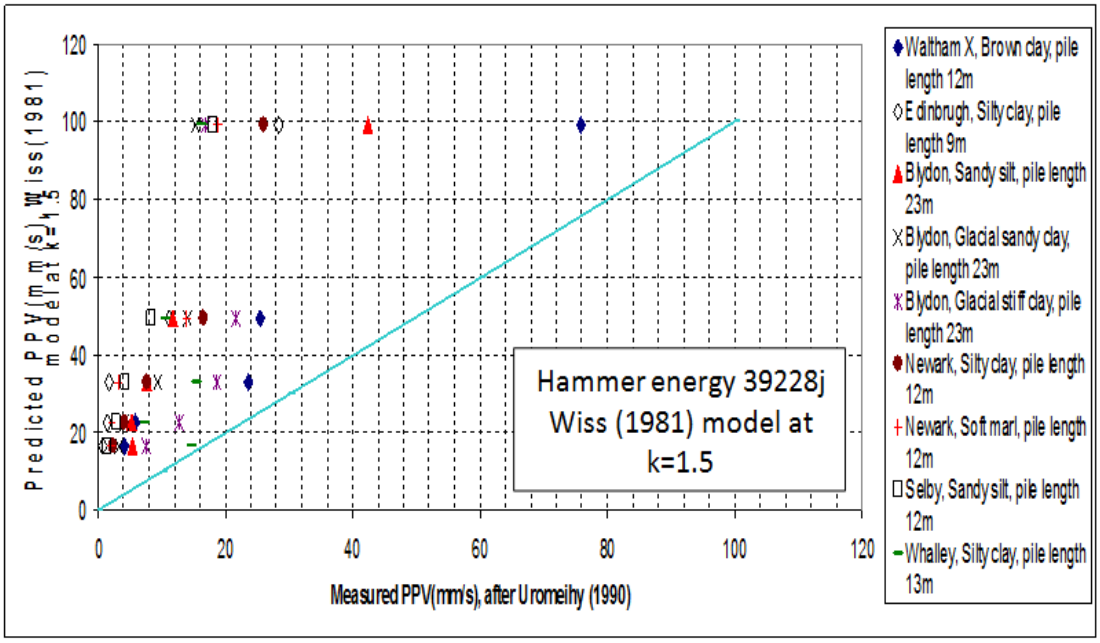

Figure 3.128: The comparison between predicted and measured PPV at energy of driving 39228 joule.

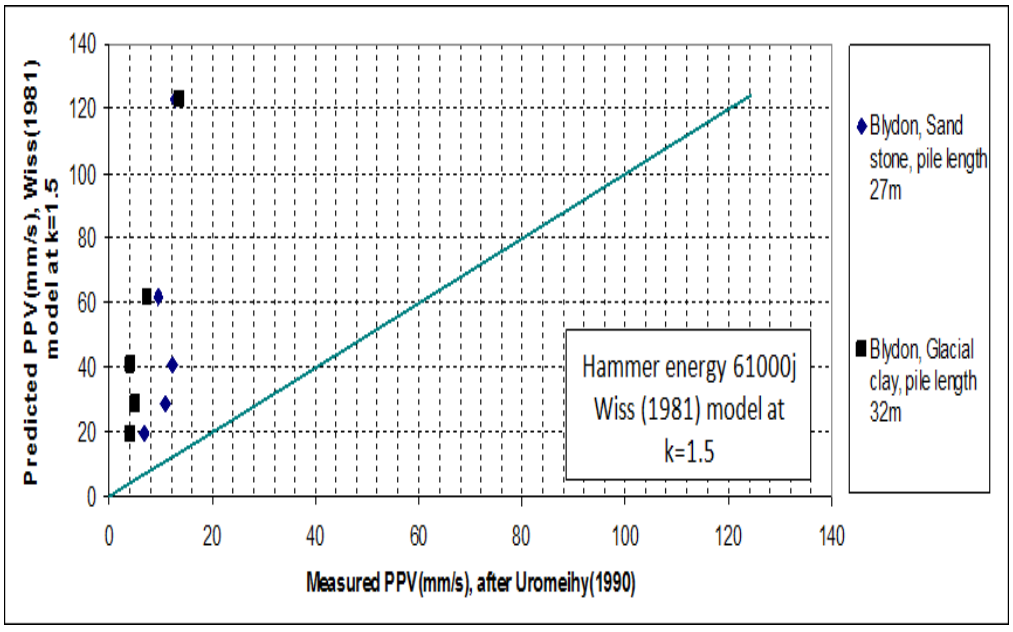

Figure 3.129: The comparison between predicted and measured PPV at energy of driving 61000 joule.

From the previous graphs for the comparison between measured and predicted PPV it can be seen that for both models of Attewell & Farmer at k=0.25 and Attewell et al (1992) best fit give a close trend to the infield measurements

especially at lower values for measured PPV. The following conclusion and review for each model show reasonable and accepted point of view to illustrate the difference between PPV values (measured and predicted).

Heckman and Hagerty (1978)

The authors measured the intensity of ground vibration at different distances away from piles being driven. The piles were of different type, size and material. Heckman & Hagerty (1978) prediction model is expressed in Eq.3.3, which is a measure of ground intensity (usually the vertical vibration velocity).

The vibration velocity is not defined in terms of direction (vertical, horizontal or resultant components). The empirical factor is not dimensionless which has caused some confusing in the literature (Santos 2008), (Massarsch 2005). The authors related the K factor with a strong correlation with the pile impedance as shown in Figure 3.127, the ground vibration increased markedly when the pile impedance decreased (Massarsch 1992).

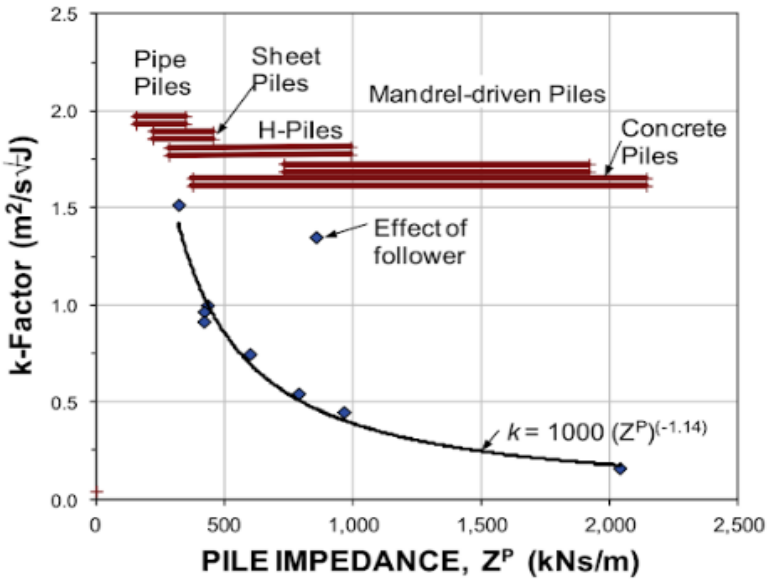

Figure 3.130: Influence of pile impedance on the vibration factor K, Heckman and Hagerty (1978).

By comparing the results from Heckman and Hagerty prediction model and other infield measurements it has been found the following:

- K factor is given for only 5 types of piles neglecting other types starting from timber piles, composite piles.
- The model shows that PPV depends only on three factors (pile impedance, source energy and distance from the source), but it has been found that there are different parameters affecting on PPV such as soil type, pile length, the cyclic loading effect.
- The type of driving machine and the method of driving are not mentioned briefly by the authors, it is known that the both parameters are very important and affect clearly on PPV values.
- Heckman & Hagerty (1978) model always gives a higher values close to the driving source especially in the first 9m away from the source of vibration.

Attewell and Farmer (1973) model

The authors analyzed the vibrations from driving various types of piles in different soil conditions. They proposed that PPV measured at distance from the energy source can be estimated as shown in Eq.3.10.

$$V = \mathrm{k}\frac{\sqrt{\mathrm{E}}}{\mathrm{r}} \qquad \text{(Eq.3.10)}$$

Where V is PPV (mm/s), E is the theoretical energy input at the source (joule), k is empirical factor ($m^2/s.\sqrt{j}$) and r is the distance from the driving source (m).

Attewell & Farmer (1973) concluded that losses due to material damping are small compared to losses due to geometrical damping. As a result, they suggested that material damping can be neglected for practical estimates of vibration from pile driving.

However, Attewell & Farmer (1973) suggested that a constant of proportionality, k, of 1.5 should be used for practical conservative prediction of ground vibrations due to pile driving.

Attewell and Farmer (1973) suggest an upper bound value of l.5 for sheet piles and 0.75 for other piles (SI units with velocity in mm/sec).

By comparing the results from Attewell and Farmer prediction model and other infield measurements it has been found the following:

- The author neglected other factors could affect on PPV values such as pile material, pile length and soil type.
- The prediction model didn't give the option for the design engineer to calculate the PPV at different depths in the ground or at the foundation base.
- The type of driving machine and the method of driving haven't been taken in consideration for the prediction model.
- At k = 0.25 the PPV values give a close trend to the infield measurements in case of clay soil and medium granular soil.
- At K= 1.5 PPV values relatively higher than other infield measurements.

Whyley and Sarsby (1992) suggested values for factor K depends on soil type, stated that k = 1.5 as upper bound for stiff or dense sand, k = 0.75 as upper bound for firm to stiff or medium dense sand and k = 0.25 upper bound for soft or loose soil.

Other researchers have modified different conditions to reach the optimum value for the factor k and x for the following term in calculating PPV as shown in Eq.3.11

$$V(mm/s) = \mathrm{k}\left(\frac{\sqrt{\mathrm{W}}}{\mathrm{r}}\right)^{x} \qquad \text{(Eq.3.11)}$$

Where k = empirically determined constant of proportionality ($m^2/s\sqrt{J}$)

W = input energy (hammer energy) (J)

r = radial distance between pile and monitoring point (m)

x = empirically determined index (-).

simplified models are employed to gain a useful insight; for example, the soil may be represented as an elastic half-space or as a layered medium (Skipp 1984). Soil is an elasto-plastic material. Since a suitable equation for vibration propagation cannot be derived for such a material, propagation is assumed as shown in Eq.3.12.

$$V = C.E^{y}/r^{x} \qquad \text{(Eq.3.12)}$$

where V = peak particle velocity, E = energy, r = distance between source and receiver C, x, y = constants.

Martin (1980) stated that a propagation law of the form: $V \alpha E^{0.5} r^{x}$ is often assumed, where the distance is considered equal to radial distance (measured horizontally) as surface or Rayleigh waves are the main provider of vibration. The constant x said to take into account both geometrical and internal damping. The value of x usually taken between 0.5 and l.5. The constant of proportionality (C) is probably influenced by soil conditions and/or source of energy (i.e. hammer or pile type).

Nilsson (1989) stated that several field studies have shown that k does not exceed 0.75 for driving of piles and 1.5 for driving of sheet piles.

Table 4:14 summarize the different proposed values for factors k and x for the best prediction of PPV.

Table 3.14: Summary of values of parameters used in different prediction models, modified after Hope & Hiller (2000).

Author	Parameters		Velocity component
	X	K	
Attewell & Farmer (1973)	**1**	1.5	Vertical PPV
Whyley & Sarsby (1992)	1	0.25 (soft or loose soil) 0.75 (stiff or medium dense soil) 1.5 (stiff or dense soil)	
Attewell et al. (1992a)	0.87	0.76	Vertical PPV
Hiller & Crabb (1998)		3 (stiff or medium dense soil)	
Head & Jardine (1992)	1	1, 5 (for $r > 0.5$ m)	SRSS
	1.54 at foundation base	0.2 at foundation base	
BSI (1992a)	1	0.75	
CEN (1998)	1	0.5 (soft cohesive soil) 0.75 (stiff cohesive soil) 1.0 (very stiff cohesive soil)	
ArcelorMittal (2008)	1	**Impact driving** 0.5 (soft cohesive soil, loose granular media, loose fill and organic soils) 0.75 (stiff cohesive soils, medium dense granular media, compact fill) 1.0 (very stiff cohesive soil, dense granular media, rock, fill with large obstructions) **Vibratory driving** 0.7 (all soil conditions)	

Svinkin (2008) empirical model

Svinkin (2008) presented a development of the energy-based relationship for the prediction of ground vibrations due to pile driving. Svinkin's model is based on determination of the vibration velocity on the pile head, and from that computes the ground vibrations. The relationship in Eq.3.8 is proposed for the ground vibration due to pile driving

Where Vg = ground vibration (mm/s) (PPV), Vp = pile vibration at the pile head and it can be calculated from Eq.3.9

The pile impedance Zp is dependent of the pile density, the wave propagation velocity in the pile and the cross section area of the pile. The pile impedance can also be expressed as a function of the modulus of elasticity, see Eq. 3.13, after (Massarsch, 2000).

$$Zp = \rho . C . Ap = \frac{E.Ap}{C} \qquad \text{(Eq.3.13)}$$

Where: Zp = pile impedance [Ns/m], ρ = pile material density [kg/m3], C = wave propagation velocity in the pile [m/s], Ap = cross section area of the pile [m^2] and E = modulus of elasticity [Pa]

Taking a general look at Svinkin (2008) model, it can be seen that is the only model which include a lot of effective parameters on PPV values. Pile impedance (pile material) and pile length affect directly on energy transfer to the soil which could lead to higher or lower PPV values. Using the term of wave propagation velocity in the pile to estimate PPV gives the model more realistic expectation for calculating PPV because it is confirmed by (Massarsch 1993) that the energy of driving transfer through the pile first then to the soil, therefore the velocity in the pile could be responsible for producing waves in soil. Svinkin model shows that the velocity in pile depends on pile density, modulus of elasticity of the pile which may gives higher prediction of PPV.

By comparing the results from Svinkin (2008) model and other infield measurements it has been found the following:

- The velocity in the pile CB at Svinkin model always tend to be very high due to the high magnitudes of pile impedance and pile stiffness which leads to high values of PPV.
- Svinkin model at high value of CB and high value of driving energy gives very high PPV values compared with other infield measurements at the same conditions.
- Svinkin model could give reasonable PPV values for low energy driving and low pile impedance.
- Svinkin model don't include soil stiffness and its effect on PPV values.
- Measuring PPV at different depths is not available in Svinkin model.
- The method of driving is not taken into account by the author, it is known that the method of driving affect clearly on PPV values.

Attewell et al. (1992) model

Attewell et al. (1992a and 1992b) found that a quadratic regression curve was a better fit to field data from measurements of ground vibrations due to pile driving than the previously used linear regression curve (Attewell & Farmer, 1973). The developed model is shown in Eq.3.5

Where v (PPV) = vibration velocity (mm/s), x_1, x_2 and x_3 = constants of proportionality, W_0 = input energy (J), r = distance between source and point of interest (m). Constants x_1, x_2 and x_3 are functions of the soil conditions at the site of pile driving. Proposed values of the constants of proportionality are given according to Deckner (2013) as shown in Table 3.6. For impact vibratory pile driving, Table 3.7 illustrated constants value

The authors proposed that the values for half a standard deviation should be used for normal construction work while one standard deviation should be used where high security against vibration is needed. For the best fit line there is a

risk of exceeding the estimated values of 50%, for half a standard deviation the risk is 31% and for one standard deviation the risk is reduced to 16% (Attewell et al., 1992b), adapted from (Deckner 2013).

By comparing the results from Attewell et al., 1992b model and other infield measurements it has been found the following:

- The model doesn't include soil stiffness and its effect on PPV values.
- Measuring PPV at different depths is not available by the model.
- For the best fit line the PPV is higher than the PPV at using half standard deviation and one standard deviation.
- One standard deviation constants gives lower PPV values.

J. M. Ko, et al. (1990) model

The authors performed an experimental study for calculating PPV values in a specified distance from the vibration source. PPV values were plotted vs. distance from the vibration source. The investigation yielded the attenuation curve which accommodates energy, distance and damping coefficients (material and geometric damping). J. M. Ko, et al. used data from a study location and obtained α dan V parameters at distance r = 1m from the driving source for alluvial silty sand soil. The reference values are $\alpha = 0.04m^{-1}$ dan V = 70 mm/s. J.M.Ko et al. model is given in Eq.3.4.

Where V is PPV, r is the distance from the driving source. It can see that J.M.Ko et al model included the damping coefficient in calculating PPV and it consider being one of the few models which depend on soil type effect on PPV values represented in material and geometric damping. Each different type of soil has its own damping coefficients. Damping control the propagation of wave through the soil by attenuates the velocity by the distance from the driving source.

By comparing the results from J. M. Ko et al. (1990) model and other infield measurements it has been found the following:

- The model gives reasonable and accepted values of PPV in general and a close trend to the infield measurements.
- The model is based on experiments for granular soil (silty sand), it may be gives other values for damping coefficient for other types of soil which will affect on PPV results.
- The model doesn't depend directly on driving energy which is very effective parameters for calculating PPV.
- J. M. Ko, et al model gives relatively high values of PPV close the vibration source for (r < 6m).
- For the same distance of measuring PPV J. M. Ko et al model gives the same PPV values however the soil, energy, pile material, pile length or any other variables are different, this consider technically not realistic.
- The model doesn't include soil stiffness and its effect on PPV values, however the model depends on geometric and material damping the model cannot express the different types of soil on PPV.
- Measuring PPV at different depths is not available by the model.

Wiss (1981) model

Wiss (1981) performed an independent research and state that the maximum particle velocity can be closely related to Eq.3.21.

$$V = \left(\frac{\sqrt{W0\ (joules)}}{r\ (m)}\right) \qquad \text{(Eq.3.14)}$$

Wiss suggested that the value from above equation is scaled energy which is similar with Attewell & Farmer (1973) for determining maximum particle velocity as shown in Eq.3.2.

Where K is a constant relied on type of soil. Wiss also conclude that vibration level produced by pile driver is different for clay soil and sand soil, and dry sand or wet sand as well. Therefore, Wiss used K factor to distinguish the

effect of soil type. Wiss attributed to different between PPV values for different types of soil to the difference between the frequencies of soil.

Wiss stated that particle velocity can be expressed as $2\pi fA$, in which f is frequency (cps) and A is amplitude (displacement). Impact vibrations produced by pile driving have characteristic frequencies depending on the type of soil. A loose alluvial fill has natural frequencies of about 5 to 10 cps, clay soils vary between 15 and 25 cps, sand between 30 and 40 cps. That leads to different values of PPV depends on soil type. It could be other reason support the effect of soil type on PPV values with the other views of the effect of damping coefficients and soil stiffness.

3.14 Conclusions

Pile driving is a serious problem producing vibration due to the increase in establishing new communities including pile driving, therefore the hazard of pile driving earthborn vibration on the soil and the adjacent structures have to be studied to avoid any kind of damage. The chapter is summarized in the following points:

1. PPV prediction equations show many parameters to calculate PPV. The most effective parameters as shown in most previous equations were the hammer energy and the distance from the vibration source. There are other important not included in the prediction equations such as soil type. Svinkin (2008) illustrated enough parameters control PPV (i.e. wave propagation velocity in the pile, pile impedance, pile length beside hammer energy and the distance from the source.
2. A lot of models proved that the numerical analysis using finite element programmes such as (PLAXIS, ABAQUS, and COMSOL) are valid to drive a simply method to predict PPV values.
3. Theoretical, numerical, engineering models predicting PPV were investigated and show a good agreement with field measurement and

consider being valid methods to predict PPV and simulate the construction vibration effect.

4. Pile driving is considered as one of the main sources of vibration which are very harmful to the soil and the adjacent structures, due to their higher energy intensity leading to high values of PPV.
5. Plaxis model shows a validity to simulate pile driving effect on soil and predict PPV values. An agreement is done between Plaxis model and Petřík et al (2012) infield measurement to complete the verification of Plaxis model.
6. The decrease in peak particle velocity (PPV) with distance from the pile driving source is confirmed by the analysis.
7. The PPV of the born vibrations increases with the increase of the stiffness of surrounding soils.
8. Driving hammer or damping mass increases the levels of PPV in the surrounding soil due to the increase of the energy level of the vibration source.
9. For different embedment lengths investigation, show that the PPV generate at pile toe and confirmed by the analysis. The smallest pile length gives the large PPV on the ground surface.
10. Ram drop height is very effective parameter controlling the energy of driving, as the importance of hammer mass the ram drop height is also very important for the design engineer, the more the ram drop height increased, the PPV increased.
11. Pile material is a significant parameter in measuring PPV values. timber piles give high PPV values and keep reducing as using high stiffness pile material (e.g. steel or precast reinforced concrete).
12. Existing of a building or any other type of structures can lead to increasing PPV values because of the mass of the structure causes consolidation to the soil beneath it, which leads to improving soil properties and increasing soil stiffness.

13. The results of Finite Element analysis of pile driving compare very well with the prediction of PPV by empirical formula Svinkin (2008) and Attewell & Farmer (1973) in cases of medium dense sand and loose sand, respectively.
14. SAP model illustrates the direct effect of vibration on the adjacent structure close to pile driving.
15. Vibration can increase the straining action in building member, causing structural or cosmetic damage depends on how close the building to the driving source or the vibration magnitude.
16. Pile driving earthborn vibration is extremely dangerous to wall bearing or heritage building.
17. Attewell &Farmer (1973) prediction model consider very suitable to be used in estimating PPV when K = 0.25 and 0.75 based on the previous comparison.
18. Attwell et al (1992) prediction model gives reasonable and accepted values for PPV for the best fit curve.

Chapter 4

Effect of Dynamic Compaction on Soil and Structures

Chapter 4

Dynamic Compaction

The effect of dynamic compaction earthborn vibration on soil and adjacent structures.

4.1 Introduction:

Dynamic Compaction is an effective way for soil improvement; it is used to achieve deep ground densification for building foundations, or road and rail embankment foundations, airport runways and facilities, power plant facilities, dams, tank farms and…… etc, for loose materials, granular soils such as sand deposits and gravel. It is also used to form Dynamic Replacement, stone pillars in soft ground (silty clay or peat) as a means to reinforce these soil types.

4.2 Method of compaction:

The method of Dynamic compaction is when a10-40 tone weights are propped in free or quasi-free fall, from a height of about 10-30m. The spacing of the impact points and the unit energy, phasing and rest periods, depending on the soil types and level of improvement required. Specially designed 80-120t Cranes are normally used.

This technique uses the dynamic effect of high energy impacts, caused by dropping large steel ram weighing 15 to 40 tons from a height of 10-30 meters depends on soil condition and the requested densification as shown in Figures 4.1 and 4.2.

For compaction of soils to more than 10-12m, High Energy Dynamic Compaction can be performed. This technique employs High Energy of more than 600 t.m using drop weights of more than 30t, drop heights of more than 30m and cranes weighing more than 120t. That higher energy can be very dangerous to the adjacent structures due to producing high values of PPV which consider being a sign of damage level.

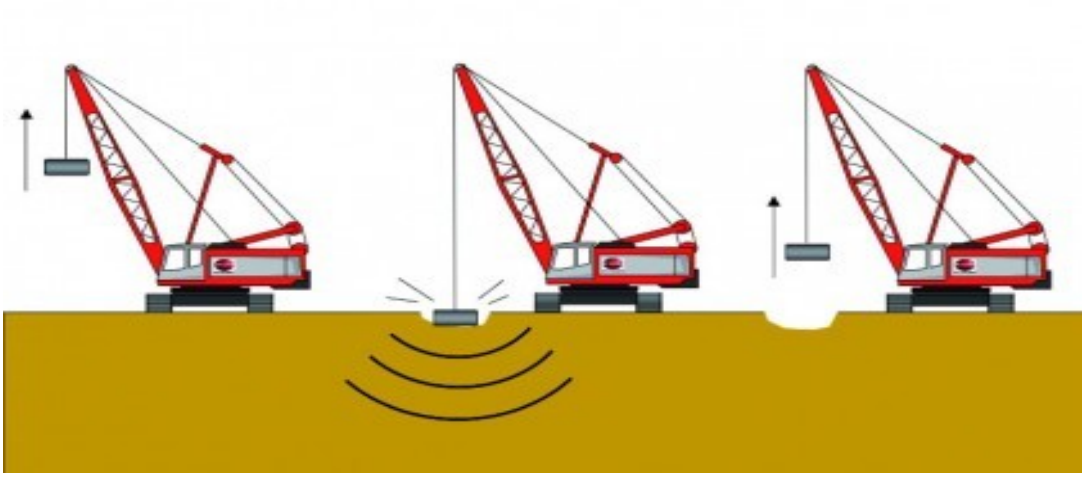

Figure 4.1: Dynamic compaction machine (www.vibromenard.co.uk).

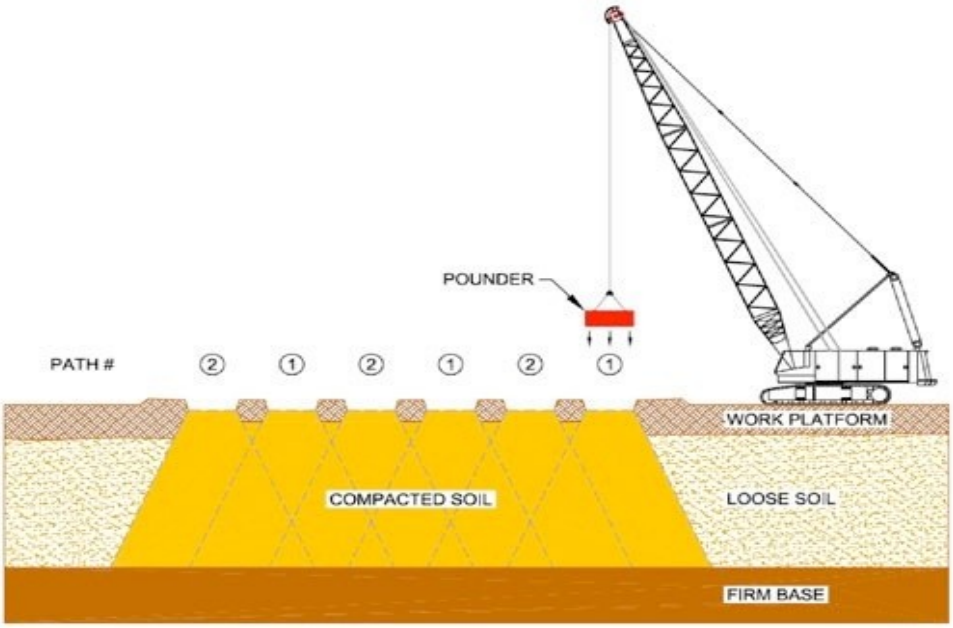

Figure 4.2: Dynamic compaction, work mechanism (www.densification.com).

4.3 Dynamic compaction technique:

Dynamic Compaction technique was invented by Louis Menard in the late 1960s but the first known technical reference on the subject involved a site in Germany (Loos, 1936). It has been developed on numerous sites and applications since this time successfully.

The basic principle behind the technique consists in the transmission of high energy waves through a compressible soil layer in order to improve at depth its

geotechnical properties. Dynamic Compaction is normally associated with an intensive programme of in-situ-testing in order to verify that the specified improvement has been achieved. Dynamic Compaction (DC) (also referred to as impact densification, heavy tamping and dynamic consolidation) has become an accepted method of site improvement, Lauzon et al (2011)

4.4 Rapid impact compaction:

Another type of dynamic compaction technique is also used, is known as the Rapid Runway Compactor, and is marketed as a ground improvement technique under the name of Rapid Impact Compaction (RIC), Lauzon et al (2011), as shown in Figures 4.3 and 4.4.

Dynamic Compaction and Rapid Impact Compaction generate vibrations that are annoying to neighbors and potentially hazardous to adjacent structures, the two techniques have many advantages in terms of cost, schedule, and effectiveness. With less energy per blow, Rapid Impact Compaction is typically presented as a technique generating lower vibrations than the heavier tampers used with Dynamic Compaction.

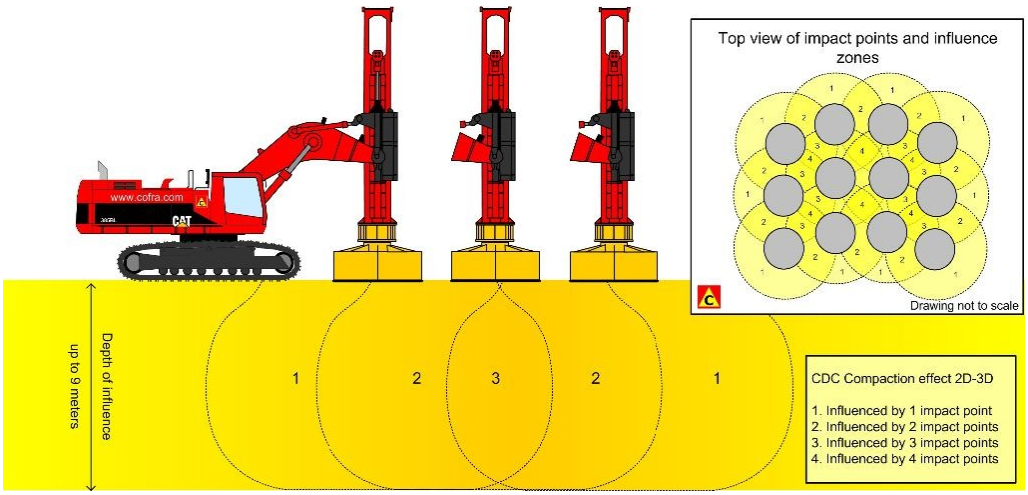

Figure 4.3: Rapid impact compaction technique,
(http://cofra.com/activities/rapid-impact-compaction/)

Figure 4.4: Rapid impact compaction machine,
(http://www.menardgroupusa.com)

4.5 Comparison between Rapid impact compaction and Dynamic compaction:

Both techniques of dynamic compaction and rapid impact hammer were compared to by Lauzon et al (2011) by measurement in different sites, to evaluate the PPV values for estimating any possible damage, they concluded the following:

- At equal distances, vibrations generated by the RIC methods are less than those produced by the DC method. This could be explained by the combined effect of a smaller drop height of the hammer used in RIC and the smaller diameter of the tamper.
- The data also shows that vibration frequencies produced by RIC are higher than those produced by the DC rig. Since RIC frequencies are higher than the typical natural frequencies of houses/structures, less vibration amplification can be expected to make it possible to work closer to houses since the safe level of vibrations define by USBM RI 8507 increases with increased frequency.

The process of DC design usually includes the following items: selection of tamper weight and drop height, selection of tamper base area, determination of grid spacing, establishing the number of drops per compaction point, and determination of a number of phases and their tamping patterns. In usual design approaches, the degree and depth of improvement are assumed to depend on the applied energy per unit volume of soil, and the applied energy per drop, respectively, Shahir et al (2009)

4.6 Records of PPV field measurements due to dynamic compaction

A compilation of available PPV data from several dynamic compaction projects is presented in Figure 4.5. Soil types at these sites included silty sands, sandy fills, sandy clay, rubble, coal spoil, and debris fill, Mayne et al. (1984).

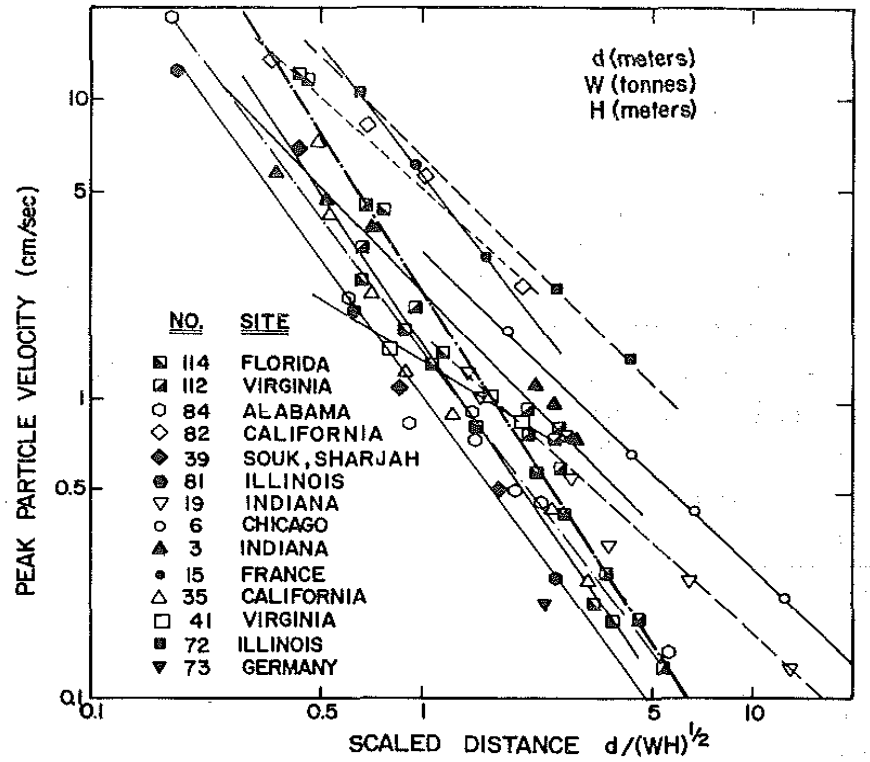

Figure 4.5: Attenuation of Ground Vibrations Measured on Different Dynamic Compaction Projects, Mayne, et al. (1984).

For preliminary estimates of ground vibration levels, a conservative upper limit appears in Eq.4.1, after Mayne, et al. (1984).

$$\text{PPV} \leq 70 \left(\frac{\sqrt{\text{WH}}}{\text{d}}\right)^{1.4} \qquad \text{(Eq.4.1)}$$

When PPV is in mm/s, d distance from the impact and H (pounder drop height) are in meters and W (pounder weight) is in tons. PPV measurements tend to increase with the number of blows as the materials become more dense after Dumas (1981) and (1982), Pearce (1977). Recommendations concerning safe vibration levels during dynamic compaction are given by Mitchell (1979, 1981) and Wiss (1981).

To normalize the data for energy variations in each project, the PPV has been plotted against the inverse scaled distance as shown in Figure 4.6. The inverse scaled distance is the square root of the drop energy, $(WH)^{0.5}$, divided by the distance, d, from the impact point. The best-fit line for the data points is given as shown in Eq.4.2.

$$PPV \leq 20\left(\frac{\sqrt{WH}}{d}\right) \qquad \text{(Eq.4.2)}$$

Where the PPV is in millimeters per second; W=tamper weight in tons; and H=drop height in meters. This equation, based on 298 data points, has an r^2 value of 0.82. The best-fit line is shown in Figure 4.6 along with the ± 2 standard deviation bounds. The upper limit line, defined by Mayne (1985) based on measurements at a large number of sites involving non collapsible soils, is also shown in Figure 4.6 for comparison. In general, the PPV values for collapsible soils are lower for distances close to the drop point but attenuate at a slower rate with distance from the source than for non collapsible soils as indicated by the flatter slope. These data suggest that it may be possible to compact somewhat closer to adjacent buildings when performing the DC on collapsible soils.

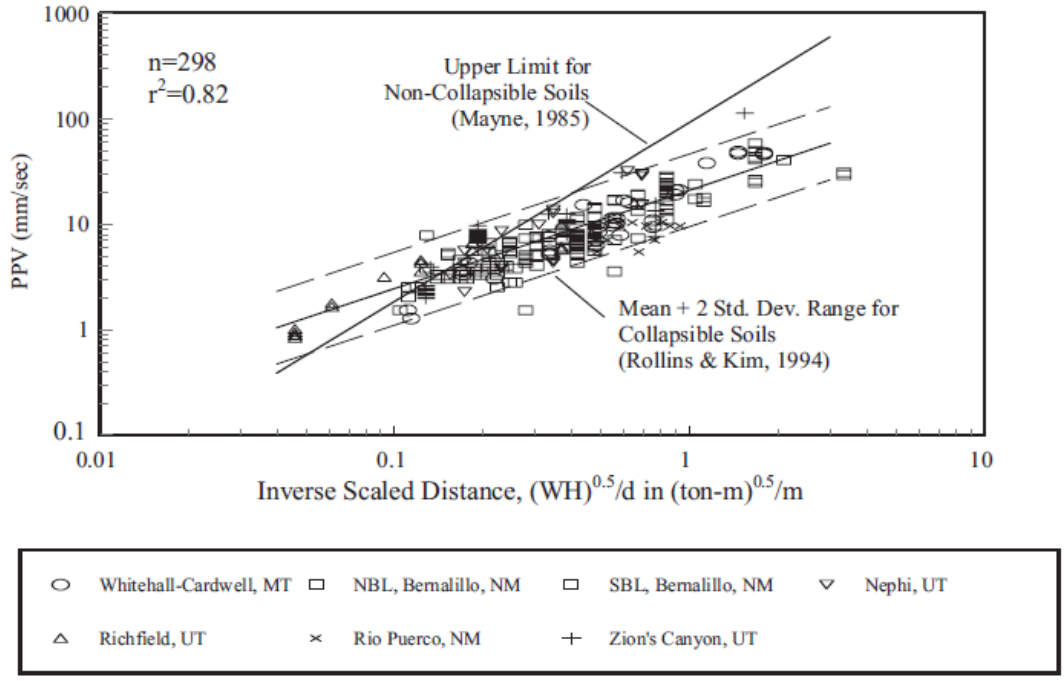

Figure 4.6: PPV versus inverse scaled distance for collapsible soils along with best-fit line and ±2 standard deviation bounds; upper bound curve for non collapsible soils (Mayne 1985) is shown for comparison

4.7 Prediction models of PPV due to dynamic compaction

Wiss (1981) has proposed to express peak particle velocity in terms of distance, d, and energy, E, in a single expression for dynamic compaction as shown in Eq.4.3. Wiss (1981) reproduced his formula to adapt the soil type changes as illustrated in Eq.4.4.

$$PPV = k\left(\frac{d}{\sqrt{E}}\right)^{-n} \qquad \text{(Eq.4.3)}$$

$$PPV = K\left(\frac{\sqrt{W0\ (joules)}}{r\ (m)}\right) \qquad \text{(Eq.4.4)}$$

Where K is a constant relied on type of soil, Therefore, Wiss used K factor to distinguish the effect of soil type.

Chapot et al. (1981) founded a new form of equation to predict PPV for dynamic compaction as shown in Eq.4.4. Where d is the distance from the impact point.

$$PPV = 340d^{-1.1} mm/s \qquad (Eq.4.5)$$

Mayne et al. (1984) gathered the measurements of fourteen Dynamic Compaction sites. Soil types at these sites included silty sands, sandy clay, rubble, coal spoil and debris fill. For estimating of ground vibration levels, a conservative upper limit appeared to be in Eq.4.6.

$$PPV \leq 70 \left(\frac{\sqrt{WH}}{d}\right)^{1.4} \qquad (Eq.4.6)$$

When PPV is in mm/s, d distance from the impact and H (pounder drop height) are in meters and W (pounder weight) is in tons

Later and based on a mix of single maximum component and TVS measurements of 12 sites,

Mayne (1985) proposed an upper limit conservative PPV in Eq.4.7. When PPV is in mm/s, d distance from the impact and H (pounder drop height) are in meters and W (pounder weight) is in tons.

$$PPV \leq 92 \left(\frac{\sqrt{WH}}{d}\right)^{1.7} \qquad (Eq.4.7)$$

In order to get a close trend and based on information accrued by monitoring vibrations realized by different drop heights from a site in Alexandria, Virginia, Mayne (1985) has also postulated that while pounder weight may affect vibration frequency, the magnitude of particle velocities is slightly more influenced by the drop height of the pounder.

Thus as formulated in Eq. 4.8, Mayne (1985) proposed to estimate PPV by normalization (dividing by the theoretical impact velocity of the falling weight) and plotting it against the normalized distance to impact by dividing d by the pounder radius r_o).

$$\frac{PPV}{\sqrt{2gH}} \leq 0.2 \left(\frac{d}{r0}\right)^{1.7} \quad (Eq.4.8)$$

Models for PPV due to dynamic compaction are summarized in Table 4.1.

Table 4.1: Models for Prediction of PPV for dynamic compaction

Prediction method /model	Reference
$$p.pv = k\left(\frac{d}{\sqrt{E}}\right)^{-n}$$ Where K is the intercept with the ordinate and n is the slope or attenuation rate. Distance, d, and energy, E $$p.pv = K\left(\frac{\sqrt{W0\ (joules)}}{r\ (m)}\right)$$ Where K is a constant relied on type of soil, Therefore, Wiss used K factor to distinguish the effect of soil type	Wiss (1981)
When PPV is in mm/s, d distance from the impact and H (pounder drop height) are in meters and W (pounder weight) is in tons.	Mayne et al. (1984)
$$p.pv \leq 92\left(\frac{\sqrt{WH}}{d}\right)^{1.7} \qquad \frac{p.p.v}{\sqrt{2gH}} \leq 0.2\left(\frac{d}{r0}\right)^{1.7}$$ When PPV is in mm/s, pounder radius r_o, d distance from the impact and H (pounder drop height) are in meters and W (pounder weight) is in tons.	Mayne (1985)
$$p.pv = 560d^{-1.1}mm/s \qquad p.pv \leq 25\left(\frac{\sqrt{WH}}{d}\right)^{1.1}$$ d, distance from the impact and H, pounder drop height are in meters and W pounder	Hamidi et al (2011)
d, distance from the impact	Chapot et al. (1981)

4.8 Vibro-Compaction

Some researchers suggested ways to reduce the damage effect of construction vibration as illustrated before in chapter two, such as wave barriers as simple

solution to reduce the vibration effect. The ways of vibration isolation will be investigated in chapter five.

For dynamic compaction another types of compaction start to be used to reduce the vibration effect on the ground surface and also the adjacent structures, therefore another technique is used to achieve the needed compaction, it called vibro-compaction.

Vibro Compaction is an established ground improvement method for stabilizing granular soils such as loose sands, gravels and some hydraulic fills. The technique is primarily used for seismic mitigation and in-situ densification of loose sands up to 30m deep.

The vibrator is typically hung from a crane and lowered vertically into the soil under its own weight and vibrations. Penetration is usually helped by water jets integrated into the vibrator assembly. After reaching the bottom of the treatment zone, the soils are densified as the vibrator is raised in lifts as shown in Figure 4.7.

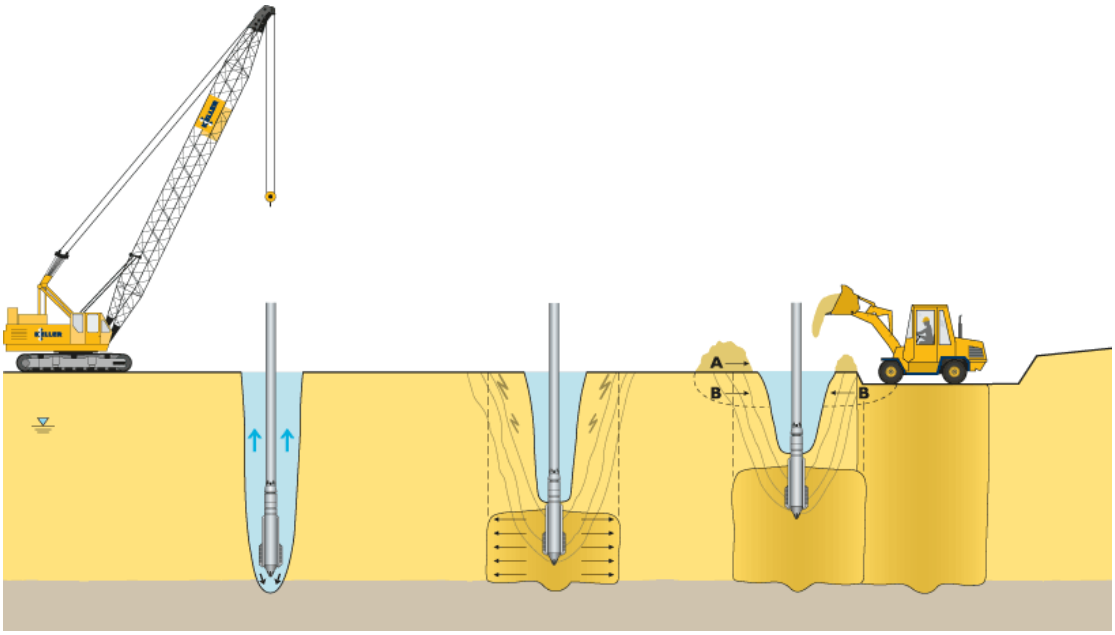

Figure 4.7: Consequence of vibro compaction.

In vibro-compaction case the vibration generated under the ground which makes the values of PPV is lower than the case of surface dynamic compaction

as shown in Figures 4.8 and 4.9, also it shows the difference between the effective depths for the both ways of compaction.

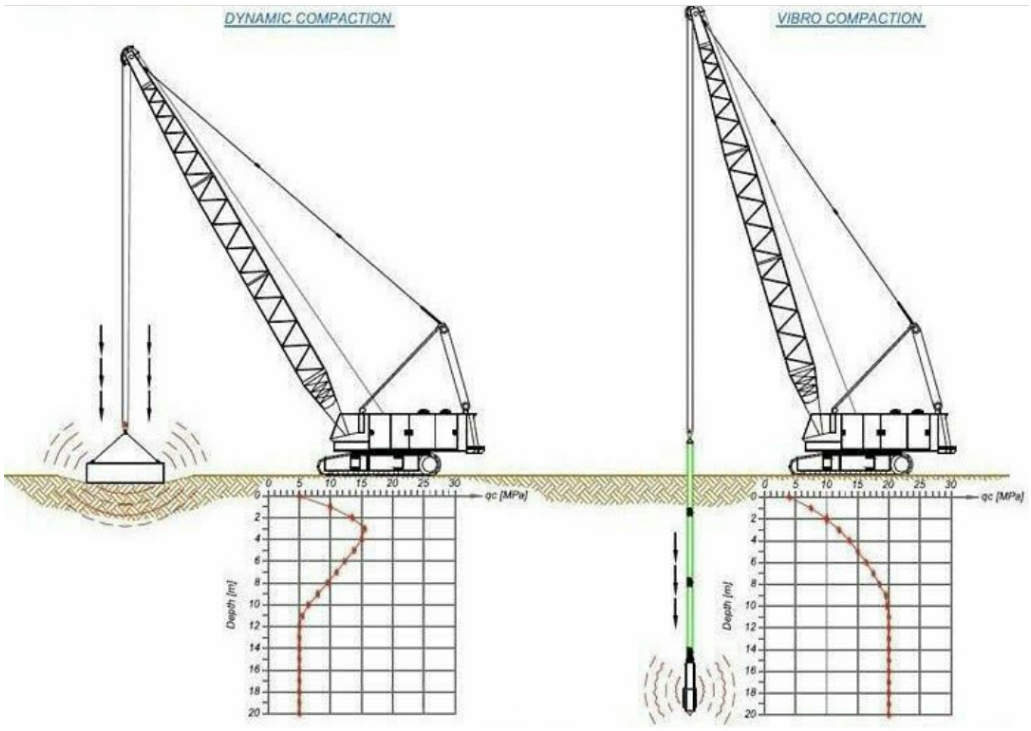

Figure 4.8: The difference between Dynamic compaction and Vibro compaction.

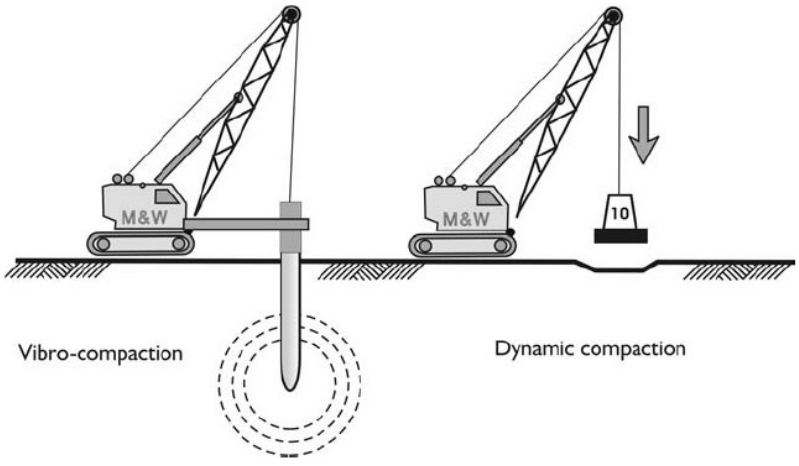

Figure 4.9: The difference mechanisms of Dynamic compaction and Vibro compaction.

NUMERICAL MODELING

4.9 Analysis

In this chapter, the analysis of the results of the effect of construction vibration from dynamic compaction on soil and the adjacent structures are presented. A series of models were run under both different soil types and other different parameters to show the effect of construction vibration on soil and the nearby structures.

4.10 Finite Element Models

Finite element analyses of Dynamic compaction (DC) are carried out using Plaxis 8.2 2D dynamic version. A set of general fixities to the boundary conditions of the problem are considered automatically by the Plaxis program. The Rayleigh damping is considered at vertical boundaries with $\alpha, \beta = 0.01$ in order to resist the Rayleigh waves. While the plastic properties of soil are defined by using material damping, which is defined in Plaxis by Rayleigh (α and β), where The Rayleigh damping is considered to be object-dependent in material data set to consider the plastic properties of soil during the dynamic analysis in Plaxis.

Plaxis model for dynamic compaction is shown in Figure 4.10. The mesh was generated and refined twice around the pile to improve the accuracy of the results as shown in Figure 4.11. For impact hummers, the analysis was based on three phase's plastic (staged construction) and two phases for dynamic analysis (total multipliers). The dimensions of the soil model for pile driving are taken around 50 m in depth and 150 m in width after some mesh experiments, the Plaxis model for dynamic compaction is taken after case study of airport Hilton construction at Norfolk, VA after Terra Systems for geotechnical contracting in 1985 by geotechnical engineer Law Engineering. Different parameters used in the Plaxis model are illustrated as shown in Table 4.2. "Mohr Columb" undrained model is used for modeling sand, while "hardening soil" for modeling clay.

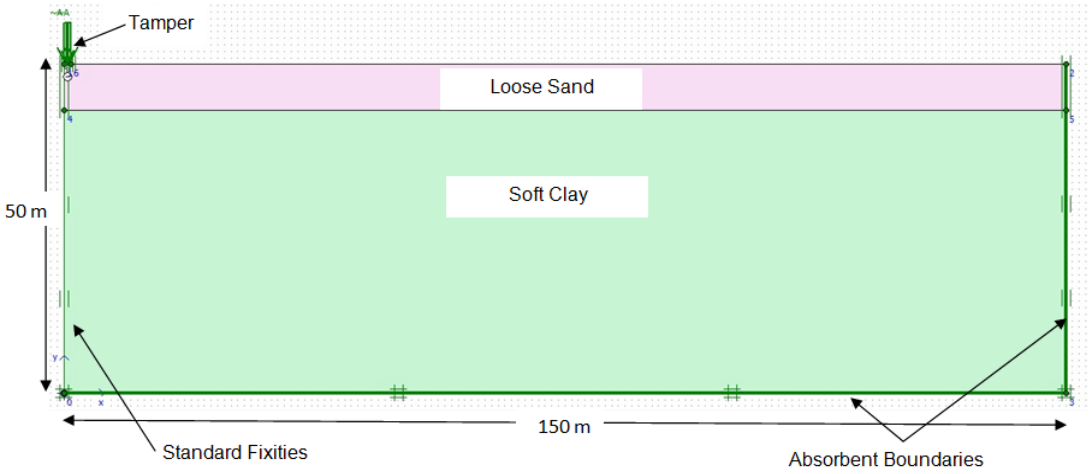

Figure 4.10: Plaxis model for dynamic compaction simulation

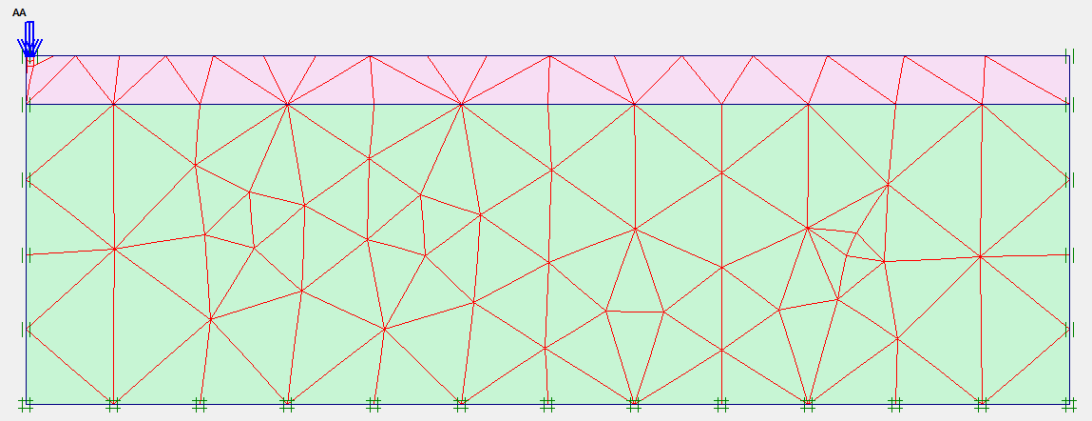

Figure 4.11: Mesh generation of Plaxis model for dynamic compaction simulation.

4.10.1 Studied parameters

In this research, the parameters are varied to evaluate their effects on the soil response under the effect of dynamic compaction. The effect of soil stiffness is investigated on peak particle velocity PPV due to dynamic compaction. On the other hand, the effect of the compaction energy on PPV is studied

Table 4.2: The different parameters used in the models under investigation.

Parameter	symbol	Clay1	Sand1	Sand2	Sand3	Pile	Units
Unit weight above pheratic line	γ_{unsat}	14	17	18	20	25	kN/m^3
Unit weight below phreatic line	γ_{sat}	16	19	20	22	—	kN/m^3
Elastic modulus	E_{ref}	5000	25000	33000	40000	22×10^6	kN/m^2
Oedometer modulus	E_{oed}	—	25000	33000	40000	—	kN/m^2
Power	M	—	0.5	0.5	0.5	—	—
Unloading modulus	E_{ur}	—	75000	99000	120000	—	kN/m^2
Poisson's ratio	ν	0.2	0.3	0.33	0.35	0.15	—
Cohesion	C_u	25	1	1	1	—	kN/m^2
Friction angle	ϕ	1	30	35	40	—	°
Dilatancy angle	ψ	0.0	0.0	5	10	—	°
Interface strength reduction	R_{inter}	0.6	0.67	0.67	0.67	—	—

4.10.2 Effect of soil stiffness on Dynamic Compaction PPV

The maximum velocity due to dynamic compaction is shown in Figure 4.12. It can be noticed that the great values of velocity exist close to the vibration source, and start to be reduced by the distance from the driving source.

The variations of the PPV with distance from the vibration source in both loose and medium sand are illustrated in Figure 4.13. As expected, the velocity decreases with the increase in distance from driving source. The PPV increases with the increase in the stiffness.

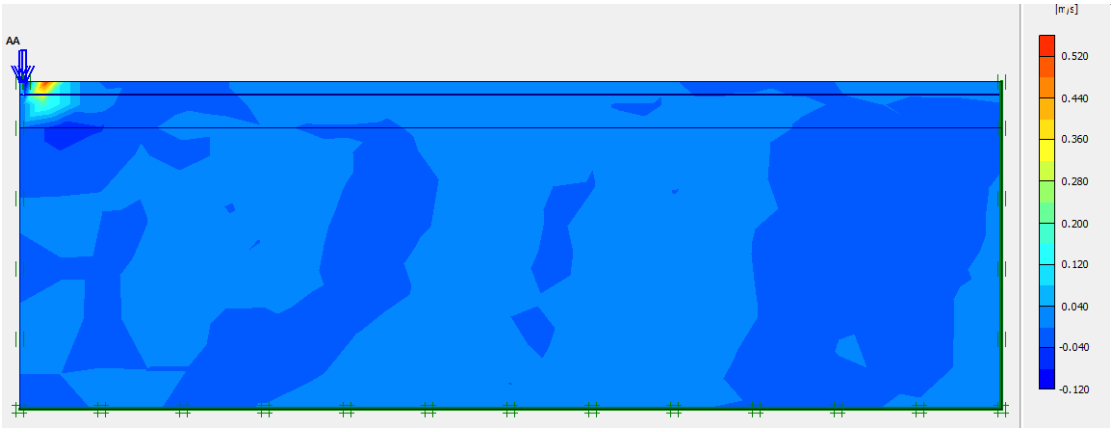

Figure 4.12: Maximum velocity in the sand at E 25000 kPa adapted from Plaxis model.

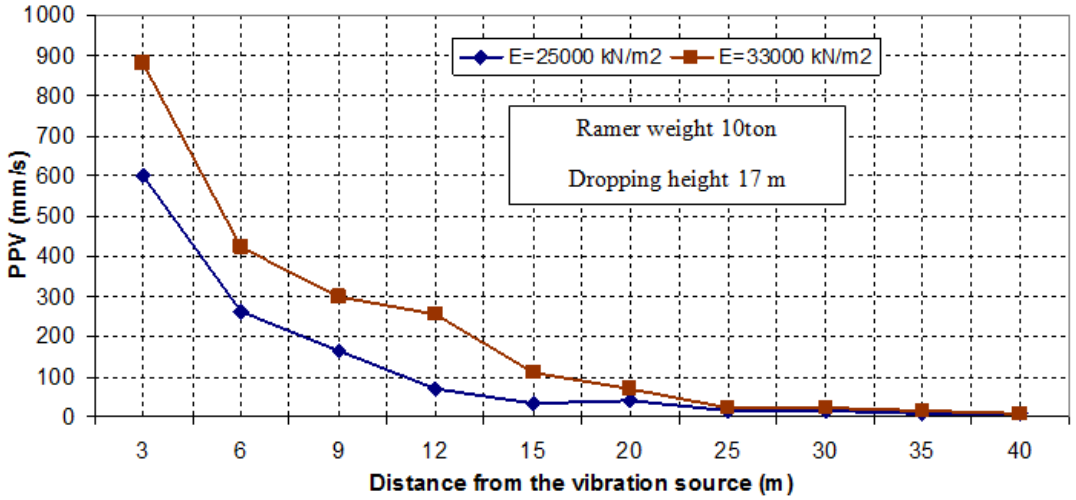

Figure 4.13: Maximum vertical PPV for different soil stiffness at different distances from the vibration source in case of using dynamic compaction.

4.10.3 Effect of Damper Weight/ Energy on Dynamic Compaction PPV

Dynamic compaction can cause significant damage to adjacent structures due to the high impact energy. The generated waves of Dynamic compaction have very large magnitude comparing to the other sources of vibration. The rammer weight and the dropping height are very effective parameters controlling the values of the propagated waves; therefore the design engineer should choose a suitable rammer weight and the proper dropping height. Pre observation for the field before starting the dynamic compaction process, monitoring any adjacent structures or facilities also any underground structures should be set to avoid any possible damage due to vibration. The maximum velocity due to dynamic compaction at different rammer weights (5ton, 8ton and 10ton) adapted from Plaxis model are shown in Figures 4.14, 4.15 and 4.16, respectively.

For compaction of soil to depths for example exceeding 10 to 12 m, High Energy Dynamic Compaction (HEDC) can be performed. High compaction energy of more than 600 t.m is achieved using specialized equipment (weights > 30 tons, drop heights > 30 m, Cranes >120 tons). The effect of damper weight on PPV is also investigated as shown in Figure 4.27. In general, the increase in tamper weight increases PPV. Increasing damper weight increases the input energy to the soil thus higher born vibration levels gives higher PPV.

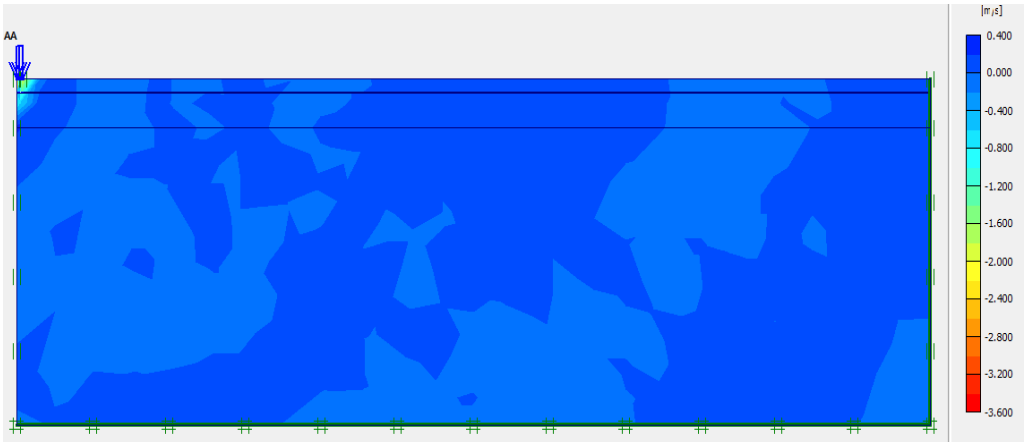

Figure 4.14: Maximum velocity in sand at rammer weight 5ton adapted from Plaxis model.

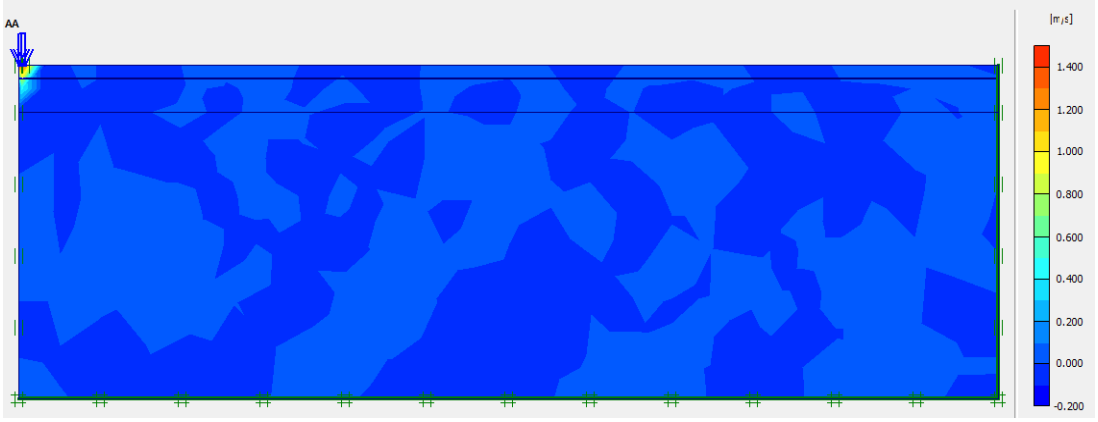

Figure 4.15: Maximum velocity in sand at rammer weight 8ton adapted from Plaxis model.

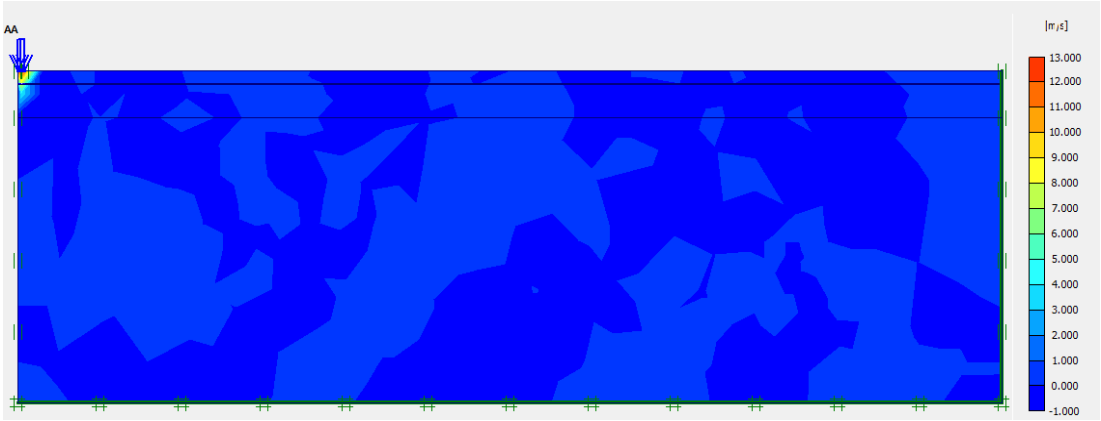

Figure 4.16: Maximum velocity in sand at rammer weight 10ton adapted from Plaxis model.

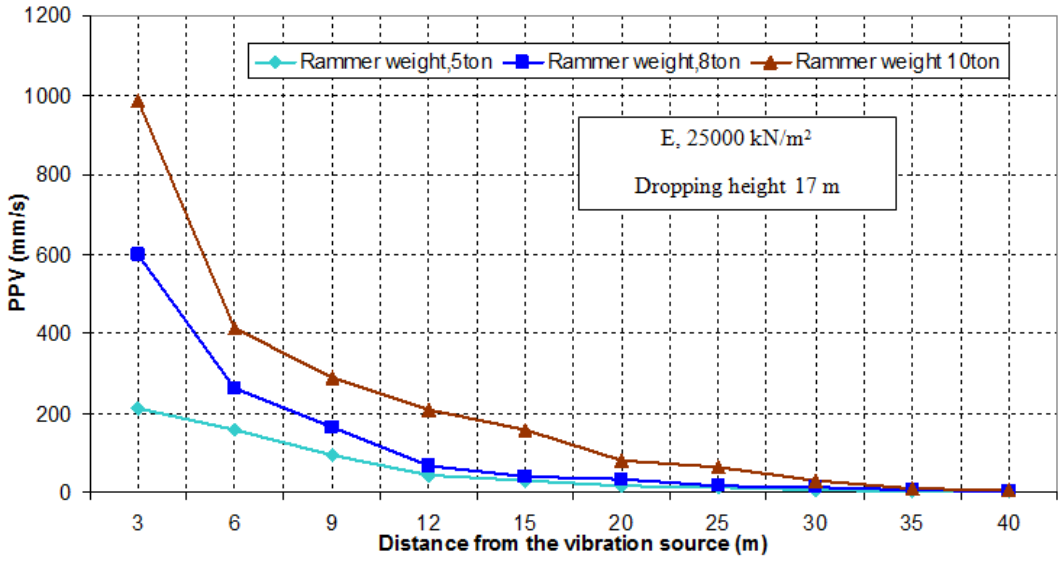

Figure 4.17: Maximum PPV in sand at E, 25000kN/m^2 adapted from Plaxis model for different rammer's weight with distance from the vibration source.

4.10.4 Comparison between pile driving and dynamic compaction response.

The effect of pile driving on soil and the adjacent structures is illustrated in chapter three, it was noticed that pile driving has a harmful effect on both soil and the structures by discussing the PPV values and comparing it with the standards and the vibration limits. A comparison between PPV values due to pile driving and dynamic compaction is investigated to figure out which process of them produces higher values and thus higher damage.

Figure 4.18 shows the variation between PPV values at a different horizontal distance due to both dynamic compaction and pile driving technique. It can be noticed that dynamic compaction has a large value of PPV due to the higher magnitude of energy which increases PPV values at the ground surface. It is found that there is no loss in energy by friction in comparing with the case of pile driving where much energy gets loosed through transferring from hammer to the pile then to the adjacent soil. The degree of damage due to PPV was classified by Cenek et al (2012) and Dowding (1996) and by comparing PPV values from dynamic compaction with these classifications of damage or any other limits, it is clear that they can be classified as "very dangerous".

It can be concluded that dynamic compaction has more significant damage than pile driving. Studying the effect of vibration on soil should be investigated before starting any project containing any source of vibration to avoid any possible occurred damage. Observation and monitoring settlement due to vibration while pile driving or dynamic compaction process shouldn't be neglected. Mayne (1985) suggested that if vibration levels are anticipated to cause off-site problems, isolation trenches can be dug between the point of impact and the area to be protected. The vibration levels can be reduced by factors of 2 to 10, depending on some factors such as the soil type, the depth of the trench and the position of the weight dropping to the trench.

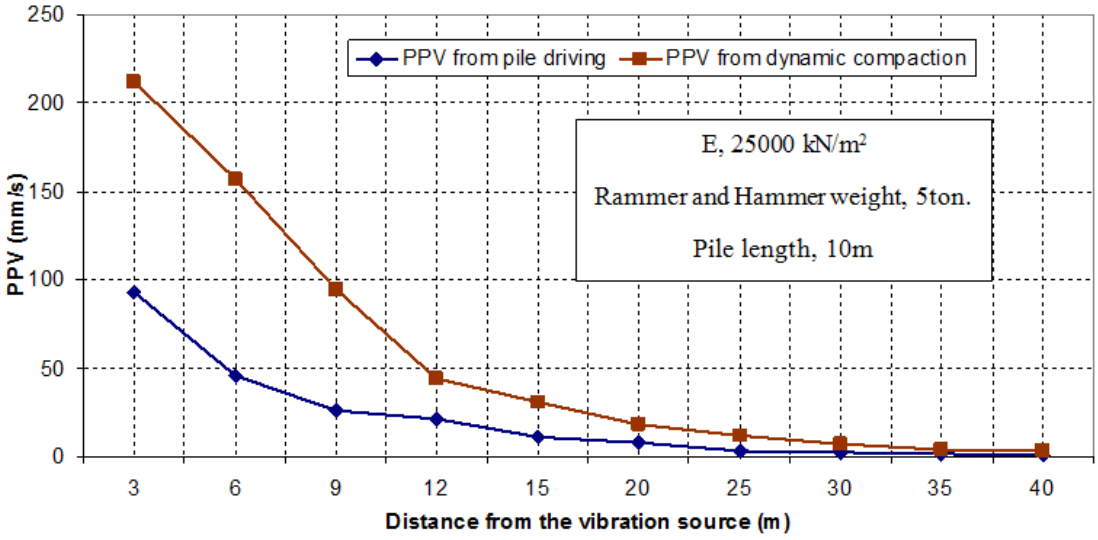

Figure 4.18: The maximum PPV values for pile driving and dynamic compaction vs. distance from the vibration source.

4.10.5 Comparison between Finite Element model results and predictive empirical relationships for calculating Dynamic Compaction PPV

Models for PPV prediction has been set to evaluate the PPV values for helping design engineers to avoid any possible damage occur to the adjacent structures. A comparison between Mayne et al (1984) formula for calculating PPV and PPV values from Plaxis model is investigated.

Mayne et al (1984) proposed a formula for calculating PPV due to dynamic compaction as shown in Eq.4.3 also see Table 4.1.

$$PPV\ (mm/s) = 70\ (\sqrt{(WH)} / d)^{1.4} \qquad (Eq.4.3)$$

Where; d is the distance from the point of impact, H is the dropping height of the tamper, and w is the tamper weight.

Figure 4.19 shows the variation between PPV values from Plaxis model at different soil stiffness and other function proposed by Mayne et al (1984). A difference is noticed between the values of PPV especially at 3m and 6m far from the impact point.

With the increase of the distance from the impact point the values of PPV become more similar to each other especially between the values of Plaxis and Eq.2.1. It can be seen that the effect of the tamper weight is a very effective parameter and shouldn't be neglected. It can be seen, also, that by increasing the soil stiffness the PPV increases. It can be concluded that soil stiffness is a very effective parameter in calculating PPV.

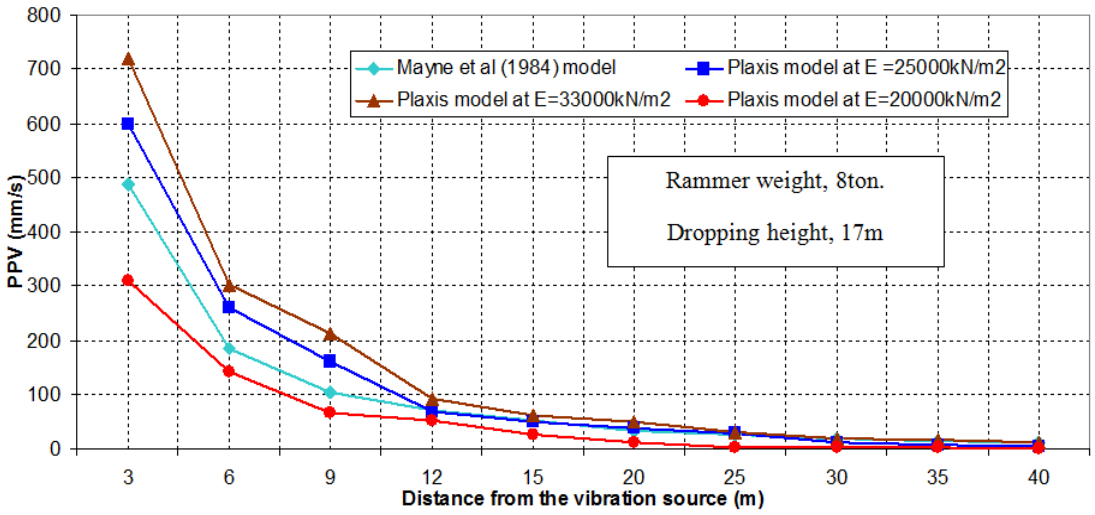

Figure 4.19: Comparison between PPV values from Finite Element and other prediction models for PPV values due to dynamic compaction.

4.11 Conclusions

Effect of the dynamic compaction on the Peak Particle Velocity (PPV) is investigated using Finite Element Analysis. Based on the data and the results of the analysis presented in this chapter, the following main conclusions can be drawn.

1. Dynamic compaction is widely used as a tool for soil improvement, therefore facing a lot of vibration problems in structures and underground facilities become more common and are important to be evaluated to avoid damages.
2. There are many types of soil improvement techniques. The main systems are DC and RIC; both techniques generate vibration but with different values. RIC produce lower vibration due to its small dropping

height, so it can be the suitable choice for design engineers to reduce the vibration effect.

3. Another type of compaction is the vibro compaction; it has the same concept of generation vibration under the ground, not at the surface like the case of dynamic compaction. That is why it has less effect on the adjacent structures.
4. The propagated waves of dynamic compaction have the same features of pile driving waves; the difference only is the place where dynamic compaction vibration waves generate.
5. Many researchers developed approaches for calculating PPV values through field measurements and with a scaled distance approaches, a formula or models for PPV prediction can be set.
6. Driving hammer or damping weight increases the levels of PPV in the surrounding soil due to the increase of the energy level of the vibration source.
7. The PPV values due to dynamic compaction are much greater than those due to pile driving. This is because of the great difference in the input energy in the two cases.
8. The prediction of PPV due to dynamic compaction by the empirical formula Mayne et al (1984) model provides comparable results of average PPV values computed by Finite Element model for relatively wide range of sand stiffness. Such an agreement is encouraging and promotes the idea of introducing the soil stiffness to the empirical prediction equations.

Chapter 5

Soil Settlement due to Construction Vibration

Chapter 5
Ground Settlement due to construction vibration

5.1 Introduction

This chapter presents the behavior of the soil layers during construction vibration processes such as pile driving or dynamic compaction. As illustrated in pervious chapters when vibration generates through soil in all directions, the vibrations transfer to the surrounding soil and it begins to vibrate with the same magnitude which leads to densification to the soil layers. Waves propagate from the vibration source and by the distance from the source the wave start to attenuate which cause differences in the values of densification and it may leads to differential settlement to the adjacent structures. The soil is loaded cyclically due to these vibrations. It is this loading that is responsible for the densification and the excess pore pressures. In case of saturated soil at first some excess pore pressure is developed. Dissipation of the excess pore pressure results in densification. The process of earth born vibration and its propagation due to pile driving is shown in Figure 5.1.

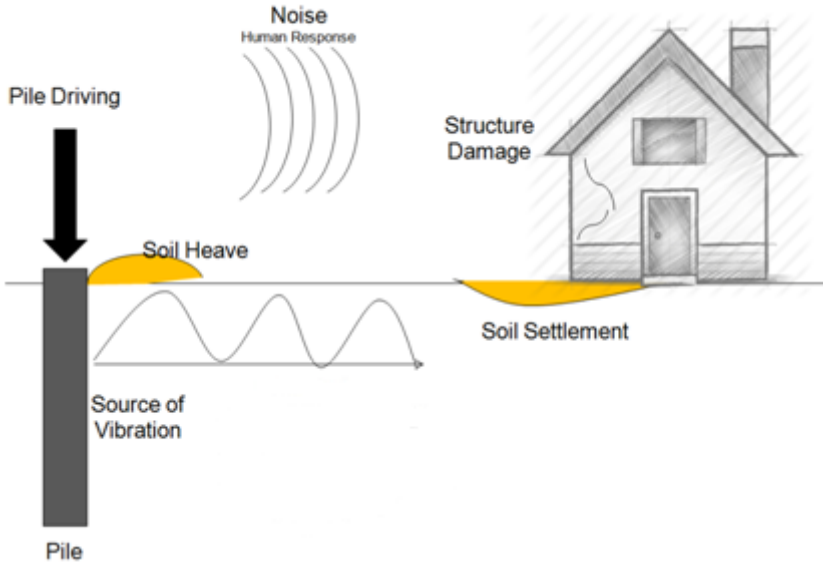

Figure 5.1: Construction vibration induced soil heave and settlement.

5.2 Examples of damage due to vibration

Existing roads and railways may show local settlements, resulting in discomfort to the traffic and, in case of railways, risk of derailment. Lifelines as sewage lines and water mains may suffer differential settlement, bending and cracking. Another problem may be the development of excess pore pressures. In saturated sand excess pore pressures precede the settlement. These temporary excess pore pressures may endanger the stability of buildings, dikes and etc. The main reason of the damage due to construction vibration is soil settlement because it affects directly beneath the foundation, for heritage or old buildings this may cause significant damage and may be failure.

Siskind et al. (1980) and Dowding (1996) defined the possible damage into three categories depending on the place of cracks (the affected element of the structures), major or minor cracks and structural or architectural damage as following.

1. Cosmetic cracking threshold, opening of old cracks and formation of new plaster cracks.
2. Minor or architectural damage, cracks not affecting structural capacity (broken windows, cracked plaster).
3. Major or structural damage, cracks affecting the integrity of building support (large cracks in beams, columns or foundations, shifted foundations, wall put out of plumb).

Many types of damage can be occurred due to construction induced vibration. Figure 5.2 shows the settlement of pavement due to vibration. Construction vibration can cause differential settlement cracks or increasing the existed cracks in the structures. Figures 5.3 and 5.4 show different types of settlement cracks are look like.

Figure 5.2: Cracks in exterior property wall, (http://vibrationdamage.com/understanding_vibration_damage.htm).

Figure 5.3: Cracks in a wall due to construction vibration, (http://vibrationdamage.com/understanding_vibration_damage.htm).

Figure 5.4: Sign of damage from the blasting, photo by Molly Moore, West Virginia USA. (http://appvoices.org/2016/02/18/blasting-homeowners-property-damage-coal/).

The following Figures show the damage due to construction of new road which caused failures for façade walls. Figures 5.5 and 5.6 show the damage in walls and plaster

Figure 5.5: Damage in plaster due to road construction, recent insurance adjustment claim for a home damaged by construction next door, Florida, USA. (ww.toddclaimservice.com)

Figure 5.6: Damage in wall due to road construction, recent insurance adjustment claim for a home damaged by construction next door, Florida, USA. (ww.toddclaimservice.com)

There are some characteristics of vibration cracks which settling cracks rarely share. Cracks at drywall corner beads and sheet joins can occur from normal settling, temperature cycling and construction vibration. However, cosmetic drywall cracks from vibration often appear at the corners of windows and doors, running roughly diagonally from the corners. Corresponding cracks often manifest themselves outside around wall penetrations in rigid finishes like stucco. These diagonal cracks are due to the house being placed in shear (i.e. sections of the house moving in different directions or speeds with respect to one another) by vibrations.

Svinkin (2008) illustrated the possible damge due to dynamic settlement as following:

5.3 Pre-survey documentation

Most construction sites that involve the use of explosives are required to do pre-blast surveys to map the existing cracks or other defects in buildings within a certain radius from the blasting activity and to measure the vibrations produced during construction. If the vibrations from the blasting exceed the threshold level and damage is reported by the homeowner or business owner, the contractor can determine what damage existed prior to the blast so a comparison can be made, and any damage caused by the construction can be repaired.

A pre-construction survey is the first step in the control of construction vibrations to ensure safety and serviceability of adjacent and remote houses, buildings and facilities. In a situation where the soil has high liquefaction potential, construction vibration can cause ground settlement or shifting that significantly reduces support provided by the soil. Rather than vibration itself, this ground settlement or shifting of the ground can cause damage to the building. This situation requires a geotechnical engineer and a review of analysis, mitigation, and monitoring processes. Some types of construction-caused damage can look very similar to settling damage or can involve

construction vibration-caused settling, so you will need to try to differentiate the two.

The steps of pre construction survey to document the damage due to vibration, because few structures begin free of distress. It is often possible to resolve construction damage from other sources by comparing post-construction and pre-construction photographs and elevation surveys, (Svinkin 2008).

- The pre-driving condition survey has to be provided after the accomplishment of excavating and dewatering at a site.
- A pre-construction survey is the first step in the control of construction vibrations to ensure safety and serviceability of adjacent and remote houses, buildings and facilities.
- Surveys of structure responses provide more objective information about vibration effects on structures than vibration measurements.

There are four goals of preconstruction survey:

- Document the existing cracks and other damage.
- Analyze probable causes of existing damage.
- Classify susceptibility rating of structures.
- Determine mitigation measures of pile driving effects on structures.

5.4 Mechanism of settlement due to vibration

There are two fundamental mechanisms for vibration damage 1) distortion from inertial loads, and 2) settlement of the soils supporting the foundation. If the soil settlement is not uniform, distortion and damage can occur. Such differential settlement can also be due to deep excavations adjacent to existing foundations.

Massarsch(1993) has, based on a review of existing vibration codes in different countries, suggested that damage to buildings caused by "pseudo-static" ground distortions occur at a critical deflection ratio $d/L = 1.5 \cdot 10^{-5}$. simple relationship can be used to estimate a critical vibration velocity V_{cr} in the following Eq.5.1.

$$V_{cr} = 4.7\ 10^{-5}\ C \qquad \text{(Eq.5.1)}$$

Where (C), is the wave propagation velocity and it equals to L/f (where L is the wave length and f is the frequency of the wave. This simple relationship is valid if the wave length is smaller than twice the building length B (i. e. for wave propagation in soft soils, Massarsch (1993).

The ground vibration velocity V depends on the wave propagation velocity C and the two non-dimensional numbers ground distortion (d/L) and relative building length (B/L). Figure 5.7 shows the effect of wave propagation below building, subjected to surface waves of different wave length.

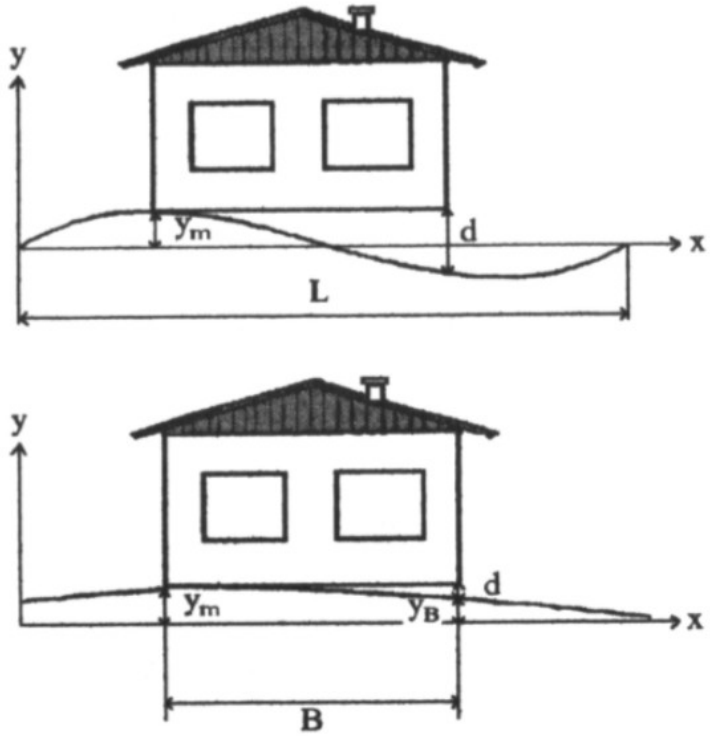

Figure 5.7: Influence of wave length on ground distortion below the building, (after Massarsch 1993).

Vibration induced settlements can occur in loose soils subject to ground borne vibrations from any contiguous source like construction operations, forging operations, or other dynamic event like blasting. The soil may be saturated in which case liquefaction may occur or non-saturated in which case

shakedown settlement may occur. The liquefaction process due to construction vibration is similar to the liquefaction due to earthquake as it shown in Figure 5.8

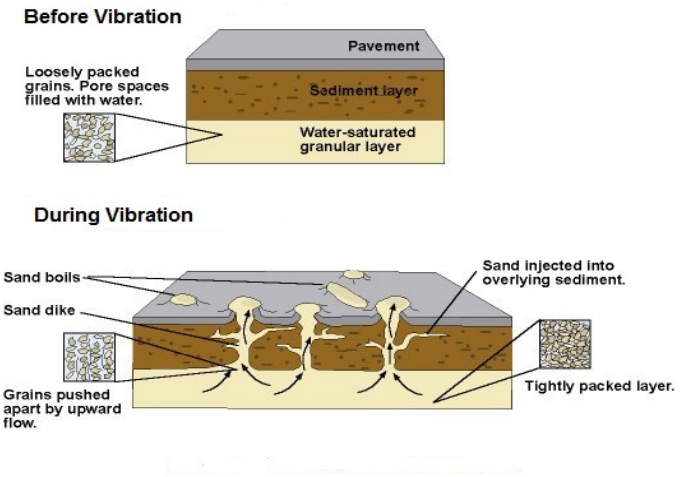

Figure 5.8: The process of soil liquefaction due to vibration, modified from theconstructor.org

Damage may occur to structures supported on soils due to settlement by vibrations. Factors that increase the total vibration energy input will increase settlements. Such factors are: depth of overburden, intensity of final driving resistance, number of piles and size of the site.

5.5 Soil densification

Clean sands with relative densities less than or equal to (50-55) % are considered susceptible to densification as illustrated by Lacy and Gould (1985).

Vibration-induced settlements and soil shakedown is known to occur due to densification of loose saturated sands subjected to vibrations, Therefore, understanding vibrations resulting from pile driving is essential to alleviate risk of damage to buildings and structures in the vicinity of pile driving activities.

It has been indicated in many cases that settlements can occur even at low vibration levels in loose granular soils. As the vibration amplitude is largest close to the ground surface, settlements will be larger in the upper soil layers, where the confining stress is low.

5.6 Shear strain effect on soil settlement

Drnevich and Massarsch (1979) and Mohamed and Dobry (1987) have shown that soil disturbance will not occur if shear strain are below a threshold value of γ_t ≈0.001% ($10*10^{-6}$). When this level is exceeded, the risk of particle rearrangement and thus settlement increases. At a shear strain level of ≈0.010 %($100*10^{-6}$), vibrations can start to cause settlement and this value should not be exceeded. Significant risk of settlements exists when the shear strain level exceeds ≈0.100 % ($1{,}000*10^{-6}$). It is important to note that shear modulus and shear wave speed are affected by shear strain. Massarsch (2004a) has shown that the shear wave speed decreases with increasing shear strain and that this reduction depends on the fines content (plasticity index) of the soil. The reduction of shear wave speed is more pronounced in gravel and sand than in silt and is even smaller in clay. The effect must be appraised when determining the shear wave speed at a given strain level and taking into account the reduction in shear wave speed with shear strain level.

5.7 Methods of estimating soil settlement

Vibrations, which are caused by driving piles into dry or permeable soils, can cause settlements. The magnitude of settlement depends on several factors, such as soil type and stratification, groundwater conditions (degree of saturation), pile type, and method of pile installation (driving energy). For estimating settlements in homogeneous sand deposit adjacent to a single pile

Massarsch (1993) suggested an embirical graph for settlement measuring based on the amplitude of acceleration once the amplitude is available the corresponding volume strain can be derived from the following graph in Figure 5.9 for vibratory pile driving and vibratory soil compaction.

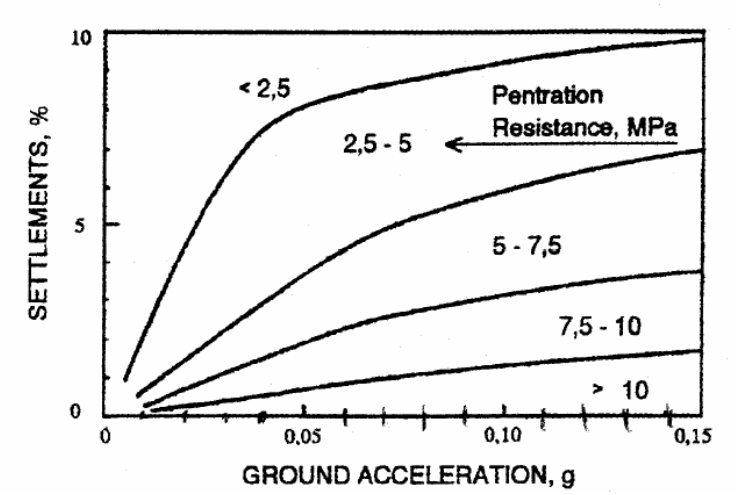

Figure 5.9: Settlement value as a function of cone resistance and ground acceleration, after (Massarsch 1993).

It is agreed that the most relevant parameter to assess the risk of settlement is the ground acceleration. Massarsch (1993) set an empirical graph for pile driving as shown in Figure 5.6 to calculate settlement value as a percentage of soil layer thickness. The density of the soil is expressed in terms of cone penetration resistance. Settlements can range between 10% in very loose sand and silt and 1% in dense sand and gravel. This uneven foundation can lead to large differential settlement below light weight buildings, even at very low vibration levels, however it can't be harmful as direct wave propagation.

Massarsch (2000) illustrated a second method to assess settlement. The method consists of two steps, the first one is to estimate shear strain value, and the second step is to estimate the volume strain from the shear strain.

It suggests evaluating the total settlement Δ of a sand layer, due to vibrations caused by the propagation of superficial waves, by means of the sum of settlements Δ_z of each single layer then, this result has to be multiplied by the number of vibration cycles as it shown in Eq.5.2:

$$\Delta z = \sum_{i=1}^{n} \Delta z . N \qquad \text{(Eq.5.2)}$$

For the evaluation of the settlement Δ_Z (mm) of each layer is the following Eq.5.3:

$$\Delta_z = f_1.m_z.v.\ \Delta H/\ (R_c.\ C_s) \qquad \text{(Eq.5.3)}$$

- Where Δ_z is the settlement in the considered layer.
- f_1 is the empirical parameter relating the plastic vertical strain to the shear strain amplitude.
- m_z is the parameter relating the vibration amplitude at depth z to the vibration amplitude at ground level. (f_1 and m_z are factors of shear strain)
- v is the vibration amplitude (velocity amplitude of particles) at ground level,
- ΔH is the thickness considered layer.
- R_c is the ratio between Rayleigh wave velocity and shear wave velocity (taken as 0.93).
- C_s is the shear wave velocity.

The parameter f_1 is the ratio between the vertical strain ε_z and the shear strain amplitude $\Delta\gamma$. It is a function of the shear strain amplitude and the number of equivalent cycles. The value of f_1 is derived from the test results published by (Seed and Silver 1972) and (Youd 1972) and is presented in a graph. This graph is reproduced as shown in Figure 5.10.

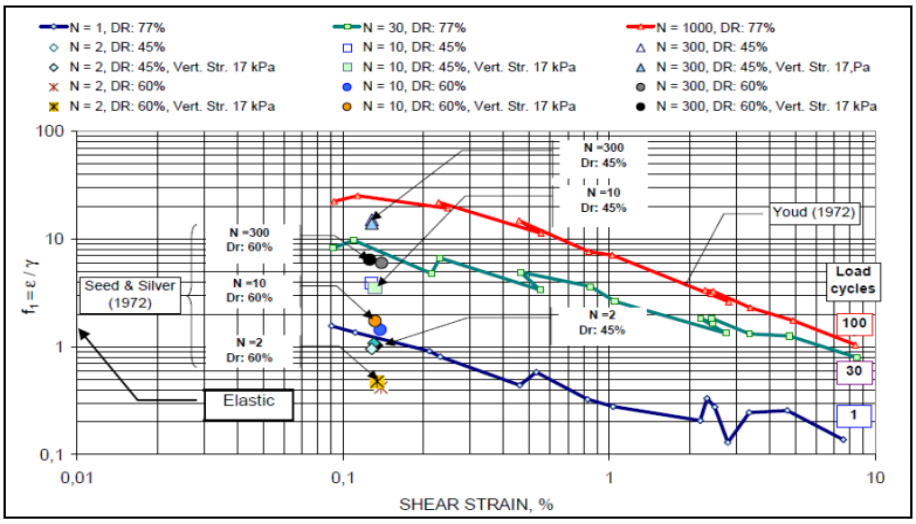

Figure 5.10: Shear strain factor f1 as function of shear strain for different values of load cycles and relative density (data modified after Seed and Silver (1972); Youd(1972))

Relative density (DR) is an important parameter in the laboratory testing of the dynamic properties of sandy soils. Relative density of cohesion less soils is defined as the ratio of the difference between the void ratio of cohesion- less soil in the loosest state and in-situ void ratio to the difference between its void ratios in the loosest and the densest states. Thus relative density (D_r), also called density index (I_d), is defined in Eq.5.4.

$$D_r = [(e_{max} - e) / (e_{max} - e_{min})] \times 100 \qquad \text{(Eq.5.4)}$$

Where e_{max} is the maximum void ratio of soil corresponding to the loosest state, e is the in-situ void ratio, and e_{min} is the minimum void ratio of soil corresponding to the densest state.

Relative density represents the initial state of sands and is usually expressed as a function of soil resistance such as SPT blow counts (Terzaghi and Peck 1967) or CPT tip resistance (Yi, 2009a).Several relationships between relative density and SPT blow counts have been proposed in the past (Terzaghi and Peck 1967; Tokimatsu and Seed 1987; Idriss and Boulanger 2008).

The shear strain amplitude is derived from the vibration velocity amplitude as shown in Eq.5.5

$$\gamma = \frac{Vs}{Cs} \qquad \text{(Eq.5.5)}$$

Where γ is the shear strain amplitude, v_s is the amplitude of vibration velocity and C_s: is the shear wave velocity. Cs is always fixed equal to 540 m/s (about 7% major than the Rayleigh waves velocity; Massarch, 2000)

The parameter $m_z * \nu$ is in fact the velocity amplitude at depth z. The value of m_z can be obtained from theoretical values derived for Rayleigh wave. The relation has been simplified as in Eq.5.6.

$$m_z = 0.9 - 0.6 * z / \lambda \qquad \text{(Eq.5.6)}$$

Where z is the depth below ground level, λ is the wave length. The wave length λ follows from $\lambda = C_R/f$ with C_R the Rayleigh wave velocity and f the dominate

frequency of the propagating wave and according to Massarch (1993) at vibration frequencies on the order of (10-30)Hz the wave length range between (5-20)m these values are just within the critical range of many buildings affected by pile driving. The value of m_z for a homogeneous soil layer can be considered equal to 0.5 it can be obtain following the graph in Figure 5.11

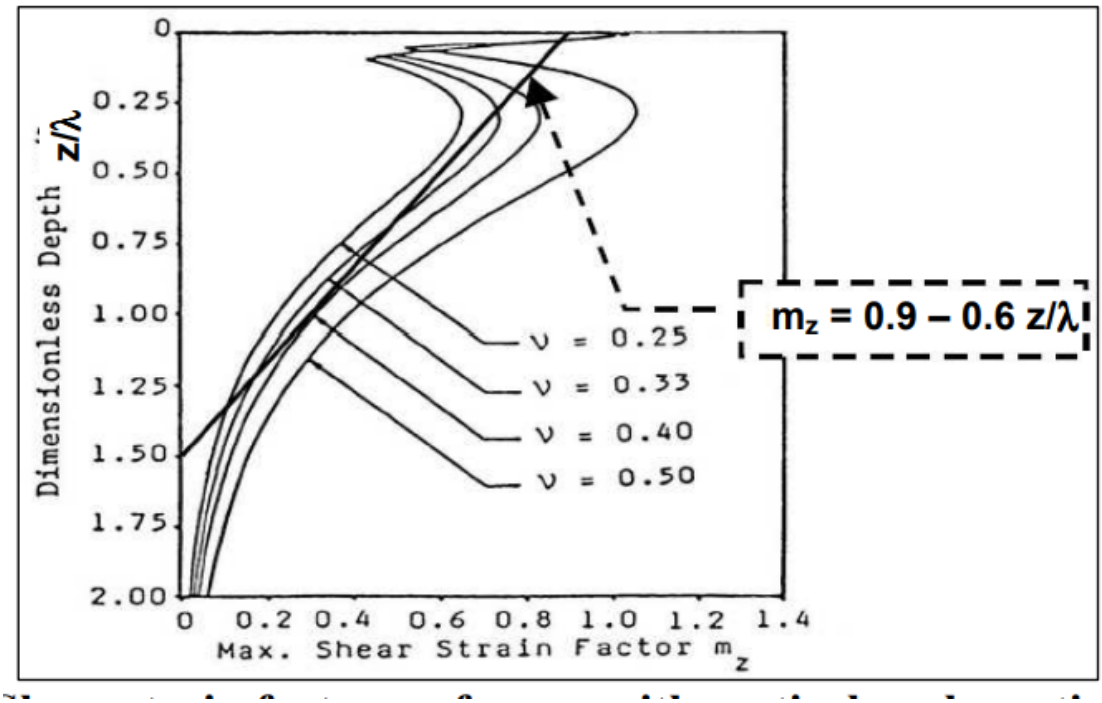

Figure 5.11: Shear strain factor m_z for use with vertical peak particle velocity, with indication of simplified relationship (after Massarch, 2000)

Massarsch (2004b) proposed the basic procedure for estimating ground settlement due to pile driving, the model description is illustrated in Figure 5.9. It is presumed that the most considerable densification due to pile driving occurs within a range corresponding to three pile diameters (3D) around the driven pile. The volume reduction resulting from ground vibrations will cause significant settlements in a cone with an inclination 2(V):1(H) after Massarch (2004b), with its apex at a depth of 6 pile diameters (6D) below the pile toe. Thus, the settlement trough will extend a distance of 3D + L/2 from the centre of the pile, with maximum settlement at the centre of the pile. Maximum and average settlements (s_{max} and s_{avg} (m)) settlement can be estimated using the

Eq. 5.7 relationship adapted from Massarch (2004b) , for an appropriate value of the soil compression factor, α (Table 5.1).

$$Smax = \alpha(L + 6D) \quad | \quad Savg = \frac{\alpha(L+3D)}{3} \qquad \text{(Eq.5.7)}$$

Table 5.1 shows compression factors, based on experience from soil compaction projects, which are applicable to driving in very loose to very dense sand. The intensity of ground vibrations can be assessed based on vibration levels indicated in Figure 5.12

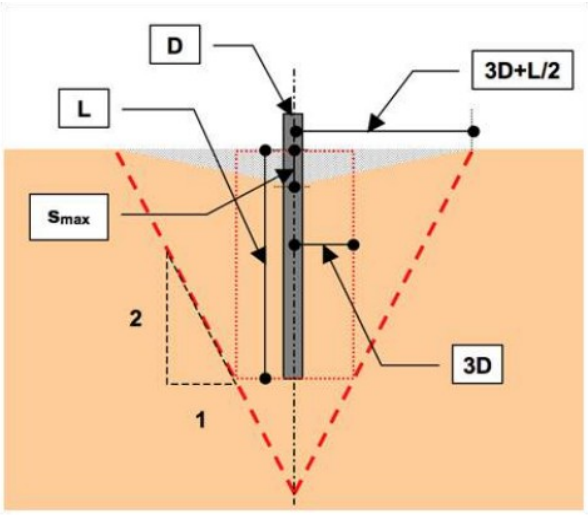

Figure 5.12: Basic method of estimating settlements adjacent to a single pile in homogeneous sand. Massarsch(2004).

Table 5.1: Compression factor, α, for sand based on soil relative density and level of driving energy.(Massarch and Fellenius 2014)

Soil Density	Driving Energy		
	Low	Medium	High
	Compression factor α		
Very loose	0.02	0.03	0.04
Loose	0.01	0.02	0.03
Medium	0.005	0.01	0.02
Dense	0.00	0.05	0.01
Very Dense	0.00	0.00	0.005

Drabkin et al. (1996) proposed a polynomial model to estimate settlement taking into consideration several factors including soil properties. This method allows for good estimation of settlement, however, it is based on a laboratory approach modeling vibration data obtained from field ground surface measurements. The model describes a method to predict in-situ settlement of sands caused by pile driving or vehicular traffic with a laboratory developed polynomial model.

A model of vibration-induced settlement for small to intermediate vibration levels was developed using multifactorial experimental design. Such factors affecting vibration-induced settlement as vibration amplitude, deviatoric stress, confining pressure, soil gradation, number of vibration cycles, relative density, and moisture content. Settlement evaluation is illustrated in Eq.5.8

$$LnY=2.27+1.19(X_1) - 0.71(X_1)^2 + 0.49(X_2) - 0.68(X_2)^2 - 0.80(X_3) +1.09(X_3)^2 - 0.46(X_4) + 0.06(X_4)^2 + 0.45(X_5) - 0.38(X_5)^2 - 0.19(X_6) - 0.10(X_7). \quad \text{(Eq.5.8)}$$

The natural values of factors should be replaced by their coded values Xi and substituted in the polynomial equation as it shown in Tables 5.2 and 5.3.

Table 5.2: Tested Ranges of Factors

No	Factors	Tested ranges	Designation coded value
1	Vibration amplitude	2.5-18 mm/s *(v* =0.1- 0.7 in./sec)	X_1
2	Deviatoric stress	14-104 kPa (s = 2-15 psi)	X_2
3	Confining pressure	69-207 kPa (p = l0- 30 psi)	X_3
4	Sand mixture	Coarse, medium, fine	X_4
5	Number of vibration cycles	N =60-500,000	X_5
6	Moisture content	Dry, saturated	X_6
7	Initial relative density	Loose, medium dense	X_7

The method has been validated by the authors with field data. The considered cases contain situations with impact and vibratory driving of foundation piles and sheet piles. They concluded that a reasonable agreement between observed and calculated settlements exists

Table 5.3: Coding of variable factors

No	Factors	Coding of factors
1	Vibration amplitude	$X_1 = -1 + (v - 0.1)/0.3$
2	Deviatoric stress	$X_2 = -1 + (s - 2)/6.5$
3	Confining pressure	$X_3 = -1 + (p - 10)/10$
4	Coarse sand	$X_4 = -1$
4	Fine sand	$X_4 = 1$
5	Number of vibration cycles	$X_5 = -1 + (N - 60)/26997$
6	Saturated sand	$X_6 = -1$
6	Dry sand	$X_6 = 2$
7	Initially loose sand	$X_7 = -1$
7	Initially medium dense sand	$X_7 = 2$

Bement and Shelby (1997) used the cyclic loading test for sand samples vibrated vertically a new formula is developed to determine the densification of sand. The new formula is derived as a result from large series of cyclic loading tests. Different parameters are varied: type of sand, relative density, vertical (static) stress, frequency of loading (25 Hz, 40 Hz and 120 Hz) and degree of saturation. The vertical acceleration in the tests is increased stepwise. In general each 10 to 20 minutes the acceleration level is increased. From the test results the following expression for the volume reduction is obtained in Eq.5.9.

$$S = \frac{2.8\ \mathrm{Ln}(Dc)\ (\eta)^2}{0.01 \times \sigma'v0} \qquad \text{(Eq.5.9)}$$

With; S: settlement (unit: %), η: acceleration amplitude (unit: g), D_c: parameter describing the grain size distribution (unit mm^{-1}), I_D: relative density (unit: unity), and σ'_{v0}: vertical stress (unit kPa), Where D_C is determined by Eq.5.10.

$$Dc= D_{90}/ (D_{60}\times D_{30}) \qquad \text{(Eq.5.10)}$$

D_{90}: particle size with 90% passing

For acceleration levels exceeding 2g and the possible hazard increased, it is stated by the authors that fluidization will occur and a different equation is given, as shown in Eq.5.11:

$$S= \frac{4\ Ln(Dc) +0.7\ln(\eta)}{0.01\times\sigma'v0+0.75(1-I_D)} \qquad \text{(Eq.5.11)}$$

(Hergarden 2000), developed a method for assessing the settlement due to vibratory sheet piling. The densification is a function of the acceleration amplitude. For the source model empirical data from the Dutch manual on sheet piling C 166 (CUR 1993) are used. The horizontal and vertical velocity at 5 m from the sheet pile are given for 6 different soil profiles, that are typical for Dutch subsoil conditions. The given values are valid for a vibrator with a centrifugal force of 350 kN. For vibrators with a higher centrifugal force the velocity amplitude is to be corrected according to Eq.5.12.

$$V_{0,cor}=V_{ref}+0.002\times(F_{dyn}-350) \qquad \text{(Eq.5.12)}$$

Where F_{dyn} is the centrifugal force (in kN), V_{ref} is the velocity amplitude (in mm/s) at reference distance r_0, for a centrifugal force of 350 kN and $V_{ref,cor}$ is the corrected velocity amplitude at reference distance r_0 (in mm/s),corrected for capacity of the vibrator.

The densification model is based on a publication by Barkan (1962). Following Barkan, Hergarden assumes that there is a threshold acceleration below which no

densification occurs. This threshold acceleration is a function of the relative density and stress level. The threshold acceleration follows from Eq.5.13.

$$\eta_0 = \frac{\text{Ln}\,(1-I_{D,0})}{-\alpha_B} \qquad \text{Eq.5.13}$$

Where η_0 is the threshold acceleration, I_{D0} is the initial relative density and α_B is the empirical parameter, depending on soil strength and stress level. For α_B values are varied between 3 for high stress and strength level and 5 for low stress and strength level.

The change in relative density as function of acceleration and time is described with the following equation, Eq.5.14

$$\Delta I_D(\eta,t) = [\exp(-\alpha_B.\eta_0) - \exp(-\alpha_B.\eta)] \qquad \text{(Eq.5.14)}$$

Where η is the acceleration amplitude (a/g).

Knowing the change in relative density the volume strain can be determined as shown in Eq.5.15.

$$\zeta_{vol} = \Delta I_D \times (e_{max} - e_{min}) / (1+e_0) \qquad \text{(Eq.5.15)}$$

With, e_{max} is the maximum void ratio, e_{min} is the minimum void ratio and e_0 is the initial void ratio.

The amount of densification can be calculated using the mentioned formulas. It is also possible to use the nomogram of Figure 5.13. Starting point is the cone resistance and the vertical effective stress. From this follows in the left hand graph the relative density I_D. For this the correlation of Lunne and Christoffersen (1983) is used. Going to the right hand graph the threshold acceleration can be found when the value of α_B is selected. If the acceleration at the considered point is above the threshold value the relative density after vibrating can be found going from the right hand graph to the left hand graph.

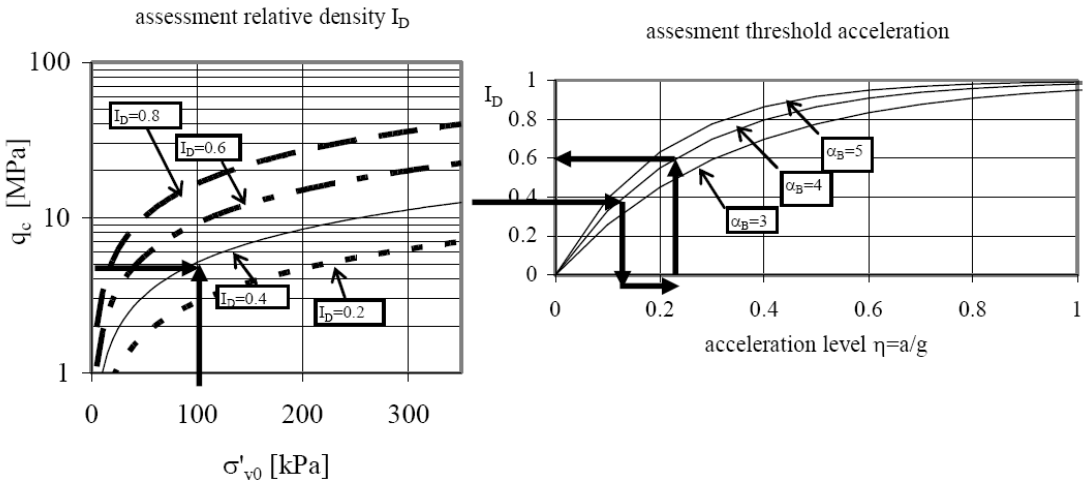

Figure 5.13: Nomogram for assessing the volume strain, after Hergarden (2000)

The procedure will be illustrated with an example. In the example the cone resistance is 5 MPa, the effective vertical stress is 100 kPa and the acceleration amplitude is 2.3 m/s^2 (η= 0.23). From the left hand graph the relative density is assessed to be I_D = 0.4. This value is used as input in the right hand graph. It is assumed that for this situation α_β =4. Going horizontally from I_d = 0.4 to the line of α_β =4 and then going vertical downward the threshold acceleration is found to be η_0 = 0.13. The actual acceleration amplitude is η= 0.23, so above this value. Densification due to vibrating is expected. The final relative density due to vibrating can be read from the right hand graph. Going from η = 0.23 to the line of α_β =4 and then going to the left the final relative density is found to be I_D = 0.5, This gives a change in relative density of ΔI_D = 0.2. From this the volume strain can be calculated.

This procedure can be performed for each point in the densification zone. The result is the local volume strain in the subsoil due to vibrating. The settlement at surface follows from integration of the effect of all local volume strains. It is assumed that the effect of local volume change spreads to the surface at an angle θ. For θ a value of 30° is proposed. With this the width of the settlement trough due to densification of element ij is given from Eq.5.16.

$$B_{ij} = 2\ Z\ \tan\theta \qquad \text{(Eq.5.16)}$$

Where Bij: influence width at surface, z: depth of considered point below ground surface and θ: angle of volume change spreading, as illustrated in Figure 5.14.

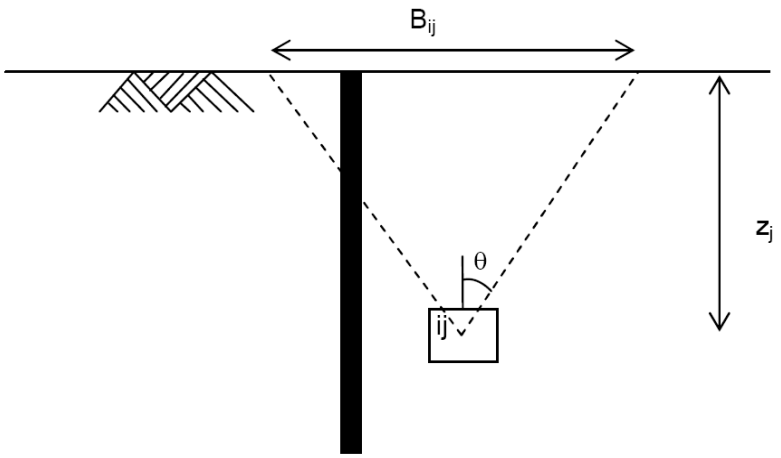

Figure 5.14: Translation of local densification to surface settlement.

The contribution to the settlement follows from the volume change of element I divided by the width B_{ij} as shown in Eq.5.17.

$$\Delta Z_{ij} = \zeta_{vol} A_{ij} / B_{ij} \qquad \text{(Eq.5.17)}$$

Where, Z_{ij} is contribution to surface settlement due to densification of point i, ζ_{vol} is the volume strain at point ij and A_{ij} is the representative area (volume per meter) of point ij.

Meijers (2007) summarized a comparison between the different models for evaluating settlement as shown in Table 5.4. Most of the methods assess the local volume strain or vertical strain. For assessing the surface settlements mostly a vertical integration of the assessed strains is used. This implies that spreading is neglected. Also the effect of the sheet pile volume on the settlement is neglected. In fact Hergarden is the only author that takes this aspect into account.

Table 5.4: Comparison models for assessing settlement due to sheet piling

Model	Driving force for densification	Number of cycles incorporated	Excess pore Pressure Generation	Density of Sand Considered	Type of Piling	Remarks
Massarsch (1993)	Acceleration	No	No	Yes	Vibratory Pile driving	
Massarsch (2000)	Shear strain Amplitude	Yes	No	Partly (only id = 45% and 60%)	Not Mentioned	
Massarsch (2004)	None	No	No	Yes	Not Mentioned	
Drabkin, Kim et al.	Velocity Amplitude	Yes	No	Yes	Not Mentioned	
Hergarden	Acceleration	No	No	Yes	Vibratory Sheet piling	
Bement	Acceleration	No	No	Yes	Vibratory Sheet piling	

5.8 Case Histories records

A lot of documented case histories for settlement infield measurements are illustrated in previous chapters, it can be noticed that the great values of soil settlement are ranged between 16m to 300m from the vibration source, (D'Appolonia 1971 and Kaminetzky 1991 and Bradshaw et al. 2005). By comparing these values of settlement to the standard limits and with the Egyptian code, it can be easily expect a great damage to the structures especially the isolated footings buildings. It becomes very urgent to find ways or models to expect the values of settlement due to construction vibration. Massarch (2004) proposed the basic procedure for evaluating settlement due to pile driving.

Settlement records for case histories are summarized in Table 5.5, for sandy soil or generally coarse soils.

Table 5.5: Values of soil settlement due to pile driving in sand soil.

Reference	Soil type	Measured settlement	Pile type
Swiger (1948)	saturated loose fine silty sand	1.5 ft	H-pile
Lynch(1960)	sand fill, organic silt, loose to medium dense sand, limestone, and compact sand	7 in	
Horn (1966)		5.9 in	
Feld & Craper (1997)	uniform medium dense sand	significant settlements and severe damage	H-pile

From a consideration of various vibration-related standards, the following two criteria are suggested for preliminary assessment of predicted ground vibrations after AJ Sutherland and IR McIver (2012) 0.5mm/s PPV for disturbance of building occupants 5mm/s PPV for building damage. The above criteria do not apply to soils susceptible to vibratory densification or liquefaction. In general, these soils comprise uniform grain size (ie low cohesion) silts below the water table and have a very low scala count, ie about two blows per 50mm. For such cases, specialist geotechnical advice should be sought on the vibration levels that could cause consolidation or densification of the soil, which would result in differential settlement and consequent building damage.

Settlement and heave records case histories are summarized in Table 5.6. In case of clayey soils or adhesive soils

Table 5.6: Values of soil settlement and heave due to pile driving in sand soil.

Measured heave	Measured settlement	Pile type	Reference
adjacent structures heaved up to 9 mm	38 mm during five years		D'Appolonia (1971).
26 to 86 mm at the distance about 16 m from driven piles.		Concrete piles	Bradshaw et al. (2005).

Evaluation of case histories of vibration induced settlement by Drabkin et al.1995.

- **Southern Brooklyn Site (New York City)**

Differential settlement of aeration tanks was described by Lacy and Gould (1985) and Lacy et al. (1994). The 5 m high, 80 m wide tanks were supported by timber piles as shown in Figure. 5.12. Closed-end 10.75 in. (273.1 mm) pipe piles were driven to depths exceeding 40 m in close proximity to the tanks to support the new structure. Pile driving in medium dense, fine to coarse sand was performed with Vulcan 08 impact hammer. Settlement was noticed when about 100 new piles had been installed. When settlement exceeded 25 mm, all fluid was removed from the tanks, reducing loading by about one half. Nevertheless, the settlement continued and reached 70 mm during the driving of additional piles. Augered cast-in-place piles (ACIP) replaced the remaining piles to be driven, which were generally those closest to the existing structures. The possible settlement was assessed using one- and 10 layer extrapolation schemes.

The natural and coded values of factors are shown in Figure 5.15. Calculated settlement of 58.9 to 74.3 mm matched well the observed settlement Vibrations were monitored with a seismograph on the surface of both structure and the

adjacent ground. Peak particle velocities on the structure were always less than 2.5 mm/s. On the ground the vibration amplitude ranged from 2.5 to 23 mm/s. Estimates of α from ground and surface measurements ranged from 0.02 to 0.05 mm^{-1} These values indicate attenuation in organic soils forming the upper strata on site. The vulnerable zone was formed by medium dense fine sand, and the Vulcan 08 impact hammer generated frequencies of about 20 Hz. Hence an assumed value of $\alpha = 10^{-5}$ mm^{-1} was used in 10-layer extrapolation method.

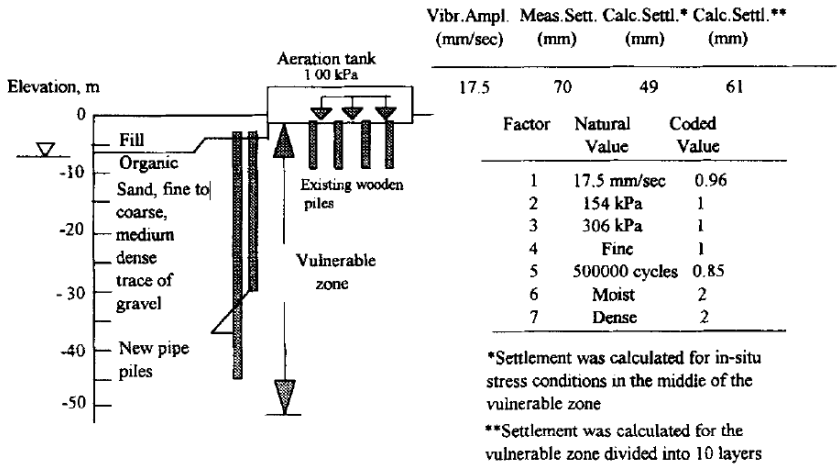

Figure 5.15: Case History at South Brooklyn Site, New York, after Drabkin et al. (1996).

- **Cedar Creek Site in Wantagh (New York)**

Evaluation of vibration effects on settlement was performed by Lacy (unpublished report, 1986) to permit the use of a vibratory hammer to drive sheeting in close proximity to existing structures, The study consisted of pile-hammer testing and monitoring of vibration-induced settlement during pile driving at the Cedar Creek site.

Several effluent tanks were planned to be constructed close to the existing 2.4 m diameter effluent and 2.1 m diameter outfall pipes as shown in Figure 5.16. Subsurface conditions are shown in Figure 5.17 as interpreted from borings made in the vicinity of the pipes. The upper 4-5 m layer was hydraulically placed lose to very compact gray and brown medium sand with a trace of silt and gravel. The

sand's density varied substantially from boring to boring. Next followed 1-2 m of organic silty clay, peat, and medium dense sand. The pipes were founded below this layer. Under the pipes to the elevation -12 m is medium compact gray fine to coarse sand with a trace of silt and gravel. This layer was vulnerable to vibration densification.

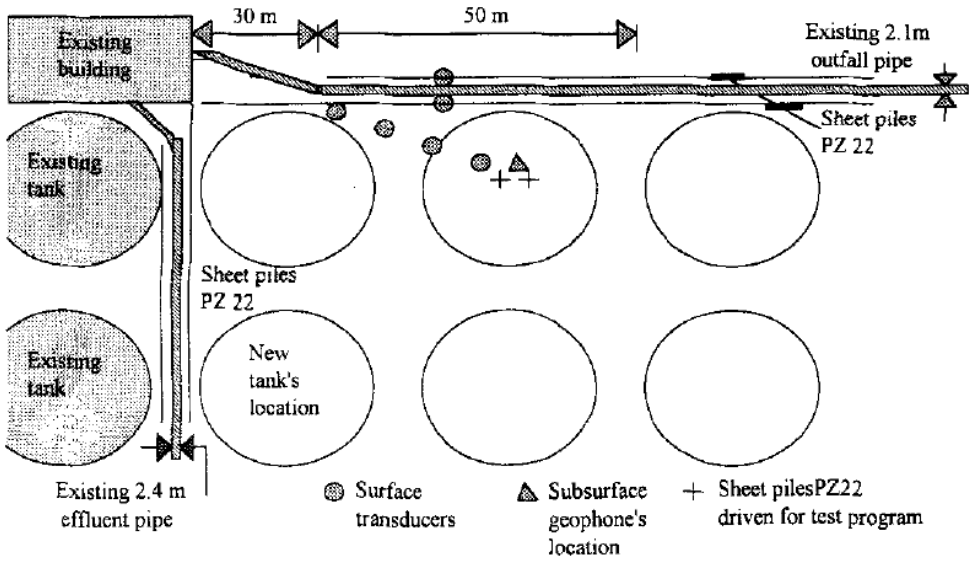

Figure 5.16: Settlement Monitoring Location Plan at Cedar Creek Site, after Drabkin et al (1996)

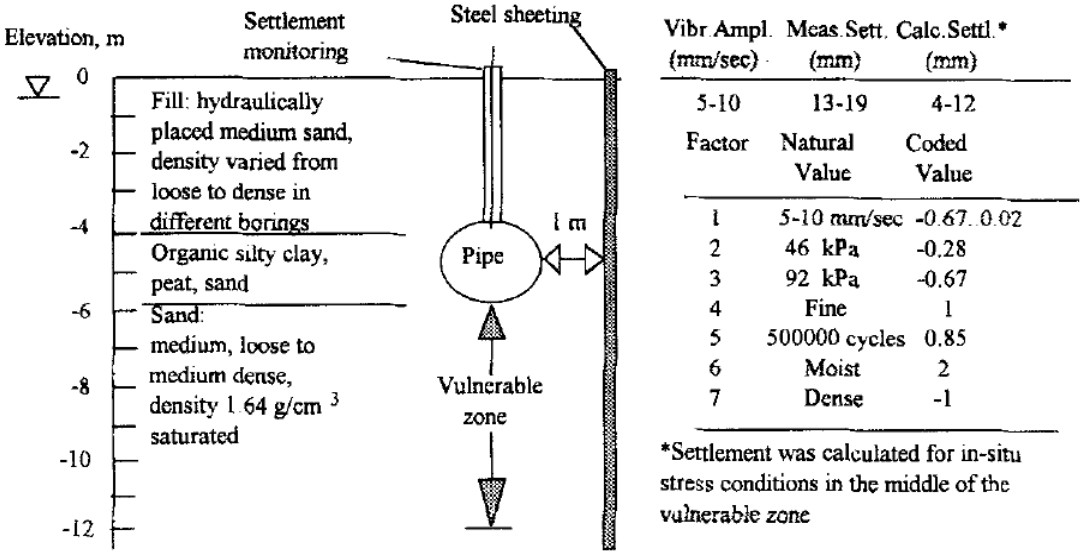

Figure 5.17: Cedar Creek Site, after Drabkin et al (1996)

Based on the test driving data, settlement was evaluated using a one-layer extrapolating method. Calculations with the 10-layer extrapolation method were

unnecessary at this site because of the small thickness of vulnerable zone. Settlements were evaluated for vibration amplitudes of 5 mm/s and 10 mm/s. The vulnerable 7 m zone was below a 5 m sand fill layer, hence confining pressure in the middle of the zone was 92 kPa and the deviator stress was 46 kPa for the at-rest earth pressure coefficient condition. The levels of all factors are shown in Figure 5.14. The predicted settlement due to driving of a small number of test piles was about 2 mm and could be within the error margins of settlement observations. The calculated settlement after driving of sheeting along the pipeline ranged from 9 to 15 mm. Therefore, the polynomial model was able to predict settlement better than test pile driving.

- **Lesaka Site (Northern Spain)**

Picornell and del Monte (1985) discussed a case of pile driving-induced settlement of a pier foundation. The building of a steel mill factory was supported by cast-in-place concrete 1.08 m diameter piers embedded to a depth of 20 m into sandy soil. The vertical pressure on each pier did not exceed 534 kPa. New equipment foundations had been designed on steel H-piles to be driven to bedrock. Upon driving steel H-piles, one of the pier foundations settled 250 mm. The investigation of this settlement included field plate-load tests, pier-load tests, and laboratory consolidation tests. They showed that static design loads would cause only minimal settlement (less than 9 mm). At the time the settlement was noticed, a visual inspection did not reveal the presence of cracks or any other feature on the ground surface that would suggest some type of cave-in effect. Using an analogy between this settlement and the settlements observed at the Embarcadero site (Clough and Chameau 1980) and at the Leningrad site (Dalmatov et al. 1968), dynamic compaction induced by the pile driving on the sand layer was considered to be the only cause of settlement. Analysis of the vibration-induced settlement using the polynomial settlement model raises doubt as to that conclusion.

In their investigation, Picornell and del Monte provided neither observed vibration amplitudes and duration of pile driving nor the type of driving

equipment. A maximum v = 17.5 mm/S was assumed. The mean effective stress (confining pressure) in the middle of vulnerable zone at a depth of 35 m was 562 kPa assuming an earth pressure coefficient at rest as 0.5. The deviator stress was 188 kPa. The stresses exceed those used for the development of the polynomial model. Thus, the combination of maximum tested level of confining pressure and deviator stress was chosen to get the possible upper bound of settlement. The number of vibration cycles were also maximum. The natural and coded values of factors are shown in Figure 5.18.

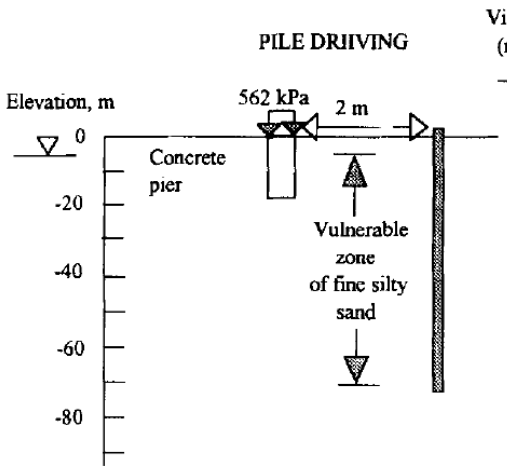

Vibr.Ampl. (mm/sec)	Meas.Sett. (mm)	Calc.Settl.* (mm)	Calc.Settl.** (mm)
17.5	250	80-100	100-120

Factor	Natural Value	Coded Value
1	17.5 mm/sec	0.96
2	188 kPa	1
3	374 kPa	1
4	Fine	1
5	500000 cycles	0.85
6	Moist	2
7	Loose	-1

*Settlement was calculated for in-situ stress conditions in the middle of the vulnerable zone

**Settlement was calculated for the vulnerable zone divided into 10 layers

Figure 5.18: Case History of Pier Settlement in Lesaka, Spain, after Drabkin et al.(1996).

The calculated settlement using both computational methods is about 120 mm, which is two times smaller than was observed at the site. Vibration-induced densification could not be totally responsible for settlement of this magnitude. Still, pile driving was definitely responsible for settlement. The explanation is probably the combined effect of vibration on both soil densification and the reduction of skin friction on the piers. These piers were not supported by bedrock, so settlement of surrounding soil could cause pier settlement. The quantitative effect of vibration on stability of friction piles in sands was not properly investigated.

- **Tri Beca Site in Manhattan (New York City)**

The settlement that accompanied pile driving at the Tri-beca site in Manhattan was described by Lacy et al. (1994). A 52 story residential building, Tri-beca Tower, was planned in close proximity to two other buildings Figure.5.19. The original foundation project considered installation of 178 mm outside diameter open-ended 30 m long pipe piles. The subsurface conditions are shown in Figure 5.20. Medium compact fine to medium sand was expected to density due to vibrations. Test piles were driven to evaluate expected settlement of an adjacent two story building and a historic landmark six story building. Extrapolation from field measurements of ground settlement predicted 25-50 mm settlement for the two story building and 13-25 mm settlement for historic building. The values of vibration amplitudes during test pile driving are now not available. They were limited by 25.4 mm/s to prevent direct damage to the structures from vibrations.

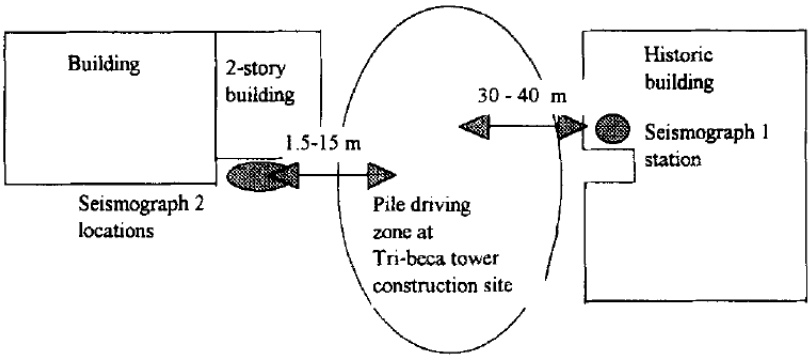

Figure 5.19: Plan of Tri-Beca Site in Manhattan, after Drabkin et al (1996).

The observed settlement of the two story building was 38-69 mm at different stages of construction. Settlement of both buildings was evaluated using the polynomial prediction model using one-layer and 10-layer extrapolation methods assuming $\alpha = 10^{-5}$ mm^{-1} The predicted settlement for the historic building was less than 10 mm and that matched the observations.

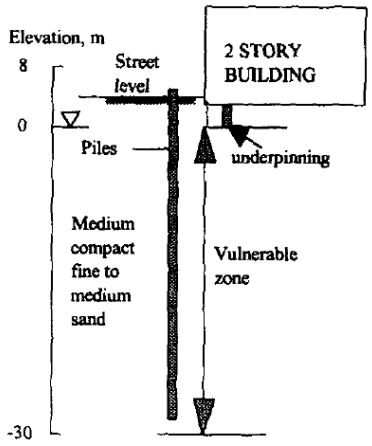

Vibr.Ampl. (mm/sec)	Meas.Sett. (mm)	Calc.Settl.* (mm)	Calc.Settl.** (mm)
5-13	38-69	12-49	18-65

Factor	Natural Value	Coded Value
1	5..13	-0.67..0.37
2	53 kPa	-0.13
3	106 kPa	-0.46
4	Fine	1
5	500000 cycles	0.85
6	Moist	2
7	Dense	2

*Settlement was calculated for in-situ stress conditions in the middle of the vulnerable zone
**Settlement was calculated using 10-layers extrapolation scheme

Figure 5.20: Case History at Tri Beca Site in Manhattan, after Drabkin et al (1996).

Studied case histories showed that usually the use of the one-layer method was sufficient for estimation of settlement. The l0-layer extrapolation showed the effect of different layers on settlement and provided the upper limit of expected settlement. That approach may be recommended for evaluation of effects of pile driving in highly non homogeneous soils.

The maximum densification happens when high deviatoric stress is combined with low confining pressure. In case of high confining pressure, the model will be valid approximately up to double values of stresses observed in the field as compared to laboratory tested. The authors (Drabkin et al) do not recommend use of the model beyond that range.

Drabkin et al (1996) compared the settlement values due to pile driving from infield measurements and the calculated values using one layer method and 10 layers method as it illustrated in Table 5.7.

Table 5.7: Case histories of vibration induced settlement, Drabkin et al.(1996)

Investigated sites	Vibration amplitude (mm/s)	Settlement (mm)		
		Observed in situ	Calculated	
			One layer scheme	10 layers scheme
Back Bay (Leathers 1994)	5.4-15	18-54	18-63	24-78
Brooklyn, South (Lacy et al. 1994)	17.5	70	59	74
Brooklyn, West (Lacy et al. 1985)	2.5-15.2	61	5-56	8-63
Cedar Creek (Lacy 1986)	5-10	13-19	9-15	-
Embarcadero (Clough and Chaomeau 1980)	1-5	8-51	8-58	-
Leningrad (Dalrnalov el al. 1967)	2.8	6-11	4.5	8.1
Lesaka (Picomell and del Monte 1985)	17.5	250	111	117
Northbrook pipeline (Linehan 1992)	2.8	38	37	48
Tri-beca (Lacy el aI. 1994)	2.5-18	38-69	15-112	27-135

5.9 Conclusions

Different methods are available to aid the design engineer in assessing the surface settlement due to construction vibration. In this chapter, the common models of settlement prediction are mentioned and briefed. The possible damage due to settlement is illustrated using lots of figures describing the resulted damage. Some of case histories represented as measurements of soil settlement due to construction vibrations. The following points of conclusions are briefed:

1. Cracks in structure systems occurred due to differential settlement beneath the foundation.
2. Construction vibration could be destructive for old or heritage buildings.

3. Case histories documented the settlement values along away from the vibration source show that the settlement can occur at far distances and with high values and could be harmful.
4. Preconstruction survey should be set before starting any vibration process to document any cracks exist on the adjacent structures and to predict and estimate the values of settlement.
5. Shear strain is very effective parameter for calculating settlement due to construction vibration.
6. Models for settlement prediction were done to estimate the values of settlement to help the engineers to predict soil settlement to avoid the possible damage.

Chapter 6
Wave Barriers

Chapter 6
Wave Barriers

6.1 General:

Ground vibrations are generated by construction activities (i.e. dynamic compaction, roadbed compaction, pile driving, blasting), are considered as a serious problem facing the structures and heritage buildings. Many solutions are discussed by many researchers to control and may be prevent the effect of construction vibration, which would be the scope of this chapter.

In most cases, the major part of the vibration energy induced by dynamic sources transferred by the Rayleigh waves propagating in the region nearby soil surface may cause strong ground motions and stress levels that transmit the vibrations through the subsoil to the structures. Therefore, the permanent adversely affects these excessive vibrations on the foundations, particularly supported on the soft soil deposits, cause structural damage to the adjacent structures.

6.2 Introduction:

In severe cases, buildings and buried services in the near vicinity may be at risk of cosmetic or minor structural damage, (Head & Jardine 1992), (Wiss 1967) and (Todd 1994). This transit vibration can cause feelable movement of building floors, rattling of doors and windows, and shaking items on shelves along with rumbling sounds.

6.3 Reduction of construction-induced vibration:

For an effective protection of the buildings from structural damage due to dynamic loads generated by man-made activities, there are many possibilities to be considered as vibration screening systems.

The reduction of the structural response may be accomplished as a) by adjusting the frequency contents of the excitation, b) by changing the location

and direction of the vibratory source, c) by modifying the wave dissipation characteristics of the soil deposit, and d) by partially interrupting the spreading of waves into the structure or by providing the structure more damping by means of installation certain devices such as additional dampers or other base isolation systems, (Firat et. al.2010). Figures 6.1 to 6.5 show the process of wave control by using wave barriers with different types of trenches.

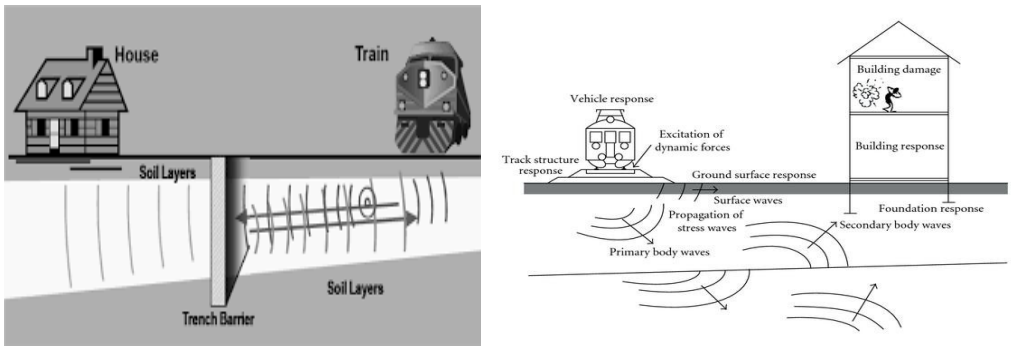

a) Wave control by trench b) Wave propagation

Figure 6.1: Wave propagation from vibration source and path control for wave reduction.

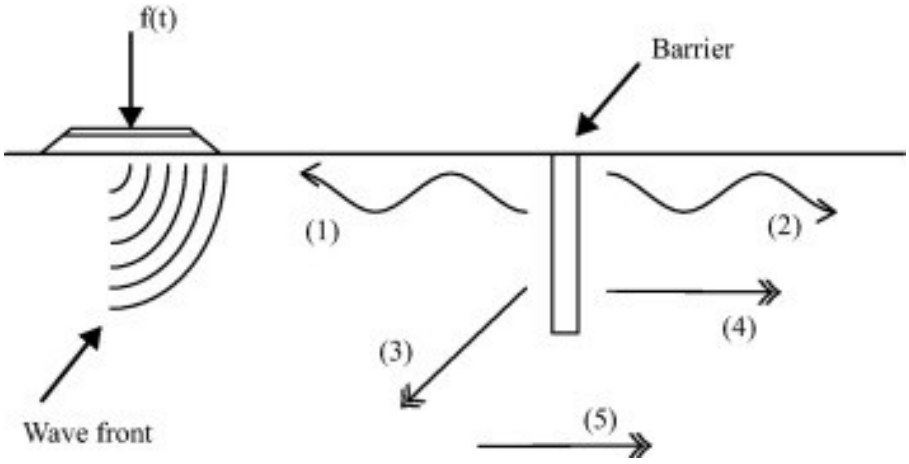

Figure 6.2: Reduction in ground vibrations by using barriers, after Persson et al. (2016)

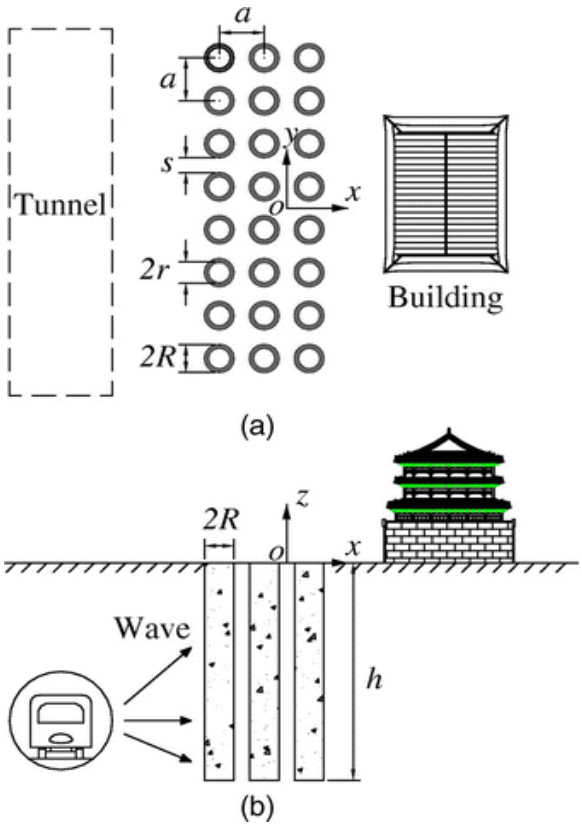

Figure 6.3: Vibration Reduction of Plane Waves Using Periodic In-Filled Pile Barriers, from Huang and Shi (2016)

Figure 6.4: The site of Furet: (a) track, noise barrier and buildings close to the track, and (b) plan view with indication of the sheet pile wall and the setup for the measurement of the free field response due to train passages**,** adapted from Dijckmans et al (2016).

Figure 6.5: Installation of the sheet pile wall: (a) general view after installation of sheet piles up to a depth of 10=16 m with the small rig, (b) welding of the top 0.3 m, adapted from Dijckmans et al (2016).

6.4 Methods of reduction vibration:

Selection of the pile installation method may provide the solution to some difficult pile driving vibration problems. Among the methods that might be chosen are (1) pre-drilling, (2) jetting, (3) cast-in-place (CIP) or auger cast piles, (4) non displacement piles like H-piles, and (5) pile cushioning, (Nam et al 2013). Several researchers have introduced multiple alternatives of pile installation techniques for minimizing the ground vibrations (Woods 1997; Svinkin 2010; Jones and Stokes 2004), However, these alternatives could not be available in most of the construction sites due to special design or different purposes.

Therefore a new way to protect structures from damage is needed and it is under investigation by many researchers and it is the wave barriers.

6.5 Wave Barriers:

Controlling a vibration source would be the most effective and easiest method of minimizing construction vibration (Webb 1976) but they are sometimes insufficient and inapplicable depending on site and construction conditions. Therefore, a second mitigation strategy to control vibration and noise is “path control”, which can be wave barriers (or vibration isolation system).

The installation of a wave barrier in the soil can significantly minimize ground vibrations by preventing the transmission of stress waves (Luong 1994). The barriers absorb or reflect propagated surface wave and reduce the energy of propagated wave from the source to nearby structures. Wave barrier is typically either a trench or a thin wall made of sheet piles or similar structural members.

6.5.1 Wave barriers types:

Both open trench and solid barrier, such as an in-filled trench with suitable materials, can be useful as vibration measures. There is a wide range of construction types of wave barriers, varying from very stiff concrete walls or row of piles to very flexible gas mattresses or wave impeding barriers, bentonite trenches, solid or hollow concrete walls, sheet pile walls, and expanded polystyrene (EPS) geofoam trenches.

Because of screening efficiency, without great difficulty to realize and low cost, both open and in-filled trenches are the most common in practical engineering applications as isolation systems.

Some studies have indicated that open trenches perform better than in-filled trenches (Beskos et al., 1985); (Ahmad and Al-Hussaini, 1991); (Luong, 1994); (Segol et al., 1978). On the other hand, (Massarsch 2005) reported that the performance of in-filled barriers relies on the type and characteristics of filling materials. As well as reporting that a gas cushion barrier made of cement-bentonite shows almost the same performance as the open trenches. (Xu et al. 2008) concluded that soil bags can be used to reduce the vibration induced by traffic and construction machine. The researchers have made further investigations on the effect of barrier depth, trench filling materials, and geometrical criteria published.

6.5.2 Case histories of using wave barriers:

6.5.2.1 (Barkan 1962) committed a number of field experiments to study the isolation performance of open and sheet-wall barriers, trying to isolate a

building from traffic-induced vibration, as shown in Figure 6.6. After comparing the vibration of building foundations before and after the installation of sheet-wall barriers, he found that the vibrations from the street continued to affect the building. Based on this, he concluded that the mitigation effect of the installation of wave barriers was so small that wave barriers were useless in reducing the ground vibration. However, (Barkan 1962) also mentioned later in his study that the failure of vibration reduction by wave barriers could be attributed to the lack of clear understanding of surface wave propagation in the presence of wave barriers in soil media.

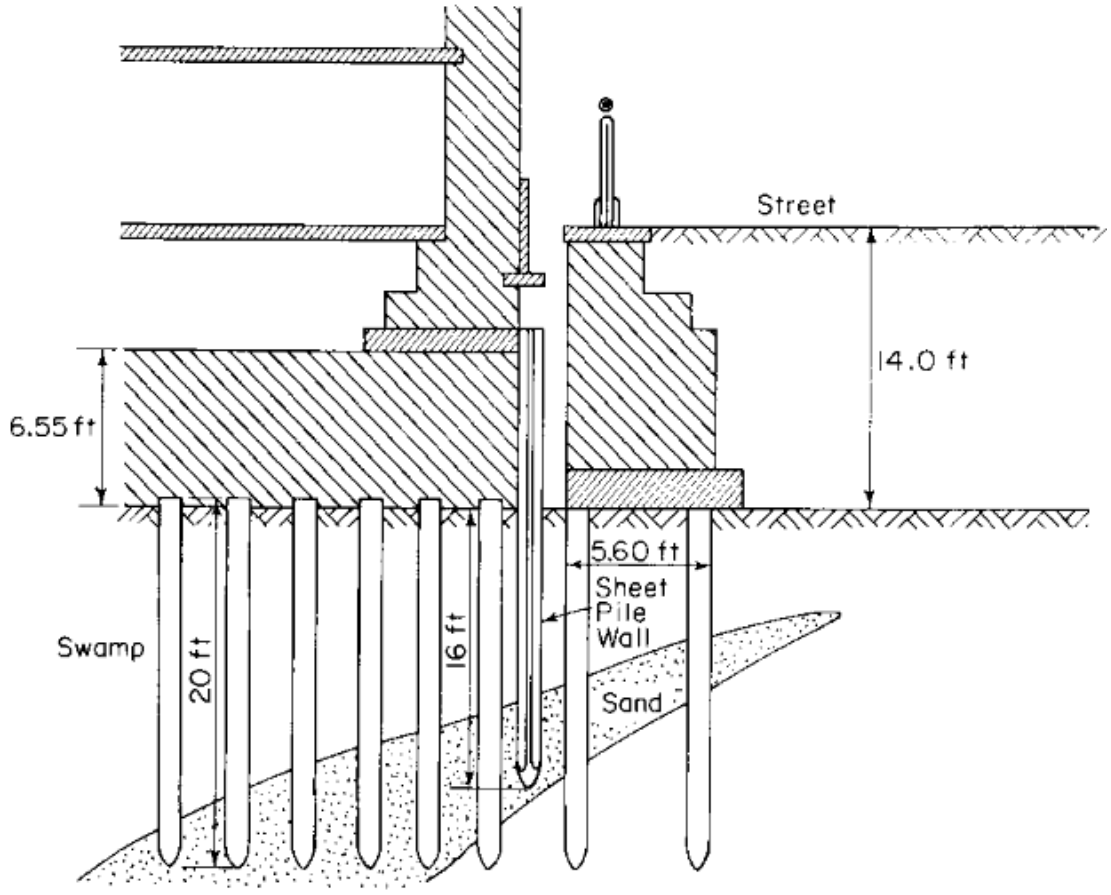

Figure 6.6: Vibration isolation of buildings from traffic-induced vibrations, after (Barkan 1962)

6.5.2.2 Dolling (1965) and Neumeuer (1963) used a bentonite-slurry-filled trench to protect a printing plant from the subway train induced vibrations, as

shown in Figure 6.7. This application of the trench seemed to be effective since the magnitude of vibration of the printing plant after the installation of the trench was only half of the one before the appearance of trench.

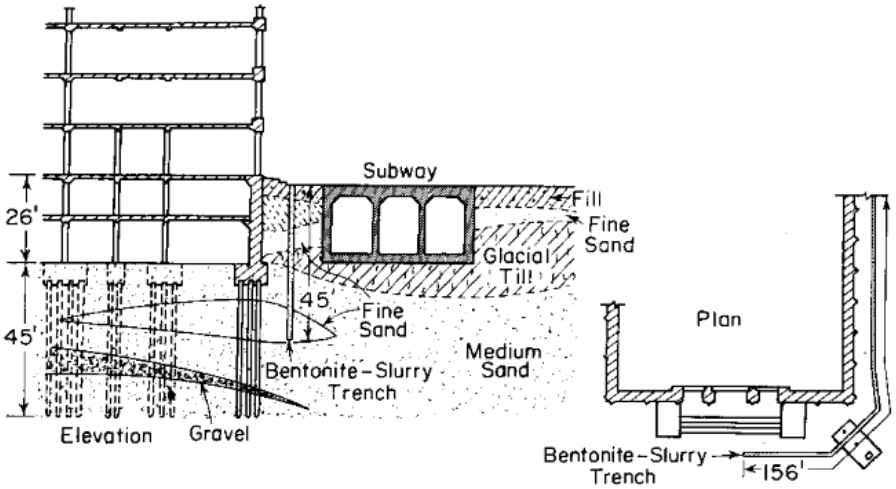

Figure 6.7: Vibration isolation of buildings from train-induced vibration after (Dolling 1965)

6.5.2.3 McNeill et al. (1965) presented another successful application of wave barriers by using a trench and a sheet-wall barrier to isolate a sensitive dimensional-standards laboratory see Figure 6.8. It was reported that the measured acceleration of the slab met the owner's specification (maximum acceleration smaller than 0.1 g).

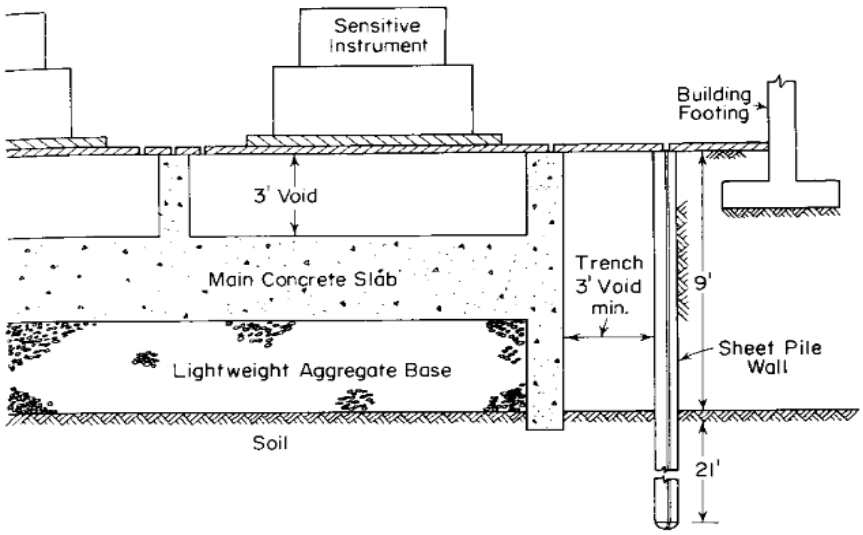

Figure 6.8: Isolation of sensitive instrument from vibration after Meneill et al. 1965.

6.6 Wave Barriers location:

Wave barriers can be divided into two groups: (1) active and (2) passive systems (Woods 1968). The two wave barrier types are seen in Figures 6.9.a and 6.9.b respectively. Trenches located close to the vibration source are called active isolation systems (range between 1 and 1.5 wavelengths from the vibration source), while trenches far from the source are called passive systems. The passive systems placed in the far field from the source are designed to shield surface waves propagated.

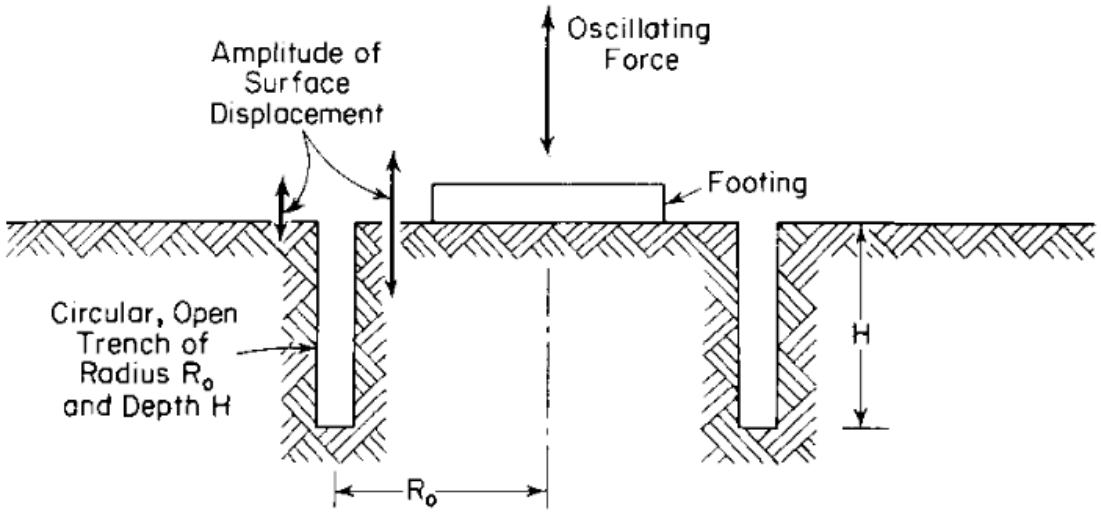

Figure 6.9.a: Active isolation vibration: circular open trench surrounding vibration footing after (woods 1968).

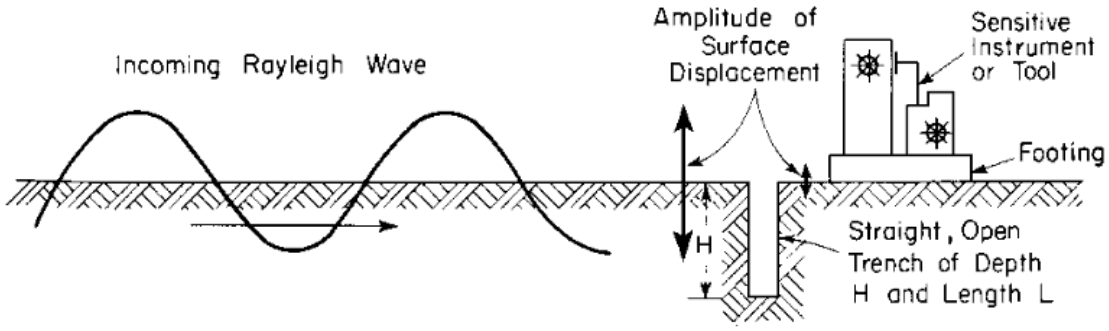

Figure 6.9.b: Passive open trench to protect buildings with sensitive installations after (woods 1968).

6.7 Barriers Depth

Barriers depth could be the most important parameter for the trench design. Consequently, using the open trenches is somewhat limited to small to medium depth because problems regarding soil instability and groundwater table may occur during construction (Woods, 1968).

May and Bolt (1982) reported that, in the active system, the distance between vibration source and barrier is not significant from a practical viewpoint but the depth has a significant influence on the vibration reduction. (Haupt 1995) also indicated that the effectiveness of passive systems does not depend on the distance from the vibrating source but the dimension (depth and width) of the system. There have been studies showing the relationship between the trench depth and the wavelength of the relevant Rayleigh wave (Ahmad and Al-Hussaini 1991; Al-Hussaini and Ahmad 1991; Al-Hussaini and Ahmad 1996). For the influence of trench width, (Fuyuki and Matsumoto (1980) reported that the width is an important affecting factor for the shallow open trenches whereas (Woods 1968) and (Segol et al. 1978) concluded that the width is not a relevant factor.

6.8 Trench Material

Many studies have shown good performance of in-filled trenches and they addressed the influence of trench filling materials. Beskos et al. (1985), Ahmad and Al-Hussaini (1991), Luong (1994), and Segol et al. (1978) concluded that open trenches are more effective wave barriers than in-filled trenches but they also addressed that the open trench applications are not very practical due to the soil (or wall) stability. Al-Hussaini and Ahmad (1996) indicated that concrete, bentonite, soil-bentonite mixtures are the most common filling materials. Other materials such as extended polystyrene (EPS) and rubber modified asphalt have been used to fill the trench (Zeng et al., 2001; Zhong et al., 2002; Itoh, 2003; Itoh et al., 2005). A gas cushion barrier made of cement-bentonite was introduced by Massarsch (1991) and the study shows the

comparable performance to open trenches. Itoh et al. (2005) investigated the performance of aluminum and geofoam as trench materials and his conclusion was that geofoam works better than aluminum. Wang et al. (2006) also studied the performance of geofoam wave barrier and showed the attenuation of stress waves in a concrete layer barrier.

6.9 Experimental investigation of wave barriers (open-in filled)

An experimental study by (Flrat et al. 2010) was made to investigate the wave propagation in case of wave barriers, electrodynamic shaker is used to produce vertical harmonic vibrations in the certain frequency range and accelerometers are used to obtain generated values that are stored on the computer by using signal calculator program. Two footings are constructed with clear distance where Rayleigh wave becomes dominant on site close to Sakarya city (Turkey) as shown in Figures 6.10 and 6.11. The first footing is used to produce the harmonic load and the other for accelerometers record and vice versa. A number of experiments are carried out on site in order to examine the screening efficiency of open and in-filled trench barriers, such as backfilled with water, bentonite, and concrete. The screening effectiveness of those barriers is determined from field measurements by comparing site data without barriers. Two different approaches are considered for vibration isolation, namely active and passive isolations.

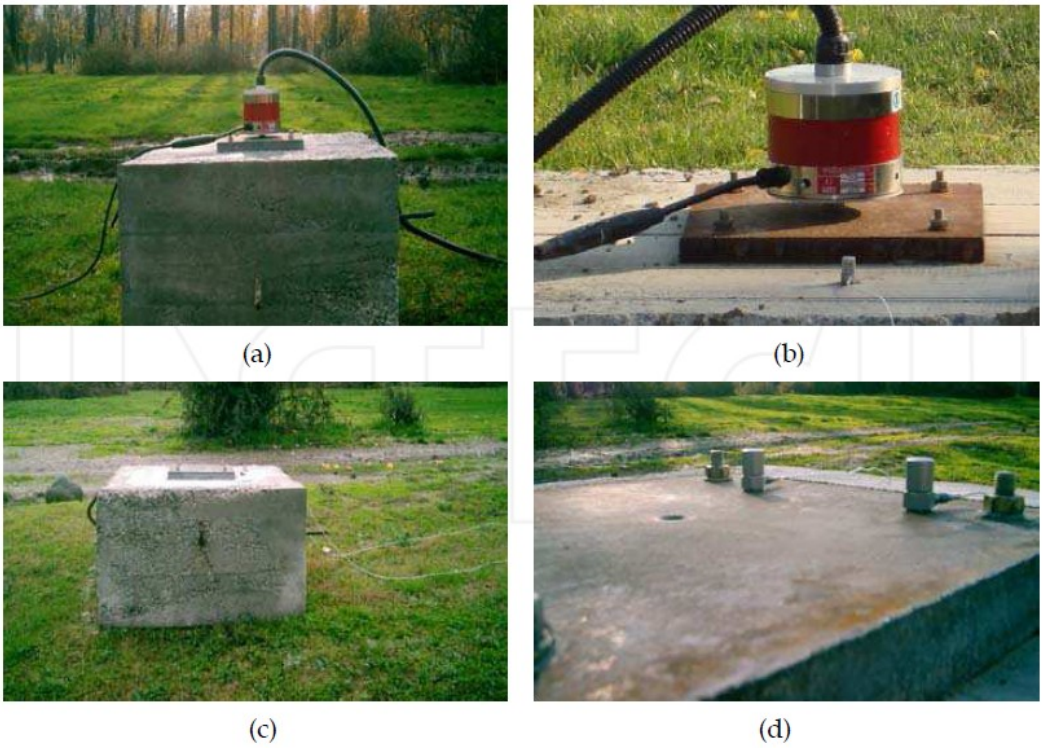

Figure 6.10: Electrodynamic shaker and accelerometers placed on the foundations, after (Flrat et al. 2010).

Figure 6.11: Trench barriers, after (Flrat et al. 2010).

Flrat et al. (2010) studied the effect of different trench materials, a comparison between open, in-filled trenches on wave propagation. By doing several infield experiments with different parameters on the reduction of foundation vibrations due to a harmonic load which is produced by electro dynamic shaker using a trench barrier.

Flrat et al. (2010) reached the following conclusions:

- Using open or in-filled trench barriers can reduce the vibrations of a structure and the resulting internal forces significantly.
- The use of an open trench is more effective than using an in-filled trench but its practical application is limited to relatively shallow depths.
- Using softer backfill material increases the effectiveness of in-filled trench and allows for larger trench depth with no supporting measures of the vertical walls of the trench.
- The barriers have been found to be generally more effective in passive isolation compared to active isolation for both measurement points.

6.10Numerical Study on Vibration Isolation by Wave Barrier and Protection of Existing Tunnel under Explosions (QIU2014):

In his study, Qiu(2014) focuses on the investigation of the influence of various parameters of a soil-barrier system on the barrier isolation efficiency. It helps the design engineer to be able to provide a good reference for the optimization design of wave barrier in reducing ground vibration in protected site and for the design of practical mitigation measures to protect existing tunnel from nearby explosions.

Qiu (2014) has concluded the following:

- Soft barriers with large depth are particularly effective in reducing the ground motion in protective sites.
- The barrier width and inclination angle seem to have little influence on the isolation effectiveness in the case of subsurface explosions, but their influences cannot be ignored in the case of a surface harmonic load. Specifically, under the surface harmonic load.
- A proper increase in the barrier width is beneficial, wave barrier with a width slightly larger than its depth performs better than the one with other widths.

- Wave barrier with a small inclination angle away from vertical direction has a better screening effect than vertical ones.
- Other parameters like the barrier Poisson's ratio, damping ratio, the barrier location, the magnitude of the external load has negligible or no influence on the vibration isolation effectiveness under the surface harmonic source and subsurface explosions.
- Numerical results show that the elastic model can be used for simulating the dynamic behavior of the main tunnel under weak explosions.

6.11. Numerical analysis

Finite element analyses of pile driving are carried out using Plaxis 8.2 2D dynamic version. A set of general fixities to the boundary conditions of the problem are considered automatically by the Plaxis program. The Rayleigh damping is considered at vertical boundaries with α, $\beta = 0.01$ in order to resist the Rayleigh waves. While the plastic properties of soil are defined by using material damping, which is defined in Plaxis by Rayleigh (α and β), where The Rayleigh damping is considered to be object-dependent in material data set to consider the plastic properties of soil during the dynamic analysis in Plaxis. Plaxis models for pile driving with and without the existing of wave barriers are shown in Figures 6.12 and 6.13. For impact hummers, the analysis was based on three phase's plastic (staged construction) and two phases for dynamic analysis (total multipliers). The dimensions of the soil model for pile driving are taken around 50m in depth and 100m in width after some mesh experiments.

The pile in Plaxis is modeled as a linear elastic nonporous. The pile has a circular cross-section with a diameter of 0.4 m with length (L_{pile}) of (10m). For representing the behavior of reinforced concrete pile in the Plaxis model, the Poisson's ratio is taken "ν" 0.1, unit weight "γ_c" 25 kN/m^3 and modulus of elasticity of 22E^6 kN/m^2.

The output of peak particle velocity (PPV) has two components horizontal and vertical but in this research vertical velocity is used for the analyses.

The layers which used in the model are soft clay stretched to 9m below ground surface overlaid on a stiff clay soil with a depth of 11m and another layer of sand stretching into great depths the properties of the soil are taken as mentioned in the previous chapters .

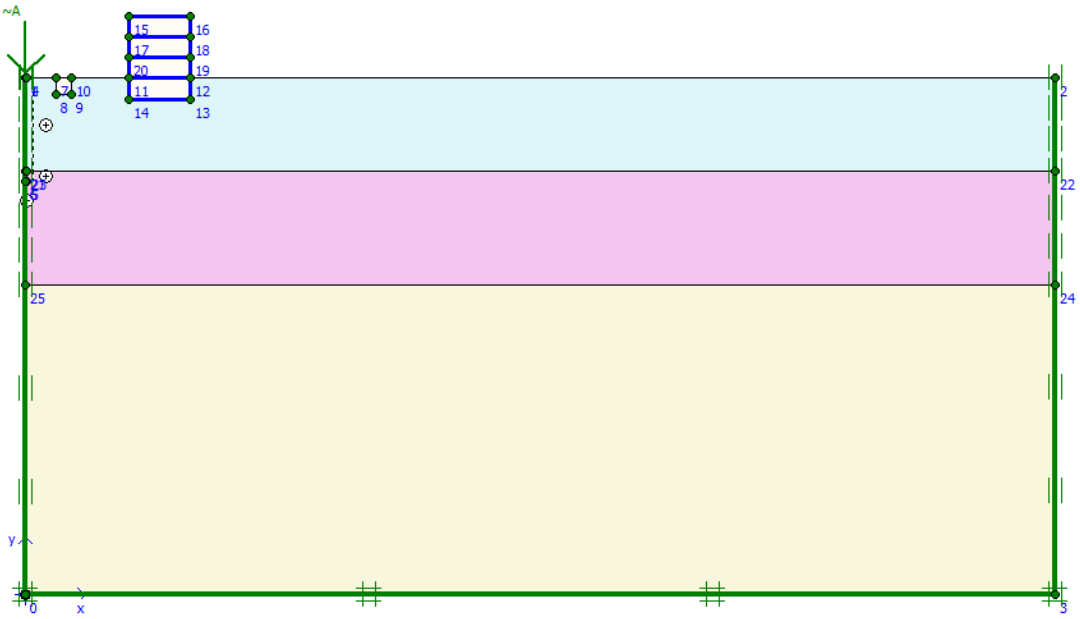

Figure 6.12: Active wave barrier system during pile driving, Plaxis model.

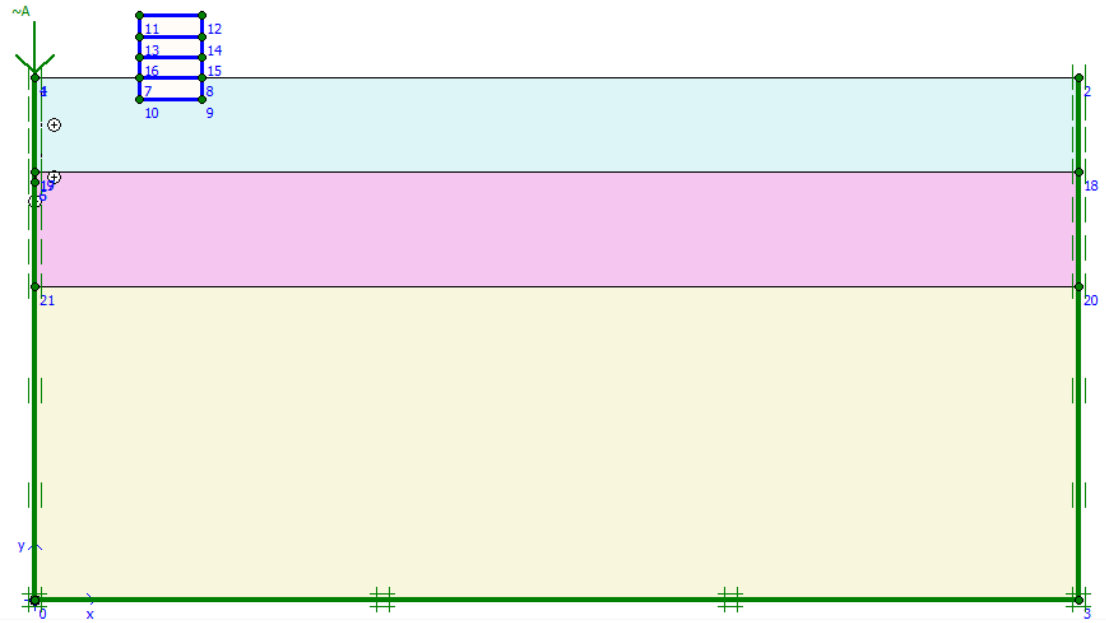

Figure 6.13: Pile driving process without existing the wave barriers, Plaxis model.

6.11.1 Studied parameters

In this chapter the parameters are varied to evaluate the effect of: 1) wave barriers existing, 2) the proper dimensions for trenches, 3) the location of the trench from the vibration source and 4) the type of the material for in filled trenches on the wave propagation through the soil under the effect of pile driving.

6.12 Results and discussion

PPV values due to pile driving in case of with and without existing wave barriers:

The first investigation is to show the clear effect of wave barriers on the propagation of waves through the soil due to pile driving, therefore the model is set using Plaxis 2D dynamic analysis V.8.2 to simulate the pile driving process. A structure consists of 3 floors is placed at a distance of 10m from the vibration source, an open trench is placed at a distance of 6m from the driving source.

Figure 6.14 shows the difference between the values of PPV during the pile driving process in case of using open wave barriers and in case of nonwave barriers.

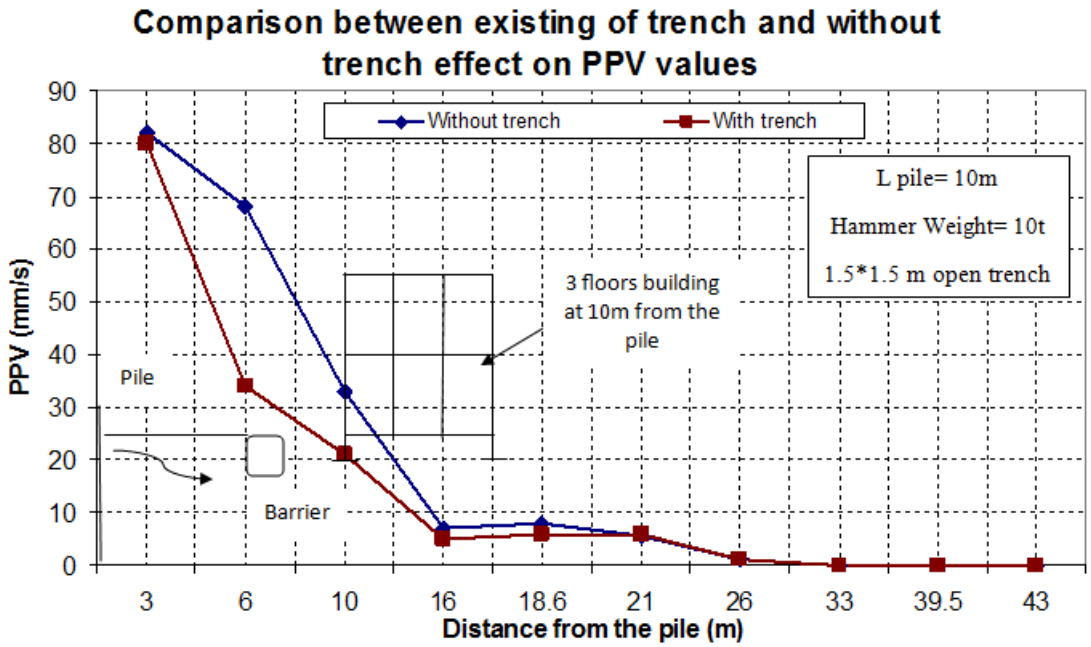

Figure 6.14: The effect of wave barriers on PPV values during pile driving, Plaxis model.

It can be noticed that in the case of using wave barrier the PPV reduced with high percentage compared with the normal case of pile driving. The barrier prevents the propagation of the wave through the soil due to the properties of the propagated waves which depends on soil particles to be transferred.

A trench as a wave barrier considers a very efficient way to reduce the possible hazard of construction vibration on the adjacent structures.

PPV values due to pile driving in case of active and passive wave barriers:

The active wave barrier defines as the barrier that is close to the vibration source when the passive barrier is placed close to the structure or the purpose which needed to be protected.

To simulate the effect of both active and passive systems another two models are done, where the open trench is placed at 3m from the driving source and 9m

from the building to represent the active system of protection, while the other model, the open trench is placed at 9 m from the driving source and 3m from the building to represent the passive protection system.

Figure 6.15 shows the difference between PPV values while using active and passive barriers.

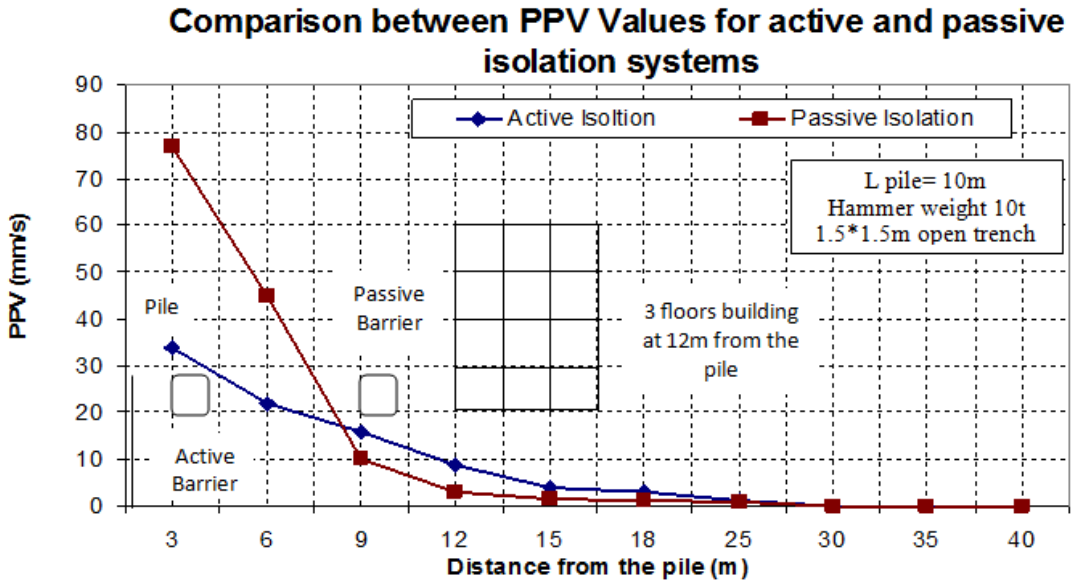

Figure 6.15: The effect of type of wave barriers active and passive on PPV values during pile driving, Plaxis model.

It can be seen that the passive barrier gives reasonable and accepted values due to different reasons, one of them is the maximum values of PPV are already exist close to the vibration source and start to attenuate by the distance from the source, therefore the passive barrier already reduces a lower magnitude of PPV that is why the effect of passive barriers is more clear than active barriers.

PPV values due to pile driving at using different widths of wave barriers:

The main idea of wave barriers is to prevent the propagation of the vibration waves through the soil, therefore, the width of the barrier is a very important parameter in the barrier efficiency. The long wave length needed a wider length to overcome the continuity of the vibration. Figure 6.16 shows the different values for PPV at different widths of trenches.

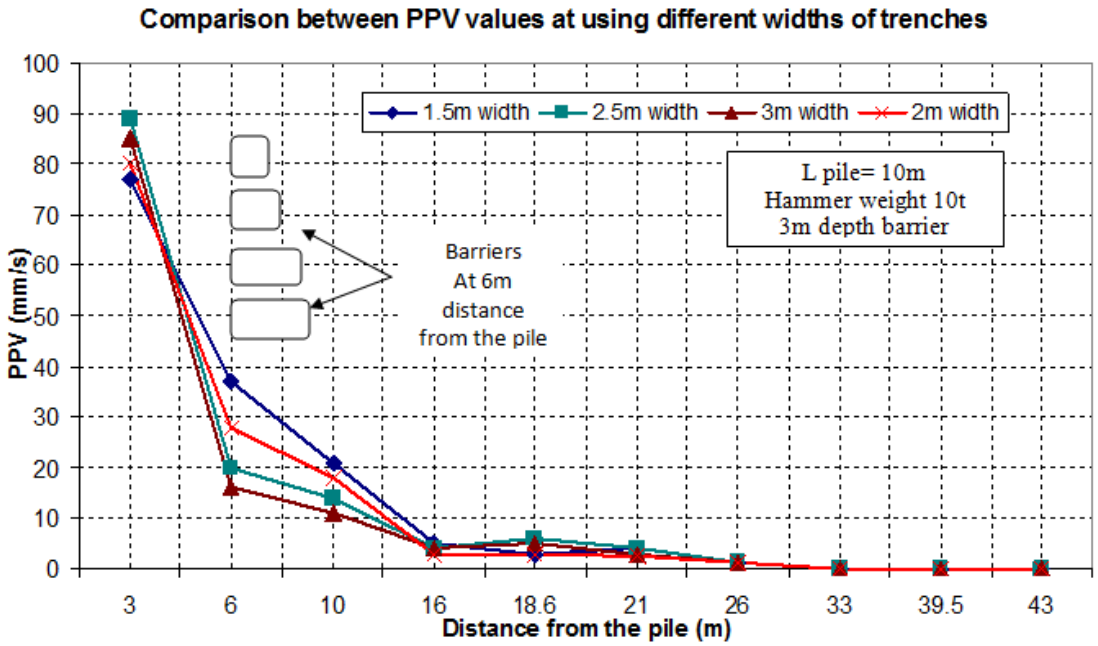

Figure 6.16: The effect of different wave barriers widths on PPV values during pile driving, Plaxis model.

It illustrated that by increasing the width of the barrier the PPV start reducing but for the appropriate dimensions lots of trials should be done to choose the ideal dimensions.

PPV values due to pile driving at different depths of wave barriers:

The proper dimensions of the barrier are the first and the most important parameter which controls the PPV values. Figure 6.12 shows the effect of different trenches depths on PPV values. As it illustrated before by increasing the width the PPV reduced, also by increasing the trench depth the PPV decreased. Unfortunately increasing the depth is not always an available option due to the need of excavation stabilization also the deep depth of a trench can be harmful to the adjacent structure in case of passive isolation. By comparing the values from Figure 6.16 and 6.17 it can be seen the increasing the width of the trench is more effective than increasing the depth for reducing PPV values.

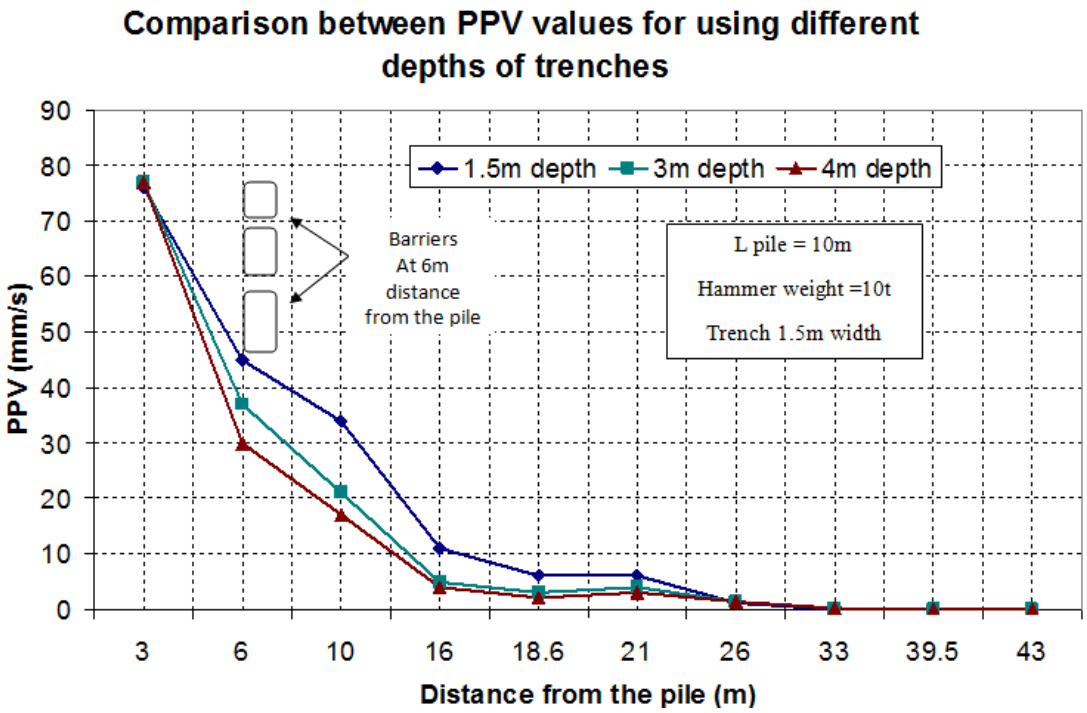

Figure 6.17: The effect of different wave barriers depths on PPV values during pile driving, Plaxis model.

PPV values due to pile driving at different materials of in-filled trenches for wave barriers:

To overcome the previous problem of the deep depths of the open trenches, in-filled trenches are considered as a practical solution for preventing vibrations from the adjacent structures. It is already known that the empty trenches give the lowest values of PPV. A lot of materials are available for in-filled trenches such as bentonite, soil bags, water, concrete, fill soil and some of petroleum heavy liquids (Bitumen), these different materials represented in the model with variety of densities varying from 1000 kN/m^2 to 4000 kN/m^2. Choosing the material depends on many parameters like the magnitude of vibration, soil type, the importance of the structure and of course on the cost of the material. Fill soil and petroleum products are the most common materials for in-filled trenches. Figure 6.18 shows a comparison between PPV values for different types of filling materials.

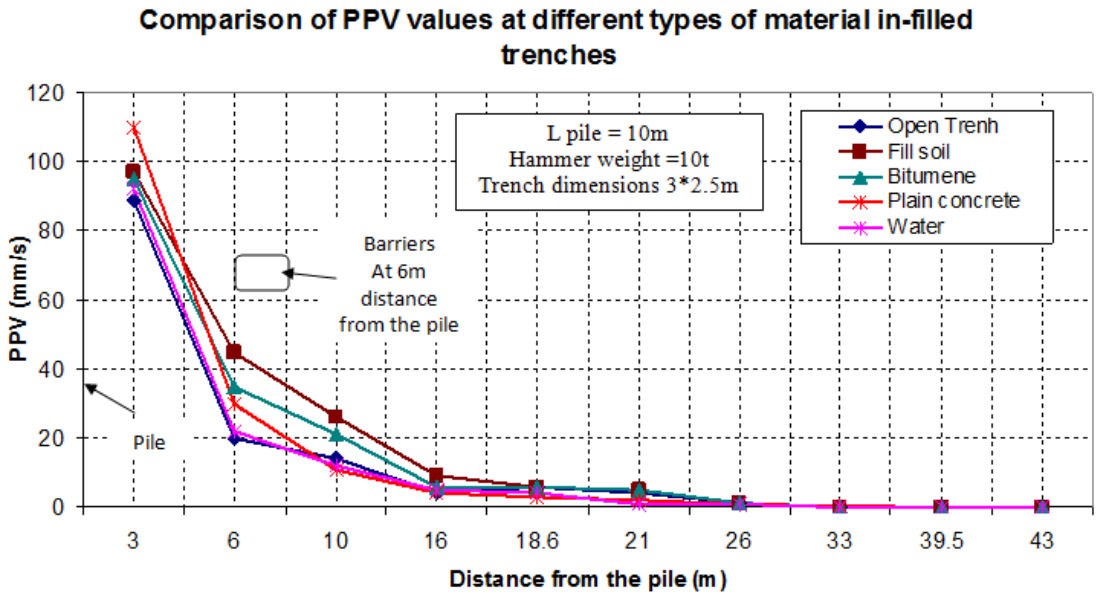

Figure 6.18: The effect of different wave barriers materials on PPV values during pile driving, Plaxis model.

It can be noticed that the open trench is more effective but as it is shown before it may be difficult to be used especially in passive isolation in great depths. Bitumen material and fill material give a close trend for reducing PPV values. Water and plain concrete gives reasonable values in PPV reduction where plain concrete trench reduce the vibration amplitude by 70% followed by water by reduction factor reach 75%.

Large impedance change between the wave barrier and the soil is required in order to achieve significant isolation. An open trench (with impedance close to zero) is more effective than a stiff barrier, (Massarsch 1993).

The effect of using sheet piles as a wave barrier in reducing PPV:

Another method of isolation is using sheet piles for building or the structure needs to be protected and it is widely used as it is shown in the literature previously. Plaxis model is set to investigate the existing of sheet piles on the behavior of vibration through the soil. The passive system is used by placing the sheet piles at distance 10m from the vibration source and at a distance of 5m from the building. Trench width is taken 2m with depth 2.5m. Figure 6.19

shows the variation of PPV values at using both of open trench and open trench with sheet piles.

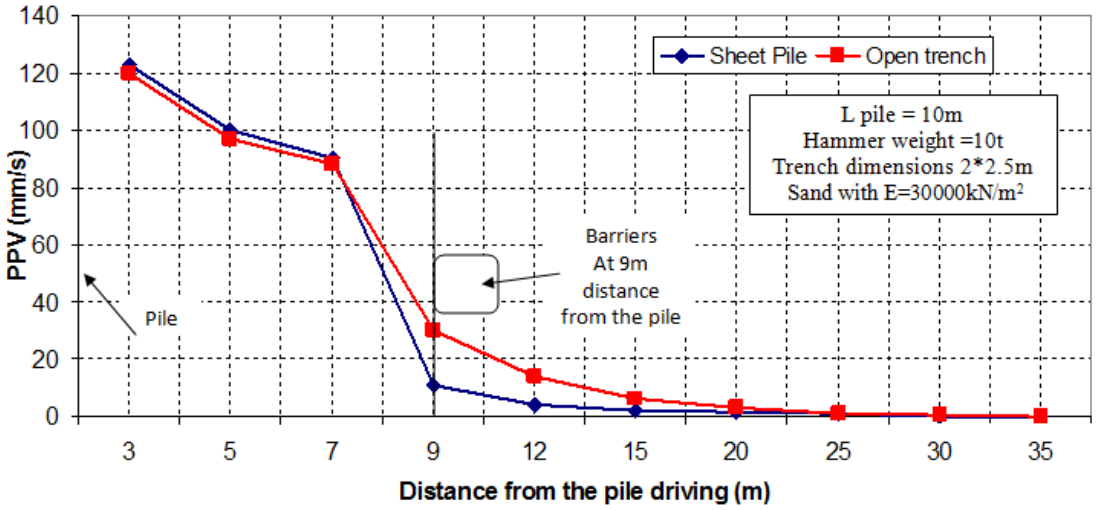

Figure 6.19: The effect of sheet piles as a wave barrier on PPV values during pile driving, Plaxis model.

It can be noticed that sheet pile as a wave barrier prevents vibration much better than open trench with higher reduction factor reaches to 60%, maybe some problem which could face the design engineer such as the economical issues and how to install the sheet piles in the soil because that installation produce vibration and that will not be reasonable, but it could be overcome by using low-frequency vibratory machine.

6.13 Conclusions

In this chapter, the ideas of preventing the vibration hazard from the structures and heritage buildings are discussed. The focus is how to get the proper dimensions of the trench, the suitable material for in-filled trenches and the difference between active and passive isolation. The main ideas of the chapter can be expressed as the following:

1. The open trench is more effective than infilled trench due to preventing the waves passing through the soil.

2. Increasing the depth and the width of the trench increase the efficiency of the trench in preventing the wave propagation because it helps to increase the efficiency of path control.
3. Using liquid material to fill the trench reduce the PPV values more than using fill soil as in filled material the reason behind that is its ability to attenuate the vibration waves also it helps in excavation stabilization for the trench.
4. Passive isolation considers being better than active isolation but it could be difficult to construct the trench next to the structure in many sites.

Chapter 7
Conclusions

Chapter 7
CONCLUSIONS

7.1 General Conclusion:

Construction and industrial dynamic sources can produce environmental vibration problems for the surrounding soils and adjacent structures. Construction vibration through soil can cause significant damage to surrounding structures. Human activity can generate soil vibration with variation in intensity, which mainly depends upon the source of vibration. This process (construction vibration) induces vibrations into the ground which can be transmitted to nearby structures. The vibration waves may cause potential damage of existing building induced by vibration source. More specifically, these vibrations can cause ground settlements and deformations that may lead to differential settlements of foundations and deformations or cracking in the structures. Vibrations create the stress waves traveling outward from the source through the soil and cause damage due to dynamic vibration induced settlement.

7.2 Chapter 1

There are many sources for construction vibration activities and they all considered being harmful to the adjacent structures.

7.3 Chapter 2

In this chapter, the available limits and criteria of vibration are briefed. The available data could be compared with the measured or the predicted values of PPV which will be a good sign for damage prediction.

7.4 Chapter 3

Pile driving is a serious problem producing vibration due to the increase in establishing new communities including pile driving, therefore the hazard of pile driving earthborn vibration on the soil and the adjacent structures have to be studied to avoid any kind of damage.

7.5 Chapter 4

Dynamic compaction process produces very high magnitude of vibration due to the higher magnitude of the input energy, therefore dynamic compaction considered to be very harmful to any adjacent structure.

7.6 Chapter 5

Different methods are available to aid the design engineer in assessing the surface settlement due to construction vibration. In this chapter, the common models of settlement prediction are mentioned and briefed. The possible damage due to settlement is illustrated using number of figures describing the resulted damage. Some of case histories represented as measurements of soil settlement due to construction vibrations.

7.7 Chapter 6

In this chapter, the ideas of preventing the vibration hazard from the structures and heritage buildings are discussed. The focus is how to get the proper dimensions of the trench, the suitable material for in-filled trenches and the difference between active and passive isolation.

References

References

1. Adam, M., Pflanz, G. and Schmid, G., (2001). "Two- and three-dimensional modeling of half-space and train-track embankment under dynamic loading. Soil Dyn. Earthquake Eng. 19 (8);559–573.
2. Ahmad, S., Al-Hussaini, T. M. (1991). "Simplified Design for Vibration Screening by Open and In-filled Trenches," J. Geotech. Engrg., Vol. 117, No. 1, pp. 67-88.
3. Ashraf, S., Jayakumaran, S., and Chen, L., (2002). "Case history: pile driving and vibration monitoring for Avenue P Bridge in Brooklyn, New York." Deep Foundations 2002, Geotechnical Special Publication No. 116, ASCE, New York, Vol. (1), pp. 500 509.
4. Athanasopoulos, G. & Pelekis, P., (2000). "Ground vibrations from sheetpile driving in urban environment: measurements, analysis and effects on buildings and occupants. Soil Dynamics and Earthquake Engineering, 19(5), pp. 371-387.
5. Attewell, P.B, A.R. Selby & A. Uromeihy. (1991). "Nonmonotonical decay of ground surface vibrations caused by pile driving. Earthquake, Blast and Impact ed SECED". London Elsevier :463-481 BS 5228 Pt 4 [1992].
6. Attewell, P.B. and Farmer, I.W., (1973). "Attenuation of ground vibrations from piles. Ground Engineering", Vol. 6(4), pp. 26-29.
7. Attewell, P.B., Selby, A.R., and O'Donnell, L., (1992). Estimation of ground vibration from driven piling based on statistical analyses of recorded data, Geotechnical and Geological Engineering, Vol. 10 (1), pp. 41-59.
8. Attewell, P.B., Selby, A.R., and O'Donnell, L., (1992). "Estimation of ground vibration from driven piling based on statistical analyses of recorded data", Geotechnical and Geological Engineering, Vol. 10 (1), pp. 41-59.
9. Badsar, S. A., Schevenels, M. and Degrande, G., (2009). The determination of the damping parameter of soils with the sasw method,

in COMPDYN 2009 ECCOMAS Thematic Conference on Computational Methods in Structural Dynamics and Earthquake Engineering.

10. Barkan, D. D. (1962). Dynamics of Bases and Foundations, translated from the Russian by L. Drashevska, edited by G. P. Tschebotarioff, McGraw-Hill.10. (original publication in Russian 1948)
11. Barkan, D.D., (1964), "Dynamics of Bases and Foundations", MacGraw-Hill Book Company, Inc. pp. 374- 406.
12. Bayraktar, M.E., Svinkin, M., and Arif, F., (2013). Florida Department of Transportation Research Center 605 wannee Street, MS30 Tallahassee, FL 32399.
13. Bement, R.A.P., Selby, A.R., 1997. Compaction of granular soils by uniformvibration equivalent to vibrodriving of piles. Geotechnical and Geological Engineering, 15, 1997, pp 121-143
14. Beskos, D. E., Dasgupta, G., Vardoulakis, I. G. (1985). Vibration isolation of machine foundations. ISBN 0872624926. In: Gazetas, G., Selig, E.T. (Eds.), Vibration Problems in Geotechnical Engineering. ASCE, New York, pp. 138-151.
15. Bodare, A., (1996). Jord- och bergdynamik, Stockholm: Div. of Soil- and Rock Mechanics Royal Institute of Technology.
16. Boscardin, M.D. and Cording, E.G. (1989). Building Response to Excavation- Induced Settlement. Jnl. Geo. Engrg. ASCE, 115;1;1-21.
17. Bradshaw, A.S., Baxter, C.D.P., and Osborn, P. (2005). “Lessons learned from pile driving at the Central Artery/Tunnel project.” Proceeding of Geo-Frontiers 2005 (CDROM),ASCE, Reston, V.A.
18. Brumund, W.F. and Leonards, G.A. (1972). Subsidence of sand due to surface vibration. Journal of the Soil Mechanics and Foundation Division, Proceedings ASCE, 98(1) 27-42.
19. Burland, J. B. and Wroth, c., (1974). Settlements of buildings and associated damage, Proceedings, conference on Settlements of Structures, Pentech Press, London, pp. 611 - 654.

20. Burland, J.B., (1995). Assessment of Risk of Damage due to Tunneling and Excavations. Invited Special Lecture to IS-Tokyo, 1995: 1st Int. Conf. on Earthquake. Geotechnical Engineering.
21. Celebi, E., Fırat, S. and Cankaya, Y., (2006). The evaluation of impedance functions in the analysis of foundations vibrations using boundary element method, Applied Mathematics and Computation 173 (1) 636–667.
22. Cenek, P.D., Sutherland, A.J. and McIver, I.R, (2012), "Ground Vibration from Road Construction", NZ Transport Agency Research Report 485.
23. Chae, Y. S., (1978). Design of excavation blasts to prevent damage. Civil Engineering—American Society of Civil Engineers 48(4):77–79.
24. Chapot, P., et al. (1981). Revue Francaise de Geotechnique (from Queyroi D, Chaput D, and Pilot G: Amelioriation des sols de fondation," Note Technique de Labratoire Central de Ponts et Chaussees, 1981, pp 55.
25. Clough, G.W. & Chameau, J- L. (1980). Measured Effects of Vibratory Sheetpile Driving. Journal of Geotechnical Engineering Division, ASCE, Vol. 106, No. GT10, pp. 1081-1099.
26. Cumrnings. A. E., Kerkhoff, G. O. and Peck, R. B., (1950). Effect of Driving Piles Into Soft Clay. Transactions, ASCE. Vol. 115. pp. 275-285.
27. D'Appolonia, D.J., (1971). Effects of Foundation Construction on Nearby Structures. Proceedings of the Fourth Panamerican Conference on Soil Mechanics and Foundation Engineering, San Juan, Puerto Rico, Vol. 1, pp. 189-236.
28. D'Appolonia, D.J., Whitman, R.V., D'Appolonia, E.D., (1969). Sand compaction with vibratory rollers. Journal of the Soil Mechanics and Foundations Division, Proceedings of the American Society of Civil Engineers, SM 1, January 1970,pp 263-284

29. Dalmatov, B.I., Ershov, V.A., Kovalevsky, E.D., 1985. Some Cases of Foundation Settlement in Driving Sheeting and Piles. Proceedings International Symposium on Wave Properties of Earth Materials, 1968, pp. 607-613
30. D'Appolonia, D. and Lambe, T. (1971). Performance of Four Foundations on End Bearing Piles", Journal of the Soil Mechanics, Foundation Division, ASCE, Vol. 97, pp.77-93.
31. Davis, D., (2010). A Review of Prediction Methods for Ground-Borne Noise due to Construction Activities. Proceedings of the 20th International Congress on Acoustics, 23- 27 August2010, Sydney, Australia.
32. Deckner, F., (2013). Ground vibrations due to pile and sheet pile driving –influencing factors, predictions and measurements, Licentiate thesis,Division of Soil and Rock Mechanics Department of Civil and Architectural Engineering School of Architecture and the Built Environment KTH, Royal Institute of Technology Stockholm 2013.
33. Dolling H. J., (1965), "Schwingungsisolierung von Bauwerken durch tiefe, auf geeignete Weise stabilisierte Schiltze", Sonderdruck aus VDI-Berchte 88. S. 3741.
34. Dowding, C.H. (1996). Construction Vibrations. Prentice- Hall, Upper Saddle River, USA.
35. Dowding, CH., (2000). Construction vibrations. Second edition. Upper Saddle River, NJ: Prentice Hall Engineering/Science/Mathematic.
36. Drabkin, S., Lacy, H. and Kim, D.S. (1996), Parametric Assessment of Settlement on Sands Caused by Low Level Vibrations due to Operation of Construction Equipment, Pile Driving and Traffic", Journal of Geotechnical Engineering, Vol. 122, No. 11, November 1996, pp. 920-928.
37. Drabkin, S., Lacy, H., Kim, D.S., (1995). Estimating settlement of sand caused by construction vibration. Journal of Geotechnical Engineering, November 1996, pp 920-928

38. Drnevich, V.P. and Massarsch, K.R. 1979. Sample Disturbance and Stress - Strain Behaviour, ASCE Journal of the Geotechnical Engineering Division, 105(GT 9) 1001-1016.
39. Dumas, J., (1981). Densification of Foundation Soils for Cold Storage Warehouse, Prince Rubert, B.C, GEOPAC Report to B.C. Pakers Ltd.
40. Dumas, J., (1982). Densification of Foundation Soils, Port Mellon, B.C., GEOPAC Report to Canadian Forest Products. Ltd. June.
41. Dumas, J., (1982). Dynamic Consolidation, Case Histories Canadian Realization. Reports by GEOPAC, Inc., st. Lambert, Quebec.
42. Duvall, W. I. and Folgelson, D. E., (1962). USBM Report of Investigation 5968 - Review of Criteria of Estimating Damage to Residences from Blasting Vibrations", US Bureau of Mines (USBR),
43. E. Celebi, G. Schmid.(2005)."Investigation of ground vibrations induced by moving loads. Engineering Structures 2005;27:1981-1998.
44. Ekanayake, S., Liyanapathirana, D. & Leo, C., (2013). "Influence zone around a closed-ended pile during vibratory driving. Soil Dynamics and Earthquake Engineering 53, 11 July, pp. 26-36.
45. Feld, J. and Carper, K.L. (1997). Construction Failure. John Wiley and Sons, New York.
46. G. Pflanz, K. Hashimoto, N. Chouw. (2002) "Reduction of structural vibrations induced by a moving load. J. Appl. Mech. 2002;5:555–563.
47. Galitzin, B. (1912). Ueber die Dispersion und Dämpfung der seismischen Oberflächenwellen. Bulletin de l'Académie Impériale des Sciences de St.-Pétersbourg, pp. 219-236.
48. Gambin, M., Capelle, J., and Dumas, J., (1979). La Consolidation Dynamique: Une Technique Permettant De Dimineur Les Risqués De Liquefaction. Proceedings 3rd Canadian Conference on Earthquake Engineering, Montreal, June, 1979, pp.117-146.
49. Gavin, G. and Dohetry, P., (2015). Comparison of impact versus vibratory driven piles: With a focus on soil-structure interaction. Deep foundation institute. GEO. Solutions.

50. Grabe, J., Mahutka, K.-P., (2005). Finite-Elemente-Analyse zur Vibrationsrammung von Phählen. Bautechnik 82 (2005), Heft 9, pp 632–640
51. Guyot, G., et al., (1981). Ground Improvement, Geotechnical Equipment, brochure by Menard, Inc., Moroeville, Pa.
52. Hagerty, J.A and Peck, R.B., (1971). Heave and Lateral Movements due to Pile Driving. Journal of the Soil Mechanics and Foundations Division. Proceedings of ASCE. Soil Mech., 97, No. SM11, pp. 1513-1532
53. Hamidi, B., Varaksin, S., Nikraz, H., (2011),"Predicting Menard Modulus using Dynamic compaction", International Conference on Advances in Geotechnical Engineering, Perth, Australia, Nov.7-9, 2011.
54. Hansbo, S. (1994). Foundation Engineering. Elsevier, The Netherlands..
55. Hanzawa, H., (1981). Improvement of Quick Sand, proceedings 10th International Conference on Soil Mechanics and Foundation Engineering, Vol.3, Stockholm, pp.683-686.
56. Haupt W. A., (1978), “Isolation of Vibration by Concrete Core Walls”, Proc 9th Int. Conf. Soil Mech. Found Engrg, 251-256, 2, Japanese Society of Soil Mechanics and Foundation Engineering.
57. Haupt, W.A., (1981). Model tests on screening of surface waves, in: Proceedings of the Tenth International Conference in Soil Mechanics and Foundation Engineering, Stockholm, vol. 3, pp. 215–222.
58. Heckman, W.S. & Hagerty, D.J., (1978). Vibrations Associated with Pile Driving. Journal of the Construction Division, Vol. 104, No. CO4, December 1978, pp. 385-394.
59. Heerema, E.P., (1980). Predicting Pile Driveability: Heather as An Illustration of the Friction Fatigue Theory. Ground Engineering, April 1980, Vol. 13, No. 3.
60. Hendricks, R., (2004). Transportation Related Earthborne Vibrations (Caltrans experience), Technical Advisory, Vibration, TAV-04-01-

R0201, California Department of Transportation, Noise, Vibration, and Hazardous Waste Management Office, Sacramento, CA.

61. Hergarden, R.H., (2000). Gronddeformaties tijdens het trillend trekken van damwanden (Ground deformations during vibratory pull of sheet piles). M.Sc. thesis Delft University of Technology, December 2000 (in Dutch)

62. Hergarden, R.H., Tol, A.F. van, (2001). Zakkingen tijdens het trillend trekken van damwanden (Settlements during vibratory pull of sheet piles). Geotechniek, July 2001 pp 85–90 (in Dutch)

63. Hillier, D.M. and Crabb, G.I., (2000). Groundborne Vibration Caused by Mechanised Construction Works, TRL Report 429, Austin, USA.

64. Holeyman, A. E., (1993). "Keynote lecture: Vibratory driving analysis. In: Application of Stress-Wave Theory to Piles. Balkema, Rotterdam: Niyama & Beim (eds), pp. 479-494.

65. Holeyman, A., (2002). "Soil Behavior under Vibratory Driving. Proceedings of the international conference on vibratory pile driving and deep soil compaction, Louvain-La Neuve, Belgium, 9-10 September 2002, pp. 3-19.

66. Holeyman, A.E. and Legrand, C., (1997). "Soil-structure interaction during pile vibratory driving. Proceedings of the 13th International Conference on Soil Mechanics and Foundation Engineering, Hamburg, Germany, September 1997, pp. 817-822.

67. Holeyman, A.E., Legrand, C., Rompaey, D. van, 1995. A method to predict the drivability of vibratory driven piles. "Proc. 5th Int. Conf. Appl. Stress-Wave Theory to Piles, Orlando, Sept. 1996, Gainesville, Univ. Florida, Dep. Civ.Eng., 1996, pp. 1101-1112

68. Holmberg, R., Arnberg, P.W., Bennerhult, O., Forssblad, L., Gereben, L., Hellman, L., Olsson, K., Rundqvist, G., Sjöberg, C., Sjökvist, K. & Wallmark, G. (1984). "Vibrations generated by traffic and building construction activities. Swedish Council for Building Research, Stockholm, Sweden.

69. Hope, V.S. and Hiller, D.M. (2000). “The prediction of groundborne vibration from percussive piling”, Canadian Geotechnical Journal, Vol. 37, No. 3, pp. 700–711.
70. Horn, H.M., (1966). “Influence of pile driving and pile characteristics on pile foundation performance.” Lecture Notes, New York Metropolitan Section, ASCE, Soil Mechanics and Foundation Group.
71. Houzé, C. (1994). HFV Amplitude Control Vibratory Hammers: Piling Efficiency without the Vibration inconvenience. Proceedings of the Fifth International Conference and Exhibition on Piling and Deep Foundations, Bruges, Belgium, pp. 2.4.1- 2.4.10.
72. Hussien, M., Rausche, F. and Likins, G., (1992). Dynamic of Pile Driving as a Function of Ram Drop Height. Application of stress-wave theory of piles, F.B.J. Barends, 1992, Balkema, Rotterdam.ISBN.
73. Idriss, I.M. 1999. An update to the Seed-Idriss simplified procedure for evaluating liquefaction potential”, in Proceedings, TRB Workshop on New Approaches to Liquefaction, FHWA-RD-99-165, FHWA, Washington, D.C.
74. Idriss, I. M., and R. W. Boulanger, 2008. Soil Liquefaction during Earthquake, Earthquake Engineering Research Institute, EERI Publication MNO-12.
75. Jackson, NM, MI Hammons, R Walker and H Von Quintus., (2007). Use of nondestructive techniques to estimate the allowable vibratory compaction level during construction. Research report FL/DOT/SMO/07-BDB-11. Florida, USA: State Materials Office, Department of Transportation, State of Florida Department of Transportation.
76. Jastrzebska, M., Lupiezowiec, M., Uliniarz, R. & Jaron, A., (2014). "Analysis of the vibration propagation on the subsoil. Studia Geotechnica et Mechanica, XXXVI(3).
77. Jones & Stokes Associates, (2004). Transportation- and construction-induced vibration guidance manual. J&S 02-039. Prepared for

California Department of Transportation, Noise, Vibration and Hazardous Waste Management Office, Sacramento, CA.

78. Juille, Y., and Sherwood, D., (1983). Improvement of Sabkhas Soils, proceedings 8th International Conference on Soil Mechanics and Foundation Engineering, Vol.2, pp.781-788.

79. K. L. Leung, I. G. Vardoulakis, D.E. Beskos, J. L. Tassoulas. (1991) " Vibration isolation by trenches in continuously non-homogenous soil by the BEM. Soil Dynamics and Earthquake Engineering; Vol. 10(3):172-179.

80. Kaminetzky, D., (1991). Design and Construction Failures – Lessons from Forensic Investigations, McGraw-Hill, Inc., New York.

81. Khoubani, A. & Ahmadi, M. M., (2012). "Numerical study of ground vibration due to impact pile driving. Proceedings of the ICE – Geotechnical Engineering, p. 12.

82. Kim, D.S. & Lee, J.S., (1999). Propagation and attenuation of characteristics of various ground vibrations. Soil Dynamics and Earthquake Engineering, Vol. 19, No 2, pp. 115-126.

83. Kim, D.S. and Drabkin, S. (1995), "Factors Affecting Vibration Induced Settlement", Third International Conference on Recent Advances in Geotechnical Earthquake Engineering and Soil Dynamics", St. Louis, Missouri, April 2-7, 1995, Vol. 3, pp. 1111-1115.

84. Kim, D.S., Drabkin s., Laefer D., and Rokhvarger A., (1994). Prediction of Low Level Vibration Induced Settlement, Proceedings of the Conference Settlement '94, Texas, pp.806-817.

85. Kim, D.S., Drabkin, S., (1995). Investigation of vibration-induced settlement using multifactorial experimental design. Geotechical Testing Journal, 18(1995)4, pp 463-471

86. Klein, R., Antes, H., Le Houedec, D.,(1997). Efficient 3D modeling of vibration isolation by open trenches. Computers & Structures; Vol. 64, No. 1-4:809-817.

87. Ko, J.M., Luk, S.T., and Cheng, C.Y., (1990), "Vibration and Noise-Measurement Prediction and Control", Proceedings of Australian Vibration and Noise Conference.
88. Konan, W., (1985). Vibration criteria for historic buildings. Journal of Construction Engineering and Management 111(3):208–215.
89. Kramer, S., (1996). Geotechnical Earthquake Engineering. New Jersey, USA, Prentice-Hall.
90. Kuo, K. A. & Hunt, H. E. M., (2013). An efficient model for the dynamic behaviour of a single pile in viscoelastic soil. Journal of Sound and Vibration.
91. Lacy, H.S. and Gould, J.P., (1985). Settlement from pile driving in sands. American Society of Civil Engineers, Proceedings of ASCE Symposium on Vibration Problems in Geotechnical Engineering, Detroit, Michigan, G. Gazetas and E.T. Selig, Editors, pp. 152-173.
92. Larsson, R. & Mulabdic´, M., (1991). Report No 40 Shear moduli in scandinavian clays, Linköping: SGI.
93. Lauzon, M., Morel, J.F., Briet, S., Beaton, N.F., (2011). Ground Vibrations Induced by Dynamic Compaction and Rapid Impact compaction. Pan-AM. CGS. Geotechnical Conference.
94. Lee, S.H., Kim, B.I. & Han, J.T., (2012). "Prediction of Penetration Rate of Sheet Pile Installed in Sand by Vibratory Pile Driver. KSCE Journal of Civil Engineering, Vol. 16, No. 3, pp. 316-324.
95. Leung, K.L., Beskos, D.E., Vardoulakis, I.G., (1991). Vibration isolation using open or filled trenches, Part 3: 2-D non-homogeneous soil, Computational Mechanics 7 137–148.
96. Lewis,M.R., Daive,J.R., (1993). Vibrations due to pile driving, Third International Conference on Case Histories in Geotechnical Engineering, St. Louis, Missouri.
97. Leznicki, J.K., Gaibrois, R.G. and Esrig, M.E. (1994), “Displacement of Landmark Building Resulting from Adjacent Construction Activities”, Vertical and Horizontal Deformations of Foundations and

Embankments, ASCE Geotechnical Special Publication No. 40, 1994, pp. 222-232.

98. Linehan, P. W., Longinow, A., & Dowding, C. H. (1992). Pipeline response to pile driving and adjacent excavation. Journal of Geotechnical Engineering, 118(2), 300-316. DOI: 10.1061/(ASCE)0733 9410(1992)118:2(300).

99. Lo, K. and Stermac, A. (1965). Induced Pore Pressures During Pile-Driving Operation. Proceedings, 6th International Conference on Soil Mechanics and Foundation Engineering, Montreal, Vol. 2, p. 285-289.

100. Lo, K. and Stermac, A. (1965). Induced Pore Pressures During Pile-Driving Operation. Proceedings, 6th International Conference on Soil Mechanics and Foundation Engineering, Montreal, Vol. 2, p. 285-289.

101. Lo, K.-F., Ni, S.-H., Huang, Y.-H. & Lehmann, L., (2012). "Free field vibrations due to pile driving using a coupled fem with SBFEM method. Journal of GeoEngineering, 7(2), pp. 96-73.

102. Loos, W., (1936). Comparative Studies for Compacting Cohesion less Soils, Proceedings, 1st International Conference on Soil Mechanics and Foundation Engineering, Vol. III, Harvard Univ., Cambridge, Mass pp.174-178.

103. Lupiezowiec, M., Pradelok, S., Betkowski, P. & Poprawa, G., (2014). "FEM model of vibration propagation in the soil caused by prefabricated driven piles. u.o., u.n.

104. Lynch, T.J., (1960). Pile driving experience at Port Everglades." J. Soil Mechanics and Foundation Division, 85(SM2), pp. 41-62.

105. M. Adam, G. Pflanz, G. Schmid. (2000). "Two- and three-dimensional modeling of half-spaceand train-track embankment under dynamic loading. Soil Dyn. Earthquake Eng.2000; 19 (8);559–573.

106. Mahutka, K., Grabe, J., 2005. Numerical prediction of settlements and vibrations due to vibratory pile driving using a continuum model. Proc. TRANSVIB2006, Paris, September 2006, pp 243-252

107. Martin, D., (1980), "Ground vibrations from impact pile driving". Transport and Road Research Laboratory, Supplementary Report 544, Crowthorne, England..
108. Masoumi, H.R. & Degrande, G., (2008). Numerical modeling of free field vibrations due to pile driving using a dynamic soil-structure interaction formulation. Journal of Computational and Applied Mathematics, Vol. 215, No. 2, pp. 503-511.
109. Masoumi, H.R., Degrande, G. & Lombaert, G., (2006). Free field vibrations due to vibratory pile driving in a layered soil medium. Proceedings of TRANSVIB 2006, Paris 21-22 September.
110. Masoumi, H.R., Degrande, G. & Lombaert, G., (2007). Prediction of free field vibrations due to pile driving using a dynamic soil-structure interaction formulation. Soil Dynamics and Earthquake Engineering, Vol. 27, No. 2, pp. 126-143.
111. Masoumi, H.R., Francois, S. & Degrande, G. (2009). A non- linear coupled finite element boundary element model for the prediction of vibrations due to vibratory and impact pile driving. International Journal for Numerical and Analytical Methods in Geomechanics, Vol. 33, No. 2, pp. 245-274.
112. Massarch K.R and Fellenius B.H, (2014) "Ground vibration from pile and sheet pile driving" part(1) pp.131-138.
113. Massarsch, K. R., (1993), "Man-Made Vibrations and Solutions" (June 1, 1993). International Conference on Case Histories in Geotechnical. Engineering. Paper 6.
114. Massarsch, K.R and Broms, B.B, (1989), "Soil displacement caused by pile driving in clay. International conference on piling and deep foundation, London, 15-18 May, 1989, proceedings, pp.275-282.
115. Massarsch, K.R and Broms, B.B, (1991), "Damage criteria for small amplitude ground vibrations, submitted for publication to: second international conference on recent advances in geotechnical earthquake

engineering and soil dynamics, st, Louis, Missouri, March 11-25, 1991, pp. 1451-1459.

116. Massarsch, K.R. & Fellenius, B.H., (2008). Ground Vibrations Induced by Impact Pile Driving. Proceedings of the 6th International Conference on Case Histories in Geotechnical Engineering, Arlington, August 11-16, 2008.

117. Massarsch, K.R. & Fellenius, B.H., (2008). Ground Vibrations Induced by Impact Pile Driving. Proceedings of the 6th International Conference on Case Histories in Geotechnical Engineering, Arlington, August 11-16, 2008.

118. Massarsch, K.R. (2000a). Settlements and damage caused by construction-induced vibrations. Proceedings of the International Workshop Wave 2000, Bochum, Germany, pp. 299- 315.

119. Massarsch, K.R. (2000b). Vibratorers användningsmöjligheter vid drivning av pålar och spont. Pålkommissionen rapport 99, Linköping, Sweden.

120. Massarsch, K.R. (2004). Vibrations Caused by Pile Driving. Deep foundations, summer 2004 and fall 2004 (two parts).

121. Massarsch, K.R. and Fellenius, B.H., (2005). Deep vibratory compaction of granular soils. In Ground Improvement Case Histories, Geo-Engineering Series Vol.3, Chapter 19, Elsevier Publishers (UK), Edited by Buddhima Indraratna and Jian Chu, pp. 633 - 658.

122. Massarsch,K. R.,(2005).Vibration isolation using Gas-filled cushions. Soil Dynamics Symposium in Honor of Professor Richard D. Woods. Proceedings of the Sessions of the GeoFrontiers.Austin, Texas, January 24-26.

123. Massarsch, K.R., (1984). Vibration problems in soft soils symposium on recent developments in laboratory and field tests and analysis of geotechnical problems, Asian institute of technology, Bangkok, Proceedings, A.A. Balkema, pp. 539-549.

124. Mayne P. W., Jones J. S. and Dumas J. C., (1984). Ground response to dynamic compaction. Journal of Geotechnical Engineering, ASCE, 110, No. GT6, 757–773. .
125. Mayne, P.W., (1985). "Ground vibrations during dynamic compaction. American Society of Civil Engineers, Proceedings of ASCE Symposium on Vibration Problems in Geotechnical Engineering, Detroit, Michigan, G. Gazetas and E.T. Selig, Editors, pp. 247-265.
126. Mayne, P.W., B. Christopher, R. Berg, and J. DeJong, (2002). Subsurface investigations - geotechnical site characteriza-tion, FHWA-NHI-01-031, FHWA, Washington, D.C., 301 pages.
127. Mayne, P.W. and Kulhawy, F.H. (1982). “K0-OCR relationships in soil”. J. Geotech. Engrg., Vol. 108 (GT6), 851-872
128. Meijers, P., (2004b). Invloed inbrengen en verwijderen van damwanden op omgeving (Influence of installation and removal of sheet piles on the surrounding). Geotechniek 8, 2004, pp 8-13
129. Meijers, P., 2004c. Effect steel sheet pile on measurements with an electrical density probe. GeoDelft, internal report 525250-2, December 2005
130. Menard, Inc., (1981). Dynamic Consolidation- The Menard Group Internal Publication, 22 Cambridge Street, Aylesburg, England.
131. Mohamed, R. and Dobry, R., (1987). Settlements of cohesion less soils due to pile driving. Proceedings, 9th Southeast Asian Geotechnical Conference, Bangkok, Thailand, pp. 7-23.
132. McNeill, R.L., Margason, B. E., Babcock, F.M.(1965) The role of soil dynamics in the design of stable test pads. Proceedings Guidance and Control Conference, 366-375, 1965.
133. New, B.M., (1986). Ground vibration caused by civil engineering works. TRRL research report 53. Transport and Road Research Laboratory, Department of Transportation, UK.

134. Niederwanger, G. (1999). Measurement and estimation of vibration of old buildings. Transactions on the Built Environment, Vol. 39, WIT Press, pp. 67-76.
135. Nilsson, G., (1989). "Markvibrationer vid pålslagning. Master thesis Nr 3:89, Division for Soil and Rock Mechanics, Royal Institute of Technology, Stockholm, Sweden.
136. Neumeuer.H., (1963)." Untersuchungen uber die abschirmuny eines besehenden ge baudes gegen ersch utterungen beim bauund betrieb einer u-bahnstrecke. Baumaschine und bautechnik 10, 23-29.
137. Olsson, E., (2014). "A Dynamic Response Study on Optimal Piling Depth with respect to Ground Vibrations, Göteborg: MSc thesis, Chalmers University of Technology.
138. Oriad, L.L, (1999), "The effects of vibrations and Environmental forces. International Society of Explosives Engineers, Cleveland.
139. Pearce, P.W., (1979). Discussion on Dynamic Compaction, Clay Fills, Institution of Civil Engineers, London, pp. 279-281.
140. Peck,R.B., Hanson, W.E., and Thornburn, T.H., (1974). Foundation Engineering, John Wiley and Sons, New York.
141. Petřík, T., Hrubešová, E. and Lednická, M., (2012), " A comparison of numerical models results with in-situ measurement of ground vibrations caused by sheet pile driving, Acta Geodyn. Geomater, Vol.9, No. 2 (166), pp. 165–171.
142. Pflanz, G., Hashimoto, K., Chouw.,N., (2002). Reduction of structural vibrations induced by a moving load. J. Appl. Mech.;5:555–563.Randelementmethode im Zeitbereich,
143. Picornell, M. and Monte, E. (1985), Pile Driving Induced Settlements of a Pier Foundation, Proceedings of a Symposium sponsored by the Geotechnical Engineering Division in conjunction with the ASCE Convention in Detroit, Michigan, October 1985, pp. 174-186.

144. P.Persson, K.Persson and G.Sandberg, (2016)" Numerical study of reduction in ground vibrations by using barriers" Engineering Structures Volume 115, 15 May 2016, Pages 18-27
145. Qu Zhihao, Chai Shaokuan, Ye Qianyuan. Analysis of Dynamic Characteristics and Chatter Of A 1420 Cold Tandem Rolling Mill [J]. Journal of Vibration and Shock, 2006, 25(4): 25-29.
146. Rausche, F., (2002). Modeling of vibratory pile driving. Proceedings of the international conference on vibratory pile driving and deep soil compaction, Louvain-La Neuve, Belgium, 9-10 September 2002, pp. 21-32.
147. Reiher, H., and F. J. Meister, (1931). The effects of vibration on people. Forshung auf dem Gebeite der Ingenieurwesens 2(2).
148. Reuver, G., (2016). "Evaluation of vibratory pile installation effects on adjacent buried pipe structures through a coupled analytic approach. Master Thesis, Faculty of Civil Engineering and Geosciences - Delft University of Technology Fakultät Grundbau Boden- und Felsmechanik - Technische UniversitätWien Copyright ©Delft University of Technology.
149. Rezaei, M., Hamidi, A. and Farshi Homayoun Rooz, A., (2016). "Investigation of Peak Particle Velocity Variations during Impact Pile Driving Process. Civil Engineering Infrastructures Journal, 49(1): 59 – 69, June 2016 Print ISSN: 2322-2093; Online ISSN: 2423-6691 DOI: 10.7508/ceij.2016.01.005.
150. Richart, F., Hall, J., Woods, R. (1970). Vibrations of Soils and Foundations. Prentice Hall, Englewood Cliffs, NJ.
151. Robertson, I., (1966). Forced vertical vibration of a rigid circular disc on a semiinfinite elastic solid. Mathematical Proceedings of the Cambridge Philosophical Society, Volym 62, pp. 547-553.
152. Robinson, B. R., (2006). Models for Prediction of Surface Vibrations from Pile Driving. Master of Science Thesis, Raliegh, North Carolina, North Carolina State University.

153. Rollins, K.M. and Kim, J. (2010). “Dynamic Compaction of Collapsible Soils Based on US Case Histories”, J. Geotechnical and Geoenvironmental Engineering, ASCE, Vol. 136, No. 9, 1178-1186.

154. Seed, H.B. and Silver, M.L. (1972), Settlement of Dry Sands during Earthquakes, Journal of Soil Mechanics and Foundations, ASCE, Vol. 98, No. SM4, April 1972, pp. 381-397.

155. Seed, H.B., (1976). Evaluation of soil liquefaction effects on level ground during earthquakes. ASCE Annual Convention and Exposition, Liquefaction Problems in Geotechnical Engineering. Philadelphia. pp. 1–104.

156. Segol, G., Lee, P. C. Y., Abel, J. R. (1978). “Amplitude Reduction of Surface Waves by Trenches,” Journal of the Engineering Mechanics Division, ASCE, Vol. 104, No. 3, pp. 621-641.

157. Selby A.R. (1991) Ground vibrations caused by pile installation Proc of 4th Int Conf on Piling and Deep Foundations. Stresa DFI/Tespa :497-502.

158. Serdaroglu, M.S., (2010). "Nonlinear analysis of pile driving and ground vibrations in saturated cohesive soils using the finite element method. a thesis submitted in partial fulfillment of the requirements for the Doctor of Philosophy degree in Civil and Environmental Engineering in the Graduate College of The University of Iowa, December 2010. This dissertation is available at Iowa Research Online: http://ir.uiowa.edu/etd/882.

159. Setiawan, B. and Fad, Z.G., (2012). "Prediction of Ground Vibrations During Pile Driving Through Finite Element Method Simulations. Indonesian Society of Geotechnical Engineering (ISGE XVI), At Jakarta, Indonesia, Volume: ISGE XVI, pp. 345-350.

160. Seyhan Fırat .S, Celebi.E, Beyhan .G, GnkayaI, Kırtel .O and Vural. I (2010). "Field Experiments on Wave Propagation and Vibration Isolation by Using Wave Barriers" Wave Propagation in Materials for

Modern Applications, Book edited by: Andrey Petrin, ISBN 978-953-7619-65-7, pp. 526, January 2010, INTECH, Croatia.

161. Shahir, H., Pak, A. and Ghassemi, A., (2009). Validity of Menard Relation in Dynamic Compaction Operations. Proceedings of the institution of civil engineers, Ground Improvement, January 2009.

162. Shahir, H., Pak, A. and Ghassemi, A., (2009). Validity of Menard Relation in Dynamic Compaction Operations. Proceedings of the institution of civil engineers, Ground Improvement, January 2009.

163. Silver M. L. and Seed H. B., (1971). Volume changes in sands during cyclic load, J. Soil Mech. And Found. Engrg. Div., ASCE, 97(SM9), 1171-1182.

164. Silver M. L. and Seed H. B., (1971). Volume changes in sands during cyclic load, J. Soil Mech. And Found. Engrg. Div., ASCE, 97(SM9), 1171-1182.

165. Siskind, D. and M. Stagg, M., (2000). The Co-Report. Blast Vibration Damage Assessment Study and Report, Miami-Dade County, C3TS Project No.: 1322-01.

166. Siskind, D. E., M. S. Stagg, J. W. Kopp, and C. H. Dowding. (1980). Structure response and damage produced by ground vibration from surface mine blasting. (Report of Investigations 8507.) Washington, DC: U.S. Bureau of Mines.

167. Siskind, D. E., V. J. Stachura, M. S. Stagg, and J. W. Kopp., (1980). Structure response and damage produced by airblast from surface mining. (Report of Investigations 8485.) Washington, DC: U.S. Bureau of Mines.

168. Siskind, D.E., (2000). Vibration from Blasting. International Society of Explosives Engineers, Cleveland, Ohio.

169. Soderberg, L. (1967). Consolidation Theory Applied to Foundation Pile Time Effect. Geotechnique, Vol. 12, p. 217-225.

170. Sulander, R. & Olivecrona, S.A., (2016)."Numerical analysis of vibrations due to impact pile driving. Department of construction

sciences geotechnical engineering. ISRN LUTVDG/TVGT-16/5058-SE (1-78) | ISSN 0349-4977. Master's Dissertation

171. Susila, E., Siahaan, S., Sinaga, P. & Agrensa, F., (2014). Numerical and Experimental Studies of Wave Propagation Induced by Pile Driving. JURNAL TEKNIK SIPIL, 21(2), pp. 94-106.

172. Svinkin M.R., (1996b). "Velocity-impedance-energy relationships for driven piles. Proceedings of the Fifth International Conference on the Application of Stress-Wave Theory to Piles, Orlando, F.Townsend, M. Hussein and M. McVay, Editors, pp. 870-890..

173. Svinkin, M.R. (2004). Minimizing Construction Vibration Effects. Practice Periodical on Structural Design and Construction, ASCE, Vol. 9, No. 2, pp. 108- 115.

174. Svinkin, M.R. (2005). Environmental vibration problems during construction. Proceedings of the International Conference on Soil Mechanics and Geotechnical Engineering, Vol. 4, pp. 2453- 2456.

175. Svinkin, M.R. (2008). Soil and structure vibrations from construction and industrial sources. Proceedings of the 6th International Conference on Case Histories in Geotechnical Engineering, Arlington, August 11- 16, 2008.

176. Svinkin, M.R. (2010). Environmental vibration problems during construction. Proceedings of the International Conference on Soil Mechanics and Geotechnical Engineering, Vol. 4, pp. 2453- 2456.

177. Svinkin, M.R., (1973). To the calculation of soil vibrations by the empirical formulas. In Russian,Computation of building structures, Proceedings of Kharkov Scientific-Research and Design Institute for Industrial Construction, Stroiizdat, Moscow, pp. 223-230.

178. Svinkin, M.R., (1993)." Analyzing man-made vibrations, diagnostics and monitoring. Proceedings of the 3rd International Conference on Case Histories in Geotechnical Engineering, S. Prakash, Editor,Rolla, Missouri, Vol. 1, pp. 663-670.

179. Svinkin, M.R., (1996a). Overcoming soil uncertainty in prediction of construction and industrial vibrations. American Society of Civil Engineers, ASCE, Proceedings of Uncertainty in the Geologic Environment: From theory to Practice, Geotechnical Special Publications No. 58, C.D. Shackelford, P.Nelson, and M.J.S. Roth, Editors, Vol. 2, pp. 1178-1194.

180. Svinkin, M.R., (1997). "Numerical methods with experimental soil response in predicting vibrations from dynamic sources. Proceedings of the Ninth International Conference of International Association for Computer Methods and Advances in Geomechanics, Wuhan, China, J. X. Yuan, Editor, A.A.Balkema Publishers, Vol. 3, pp. 2263-2268.

181. Svinkin, M.R., 1992. Pile driving induced vibrations as a source of industrial seismology. Proceedings of the 4th International Conference on the Application of Stress-Wave Theory to Piles,The Hague, The Netherlands, F.B.J. Barends, Editor, A.A. Balkema Publishers, pp. 167-174.

182. Svinkin, M.R., (1992). Pile driving induced vibrations as a source of industrial seismology. Proceedings of the 4th International Conference on the Application of Stress-Wave Theory to Piles,The Hague, The Netherlands, F.B.J. Barends, Editor, A.A. Balkema Publishers, pp. 167-174.

183. Szechy, K. and Varga, L. (1978), Foundation Engineering, Akademiai Klado, Budapest, 1978.

184. Todd, A.[1994]. Berwick river walls - an unique scheme to safeguard an historic part of Berwick upon Tweed. ICE papers competition. London.

185. Terzaghi, K. and R. B. Peck, 1967. Soil Mechanics in Engineering Practice, 2nd edn., John Wiley, NY.

186. Tokimatsu, K. and H.B. Seed, 1987. Evaluation of settlements in sands due to earthquake shaking, J. Geot. Engrg., 113 (8), 861-878.

187. Uromeihy. A. (1990). Ground vibration measurements with special reference to pile driving. PhD thesis Univ. Durham UK.

188. Van Rompaey, D., Legrand, C. & Holeyman, A. (1995). A prediction method for the installation of vibratory driven piles. Transactions on the Built Environment, Vol. 14, WIT Press, pp. 533-542.
189. Vesic, A. (1972). Expansion of Cavities in Infinite Soil Mass", Journal of the Mechanics and Foundation Division, ASCE, Vol. 98, SM3, p. 265-290.
190. Viking, K. (2002b). Vibrodrivability and induced ground vibrations of vibratory installed sheet piles. Proceedings of the international conference on vibratory pile driving and deepMsoil compaction, Louvain-La Neuve, Belgium, 9-10 September 2002, pp. 99-112.
191. Viking, K. (2006). The vibratory pile installation technique. Proceedings of TRANSVIB 2006, Paris, France, pp. 65- 82.
192. Waarts, P.H. & Bielefeld, M.W., (1994). Prediction and Control of Vibrations due to Pile Driving and Sheet Pile Vibration. Proceedings of the 5th International Conference & Exhibition on Piling and Deep Foundations, Bruges, Belgium, pp. 2.11.1-2.11.6.
193. Warrington, D.C. (1992). Vibratory and Impact-vibration Pile Driving Equipment. Published on www.vulcanhammer.info/vibro/Vibrator, downloaded 2009-10-10.
194. Webb, J. F. (1976). Noise control in industry. Sound Research Laboratories Limited, Holbrook Hall Sudbury, Suffolk,U.K.
195. Whenham, V. & Holeyman, A. (2012). Load Transfer During Vibratory Driving. Geotechnical and Geological Engineering, Vol. 30, No. 5, pp. 1119-1135.
196. Whenham, V. (2011). Power Transfer and Vibrator-Pile-Soil Interactions within the framework of vibratory pile driving. Doctoral Thesis, University of Louvain, Belgium.
197. Whiffen, A. C., (1971). A survey of traffic-induced vibrations. (Report LR419.) Crowthorne, Berkshire, England: United Kingdom Department of Environment, Road Research Laboratory.

198. Whiffin, A. C., and D. R. Leonard. (1971). A Survey of Traffic-induced Vibrations. Road Research Laboratory Report LR418. Crowthorne, England.
199. Wiss, J. F. (1981). “Construction Vibrations: State-of-the-art,” Journal of the Geotechnical Engineering Division, ASCE, Vol. 107, No. GT2, February 1981, pp. 167-181.
200. Wiss, J. F., (1974). Vibrations during construction operations. Journal of the Geotechnical Division 100(CO3):239–246.
201. Wiss, J.F., (1967). Damage Effects of Pile Driving Vibration. Highway Research Board Record 155, pp. 14-20.
202. Wood, W.C and Theissen, J.R.,(1982), "Variations in adjacent structures due to pile driving",. Proceedings of the GEOPILE Conference, San Francisco, pp. 83-107.
203. Woods R. D. and Richart F. E. Jr., (1967), “Screening of Elastic Surface Waves by Trenches”, Proc. International Symposium on Wave Propagation and Dynamic Properties of Earth Materials, Albuquerque, N. M. Aug.
204. Woods R. D., (1968), “Screening of Surface Waves in Soils”, J. Soil Mech. And Found. Div., Proc. ASCE 94 (SM 4): 951-979.
205. Woods, R. D., Jedele, L. P. (1985). “Energy-attenuation Relationships from Construction Vibrations,” Vibration Problems in Geotechnical Engineering, Proceedings of a symposium sponsored by the Geotechnical Engineering Division, ASCE, Detroit, Michigan, October 1985, pp 229-246.
206. Woods, R.D. (1997). "Dynamic Effects of Pile Installations on Adjacent Structures. NCHRP Synthesis 253, National Cooperative Highway Research Program, Transportation Research Board, National Academy Press, Washington D.C., USA.
207. Xu, L. (2011). “Floor vibration in lightweight cold-formed steel framing”, Advanced in Structural Engineering. Vol. 14, No.4, pp. 659–672.

208. Xu, X., Xu, H. and Chen, S. (2008). “Research on influence of vibration caused by pile construction on environment and countermeasures”, Rock and Soil Mechanics, Vol. 24, No. 6, pp. 957–960.
209. Youd, T.L. (1972). Compaction of sands by repeated shear straining. Journal of the Soil Mechanics and Foundation Division, Proceedings ASCE, Vol. 98, pp. 709- 25.
210. Zekkos, A.A, Woods, R.D and Grizi A., (2003) "Effect of pile driving induced vibrations on nearby structures and other assets".

Standards

211. “ANSI S3.29-1983 (R2001) American National Standard to the Evaluation of Human Exposure to Vibration in Buildings,” American National Standards Institute, 2001.
212. “DNR.S02-4235/SA60: Buller och Vibrationer, Fran Sparburen Linjetrafik.,”Banverket (Swedish Railway Administration), 2002.
213. “NS8176:1999 Vibration and Shock - Measurement of Vibration in Buildings from Land based Transport and Guidance to Evaluation of its Effect on Human Beings,” Norwegian Council for Building Standardization, 1999.
214. AASHTO (1996). Standard Recommended Practice for Evaluation of Transportation- Related Earthborne Vibrations (R 8-96.), AASHTO, Washington, D.C.
215. AASHTO Designation: R 8-96. [2004]. Standard Recommended Practice for Evaluation of Transportation-Related Earthborne Vibrations, AASHTO, Washington.
216. ANSI (1990). American National Standard. Vibration of Buildings – Guidelines for the
217. BS 5228-2:2009. Code of practice for noise and vibration control on construction and open sites – part 2: vibration. British Standards Institution.

218. BS 6472-1:2008. Guide to evaluation of human exposure to vibration in buildings – part1: vibration sources other than blasting. British Standards Institution.
219. BS 7385-2:1993. Evaluation and measurement for vibration in buildings – part 2: guide to damage levels from ground-borne vibration. British Standards Institution.
220. California Department of Transportation. 2004. Transportation- and Construction-Induced Vibration Guidance Manual. June. Prepared by Jones & Stokes, Sacramento, CA. Prepared for Noise, Vibration and Hazardous Waste Office, Sacramento, CA.
221. Carman, R. A., G. M. Glickman, and C. H. Reyes. 2009. Sacramento Intermodal Transit Facility and Track Relocation Project; Findings and Recommendation on Ground borne Vibration Mitigation. April 22. Prepared by Wilson, Ihrig & Associates, with appendix by C. Searls and R. Mayes of Simpson, Gumpertz & Heger. Prepared for TranSystems.
222. City of New York. 1988. Technical Policy and Procedure Notice No. 10/88. June 6. New York, NY.
223. City of Toronto. 2008. Bylaw No. 514-2008. Toronto, Canada.
224. Department of Environment and Conservation (DEC) (2006) Assessing vibration: technical guideline. NSW, Australia: Department of Environment and Conservation. Accessed 7 April 2012: www.environment.nsw.gov.au/resources/noise/vibrationguide0643.pdf
225. Deutsches Institut für Normung. 1999. Structural Vibration, Part 3: Effects of Vibration on Structures. DIN 4150-3.
226. DIN 4150 Protection against Vibration in Building Construction. German Institute for Standards. Berlin 1939
227. DIN 4150-2:1999 Structural vibration - Part 2: Human exposure to vibration in buildings," Deutsches Institut für Normung (German Institute for Standardization), 1999.
228. ESA. 2004. Noise and Vibration Study, Doyle Drive, South Access to the Golden Gate Bridge. Final. December.

229. German Standards Organization, 1970, Vibrations in Building Construction, DIN 4150.
230. ISO 2631-2:2003: Mechanical vibration and shock - Evaluation of human exposure to whole-body vibration. Part 2: Vibration in buildings (1 Hz to 80 Hz).," International Standard Organization, 2003.
231. Measurement of Vibrations and Evaluation of Their Effects on Buildings, Accredited Standards Committee S2, Mechanical Shock and Vibration, (S2.47), Standard Secretariat c/o Acoustical Society of America, New York.
232. Standards Australia (1983). Explosives-Storage, Transport, and Use, AS 2187.2, Sydney, Australia.
233. Swedish Standard. 1999. Vibration and shock – Guidance levels and measuring of vibrations in buildings originating from piling, sheet piling, excavating and packing to estimate permitted vibration levels. SS 02 52 11. Swedish Institute for Standards, SIS. Stockholm 1999, 7 p.
234. Swiss Association of Standardization, Effects of Vibration on Construction, Seefeldstrasse9, CH 8008,Zurich, Switzerland.
235. U.S. Department of Transportation, Federal Highway Administration, 2006, Rock Blasting and Overbreak Control, National Highway Institute, Third Edition, Calvin J. Konya.
236. U.S. Department of Transportation, Federal Transit Administration and the Port Authority of New York and New Jersey, Final Environmental Impact Statement, Permanent WTC Path Terminal in Borough of Manhattan, New York County, Chapter 10: Noise and Vibration, May 2005.

Appendix A

PLAXIS 8.2

Introduction:

The Finite Element Analysis (FEA) is a numerical method for solving problems of geotechnical engineering. Useful for problems with complicated geometries, loadings and material properties where analytical solutions cannot be obtained and not accurate. Using FEA has helped many researchers to obtain results by increasing the numbers of solved parameters in short time.

The Purpose of FEA:

Analytical Solution:

Stress analysis for trusses, beams, and all the other structural members are carried out based on dramatic simplification and idealization:

– Mass concentrated at the center of gravity for decreasing the eccentricity of the structure.

– Beam simplified as a line segment (same cross-section).

Design is based on the calculation results of the idealized structure & a large safety factor (1.5-3) according to the Egyptian code.

FEA:

Design geometry is a lot more complex; and the accuracy requirement is a lot higher. We need

– To understand the physical behaviors of a complex object (strength, heat transfer capability, fluid flow, etc.)

– To predict the performance and behavior of the design; to calculate the safety margin; and to identify the weakness of the design accurately; and

– To identify the optimal design with confidence

Common FEA Applications:

- Mechanical/Aerospace/Civil/Automotive Engineering
- Structural/Stress Analysis

・ Static/Dynamic ・ Linear/Nonlinear

- Fluid Flow
- Heat Transfer
- Electromagnetic Fields
- Soil Mechanics
- Acoustics
- Biomechanics

Types of finite elements:

1-D plane element:

(Spring, Truss, beam, etc…)

2-D plane element

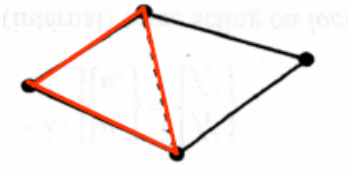

(Membrane, plate, shell, etc…)

3-D solid element

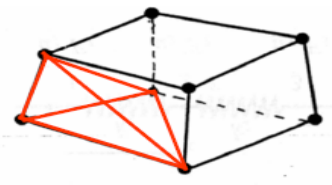

(3D fields, temperature, displacement, stress, flow velocity)

Computer program:

PLAXIS is a finite element program for geotechnical applications in which soil models are used to simulate the soil behavior. The PLAXIS code and its soil models have been developed with great care. Although a lot of testing and validation have been performed, it cannot be guaranteed that the PLAXIS code is free of errors. Moreover, the simulation of geotechnical problems by means of the finite element method implicitly involves some inevitable numerical and modeling errors. The accuracy at which reality is approximated depends highly on the expertise of the user regarding the modeling of the problem, the understanding of the soil models and their limitations, the selection of model parameters, and the ability to judge the reliability of the computational results. Hence, PLAXIS may only be used by professionals that possess the afore mentioned expertise. The user must be aware of his/her responsibility when he/she uses the computational results for geotechnical design purposes. PLAXIS 2D is a two-dimensional finite element program, developed for the analysis of deformation, stability and groundwater flow in geotechnical engineering. It is a part of the PLAXIS product range, a suite of finite element programs that is used worldwide for geotechnical engineering and design. A large range of geotechnical problems may be analyzed using this high capacity version. It is possible to use extensive 2D finite element meshes. The PLAXIS2D is supplied as an extended package, including static elasto plastic deformation, advanced soil models, stability analysis, consolidation, safety analysis, updated mesh and steady-state groundwater flow.

- **Plaxis dynamic:**

The PLAXIS Dynamics Module is an extension to PLAXIS 2D. It offers the tools to analyze the propagation of waves through the soil and their influence on structures. This allows for the analysis of seismic loading as well as vibrations due to construction activities. PLAXIS Dynamics offers the possibility to perform dynamic calculations in individual calculation phases.

- **Modeling:**

• Time-dependent dynamic load systems for point loads, distributed loads and prescribed displacements (velocities, acceleration)

• Independent application of horizontal and vertical displacement (velocity, acceleration) components

• Absorbent (viscous) boundaries to absorb waves at the model boundaries

• Rayleigh damping (α_R and β_R) per material data set for soil layers and structures)

• Smooth meshes, to prevent numerical oscillations and internal reflections

- **Calculations:**

• Automatic time stepping using dynamic sub-steps

• Selection of New mark time integration scheme (α_N and β_N)

• Free vibration analysis

• Harmonic loads

• Import of SMC files for time-dependent dynamic loading

- **Results:**

• Velocities and acceleration in addition to displacements

• Time-displacement, Time-velocity, Time-acceleration curves

• Switch from time-curves to frequency-curves using Fast Fourier Transform

• Animations (creation of AVI files)

General Information:

The information given in this chapter applies to all parts of the program

Units and sign conventions:

It is important in any analysis to adopt a consistent system of units. At the start of the input of geometry, a suitable set of basic units should be selected. The basic units comprise a unit for length, force and time.The default units are meters [m] for length, kilo Newton [KN] for force and seconds [s] for time.

Sign convention:

The generation of a two-dimensional (2D) finite element model in PLAXIS 2D is based on the creation of a geometry model. This geometry model is created in the x-y-plane of the global coordinate system (Figure 9.1), whereas the z-direction is the out-of-plane direction. In the global coordinate system the positive z-direction is pointing towards the user. In all of the output data, compressive stresses and forces, including pore pressures, are taken to be negative, whereas tensile stresses and forces are taken to be positive. Figure 9.1 shows the positive stress directions. Although

PLAXIS 2D is a 2D program; stresses are based on the 3D Cartesian coordinate system shown in Figure 9.1. In a plane strain analysis σ_{zz} is the out-of-plane stress. In an axisymmetric analysis, x represents the radial coordinate, y represents the axial coordinate and z represents the tangential direction. In this case, σ_{xx} represents the radial stress and σ_{zz} represents the hoop stress.

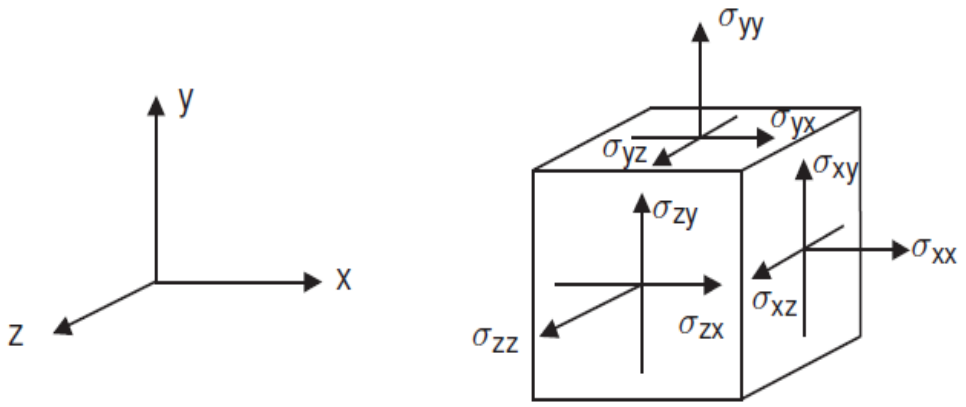

Figure 9.1: Coordinate system and indication of positive stress components
(After PLAXIS 2D Reference Manual 2011)

Input program – General over view:

To carry out a finite element analysis using the PLAXIS 2D program, the user has to create a two dimensional geometry model composed of points, lines and other components, in the x - y plane and specify the material properties and boundary conditions.

New project:

When the Start a new project option is selected, the Project properties window appears in which the basic model parameters of the new project can be defined. The Project properties window contains the Project and the model tab sheets. The Project tab sheet contains the project name and description and offers the possibility to select a company logo. The Model tab sheet contains the type of the model, the basic units for length, force and time, the unit weight of water and the initial dimensions of the model. The default values can be replaced by the current values when selecting Set as default and clicking the OK button. A more detailed description of all these options is given below.

General model properties

The general options of the project are available in the Model tab sheet of the Project properties window.

Model:

PLAXIS 2D may be used to carry out two-dimensional finite element analysis. The finite element model is defined by selecting the corresponding option in the Model dropdown-menu in the Project tab sheet.

- **Plane strain:**

A Plane strain model is used for geometries with a (more or less) uniform cross section and corresponding stress state and loading scheme over a certain length perpendicular to the cross section (z-direction). Displacements and strains in z-direction are assumed to be zero. However, normal stresses in z-direction are fully taken into account. In earthquake problems the dynamic loading source is usually applied along the bottom of the model resulting in shear waves that propagate upwards. This type of problems is generally simulated using a plane strain model.

- **Axisymmetric:**

An Axisymmetric model is used for circular structures with a (more or less) uniform radial cross section and loading scheme around the central axis, where the deformation and stress state are assumed to be identical in any radial direction. Note that for axisymmetric problems the x-coordinate represents the radius and the y-axis corresponds to the axial line of symmetry. Negative x-coordinates cannot be used. Single-source vibration problems are often modeled with axisymmetric models like pile driving or dynamic compaction. This is because waves in an axisymmetric system radiate in a manner similar to that in a three dimensional system. In this case, the energy disperses leading to wave attenuations with distance. Such effect can be attributed to the geometric damping (or radiation damping), which is by definition included in the axisymmetric model. The selection of Plane strain or Axisymmetric results in a two dimensional finite element model with only two translational degrees of freedom per node (x- and y-)direction) as shown in (Fig.9.2).

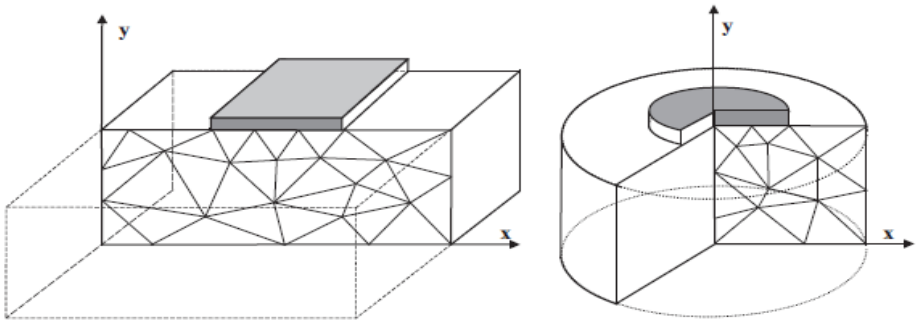

Figure.9.2: Example of a plane strain (left) and axisymmetric problem (right), (After PLAXIS 2D Reference Manual, 2002)

Elements:

The user may select either 6-node or 15-node triangular elements to model soil layers and other volume clusters.

- **15-Node:**

The 15-node triangle is the default element. It provides a fourth order interpolation for displacements and the numerical integration involves twelve Gauss points (stress points). The type of element for structural elements and interfaces is automatically taken to be compatible with the soil element type as selected here. The 15-node triangle is a very accurate element that has produced high quality stress results for difficult problems, as for example in collapse calculations for in compressible soils (Nagtegaal, Parks & Rice, 1974, Sloan, 1981 and Sloan & Randolph, 1982). The15-node triangle is particularly recommended to be used in axis-symmetric analysis. The use of 15-node triangles leads to more memory consumption and slower calculation and operation performance. Therefore a more simple type of elements is also available.

- **6-Node:**

The 6-node triangle provides a second order interpolation for displacements and the numerical integration involves three Gauss points. The type of element for structural elements and interfaces is automatically taken to be compatible

with the soil element type as selected here. The 6-node triangle is a fairly accurate element that gives good results in standard deformation analyses, provided that a sufficient number of elements are used. However, care should be taken with axisymmetric models or in situations where (possible) failure plays a role, such as a bearing capacity calculation or a safety analysis by means of phi-creduction. Failure loads or safety factors are generally over predicted using 6-nodedelements. In those cases the use of 15-node elements is preferred.

One 15-node element can be thought of a composition of four 6-node elements, since the total number of nodes and stress points is equal. Nevertheless, one 15-node element is more powerful than four 6-node elements. In addition to the soil elements, compatible plate elements are used to simulate the behavior of walls, plates and shells and geo-grid elements are used to simulate the behavior of geo-grids and wovens Moreover, compatible interface elements are used to simulate soil-structure interaction .Finally, the geometry creation mode allows for the input of embedded pile rows, fixed-end anchors and node-to-node anchors.

Prescribed displacement:

Prescribed displacements are special conditions that can be imposed to the model to control the displacements at certain locations. Prescribed displacements can be assigned to existing geometric entities by right clicking the entity and selecting the corresponding option in the appearing menu. The creation of a prescribed displacement is similar to the creation of a geometric entity. The options available in the menu displayed as the Create prescribed displacement button is selected in the side toolbar provide a faster definition of prescribed displacements. Instead of creating the geometric entity and then assigning a prescribed displacement to it, the process is completed in one step. Although the input values of prescribed displacements are specified in the Structures mode, the activation, deactivation or change of values may be

considered in the framework of Staged construction. On a geometric entity where both prescribed displacements and loads are applied and active, the prescribed displacement has priority over the load during calculations. If both prescribed and fixed displacement is assigned to a line, the fixed displacement will be taken into consideration. However, when not all the displacement directions are fixed, it is possible to apply a load in the free directions.

Material properties and material database:

In PLAXIS, soil properties and material properties of structures are stored in material data sets. There are four different types of material sets grouped as data sets for soil and interfaces, plates, geo-grids, embedded pile rows and anchors. All data sets are stored in the material database. From the database, the data sets can be assigned to the soil clusters or to the corresponding structural objects in the geometry model.

Material model:

PLAXIS supports different models to simulate the behavior of soil and other continua. The models and their parameters are described in detail below.

Linear Elastic model (LE):

The Linear Elastic model is based on Hooke's law of isotropic elasticity. It involves two basic elastic parameters, i.e. Young's modulus E and Poisson's ratio v. Although the Linear Elastic model is not suitable to model soil, it may be used to model stiff volumes in the soil, like concrete walls, or intact rock formations.

Hardening Soil model (HS):

The Hardening Soil model is an advanced model for the simulation of soil behavior. As for the Mohr-Coulomb model, limiting states of stress are described by means of the friction angle, the cohesion, c, and the dilatancy angle, however, soil stiffness is described much more accurately by using three

different input stiffness's: the triaxial loading stiffness, E50, the triaxial unloading stiffness, E_{ur}, and the odometer loading stiffness, E_{oed}. As average values for various soil types, $E_{ur} \approx 3E_{50}$ and $E_{oed} \approx E_{50}$ are suggested as default settings, but both very soft and very stiff soils tend to give other ratios of E_{oed}/E_{50}, which can be entered by the user. In contrast to the Mohr-Coulomb model, the Hardening Soil model also accounts for stress-dependency of stiffness moduli. This means that all stiffnesss increase with pressure. Hence, all three input stiffnesss relate to a reference stress, usually taken as100 kPa (1 bar).Besides the model parameters mentioned above, initial soil conditions, such aspre-consolidation, play an essential role in most soil deformation problems. This can be taken into account in the initial stress generation.

Soft Soil model (SS):

The Soft Soil model is a Cam-Clay type model especially meant for primary compression of near normally-consolidated clay-type soils. Although the modeling capabilities of this model are generally superseded by the Hardening Soil model, the Soft Soil model is better capable to model the compression behavior of very soft soils.

Soft Soil Creep model (SSC):

The Hardening Soil model is generally suitable for all soils, but it does not account for viscous effects, i.e. creep and stress relaxation. In fact, all soils exhibit some creep and primary compression is thus followed by a certain amount of secondary compression. The latter is most dominant in soft soils, i.e. normally consolidated clays, silts and peat, and PLAXIS thus implemented a model under the name Soft Soil Creep model. The Soft Soil Creep model has been developed primarily for application to settlement problems of foundations, embankments, etc. For unloading problems, as normally encountered in tunneling and other excavation problems, the Soft Soil Creep model hardly supersedes the simple Mohr-Coulomb model. As for the Hardening Soil model, proper initial soil conditions are also essential when

using the Soft Soil Creep model. This also includes data on the pre-consolidation stress, as the model accounts for the effect of over-consolidation. Note that the initial over-consolidation ratio also determines the initial creep rate.

Mohr-Coulomb model (MC):

The linear elastic perfectly-plastic Mohr-Coulomb model involves five input parameters, i.e. E and ν for soil elasticity; φ and c for soil plasticity and Ψ as an angle of dilatancy. This Mohr-Coulomb model represents a 'first-order' approximation of soil or rock behavior. It is recommended to use this model for a first analysis of the problem considered. For each layer one estimates a constant average stiffness or a stiffness that increases linearly with depth. Due to this constant stiffness, computations tend to be relatively fast and one obtains a first estimate of deformations.

Plasticity is associated with the development of irreversible strains. In order to evaluate whether or not plasticity occurs in a calculation, a yield function, f, is introduced as a function of stress and strain. Plastic yielding is related with the condition f = 0. This condition can often be presented as a surface in principal stress space. A perfectly-plastic model is a constitutive model with a fixed yield surface, i.e. a yield surface that is fully defined by model parameters and not affected by (plastic) straining. For stress states represented by points within the yield surface, the behavior is purely elastic and all strains are reversible.

Mohr coulomb behavior:

The basic principle of elastoplasticity is that strains and strain rates are decomposed into an elastic part and a plastic part as shown in (Eq.9.1):

$$\underline{\varepsilon} = \underline{\varepsilon}^{e} + \underline{\varepsilon}^{p} \qquad \dot{\underline{\varepsilon}} = \dot{\underline{\varepsilon}}^{e} + \dot{\underline{\varepsilon}}^{p} \tag{9.1}$$

According to the classical theory of plasticity (Hill, 1950), plastic strain rates are proportional to the derivative of the yield function with respect to the stresses. This means that the plastic strain rates can be represented as vectors perpendicular to the yield surface. This classical form of the theory is referred to as associated plasticity. However, for Mohr-Coulomb type yield functions, the theory of associated plasticity over estimates dilatancy. Therefore, in addition to the yield function, a plastic potential function g is introduced. The case g ≠ f is denoted as non-associated plasticity. Ingeneral, the plastic strain rates are written as shown in (Eq.9.1.2):

$$\underline{\dot{\varepsilon}}^{p} = \lambda \frac{\partial g}{\partial \underline{\sigma}'} \tag{9.1.2}$$

In which λ is the plastic multiplier. For purely elastic behaviour λ is zero, whereas in the case of plastic behaviour λ is positive as shown in relations 9.3

$$\lambda = 0 \quad \text{for:} \quad f < 0 \quad \text{or :} \quad \frac{\partial f}{\partial \underline{\sigma}'}^{T} \underline{\underline{D}}^{e} \underline{\dot{\varepsilon}} \leq 0 \quad \text{(Elasticity)} \tag{9.2}$$

$$\lambda > 0 \quad \text{for:} \quad f = 0 \quad \text{and:} \quad \frac{\partial f}{\partial \underline{\sigma}'}^{T} \underline{\underline{D}}^{e} \underline{\dot{\varepsilon}} > 0 \quad \text{(Plasticity)} \tag{9.3}$$

These equations may be used to obtain the following relationship between the effective stress rates and strain rates for elastic perfectly-plastic behaviour (Smith & Griffith, 1982; Vermeer & Borst, 1984) as shown in (Eq.9.4):

$$\underline{\dot{\sigma}}' = \left(\underline{\underline{D}}^{e} - \frac{\alpha}{d} \underline{\underline{D}}^{e} \frac{\partial g}{\partial \underline{\sigma}'} \frac{\partial f}{\partial \underline{\sigma}'}^{T} \underline{\underline{D}}^{e} \right) \underline{\dot{\varepsilon}} \tag{9.4}$$

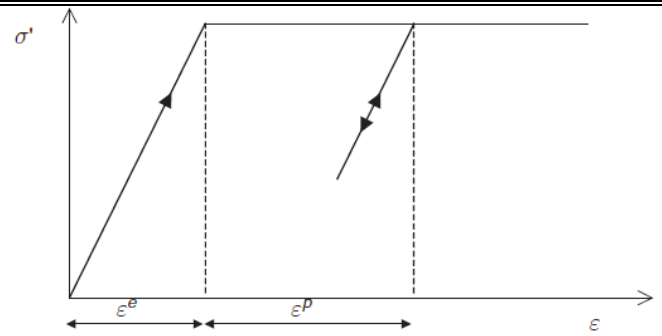

Figure 9.3: Basic idea of an elastic perfectly plastic model (After PLAXIS 2D material model Manual 2011)

Drainage type:

In principle, all model parameters in PLAXIS are meant to represent the effective soilres ponse, i.e. the relationship between the stresses and the strains associated with the soil skeleton. An important feature of soil is the presence of pore water. Pore pressures significantly influence the (time-dependent) soil response. PLAXIS offers several options to enable incorporation of the water-skeleton interaction in the soil response. The most advanced option is a fully coupled flow-deformation analysis. However, in many cases it is sufficient to analyze either the long-term (drained) response or the short-term (undrained) response without considering the time-dependent development of pore pressures. In the latter case (undrained), excess pore pressures are generated as a result of stress changes (loading or unloading). The dissipation of these excess pore pressures with time can be analyzed in a Consolidation calculation.

The simplified water-skeleton interaction, as considered in a Plastic calculation, a Safety analysis or a Dynamic analysis, is defined by the Drainage type parameter. PLAXIS offers a choice of different types of drainage:

- **Drained behavior:**

Using this setting no excess pore pressures are generated. This is clearly the case for dry soils and also for full drainage due to a high permeability (sands)and/or a low rate of loading. This option may also be used to simulate long-term soil behaviour without the need to model the precise history of undrained loading and consolidation.

- **Undrained behaviour:**

This setting is used for saturated soils in cases where pore water cannot freely flow through the soil skeleton. Flow of pore water can sometimes be neglected due to a low permeability (clays) and/or a high rate of loading. All clusters that are specified as undrained will indeed behave undrained, even if the cluster or a part of the cluster is located above the phreatic level.

- **Non-porous behavior:**

Using this setting neither initial nor excess pore pressures will be taken into account in clusters of this type. Applications may be found in the modeling of concrete or structural behavior. Non-porous behavior is often used in combination with the linear elastic model. The input of a saturated weight is not relevant for non-porous materials or intact rock.

Saturated and unsaturated weight (γ_{sat} and γ_{unsat}):

The saturated and the unsaturated weights, entered as a force per unit volume, refer to the total unit weight of the soil skeleton including the fluid in the pores. The unsaturated weight applies to all material above the phreatic level and the saturated unit weight applies to all material below the phreatic level, where the phreatic level itself is generally defined as the level where the steady-state pore pressure is zero (p_{steady} = 0).Only in the case of a fully coupled flow-deformation analysis, the phreatic level is defined as the level where the current pore water pressure is zero (p_{water}= 0). This means that during a fully coupled

flow-deformation analysis the position of the phreatic level and hence the material weight can change. For non-porous material only the unsaturated weight is relevant, which is just the total unit weight. For porous soils the unsaturated weight is obviously smaller than the saturated weight. For sands, for example, the saturated weight is generally around 20 kN/m3whereas the unsaturated weight can be significantly lower, depending on the degree of saturation.

Advanced general properties:

- **Rayleigh α and β:**

Material damping in dynamic calculations is caused by the viscous properties of soil, friction and the development of irreversible strains. All plasticity models in PLAXIS 2D can generate irreversible (plastic) strains, and may thus cause material damping. However, this damping is generally not enough to model the damping characteristics of real soils. For example, most soil models show pure elastic behavior upon unloading and reloading which does not lead to damping at all. There is one model in PLAXIS that includes viscous behavior, which is the Soft Soil Creep model. Using the model in dynamic calculations may lead to viscous damping, but also the Soft Soil Creep model hardly shows any creep strain in load / reloads cycles. There is also one model in PLAXIS that includes hysteretic behavior in loading / reloads cycles, which is the HS small model. When using this model, the amount of damping that is obtained depends on the amplitude of the strain cycles. Considering very small vibrations, even the HS small model does not show material damping, whereas real soils still show a bit of viscous damping. Hence, additional damping is needed to model realistic damping characteristics of soils in dynamic calculations. This can be done by means of Rayleigh damping. Rayleigh damping is a numerical feature in which a damping matrix C is composed by adding a portion of the mass matrix M and a portion of the stiffness matrix K as shown in (Eq. 9.5):

$$C = \alpha M + \beta K \qquad (9.5)$$

The parameters α and β are the Rayleigh coefficients and can be specified in the corresponding cells in the Parameters tab sheet of the Soil window. α is the parameter that determines the influence of mass in the damping of the system. The higher α is, the more the lower frequencies are damped. β is the parameter that determines the influence of stiffness in the damping of the system. The higher β is, the more the higher frequencies are damped. In PLAXIS 2D, these parameters can be specified for each material data set for soil and interfaces as well as for material data sets for plates. In this way, the (viscous) damping characteristics can be specified for each individual material in the finite element model.

Despite the considerable amount of research work in the field of dynamics, little has been achieved yet for the development of a commonly accepted procedure for damping parameter identification. Instead, for engineering purposes, some measures are made to account for material damping. A commonly used engineering parameter is the damping ratio £. The damping ratio is defined as £ = 1 for critical damping, i.e. exactly the amount of damping needed to let a single degree-of-freedom system that is released from an initial excitation u_0, smoothly stops without rebounding. Considering Rayleigh damping, a relationship can be established between the damping ratio £ and the Rayleigh damping parameters α and β in (Eq9.6) and shown in (Fig. 9.4):

$$\alpha + \beta w^2 = 2w£ \quad \text{and} \quad w = 2\pi f \qquad (9.6)$$

Where w is the angular frequency in rad/s and f is the frequency in Hz (1/s).

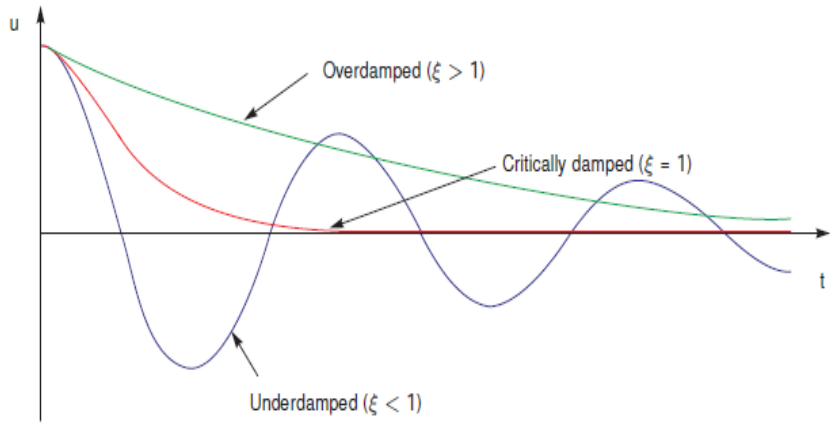

Figure 9.4 Role of damping ratio £ in free vibration of a single degree-of-freedom system (After PLAXIS 2D Reference Manual 2011)

The damping parameters (α and β) can be automatically calculated by the program when the target damping ratio (£) and the target frequencies (f) are specified in the pane displayed in the General tab sheet when one of the cells corresponding to the damping parameters is clicked.

Material data sets for plates:

In addition to material data sets for soil and interfaces, the material properties and model parameters for plates are also entered in separate material data sets. Plates are used to model the behavior of slender walls, plates or thin shells. Distinction can be made between elastic and elastoplastic behavior. A data set for plates generally represents a certain type of plate material, and can be assigned to the corresponding (group of) plate elements in the geometry model.

- **Material set**:

Several data sets may be created to distinguish between different types of plates. The material data set is defined by:

Identification: A user may specify any identification title for a data set. It is advisable to use a meaningful name since the data set will appear in the database tree view by its identification.

Comments: A user may write down comments related to the material data set.

Color: Color can be used as a distinction tool in the model.

Material type: There are two available options, describing the material type of a plate. These options are Elastic and Elastoplastic. The availability of the parameters defined in the Properties box depends on the selected material type.

- **Properties:**

The properties required for plates can be grouped into general properties, stiffness properties, strength properties in case of elasto plastic behavior and dynamic properties.

- **General properties:**

A plate has two general properties:

d: The (equivalent) thickness (in the unit of length) is automatically calculated from the ratio of the axial stiffness EA and flexural rigidity EI (see Stiffness properties).

W: In a material set for plates a specific weight can be specified, which is entered as a force per unit of length per unit width in the out-of-plane direction. For relatively massive structures the weight of a plate is, in principle, obtained by multiplying the unit weight of the plate material by the thickness of the plate. Note that in a finite element model, plates are superimposed on a continuum and therefore 'overlap' the soil. To calculate accurately the total weight of soil and structures in the model, the unit weight of the soil should be subtracted from the unit weight of the plate material. For sheet-pile walls the weight (force per unit area) is generally provided by the manufacturer. This value can be adopted directly since sheet-pile walls usually occupy relatively little volume. The weight of plates is activated together with the soil weight by means of the ΣM_{weight} parameter.

- **Stiffness properties:**

For elastic behavior, several parameters should be specified as material properties. PLAXIS 2D allows for orthotropic material behavior in plates, which is defined by the following parameters:

EA: For elastic behavior an in-plane axial stiffness EA should be specified. For both axisymmetric and plane strain models the value relates to stiffness per unit width in the out-of-plane direction.

EI: For elastic behavior a flexural rigidity EI should be specified. For both axisymmetric and plane strain models the value relates to stiffness per unit width in the out-of-plane direction.

***ν* (nu)**: Poisson's ratio.

From the ratio of EI and EA an equivalent thickness for an equivalent plate (d_{eq}) is automatically calculated from the (Eq.9.7):

$$d_{eq} = \sqrt{12\frac{EI}{EA}} \tag{9.7}$$

For the modeling of plates, PLAXIS uses the Mindl in beam theory as described in Bathe (1982). This means that, in addition to bending, shear deformation is taken into account. The shear stiffness of the plate is determined from (Eq.9.8):

$$\text{Shear stiffness} = \frac{5EA}{12(1+\nu)} = \frac{5E\left(d_{eq}\cdot 1m\right)}{12(1+\nu)} \tag{9.8}$$

This implies that the shear stiffness is determined from the assumption that the plate has a rectangular cross section. In the case of modeling a solid wall, this will give the correct shear deformation. However, in the case of steel profile

elements, like sheet-pile walls, the computed shear deformation may be too large. You can check this by judging the value of d_{eq}. For steel profile elements, deq should be at least of the order of a factor 10times smaller than the length of the plate to ensure negligible shear deformations. In addition to the above stiffness parameters, a Poisson's ratio is required. For thin structures with a certain profile or structures that are relatively flexible in the out-of-plane direction (like sheet-pile walls), it is advisable to set Poisson's ratio to zero. For real massive structures (like concrete walls) it is more realistic to enter a true Poisson's ratio of the order of 0.15.

Since PLAXIS considers plates (extending in the out-of-plane direction) rather than beams (one-dimensional structures), the value of Poisson's ratio will influence the flexural rigidity of the isotropic plate as follows:

EI: Input value of flexural rigidity

EI/1-ν^2Observed value of flexural rigidity

The stiffening effect of Poisson's ratio is caused by the stresses in the out-of-plane direction (σ_{zz}) and the fact that strains are prevented in this direction. Note that the Poisson's ration (ν) is assumed to be zero in anisotropic case.

- **Strength properties (plasticity):**

Strength parameters are required in case of plasticity:

M_p: Maximum bending moment

N_p: Maximum normal force

Plasticity may be taken into account by specifying a maximum bending moment, Mp. The maximum bending moment is given in units of force times length per unit width. In addition to the maximum bending moment, the axial force is limited to Np. The maximum axial force, Np, is specified in units of force per unit width. When the combination of a bending moment and an axial force occur in a plate, then the actual bending moment or axial force at which plasticity occurs is lower than respectively Mp or Np.

The relationship between Mp and Np is visualized in Figure 9.5. The diamond shape represents the ultimate combination of forces for which plasticity will occur. Force combinations inside the diamond will result in elastic deformations only. The Scientific Manual describes in more detail how PLAXIS deals with plasticity in plates.

Bending moments and axial forces are calculated at the stress points of the beam elements. If M_p or N_p is exceeded, stresses are redistributed according to the theory of plasticity, so that the maxima are complied with. This will result in irreversible deformations. Output of bending moments and axial forces is given in the nodes, which requires extrapolation of the values at the stress points. Due to the position of the stress points in a beam element, it is possible

that the nodal values of the bending moment may slightly exceed M_p as shown in (Figure. 4.5).

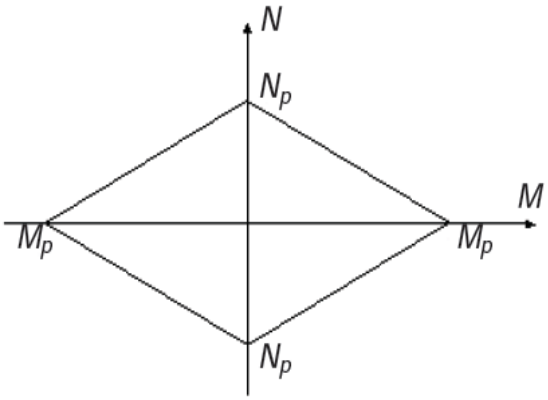

Figure 9.5: Combinations of maximum bending moment and axial force (After PLAXIS 2D Reference Manual 2011)

- **Interfaces:**

Interfaces are joint elements to be added to plates to allow for a proper modeling of soil-structure interaction. Interfaces may be used to simulate, for example, the thin zone of intensely shearing material at the contact between a plate and the surrounding soil. Interfaces can be created next to plate or geo-grid elements or between two soil volumes.

An interface can be created using the Create interface option available in the menu displayed when the Create structure button in the side toolbar is clicked. The creation of an interface is similar to the creation of a line. In this case a line with an interface assigned to it will be created. When the geometric entity (line) is already available in the model it is advised to assign an interface to it without recreating the geometry in order to prevent the model from being unnecessarily large and unwieldy.

The interface appears as a line at the side of the geometry line the interaction with the soil takes place. The side at which the interface will appear is also indicated by the arrow in the cursor pointing in the direction of drawing. To place an interface at the other side, it should be drawn in the opposite direction. Note that interfaces can be placed at both sides of a geometry line. This enables a full interaction between structural objects (walls, plates, geo-grids, etc.) and the surrounding soil. To be able to distinguish between the two possible interfaces along a geometry line, the interfaces are indicated by a plus-sign (+)or a minus sign (-).The sign of an interface is only used to enable distinguishing interfaces at either side of a surface, but it does not affect its behavior.

Mesh generation:

When the geometry model is fully defined the geometry has to be divided into finite elements in order to perform finite element calculations. A composition of finite elements is called a mesh. The mesh is created in the Mesh mode. The mesh should be sufficiently fine to obtain accurate numerical results. On the other hand, very fine meshes should be avoided since this will lead to excessive calculation times. The PLAXIS 2Dprogram allows for a fully automatic generation of finite element meshes. The generation of the mesh is based on a robust triangulation procedure. The mesh generation process takes into account the soil stratigraphy as well as all structural objects, loads and boundary conditions.

- **Local refinement:**

In areas where large stress concentrations or large deformation gradients are expected, it is desirable to have a more accurate (finer) finite element mesh, whereas other parts of the geometry might not require a fine mesh. Such a situation often occurs when the geometry model includes edges or corners or structural objects. Local refinement is based on a local fineness factor that can be specified for each geometry entity. This factor gives an indication of the relative element size with respect to the target element size as determined by the Element distribution parameter. By default, the Fineness factor value is set to 1.0 for most geometry entities whereas this value is0.25 for structural objects and loads. A Fineness factor value of 0.5 reduces the element size to half the target element size. The fineness factor can be changed by selecting the geometry entity and clicking on the Fineness factor in the Selection explorer. Values in the range from 0.03125 to 8.0 are acceptable. Using a value larger than 1.0 coarsens the mesh locally.

Calculation phases:

Finite element calculations can be divided into several sequential calculation phases. Each calculation phase corresponds to a particular loading or construction stage. The construction stages can be defined in the Staged construction mode.

- **Types of analysis:**

The first step in a PLAXIS analysis is defining a calculation type of a phase in the Calculation type drop-down menu in the Phases window. The options available are K0procedure and Gravity loading for the initial phase to generate the initial stress state of soil. The Groundwater flow only option can be used only if groundwater flow analysis will be performed. For deformation analysis options such as Plastic, Consolidation, Safety, Dynamic and Fully coupled flow-deformation are available.

- **Initial stress generation:**

Many analysis problems in geotechnical engineering require the specification of a set of initial stresses. The initial stresses in a soil body are influenced by the weight of the material and the history of its formation. This stress state is usually characterized by an initial vertical effective stress ($\sigma'_{v,0}$). The initial horizontal effective stress $\sigma'_{h,0}$ is related to the initial vertical effective stress by the coefficient of lateral earth pressure K_0 in (Eq.9.10)

$$(\sigma'_{h,0} = K_0 \cdot \sigma'_{v,0}). \qquad (9.10)$$

- **K_0 procedure**

K0 procedure is a special calculation method available in PLAXIS to define the initial stresses for the model, taking into account the loading history of the soil.

In practice, the value of K0 for a normally consolidated soil is often assumed to be related to the friction angle by Jaky's empirical expression in (Eq.9.11):

$$K_0 = 1 - \sin\varphi \qquad (9.11)$$

When the K_0 procedure is adopted, PLAXIS will generate vertical stresses that are in equilibrium with the self-weight of the soil. Horizontal stresses, however, are calculated from the specified value of K_0. Even if the value of K_0 is chosen such that plasticity does not occur, the K_0 procedure does not ensure that the complete stress field is in equilibrium. Full equilibrium is only obtained for a horizontal soil surface with any soil layers parallel to this surface and a horizontal phreatic level. Therefore, the K_0 procedure is not recommended when dealing with non-horizontal surfaces.

- **Results of initial stress generation:**

After the generation of initial stresses the plot of the initial effective stresses can be inspected. It is also useful to view the plot of plastic points.Using K0 values that differ substantially from unity may sometimes lead to an initial stress state that violates the Mohr-Coulomb criterion. If the plot of the plastic

points shows many red plastic points (Mohr-Coulomb points), the value of K0 should be chosen closer to 1.0.

If there are a small number of plastic points, it is advisable to perform a plastic nil-step. When using the Hardening Soil model and defining a normally consolidated initial stress state (OCR = 1.0 and POP = 0.0), the plot of plastic points shows many hardening points. Users need not be concerned about these plastic points as they just indicate a normally consolidated stress state.

- **Plastic calculation**:

A Plastic calculation is used to carry out an elastic-plastic deformation analysis in which it is not necessary to take the change of pore pressure with time into account. If the Updated mesh parameter has not been selected, the calculation is performed according to the small deformation theory. The stiffness matrix in a normal plastic calculation is based on the original un deformed geometry. This type of calculation is appropriate in most practical geotechnical applications. Although a time interval can be specified, a plastic calculation does not take time effects into account, except when the Soft Soil Creep model is used. Considering the quick loading of saturated clay-type soils, a Plastic calculation may be used for the limiting case of fully undrained behavior using the undrained option in the material data sets. On the other hand, performing a fully drained analysis can assess the settlements on the long term. This will give a reasonably accurate prediction of the final situation, although the precise loading history is not followed and the process of consolidation is not dealt with explicitly.

An elastic-plastic deformation analysis where undrained behavior is temporarily ignored can be defined by checking the Ignore undrained behavior parameter. In this case the stiffness of water is not taken into account.

In a Plastic calculation loading can be defined in the sense of changing the load combination, stress state, weight, strength or stiffness of elements, activated by

changing the load and geometry configuration or pore pressure distribution by means of Staged construction. In this case, the total load level that is to be reached at the end of the calculation phase is defined by specifying a new geometry and load configuration, and/or pore pressure distribution, in the Staged construction mode.

- **Dynamic calculation:**

The Dynamic option should be selected when it is necessary to consider stress waves and vibrations in the soil. With PLAXIS 2D it is possible to perform a dynamic analysis after a series of plastic calculations. The applied dynamic load is the product of the input value of the defined dynamic load and the corresponding dynamic load multiplier. Besides the activation of the dynamic load or dynamic prescribed displacement, absorbent (viscous) boundary conditions can be defined for a Dynamic calculation. The possible vibrations of a system that occur when an existing static load is released can be analyzed by performing a free vibration analysis. A free vibration analysis can be performed in a Dynamic calculation type. To perform a free vibration analysis the active static external load in a previous calculation needs to be deactivated. In a Dynamic calculation loading can be defined in the sense of applying a predefined combination of external loads as dynamic forces using dynamic multipliers activated in the Staged construction mode.

- **Dynamic control parameters:**

The parameters controlling a Dynamic analysis can be defined in the Dynamic control parameters sub tree in the Phases window. The New mark alpha and Beta parameters determine the numeric time-integration according to the implicit new mark scheme. In order to obtain an unconditionally stable solution, these parameters must satisfy the following conditions in (Eq.9.12):

$$Newmark\ \beta \geq 0.5 \quad \text{and} \quad Newmark\ \alpha \geq 0.25(0.5 + \beta)^2 \tag{9.12}$$

For an average acceleration scheme you can use the standard settings ($\alpha = 0.25$ and $\beta = 0.5$). Using a higher β-value and corresponding α-value results in a damped New mark scheme (e.g. $\alpha = 0.3025$ and $\beta = 0.6$).

Appendix B

SAP. 2000. V.14

Introduction

SAP2000 is the latest and most powerful version of the well- known SAP series of structural analysis programs. SAP2000 is object based, meaning that the models are created using members that represent the physical reality. A beam with multiple members framing into it is created as a single object, just as it exists in the real world, and the meshing needed to ensure that connectivity exists with the other members is handled internally by the program. Results for analysis and design are reported for the overall object, and not for each sub-element that makes up the object, providing information that is both easier to interpret and more consistent with the
physical structure.

The physical structural members in a SAP2000 model are represented by objects.

Using the graphical user inter face, you “draw” the geometry of an object, then “as -sign” properties and loads to the object to completely define the model of the physical member.

The following object types are available, listed in order of geometrical dimension:

- Point objects, of two types:

1. Joint objects: These are automatically created at the corners or ends of all other types of objects below, and they can be explicitly added to model supports or other localized behavior.
2. Grounded (one-joint) support objects: Used to model special support behavior such as isolators, dampers, gaps, multi linear springs, and more.

- Line objects, of several types but the focus will be in the frame object:

1. Frame objects: Used to model beams, columns, braces, and trusses; they

may be straight or curved.

- Area objects: Used to model walls, floors, and other thin-walled members, as well as two-dimensional sol ids (plane stress, plane strain, and axisymmetric sol ids). Only shell-type area objects are covered in this manual.

Global Coordinate System

The global coordinate system is a three-dimensional, right- handed, rectangular coordinate system. The three axes, de noted X, Y, and Z, are mutually perpendicular and satisfy the right- hand rule. The location and orientation of the global system are arbitrary. Locations in the global coordinate system can be specified using the variables x, y, and z. A vector in the global coordinate system can be specified by giving the locations of two points, a pair of angles, or by specifying a coordinate direction. Coordinate directions are in dictated using the values ±X, ±Y, and ±Z. For example, +X de fines a vector parallel to and directed along the positive X axis. The sign is required. All other coordinate systems in the model are de fined with respect to the global coordinate system.

SAP2000 always assumes that Z is the vertical axis, with +Z being upward. Local coordinate systems for joints, elements, and ground-acceleration loading are defined with respect to this upward direction. Self-weight loading always acts downward, in the –Z direction. The X-Y plane is horizontal. The primary horizontal direction is +X. Angles in the horizontal plane are measured from the positive half of the X axis, with positive angles appearing counter clockwise when you are looking down at the X-Y plane.

Local Coordinate System

Each part (joint, element, or constraint) of the structural model has its own local coordinate system used to de fine the properties, loads, and response for that part. The axes of the local coordinate systems are de noted 1, 2, and 3. In

general, the local coordinate systems may vary from joint to joint, element to element, and constraint to constraint.

There is no preferred upward direction for a local coordinate system. However, the joint and element local coordinate systems are de fined with respect to the global upward direction, +Z. The joint local 1- 2-3 coordinate system is normally the same as the global X- Y-Z coordinate system.

For the Frame and Shell elements, one of the element local axes is determined by the geometry of the individual element. You may define the orientation of the remaining two axes by specifying a single angle of rotation.

The local coordinate system for a Diaphragm Constraint is normally determined automatically from the geometry or mass distribution of the constraint. Option ally, you may specify one global axis that deter mines the plane of a Diaphragm Constraint; the remaining two axes are determined automatically.

The Frame Element

The Frame element is used to model beam, column, truss, and brace behavior in planar and three-dimensional structures. The Frame element uses a general, three-dimensional, beam-column formulation which includes the effects of bi axial bending, torsion, axial deformation, and bi-axial shear deformations. See Bathe and Wilson (1976).

Structures that can be modeled with this element include:

- Three- dimensional frames
- Three- dimensional trusses
- Planar frames
- Planar grillages
- Planar trusses

A Frame element is modeled as a straight line connecting two points. In the graphical user interface, you can divide curved objects into multiple straight objects, subject to your specification. Each element has its own local coordinate system for defining section properties and loads, and for interpreting

output. Each Frame element may be loaded by self-weight, multiple concentrated loads, and multiple distributed loads. Insertion points and end off sets are available to account for the finite size of beam and columns inter sections. End re leases are also available to model different fixity conditions at the ends of the element.

Element internal forces are produced at the ends of each element and at a user-specified number of equally-spaced output stations along the length of the element.

Degrees of Freedom

The Frame element activates all six degrees of freedom at both of its connected joints. If you want to model truss elements that do not transmit moments at the ends, you may either:

- Set the geometric Section properties j, i33, and i22 all to zero (a is non-zero; as2 and as3 are arbitrary)
- Release both bending rotations, R2 and R3, at both ends and release the torsional rotation, R1, at either end.

Each Frame element has its own element local coordinate system used to define section properties, loads and output. The axes of this local system are de noted 1, 2 and 3. The first axis is directed along the length of the element; the remaining two axes lie in the plane perpendicular to the element with an orientation that you specify. It is important that you clearly understand the definition of the element local 1-2-3 coordinate system and its relationship to the global X-Y-Z coordinate system. Both systems are right-handed coordinate systems. It is up to you to de fine local systems which simplify data input and interpretation of results.

Units

SAP2000 works with four basics units: force, length, temperature, and time. The program offers many different compatible sets of force, length and temperature units to choose from, such as “Kip, in, F” or “N, mm, C.” Time is

always measured in seconds (except for creep, shrinkage, and aging effects, which are measured in days.) An important distinction is made between mass and weight. Mass is used only for calculating dynamic inertia and for loads resulting from ground acceleration. Weight is a force that can be applied like any other force load. Be sure to use force units when specifying weight values, and mass units (force-sec^2/length) when specifying mass values.

Properties

Other properties, such as frame end releases or joint support conditions, are assigned directly to objects. These properties can only be changed by making another assignment of that same property to the object; they are not named entities and they do not exist independently of the objects.

Properties are assigned to each object to determine the structural behavior of that object in the model. Some properties, such as material and section properties, are named entities that must be defined before assigning them to objects.

Function

Options are available to define functions to describe how load varies as a function of period or time. The functions are needed for certain types of analysis only; they are not used for static analysis. A function is a series of digitized abscissa-ordinate data pairs.

Four types of functions are available:

- Response-spectrum functions: Pseudo-spectral acceleration vs. period for use in response-spectrum analysis.
- Time-history functions: Loading magnitude vs. time for use in time-history analysis.
- Steady-state functions: Loading magnitude vs. frequency for use in steady-state analysis.
- Power-spectral-density functions: Loading magnitude squared per frequency vs. frequency for use in power-spectral-density analysis.

As many named functions as needed can be defined. Functions are not assigned to objects, but are used in the definition of load cases.

Load Pattern

Loads represent actions upon the structure, such as force, pressure, support displacement, thermal effects, ground acceleration, and others. A spatial distribution of loads upon the structure is called a load pattern. As many named load patterns as needed can be defined. Typically separate load patterns would be defined for dead load, live load, wind load, snow load, thermal load, and so on. Loads that need to vary independently, either for design purposes or because of how they are applied to the structure, should be defined as separate load patterns. After defining a load pattern name, assign specific load values to the objects as part of that load pattern. The load values assigned to an object specify the type of load (e.g., force, displacement, and temperature), its magnitude, and direction (if applicable). Different loads can be assigned to different objects as part of a single load pattern. Each object can be subjected to multiple load patterns.

To calculate any response of the structure caused by the load patterns, load cases must be defined and run (described in subsequent text) to specify how the load patterns are to be applied (e.g., statically, dynamically, and so on) and how the structure is to be analyzed (e.g., linearly, nonlinearly, and so on). The same load pattern can be applied differently in separate load cases.

SAP2000 also has three built-in acceleration loads that represent unit ground translational acceleration in each of the global directions. Acceleration loads are assigned automatically to all objects in the structure that have mass.

Load Cases

A load case defines how loads are to be applied to the structure, and how the structural response is to be calculated. Many types of load cases are available. Most broadly, load cases are classified as linear or nonlinear, depending on how the structure responds to the loading.

The following types of load cases are available:

- Static: The most common type of analysis. Loads are applied without dynamical effects.
- Modal: Calculation of dynamic modes of the structure using eigenvector or Ritz-vector method. Loads are not actually applied, although they can be used to generate Ritz vectors.
- Response-Spectrum: Statistical calculation of the response caused by acceleration loads. Requires response-spectrum functions.
- Time-History: Time-varying loads are applied. Requires time history functions. The solution may be by modal superposition or direct integration methods.
- Buckling: Calculation of buckling modes under the application of loads.

Load Combination

A SAP2000 combination, also called a "combo," is a named combination of the results from one or more load cases or other combinations. When a combination is defined, it applies to the results for every object in the model.

Five types of combinations are available:

- Linear type: Results from the included load cases and combos are added linearly.
- Absolute type: The absolute values of the results from the included load cases and combos are added.
- SRSS type: The square root of the sum of the squares of the results from the included load cases and combos is computed.
- Envelope type: Results from the included load cases and combos are enveloped to find the maximum and minimum values.
- Range Add type: Positive values are added to the maximum and negative values are added to the minimum for the included load cases and combos, efficiently generating maximum and minimum responses for pattern loading.

Design is always based on combinations, not directly on load cases. A combination that contains only a single load case can be created. Each design algorithm creates it own default combinations. Additional user defined combinations can be created for design or other purposes. Design may be performed for any arrangement of user-defined and program generated combinations.

Design Settings

The design features of the program can be used on frame objects whose section properties use materials of concrete, steel, cold-formed steel, or aluminum. Several settings can be made that affect the design of a particular model:

- The specific design code to be used for each type of material, e.g., AISC-360-01/IBC2006 for steel, EUROCODE 2-1992 for concrete, AISI-ASD96 for cold-formed steel, and AA-ASD 2000for aluminum.
- Preference settings of how those codes should be applied to a model.
- Combinations for which the design should be checked.
- Groups of objects that should share the same design.
- Optional "overwrite" values for each object that specify coefficients and parameters to change the default values in the design-code formulas.

Although there are no explicit design settings for concrete shells, the program will display design stresses and the reinforcing contours necessary to carry the tensile force component of the resolved tension compression couple. This information is accessed under the Display menu for shells. The required reinforcing area is calculated using the rebar material type specified by the user under the Define menu. Design results for the design section, when available, as well as all of the settings described herein, can be considered to be part of the model.

Appendix C

GRLWEAP Hammer Database (2015). Pile dynamics, inc.

(http://www.pile.com).

ID	Hammer Manufacturer	Hammer Model	Hammer Type	Energy/Power (kip-ft)/(kW)	Ram Weight (kips)	Stroke (ft)	Energy/Power (kJ)/(kW)	Ram Weight (kN)	Stroke (m)
1288	APE	8a	ECH	24	12	2	32.553	53.4	0.61
774	APE	20E	VIB	59.67	0.15	38.3	59.67	0.668	38.3
776	APE	50E	VIB	194	0.233	30	194	1.037	30
1285	APE	7-3	ECH	42	14	3	56.967	62.3	0.914
1286	APE	8-3	ECH	48	16	3	65.105	71.2	0.914
778	APE	100E	VIB	194	0.144	30	194	0.642	30
1289	APE	10-4	ECH	80	20	4	108.509	89	1.219
781	APE	150T	VIB	260	0.17	30	260	0.759	30
784	APE	200T	VIB	466	0.341	30.83	466	1.517	30.83
787	APE	400B	VIB	738	0.78	23.33	738	3.471	23.33
596	APE	400U	ECH	400	80	5	542.544	356	1.524
1280	APE	7.5a	ECH	24	12	2	32.553	53.4	0.61
1281	APE	7.5b	ECH	20.4	10.2	2	27.67	45.39	0.61
1282	APE	7.5c	ECH	15.2	7.6	2	20.617	33.82	0.61
598	APE	750U	ECH	750	120	6.25	1017.27	534	1.905
1283	APE	9.5a	ECH	50.656	16	3.166	68.708	71.2	0.965
1284	APE	9.5b	ECH	44.324	14	3.166	60.119	62.3	0.965
779	APE	100HF	VIB	260	0.144	43	260	0.642	43
595	APE	10-60	ECH	100	20	5	135.636	89	1.524
782	APE	150HF	VIB	466	0.32	43	466	1.424	43
594	APE	15-60	ECH	150	30	5	203.454	133.5	1.524

ID	Hammer Manufacturer	Hammer Model	Hammer Type	Energy/Power (kip-ft)/(kW)	Ram Weight (kips)	Stroke (ft)	Energy/Power (kJ)/(kW)	Ram Weight (kN)	Stroke (m)
791	APE	200-6	VIB	470	0.433	30	470	1.927	30
591	APE	5.4mT	ECH	26	12	2.167	35.266	53.4	0.66
592	APE	7.2mT	ECH	51.3	16.2	3.167	69.581	72.09	0.965
570	APE	D 1-42	OED	1.317	0.208	6.333	1.787	0.926	1.93
569	APE	D 8-42	OED	19.8	1.76	11.25	26.856	7.832	3.429
785	APE	200T HF	VIB	738	0.341	43	738	1.517	43
584	APE	D 12-42	OED	29.767	2.646	11.25	40.375	11.775	3.429
1262	APE	D 16-32	OED	39.69	3.528	11.25	53.834	15.7	3.429
579	APE	D 16-42	OED	39.69	3.528	11.25	53.834	15.7	3.429
580	APE	D 16-52	OED	39.69	3.528	11.25	53.834	15.7	3.429
1263	APE	D 19-32	OED	47.126	4.189	11.25	63.92	18.641	3.429
571	APE	D 19-42	OED	47.126	4.189	11.25	63.92	18.641	3.429
1261	APE	D 19-52	OED	47.126	4.189	11.25	63.92	18.641	3.429
1264	APE	D 25-32	OED	62.01	5.512	11.25	84.108	24.528	3.429
581	APE	D 25-42	OED	62.01	5.512	11.25	84.108	24.528	3.429
1273	APE	D 25-52	OED	62.01	5.512	11.25	84.108	24.528	3.429
1265	APE	D 30-32	OED	74.419	6.615	11.25	100.939	29.437	3.429
572	APE	D 30-42	OED	74.419	6.615	11.25	100.939	29.437	3.429
1274	APE	D 30-52	OED	74.419	6.615	11.25	100.939	29.437	3.429
585	APE	D 36-26	OED	89.303	7.938	11.25	121.126	35.324	3.429
1266	APE	D 36-32	OED	89.303	7.938	11.25	121.126	35.324	3.429
573	APE	D 36-42	OED	89.303	7.938	11.25	121.126	35.324	3.429
1275	APE	D 36-52	OED	89.303	7.938	11.25	121.126	35.324	3.429

ID	Hammer Manufacturer	Hammer Model	Hammer Type	Energy/Power (kip-ft)/(kW)	Ram Weight (kips)	Stroke (ft)	Energy/Power (kJ)/(kW)	Ram Weight (kN)	Stroke (m)
1267	APE	D 46-32	OED	114.109	10.143	11.25	154.773	45.136	3.429
574	APE	D 46-42	OED	114.109	10.143	11.25	154.773	45.136	3.429
1276	APE	D 46-52	OED	114.109	10.143	11.25	154.773	45.136	3.429
583	APE	D 50-42	OED	124.031	11.025	11.25	168.231	49.061	3.429
1277	APE	D 50-52	OED	124.031	11.025	11.25	168.231	49.061	3.429
1268	APE	D 62-22	OED	153.799	13.671	11.25	208.606	60.836	3.429
575	APE	D 62-42	OED	153.799	13.671	11.25	208.606	60.836	3.429
1278	APE	D 62-52	OED	153.799	13.671	11.25	208.606	60.836	3.429
1272	APE	D 70-42	OED	173.644	15.435	11.25	235.523	68.686	3.429
1279	APE	D 70-52	OED	173.644	15.435	11.25	235.523	68.686	3.429
1269	APE	D 80-23	OED	198.45	17.64	11.25	269.17	78.498	3.429
576	APE	D 80-42	OED	198.45	17.64	11.25	269.17	78.498	3.429
789	APE	Tan 400	VIB	1476	1.368	23.33	1476	6.088	23.33
790	APE	Tan 600	VIB	1800	2.105	23.3	1800	9.367	23.3
599	APE	D 100-13	OED	300.042	23.7	12.66	406.965	105.465	3.859
1270	APE	D 100-32	OED	248.062	22.05	11.25	336.462	98.122	3.429
577	APE	D 100-42	OED	248.062	22.05	11.25	336.462	98.122	3.429
1271	APE	D 120-32	OED	349.692	27.6	12.67	474.308	122.82	3.862
582	APE	D 125-42	OED	310.084	27.563	11.25	420.585	122.655	3.429
586	APE	D 128-42	OED	317.25	28.2	11.25	430.305	125.49	3.429
587	APE	D 138-42	OED	342	30.4	11.25	463.875	135.28	3.429
588	APE	D 160-42	OED	396.9	35.28	11.25	538.339	156.996	3.429
589	APE	D 180-42	OED	446.512	39.69	11.25	605.632	176.62	3.429

ID	Hammer Manufacturer	Hammer Model	Hammer Type	Energy/Power (kip-ft)/(kW)	Ram Weight (kips)	Stroke (ft)	Energy/Power (kJ)/(kW)	Ram Weight (kN)	Stroke (m)
593	APE	D 220-42	OED	540.814	48.46	11.16	733.538	215.647	3.402
590	APE	D 225-42	OED	558	49.6	11.25	756.849	220.72	3.429
777	APE	100	VIB	194	0.318	30	194	1.415	30
772	APE	15	VIB	59.67	0.108	30	59.67	0.481	30
780	APE	150	VIB	260	0.144	30	260	0.642	30
773	APE	20	VIB	59.67	0.15	38.3	59.67	0.668	38.3
783	APE	200	VIB	466	0.289	30	466	1.284	30
770	APE	3	VIB	10.58	0.004	38.3	10.58	0.019	38.3
786	APE	300	VIB	738	0.342	25	738	1.522	25
775	APE	50	VIB	194	0.233	30	194	1.037	30
771	APE	6	VIB	10.58	0.009	38.3	10.58	0.038	38.3
788	APE	600	VIB	800	1.052	23.3	800	4.681	23.3
1287	APE	8	ECH	16	8	2	21.702	35.6	0.61
381	BSP	HH3	ECH	26.022	6.611	3.936	35.295	29.42	1.2
382	BSP	HH5	ECH	43.375	11.02	3.936	58.832	49.039	1.2
383	BSP	HH7	ECH	60.782	15.427	3.94	82.443	68.65	1.201
384	BSP	HH8	ECH	69.502	17.64	3.94	94.269	78.498	1.201
385	BSP	HH9	ECH	78.17	19.84	3.94	106.026	88.288	1.201
374	BSP	CX40	ECH	28.207	6.613	4.265	38.259	29.43	1.3
375	BSP	CX50	ECH	37.609	8.818	4.265	51.012	39.24	1.3
376	BSP	CX60	ECH	47.012	11.022	4.265	63.765	49.05	1.3
377	BSP	CX75	ECH	52.075	13.227	3.937	70.632	58.86	1.2
378	BSP	CX85	ECH	60.754	15.431	3.937	82.404	68.67	1.2

ID	Hammer Manufacturer	Hammer Model	Hammer Type	Energy/Power (kip-ft)/(kW)	Ram Weight (kips)	Stroke (ft)	Energy/Power (kJ)/(kW)	Ram Weight (kN)	Stroke (m)
600	BSP	DX20	ECH	14.109	3.308	4.265	19.137	14.721	1.3
601	BSP	DX25	ECH	18.089	4.411	4.101	24.535	19.628	1.25
602	BSP	DX30	ECH	21.706	5.513	3.937	29.442	24.535	1.2
391	BSP	HA30	ECH	260.373	66.135	3.937	353.16	294.3	1.2
392	BSP	HA40	ECH	347.164	88.18	3.937	470.88	392.4	1.2
369	BSP	SL20	ECH	14.108	3.308	4.265	19.136	14.72	1.3
370	BSP	SL30	ECH	21.693	5.51	3.937	29.424	24.52	1.2
396	BSP	CG180	ECH	131.922	26.454	4.987	178.934	117.72	1.52
397	BSP	CG210	ECH	153.91	30.863	4.987	208.757	137.34	1.52
398	BSP	CG240	ECH	175.897	35.272	4.987	238.579	156.96	1.52
399	BSP	CG270	ECH	197.884	39.681	4.987	268.402	176.58	1.52
400	BSP	CG300	ECH	219.871	44.09	4.987	298.224	196.2	1.52
379	BSP	CX110	ECH	78.112	19.84	3.937	105.948	88.29	1.2
606	BSP	CGL370	ECH	271.222	55.112	4.921	367.875	245.25	1.5
607	BSP	CGL440	ECH	325.467	66.135	4.921	441.45	294.3	1.5
608	BSP	CGL520	ECH	379.711	77.157	4.921	515.025	343.35	1.5
609	BSP	CGL590	ECH	433.956	88.18	4.921	588.6	392.4	1.5
604	BSP	LX4-SA	ECH	23.154	8.822	2.625	31.405	39.256	0.8
605	BSP	LX5-SA	ECH	28.942	11.027	2.625	39.256	49.07	0.8
610	BSP	LX7-SA	ECH	40.519	15.438	2.625	54.958	68.697	0.8
386	BSP	HH11-1.2	ECH	95.545	24.25	3.94	129.593	107.913	1.201
393	BSP	HH11-1.5	ECH	119.31	24.25	4.92	161.827	107.913	1.5
387	BSP	HH14-1.2	ECH	121.588	30.86	3.94	164.918	137.327	1.201

ID	Hammer Manufacturer	Hammer Model	Hammer Type	Energy/Power (kip-ft)/(kW)	Ram Weight (kips)	Stroke (ft)	Energy/Power (kJ)/(kW)	Ram Weight (kN)	Stroke (m)
394	BSP	HH14-1.5	ECH	151.831	30.86	4.92	205.938	137.327	1.5
388	BSP	HH16-1.2	ECH	138.866	35.272	3.937	188.352	156.96	1.2
395	BSP	HH16-1.5	ECH	173.538	35.272	4.92	235.38	156.96	1.5
603	BSP	LX2.5-SA	ECH	14.471	5.513	2.625	19.628	24.535	0.8
801	DKH	PH-5	ECH	43.396	11.023	3.937	58.86	49.05	1.2
802	DKH	PH-7	ECH	60.754	15.432	3.937	82.404	68.67	1.2
804	DKH	PH-10	ECH	86.791	22.045	3.937	117.72	98.1	1.2
805	DKH	PH-13	ECH	112.828	28.658	3.937	153.036	127.53	1.2
806	DKH	PH-20	ECH	216.978	44.09	4.921	294.3	196.2	1.5
807	DKH	PH-30	ECH	325.467	66.135	4.921	441.45	294.3	1.5
808	DKH	PH-40	ECH	433.956	88.18	4.921	588.6	392.4	1.5
803	DKH	PH-7S	ECH	60.754	15.432	3.937	82.404	68.67	1.2
809	DKH	DKH-713	ECH	112.92	28.66	3.94	153.161	127.537	1.201
56	FEC	D-18	OED	39.7	3.97	10	53.847	17.667	3.048
50	FEC	FEC 1200	OED	22.495	2.75	8.18	30.511	12.238	2.493
51	FEC	FEC 1500	OED	27.093	3.3	8.21	36.748	14.685	2.502
52	FEC	FEC 2500	OED	49.995	5.5	9.09	67.811	24.475	2.771
53	FEC	FEC 2800	OED	55.994	6.16	9.09	75.949	27.412	2.771
54	FEC	FEC 3000	OED	63.03	6.6	9.55	85.491	29.37	2.911
55	FEC	FEC 3400	OED	73.005	7.48	9.76	99.021	33.286	2.975
1340	H&M	H-150	VIB	94	0.111	28.3	94	0.494	28.3
1341	H&M	H-1700	VIB	165	0.202	20	165	0.899	20
567	HMC	19D	ECH	14	3.5	4	18.989	15.575	1.219

ID	Hammer Manufacturer	Hammer Model	Hammer Type	Energy/Power (kip-ft)/(kW)	Ram Weight (kips)	Stroke (ft)	Energy/Power (kJ)/(kW)	Ram Weight (kN)	Stroke (m)
560	HMC	28A	ECH	28	7	4	37.978	31.15	1.219
561	HMC	28B	ECH	21	7	3	28.484	31.15	0.914
568	HMC	38D	ECH	28	7	4	37.978	31.15	1.219
720	HMC	3+28	VIB	21	0.108	26.8	21	0.483	26.8
721	HMC	3+75	VIB	56	0.108	36.1	56	0.483	36.1
1620	HMC	TD19	OED	46.09	4.011	11.492	62.514	17.847	3.503
1621	HMC	TD30	OED	69.867	6.611	10.569	94.764	29.418	3.221
722	HMC	13+200	VIB	149	0.353	26.7	149	1.569	26.7
725	HMC	25+220	VIB	164	0.605	20.9	164	2.694	20.9
726	HMC	26+335	VIB	242	0.705	25.6	242	3.139	25.6
728	HMC	51+335	VIB	242	1.211	19.5	242	5.389	19.5
729	HMC	51+535	VIB	377	1.211	26.4	377	5.389	26.4
731	HMC	51+740	VIB	485	1.211	27.5	485	5.389	27.5
732	HMC	76+740	VIB	485	1.816	21.7	485	8.083	21.7
733	HMC	76+800	VIB	597	1.816	26.1	597	8.083	26.1
734	HMC	115+800	VIB	597	1.347	20.4	597	5.994	20.4
724	HMC	13H+200	VIB	164	0.353	29.8	164	1.569	29.8
723	HMC	13S+200	VIB	149	0.353	26.7	149	1.569	26.7
727	HMC	26S+335	VIB	242	0.705	25.6	242	3.139	25.6
730	HMC	51S+535	VIB	377	1.211	26.4	377	5.389	26.4
735	HMC	230+1600	VIB	1193	2.694	20.4	1193	11.988	20.4
564	HMC	119	ECH	88	22	4	119.36	97.9	1.219

ID	Hammer Manufacturer	Hammer Model	Hammer Type	Energy/Power (kip-ft)/(kW)	Ram Weight (kips)	Stroke (ft)	Energy/Power (kJ)/(kW)	Ram Weight (kN)	Stroke (m)
565	HMC	149	ECH	110	27.5	4	149.2	122.375	1.219
566	HMC	187	ECH	138	34.5	4	187.178	153.525	1.219
562	HMC	62	ECH	46	11.5	4	62.393	51.175	1.219
563	HMC	86	ECH	64	16	4	86.807	71.2	1.219
899	ICE	44B	VIB	595	1.3	30	595	5.785	30
698	ICE	50B	VIB	432	10.415	26.7	432	46.347	26.7
890	ICE	7RF	VIB	154	0.507	38.3	154	2.254	38.3
716	ICE	14RF	VIB	242	1.013	38.3	242	4.508	38.3
702	ICE	216E	VIB	130	0.46	26.7	130	2.047	26.7
880	ICE	23RF	VIB	384	0.832	38.3	384	3.702	38.3
127	ICE	30-S	OED	22.5	3	7.5	30.518	13.35	2.286
895	ICE	32RF	VIB	391	1.158	33.3	391	5.152	33.3
139	ICE	32-S	OED	26.01	3	8.67	35.279	13.35	2.643
896	ICE	36RF	VIB	431	1.302	33.3	431	5.794	33.3
128	ICE	40-S	OED	40	4	10	54.254	17.8	3.048
705	ICE	416L	VIB	242	0.92	26.7	242	4.094	26.7
129	ICE	42-S	OED	42.004	4.09	10.27	56.973	18.201	3.13
897	ICE	46RF	VIB	678	1.66	38.3	678	7.387	38.3
130	ICE	60-S	OED	59.99	7	8.57	81.368	31.15	2.612
898	ICE	64RF	VIB	663	1.158	32.5	663	5.153	32.5
131	ICE	70-S	OED	70	7	10	94.945	31.15	3.048
132	ICE	80-S	OED	80	8	10	108.509	35.6	3.048
133	ICE	90-S	OED	90	9	10	122.072	40.05	3.048

ID	Hammer Manufacturer	Hammer Model	Hammer Type	Energy/Power (kip-ft)/(kW)	Ram Weight (kips)	Stroke (ft)	Energy/Power (kJ)/(kW)	Ram Weight (kN)	Stroke (m)
1512	ICE	IP-2	ECH	17.358	4.409	3.937	23.544	19.62	1.2
1513	ICE	IP-3	ECH	26.037	6.613	3.937	35.316	29.43	1.2
1514	ICE	IP-5	ECH	43.396	11.022	3.937	58.86	49.05	1.2
1515	ICE	IP-7	ECH	60.754	15.431	3.937	82.404	68.67	1.2
715	ICE	V125	VIB	984	1.042	25.8	984	4.637	25.8
885	ICE	V360	VIB	783	0.941	25	783	4.186	25
134	ICE	100-S	OED	100	10	10	135.636	44.5	3.048
703	ICE	11-23	VIB	164	0.46	31.7	164	2.047	31.7
135	ICE	120-S	OED	120	12	10	162.763	53.4	3.048
713	ICE	1412B	VIB	597	2.036	21	597	9.06	21
714	ICE	1412C	VIB	470	2.022	23	470	9	23
717	ICE	14-23	VIB	164	1.165	35	164	5.184	35
136	ICE	200-S	OED	100	20	5	135.636	89	1.524
137	ICE	205-S	OED	170	20	8.5	230.581	89	2.591
719	ICE	22-30	VIB	250	0.917	26.9	250	4.079	26.9
700	ICE	23-28	VIB	21	0.096	26.7	21	0.427	26.7
882	ICE	23-40	VIB	30	0.192	31.8	30	0.853	31.8
883	ICE	28-35	VIB	261	1.158	27.3	261	5.152	27.3
708	ICE	44-30	VIB	242	1.3	20	242	5.785	20
709	ICE	44-50	VIB	377	1.3	26.7	377	5.785	26.7
710	ICE	44-65	VIB	485	1.3	27.5	485	5.785	27.5
888	ICE	44-70	VIB	585	0.917	28.1	585	4.08	28.1
711	ICE	66-65	VIB	485	1.95	21.7	485	8.678	21.7

ID	Hammer Manufacturer	Hammer Model	Hammer Type	Energy/Power (kip-ft)/(kW)	Ram Weight (kips)	Stroke (ft)	Energy/Power (kJ)/(kW)	Ram Weight (kN)	Stroke (m)
889	ICE	66-70	VIB	585	0.917	23	585	4.08	23
712	ICE	66-80	VIB	597	1.95	26.7	597	8.678	26.7
1502	ICE	I-8v2	OED	18.689	1.764	10.597	25.349	7.848	3.23
1516	ICE	IP-10	ECH	86.782	22.043	3.937	117.708	98.09	1.2
1517	ICE	IP-13	ECH	112.828	28.658	3.937	153.036	127.53	1.2
552	ICE	110-SH	ECH	37.72	11.5	3.28	51.162	51.175	1
553	ICE	115-SH	ECH	37.95	11.5	3.3	51.474	51.175	1.006
881	ICE	1412BT	VIB	1193	1.667	21.7	1193	7.418	21.7
555	ICE	160-SH	ECH	64	16	4	86.807	71.2	1.219
718	ICE	22-23V	VIB	164	0.917	26.9	164	4.079	26.9
887	ICE	44-30V	VIB	250	0.917	26	250	4.08	26
559	ICE	DKH-3U	ECH	26.004	6.6	3.94	35.271	29.37	1.201
1501	ICE	I-12v2	OED	29.625	2.822	10.499	40.182	12.557	3.2
1503	ICE	I-19v2	OED	46.137	4.012	11.499	62.578	17.854	3.505
1504	ICE	I-30v2	OED	76.051	6.613	11.499	103.152	29.43	3.505
1505	ICE	I-36v2	OED	93.734	7.936	11.811	127.138	35.316	3.6
1506	ICE	I-46v2	OED	119.772	10.141	11.811	162.453	45.126	3.6
1507	ICE	I-62v2	OED	172.367	14.594	11.811	233.791	64.942	3.6
1508	ICE	I-80v2	OED	208.299	17.636	11.811	282.528	78.48	3.6

ID	Hammer Manufacturer	Hammer Model	Hammer Type	Energy/Power (kip-ft)/(kW)	Ram Weight (kips)	Stroke (ft)	Energy/Power (kJ)/(kW)	Ram Weight (kN)	Stroke (m)
886	ICE	V360 T	VIB	1566	1.881	25	1566	8.37	25
140	ICE	120S-15	OED	132.45	15	8.83	179.65	66.75	2.691
884	ICE	28RF-35	VIB	261	1.158	27.3	261	5.152	27.3
891	ICE	66-70HS	VIB	585	0.916	26.7	585	4.078	26.7
892	ICE	66-80HS	VIB	597	0.916	29.2	597	4.078	29.2
1509	ICE	I-100v2	OED	260.373	22.045	11.811	353.16	98.1	3.6
1510	ICE	I-125v2	OED	310.097	27.556	11.25	420.604	122.625	3.43
360	ICE	I-12obs	OED	30.213	2.821	10.71	40.98	12.553	3.264
1520	ICE	I-138v2	OED	328.624	30.4	10.81	445.732	135.28	3.295
1511	ICE	I-160v2	OED	393.453	35.272	11.15	533.664	156.96	3.4
361	ICE	I-19obs	OED	43.242	4.015	10.77	58.651	17.867	3.283
1251	ICE	I-30 V2	OED	71.707	6.615	10.84	97.26	29.437	3.304
362	ICE	I-30obs	OED	71.453	6.616	10.8	96.916	29.441	3.292
363	ICE	I-36obs	OED	90.675	7.94	11.42	122.988	35.333	3.481
364	ICE	I-46obs	OED	107.74	10.145	10.62	146.134	45.145	3.237
365	ICE	I-62obs	OED	164.98	14.6	11.3	223.772	64.97	3.444
366	ICE	I-80obs	OED	212.4	17.7	12	288.091	78.765	3.658
893	ICE	100c-Tdm	VIB	1774	1.833	26.67	1774	8.157	26.67
368	ICE	I-100obs	OED	264.454	23.612	11.2	358.695	105.073	3.414
367	ICE	I-8v2obs	OED	17.6	1.76	10	23.872	7.832	3.048
126	ICE	1070	CED	72.6	10	7.26	98.472	44.5	2.213
554	ICE	115	ECH	46	11.5	4	62.393	51.175	1.219
556	ICE	160	ECH	64	16	4	86.807	71.2	1.219

ID	Hammer Manufacturer	Hammer Model	Hammer Type	Energy/Power (kip-ft)/(kW)	Ram Weight (kips)	Stroke (ft)	Energy/Power (kJ)/(kW)	Ram Weight (kN)	Stroke (m)
120	ICE	180	CED	8.131	1.73	4.7	11.029	7.699	1.433
701	ICE	216	VIB	130	0.46	26.7	130	2.047	26.7
557	ICE	220	ECH	88	22	4	119.36	97.9	1.219
704	ICE	223	VIB	242	0.46	38.3	242	2.047	38.3
558	ICE	275	ECH	110	27.5	4	149.2	122.375	1.219
699	ICE	3117	VIB	235	1.122	28.3	235	4.991	28.3
121	ICE	422	CED	23.12	4	5.78	31.359	17.8	1.762
894	ICE	423	VIB	377	0.915	38.3	377	4.073	38.3
122	ICE	440	CED	18.56	4	4.64	25.174	17.8	1.414
123	ICE	520	CED	30.369	5.07	5.99	41.192	22.562	1.826
124	ICE	640	CED	40.62	6	6.77	55.095	26.7	2.063
125	ICE	660	CED	51.627	7.57	6.82	70.025	33.687	2.079
550	ICE	70	ECH	21	7	3	28.484	31.15	0.914
551	ICE	75	ECH	30	7.5	4	40.691	33.375	1.219
706	ICE	812	VIB	375	1.82	26.7	375	8.099	26.7
707	ICE	815	VIB	375	1.84	26.7	375	8.188	26.7
318	IHC	S-30	ECH	21.698	3.527	6.152	29.43	15.696	1.875
320	IHC	S-35	ECH	25.525	6.63	3.85	34.622	29.504	1.173
319	IHC	S-40	ECH	28.927	4.85	5.965	39.236	21.582	1.818
321	IHC	S-70	ECH	51.25	7.73	6.63	69.513	34.399	2.021
322	IHC	S-90	ECH	65.902	9.94	6.63	89.387	44.233	2.021
323	IHC	S-120	ECH	89.372	13.48	6.63	121.221	59.986	2.021
324	IHC	S-150	ECH	110.058	16.6	6.63	149.278	73.87	2.021

ID	Hammer Manufacturer	Hammer Model	Hammer Type	Energy/Power (kip-ft)/(kW)	Ram Weight (kips)	Stroke (ft)	Energy/Power (kJ)/(kW)	Ram Weight (kN)	Stroke (m)
325	IHC	S-200	ECH	145.64	22	6.62	197.54	97.9	2.018
326	IHC	S-280	ECH	205.31	30.06	6.83	278.474	133.767	2.082
327	IHC	S-400	ECH	292.604	44.2	6.62	396.876	196.69	2.018
328	IHC	S-500	ECH	366.086	55.3	6.62	496.544	246.085	2.018
329	IHC	S-600	ECH	443.54	67	6.62	601.6	298.15	2.018
344	IHC	S-750	ECH	550.791	83.109	6.627	747.071	369.837	2.02
345	IHC	S-800	ECH	589.969	88.148	6.693	800.21	392.26	2.04
330	IHC	S-900	ECH	658.359	99.45	6.62	892.972	442.552	2.018
335	IHC	SC-30	ECH	21.808	3.76	5.8	29.579	16.732	1.768
336	IHC	SC-40	ECH	29.864	5.51	5.42	40.507	24.52	1.652
337	IHC	SC-50	ECH	36.815	7.29	5.05	49.934	32.44	1.539
338	IHC	SC-60	ECH	44.954	13.3	3.38	60.974	59.185	1.03
339	IHC	SC-75	ECH	54.797	12.15	4.51	74.324	54.067	1.375
331	IHC	S-1200	ECH	891.052	134.6	6.62	1208.587	598.97	2.018
346	IHC	S-1400	ECH	1033.839	147.94	6.988	1402.258	658.337	2.13
347	IHC	S-1800	ECH	1340.214	195.64	6.85	1817.813	870.6	2.088
334	IHC	S-2000	ECH	1473.969	222.65	6.62	1999.232	990.81	2.018
333	IHC	S-2300	ECH	1681.48	254	6.62	2280.692	1130.3	2.018
348	IHC	S-2500	ECH	1843.16	275.80	6.683	2499.989	1227.32	2.037
1371	IHC	S-3000	ECH	2211.928	332.44	6.654	3000.17	1479.37	2.028
1372	IHC	S-4000	ECH	2948.905	444.30	6.637	3999.776	1977.15	2.023
340	IHC	SC-110	ECH	81.887	17.46	4.69	111.069	77.697	1.43
341	IHC	SC-150	ECH	109.35	24.3	4.5	148.318	108.135	1.372

ID	Hammer Manufacturer	Hammer Model	Hammer Type	Energy/Power (kip-ft)/(kW)	Ram Weight (kips)	Stroke (ft)	Energy/Power (kJ)/(kW)	Ram Weight (kN)	Stroke (m)
342	IHC	SC-200	ECH	152.51	30.2	5.05	206.858	134.39	1.539
343	IHC	SC-250	ECH	179.802	37.256	4.826	243.876	165.789	1.471
332	IHC	S-1800-L	ECH	1170.387	166	7.051	1587.466	738.7	2.149
1053	J&M	416B	VIB	261	0.917	26.7	261	4.079	26.7
1054	J&M	416S	VIB	250	0.917	26.7	250	4.079	26.7
1039	J&M	11-23	VIB	164	0.917	31.7	164	4.079	31.7
1041	J&M	1412T	VIB	1119	1.667	21.7	1119	7.417	21.7
1044	J&M	22-23	VIB	164	0.917	20.8	164	4.079	20.8
1045	J&M	22-30	VIB	261	0.917	27.5	261	4.079	27.5
1050	J&M	28-35	VIB	261	1.167	27.5	261	5.192	27.5
1056	J&M	44-30	VIB	250	0.917	20	250	4.079	20
1057	J&M	44-50	VIB	399	0.917	26.7	399	4.079	26.7
1058	J&M	44-65	VIB	552	0.917	27.5	552	4.079	27.5
1060	J&M	66-65	VIB	552	0.917	21.7	552	4.079	21.7
1061	J&M	66-80	VIB	559	0.917	26.7	559	4.079	26.7
1021	J&M	82 HIH	ECH	32.8	8.2	4	44.489	36.49	1.219
1022	J&M	115 HIH	ECH	46	11.5	4	62.393	51.175	1.219
1023	J&M	160 HIH	ECH	64	16	4	86.807	71.2	1.219
1024	J&M	220 HIH	ECH	88	22	4	119.36	97.9	1.219
1025	J&M	275 HIH	ECH	110	27.5	4	149.2	122.375	1.219
1026	J&M	345 HIH	ECH	138	34.5	4	187.178	153.525	1.219
1020	J&M	70B HIH	ECH	21	7	3	28.484	31.15	0.914
1040	J&M	1412	VIB	559	1.667	21.7	559	7.417	21.7

ID	Hammer Manufacturer	Hammer Model	Hammer Type	Energy/Power (kip-ft)/(kW)	Ram Weight (kips)	Stroke (ft)	Energy/Power (kJ)/(kW)	Ram Weight (kN)	Stroke (m)
1042	J&M	216	VIB	149	0.917	26.7	149	4.079	26.7
1051	J&M	360	VIB	783	0.942	21.7	783	4.19	21.7
1052	J&M	416	VIB	250	0.917	26.7	250	4.079	26.7
1055	J&M	815	VIB	429	0.917	26.7	429	4.079	26.7
811	MGF	RBH 80	VIB	50	0.597	30	50	2.659	30
812	MGF	RBH 140	VIB	85	1.04	26.66	85	4.628	26.66
813	MGF	RBH 200	VIB	125	0.738	26.66	125	3.282	26.66
814	MGF	RBH 320	VIB	200	0.787	26.66	200	3.501	26.66
815	MGF	RBH 460	VIB	255	1.133	26.66	255	5.044	26.66
816	MGF	RBH 1050	VIB	460	1.549	22.5	460	6.893	22.5
817	MGF	RBH 1575	VIB	700	1.162	22.5	700	5.169	22.5
818	MGF	RBH 2400	VIB	975	1.769	23.5	975	7.874	23.5
304	MKT	9B3	ECH	8.752	1.6	5.47	11.871	7.12	1.667
308	MKT	S-5	ECH	16.25	5	3.25	22.041	22.25	0.991
312	MKT	S-8	ECH	26	8	3.25	35.265	35.6	0.991
305	MKT	10B3	ECH	13.11	3	4.37	17.782	13.35	1.332
309	MKT	11B3	ECH	19.15	5	3.83	25.974	22.25	1.167
314	MKT	S 10	ECH	32.5	10	3.25	44.082	44.5	0.991
315	MKT	S 14	ECH	37.52	14	2.68	50.891	62.3	0.817
317	MKT	S 20	ECH	60	20	3	81.382	89	0.914
750	MKT	V-2B	VIB	52	0.146	30	52	0.65	30
753	MKT	V-30	VIB	448	1.467	28.33	448	6.528	28.33
754	MKT	V-35	VIB	485	1.6	28.33	485	7.12	28.33

ID	Hammer Manufacturer	Hammer Model	Hammer Type	Energy/Power (kip-ft)/(kW)	Ram Weight (kips)	Stroke (ft)	Energy/Power (kJ)/(kW)	Ram Weight (kN)	Stroke (m)
751	MKT	V-5C	VIB	138	0.433	28.33	138	1.927	28.33
152	MKT	DA 45	CED	30.72	4	7.68	41.667	17.8	2.341
146	MKT	DE 10	OED	8.8	1.1	8	11.936	4.895	2.438
147	MKT	DE 20	OED	16	2	8	21.702	8.9	2.438
148	MKT	DE 30	OED	22.4	2.8	8	30.382	12.46	2.438
154	MKT	DE 35	OED	35	3.5	10	47.473	15.575	3.048
153	MKT	DE 40	OED	32	4	8	43.404	17.8	2.438
155	MKT	DE 42	OED	42	4.2	10	56.967	18.69	3.048
301	MKT	No. 5	ECH	1	0.2	5	1.356	0.89	1.524
302	MKT	No. 6	ECH	2.5	0.4	6.25	3.391	1.78	1.905
303	MKT	No. 7	ECH	4.152	0.8	5.19	5.632	3.56	1.582
755	MKT	V-140	VIB	1341	1.167	23.33	1341	5.193	23.33
752	MKT	V-20B	VIB	242	0.2	28.33	242	0.89	28.33
306	MKT	C5-Air	ECH	14.2	5	2.84	19.26	22.25	0.866
151	MKT	DA 35B	CED	21	2.8	7.5	28.484	12.46	2.286
167	MKT	DA 35C	CED	21	2.8	7.5	28.484	12.46	2.286
161	MKT	DA 55B	CED	38.2	5	7.64	51.813	22.25	2.329
168	MKT	DA 55C	CED	38.2	5	7.64	51.813	22.25	2.329
150	MKT	DE 30B	OED	23.8	2.8	8.5	32.281	12.46	2.591
159	MKT	DE 50B	OED	42.5	5	8.5	57.645	22.25	2.591
157	MKT	DE 50C	OED	50	5	10	67.818	22.25	3.048
162	MKT	DE 70B	OED	59.5	7	8.5	80.703	31.15	2.591
158	MKT	DE 70C	OED	70	7	10	94.945	31.15	3.048

ID	Hammer Manufacturer	Hammer Model	Hammer Type	Energy/Power (kip-ft)/(kW)	Ram Weight (kips)	Stroke (ft)	Energy/Power (kJ)/(kW)	Ram Weight (kN)	Stroke (m)
142	MKT	DE-20C	OED	20	2	10	27.127	8.9	3.048
143	MKT	DE-30C	OED	28	2.8	10	37.978	12.46	3.048
144	MKT	DE-33C	OED	33	3.3	10	44.76	14.685	3.048
163	MKT	DE-50B	OED	50	5	10	67.818	22.25	3.048
164	MKT	DE-70B	OED	70	7	10	94.945	31.15	3.048
316	MKT	MS 500	ECH	44	11	4	59.68	48.95	1.219
313	MKT	MS-350	ECH	30.803	7.72	3.99	41.78	34.354	1.216
165	MKT	DE-110C	OED	110	11	10	149.2	48.95	3.048
166	MKT	DE-150C	OED	150	15	10	203.454	66.75	3.048
307	MKT	C5-Steam	ECH	16.2	5	3.24	21.973	22.25	0.988
311	MKT	C826 Air	ECH	21.2	8	2.65	28.755	35.6	0.808
310	MKT	C826 Stm	ECH	24.4	8	3.05	33.095	35.6	0.93
149	MKT	DA35B SA	OED	23.8	2.8	8.5	32.281	12.46	2.591
160	MKT	DA55B SA	OED	40	5	8	54.254	22.25	2.438
145	MKT	DE333020	OED	40	4	10	54.254	17.8	3.048
669	MVE	M-12	OED	30.213	2.821	10.71	40.98	12.553	3.264
670	MVE	M-19	OED	49.384	4.015	12.3	66.983	17.867	3.749
671	MVE	M-30	OED	83.349	6.615	12.6	113.051	29.437	3.84
1142	PTC	30HP	VIB	196	0.868	27	196	3.864	27
1143	PTC	40HD	VIB	269	0.868	28	269	3.864	28
1147	PTC	60HD	VIB	305	0.868	28	305	3.864	28
1146	PTC	65HD	VIB	305	0.868	26	305	3.864	26
1148	PTC	75HD	VIB	410	0.868	25	410	3.864	25

ID	Hammer Manufacturer	Hammer Model	Hammer Type	Energy/Power (kip-ft)/(kW)	Ram Weight (kips)	Stroke (ft)	Energy/Power (kJ)/(kW)	Ram Weight (kN)	Stroke (m)
1149	PTC	100HD	VIB	451	0.868	23	451	3.864	23
1154	PTC	120HD	VIB	410	0.868	23	410	3.864	23
1155	PTC	130HD	VIB	564	0.868	23	564	3.864	23
1151	PTC	175HD	VIB	611	0.868	23	611	3.864	23
1156	PTC	200HD	VIB	710	0.868	23	710	3.864	23
1152	PTC	240HD	VIB	988	0.868	23	988	3.864	23
1157	PTC	265HD	VIB	1080	0.868	24	1080	3.864	24
1144	PTC	50HD1	VIB	255	0.868	25	255	3.864	25
1145	PTC	50HD2	VIB	290	0.868	25	290	3.864	25
1150	PTC	100HDS	VIB	564	0.868	23	564	3.864	23
1153	PTC	240HDS	VIB	988	0.868	30	988	3.864	30
1100	PVE	14M	VIB	190	1.013	28.3	190	4.508	28.3
1101	PVE	23M	VIB	234	1.66	27.5	234	7.387	27.5
1102	PVE	25M	VIB	294	0.977	28.3	294	4.348	28.3
1103	PVE	27M	VIB	294	0.977	28.3	294	4.348	28.3
1104	PVE	38M	VIB	392	0.92	28.3	392	4.094	28.3
1105	PVE	50M	VIB	440	1.2	28.3	440	5.34	28.3
1106	PVE	52M	VIB	564	0.75	28.3	564	3.338	28.3
1123	PVE	55M	VIB	403	1.173	28.33	403	5.22	28.33
1124	PVE	82M	VIB	565	1.758	28.33	565	7.823	28.33
1107	PVE	105M	VIB	784	1.52	22.5	784	6.764	22.5
1108	PVE	110M	VIB	784	0.796	22.5	784	3.542	22.5
1126	PVE	16VM	VIB	335	0.347	38.33	335	1.546	38.33

ID	Hammer Manufacturer	Hammer Model	Hammer Type	Energy/Power (kip-ft)/(kW)	Ram Weight (kips)	Stroke (ft)	Energy/Power (kJ)/(kW)	Ram Weight (kN)	Stroke (m)
1109	PVE	200M	VIB	1130	1.45	23.3	1130	6.453	23.3
1127	PVE	20VM	VIB	395	0.412	38.33	395	1.836	38.33
1128	PVE	24VM	VIB	395	0.521	38.33	395	2.32	38.33
1129	PVE	28VM	VIB	403	0.608	38.33	403	2.703	38.33
1125	PVE	300M	VIB	1796	6.206	23.33	1796	27.617	23.33
1121	PVE	40VM	VIB	564	1.45	33.3	564	6.453	33.3
1122	PVE	50VM	VIB	564	1.2	30	564	5.34	30
1130	PVE	2070VM	VIB	1130	1.519	33.33	1130	6.76	33.33
1114	PVE	2310VM	VIB	190	0.72	38.3	190	3.204	38.3
1131	PVE	2312VM	VIB	252	0.26	38.33	252	1.157	38.33
1115	PVE	2315VM	VIB	234	1.09	38.3	234	4.851	38.3
1116	PVE	2316VM	VIB	294	1.16	38.3	294	5.162	38.3
1117	PVE	2319VM	VIB	392	1.37	38.3	392	6.097	38.3
1118	PVE	2323VM	VIB	392	0.83	38.3	392	3.693	38.3
1119	PVE	2332VM	VIB	564	1.16	38.3	564	5.162	38.3
1120	PVE	2335VM	VIB	784	1.27	38.3	784	5.651	38.3
1132	PVE	2350VM	VIB	790	1.085	38.33	790	4.828	38.33
1111	PVE	1420	VIB	190	1.01	33.3	190	4.494	33.3
1110	PVE	2307	VIB	190	0.47	38.3	190	2.091	38.3
1112	PVE	2315	VIB	234	1.09	38.3	234	4.851	38.3
1113	PVE	2520	VIB	294	1.81	33.3	294	8.054	33.3
1531	SPI	D 19-42	OED	42.612	4.02	10.6	57.797	17.889	3.231
1532	SPI	D 30-32	OED	72.08	6.8	10.6	97.766	30.26	3.231

ID	Hammer Manufacturer	Hammer Model	Hammer Type	Energy/Power (kip-ft)/(kW)	Ram Weight (kips)	Stroke (ft)	Energy/Power (kJ)/(kW)	Ram Weight (kN)	Stroke (m)
350	HERA	1250	OED	24.85	2.755	9.02	33.706	12.26	2.749
351	HERA	1500	OED	29.811	3.305	9.02	40.435	14.707	2.749
349	HERA	1900	OED	44.414	4.19	10.6	60.241	18.646	3.231
352	HERA	2500	OED	49.7	5.51	9.02	67.411	24.52	2.749
353	HERA	2800	OED	55.699	6.175	9.02	75.547	27.479	2.749
354	HERA	3500	OED	69.589	7.715	9.02	94.388	34.332	2.749
355	HERA	5000	OED	99.446	11.025	9.02	134.884	49.061	2.749
356	HERA	5700	OED	113.381	12.57	9.02	153.786	55.936	2.749
357	HERA	6200	OED	123.303	13.67	9.02	167.244	60.832	2.749
358	HERA	7500	OED	149.191	16.54	9.02	202.356	73.603	2.749
359	HERA	8800	OED	174.988	19.4	9.02	237.347	86.33	2.749
507	HPSI	1000	ECH	50	10	5	67.818	44.5	1.524
501	HPSI	110	ECH	44	11	4	59.68	48.95	1.219
502	HPSI	150	ECH	60	15	4	81.382	66.75	1.219
503	HPSI	154	ECH	61.6	15.4	4	83.552	68.53	1.219
508	HPSI	1605	ECH	83	16.6	5	112.578	73.87	1.524
504	HPSI	200	ECH	80	20	4	108.509	89	1.219
512	HPSI	2000	ECH	80	20	4	108.509	89	1.219
509	HPSI	2005	ECH	95.1	19.02	5	128.99	84.639	1.524
505	HPSI	225	ECH	90	22.5	4	122.072	100.125	1.219
510	HPSI	3005	ECH	154.325	30.865	5	209.32	137.349	1.524
511	HPSI	3505	ECH	176.325	35.265	5	239.16	156.929	1.524
506	HPSI	650	ECH	32.5	6.5	5	44.082	28.925	1.524

ID	Hammer Manufacturer	Hammer Model	Hammer Type	Energy/Power (kip-ft)/(kW)	Ram Weight (kips)	Stroke (ft)	Energy/Power (kJ)/(kW)	Ram Weight (kN)	Stroke (m)
101	KOBE	K 13	OED	25.428	2.87	8.86	34.49	12.771	2.701
104	KOBE	K 25	OED	51.519	5.51	9.35	69.878	24.52	2.85
107	KOBE	K 35	OED	72.182	7.72	9.35	97.905	34.354	2.85
110	KOBE	K 45	OED	92.752	9.92	9.35	125.805	44.144	2.85
112	KOBE	KB 60	OED	130.183	13.23	9.84	176.575	58.873	2.999
113	KOBE	KB 80	OED	173.578	17.64	9.84	235.434	78.498	2.999
103	KOBE	K22-Est	OED	45.347	4.85	9.35	61.508	21.582	2.85
624	MAIT	120	VIB	674	1.74	30	674	7.743	30
620	MAIT	34	VIB	227	1.23	33.3	227	5.474	33.3
621	MAIT	42	VIB	309	1.52	33.3	309	6.764	33.3
622	MAIT	54	VIB	450	0.98	33.3	450	4.361	33.3
623	MAIT	68	VIB	531	1.23	33.3	531	5.474	33.3
999	Self	Drop/10t	ECH	300	20	15	406.908	89	4.572
535	BANUT	S3000	ECH	26.043	6.615	3.937	35.324	29.437	1.2
536	BANUT	S4000	ECH	34.724	8.82	3.937	47.099	39.249	1.2
537	BANUT	S5000	ECH	43.405	11.025	3.937	58.873	49.061	1.2
538	BANUT	S6000	ECH	52.087	13.23	3.937	70.648	58.873	1.2
539	BANUT	S8000	ECH	69.449	17.64	3.937	94.197	78.498	1.2
540	BANUT	S10000	ECH	86.811	22.05	3.937	117.747	98.122	1.2
541	BANUT	3 Tonnes	ECH	17.345	6.61	2.624	23.526	29.415	0.8
542	BANUT	4 Tonnes	ECH	23.144	8.82	2.624	31.391	39.249	0.8
543	BANUT	5 Tonnes	ECH	28.916	11.02	2.624	39.221	49.039	0.8
544	BANUT	6 Tonnes	ECH	34.716	13.23	2.624	47.087	58.873	0.8

ID	Hammer Manufacturer	Hammer Model	Hammer Type	Energy/Power (kip-ft)/(kW)	Ram Weight (kips)	Stroke (ft)	Energy/Power (kJ)/(kW)	Ram Weight (kN)	Stroke (m)
545	BANUT	7 Tonnes	ECH	40.488	15.43	2.624	54.917	68.664	0.8
1431	BRUCE	SGV-80	VIB	112.2	0.133	33.33	112.2	0.592	33.33
1432	BRUCE	SGV-100	VIB	142.6	0.179	30	142.6	0.797	30
1433	BRUCE	SGV-200	VIB	184.8	0.31	28.83	184.8	1.38	28.83
1434	BRUCE	SGV-300	VIB	211.2	0.352	27.5	211.2	1.566	27.5
1435	BRUCE	SGV-400	VIB	286	0.437	26.67	286	1.945	26.67
1436	BRUCE	SGV-450	VIB	323.4	0.478	26.67	323.4	2.127	26.67
1437	BRUCE	SGV-600	VIB	451.5	0.722	26.67	451.5	3.213	26.67
921	BRUCE	SGH-0212	ECH	17.336	4.4	3.94	23.514	19.58	1.201
530	BRUCE	SGH-0312	ECH	26.004	6.6	3.94	35.271	29.37	1.201
534	BRUCE	SGH-0412	ECH	34.672	8.8	3.94	47.028	39.16	1.201
531	BRUCE	SGH-0512	ECH	43.34	11	3.94	58.785	48.95	1.201
532	BRUCE	SGH-0712	ECH	60.676	15.4	3.94	82.298	68.53	1.201
922	BRUCE	SGH-0715	ECH	75.768	15.4	4.92	102.769	68.53	1.5
533	BRUCE	SGH-1012	ECH	86.774	22.046	3.936	117.697	98.106	1.2
923	BRUCE	SGH-1015	ECH	108.467	22.046	4.92	147.121	98.106	1.5
625	BRUCE	SGH-1212	ECH	104.129	26.455	3.936	141.236	117.727	1.2
924	BRUCE	SGH-1215	ECH	130.161	26.455	4.92	176.545	117.727	1.5
626	BRUCE	SGH-1312	ECH	112.806	28.66	3.936	153.006	127.537	1.2
627	BRUCE	SGH-1315	ECH	141.008	28.66	4.92	191.257	127.537	1.5
628	BRUCE	SGH-1412	ECH	121.483	30.865	3.936	164.775	137.348	1.2
629	BRUCE	SGH-1415	ECH	151.854	30.865	4.92	205.969	137.348	1.5
630	BRUCE	SGH-1612	ECH	138.838	35.274	3.936	188.315	156.969	1.2

ID	Hammer Manufacturer	Hammer Model	Hammer Type	Energy/Power (kip-ft)/(kW)	Ram Weight (kips)	Stroke (ft)	Energy/Power (kJ)/(kW)	Ram Weight (kN)	Stroke (m)
631	BRUCE	SGH-1615	ECH	173.548	35.274	4.92	235.393	156.969	1.5
632	BRUCE	SGH-1618	ECH	208.257	35.274	5.904	282.472	156.969	1.8
633	BRUCE	SGH-1619	ECH	219.827	35.274	6.232	298.165	156.969	1.9
634	BRUCE	SGH-1812	ECH	156.193	39.683	3.936	211.854	176.59	1.2
635	BRUCE	SGH-1815	ECH	195.241	39.683	4.92	264.817	176.59	1.5
636	BRUCE	SGH-2012	ECH	173.548	44.092	3.936	235.393	196.211	1.2
637	BRUCE	SGH-2015	ECH	216.935	44.092	4.92	294.241	196.211	1.5
638	BRUCE	SGH-2312	ECH	199.58	50.706	3.936	270.702	225.643	1.2
639	BRUCE	SGH-2315	ECH	249.475	50.706	4.92	338.378	225.643	1.5
925	BRUCE	SGH-2512	ECH	216.935	55.116	3.936	294.241	245.264	1.2
926	BRUCE	SGH-2515	ECH	271.168	55.116	4.92	367.802	245.264	1.5
640	BRUCE	SGH-3012	ECH	260.322	66.139	3.936	353.09	294.317	1.2
641	BRUCE	SGH-3013	ECH	282.015	66.139	4.264	382.514	294.317	1.3
642	BRUCE	SGH-3015	ECH	325.402	66.139	4.92	441.362	294.317	1.5
927	BRUCE	SGH-3512	ECH	303.708	77.162	3.936	411.938	343.37	1.2
928	BRUCE	SGH-3515	ECH	379.636	77.162	4.92	514.922	343.37	1.5
643	BRUCE	SGH-4012	ECH	347.095	88.185	3.936	470.786	392.422	1.2
929	BRUCE	SGH-4015	ECH	433.869	88.185	4.92	588.483	392.422	1.5
644	BRUCE	SGH-4212	ECH	364.45	92.594	3.936	494.326	412.043	1.2
930	BRUCE	SGH-4215	ECH	455.563	92.594	4.92	617.907	412.043	1.5
931	BRUCE	SGH-4512	ECH	390.482	99.208	3.936	529.635	441.475	1.2
932	BRUCE	SGH-4515	ECH	488.103	99.208	4.92	662.043	441.475	1.5
933	BRUCE	SGH-4712	ECH	407.837	103.61	3.936	553.174	461.096	1.2

ID	Hammer Manufacturer	Hammer Model	Hammer Type	Energy/Power (kip-ft)/(kW)	Ram Weight (kips)	Stroke (ft)	Energy/Power (kJ)/(kW)	Ram Weight (kN)	Stroke (m)
934	BRUCE	SGH-4715	ECH	509.796	103.61	4.92	691.467	461.096	1.5
935	BRUCE	SGH-4719	ECH	645.742	103.61	6.232	875.858	461.096	1.9
645	BRUCE	SGH-5012	ECH	433.869	110.23	3.936	588.483	490.528	1.2
936	BRUCE	SGH-5015	ECH	542.337	110.23	4.92	735.604	490.528	1.5
937	BRUCE	SGH-5715	ECH	618.263	125.66	4.92	838.588	559.202	1.5
938	BRUCE	SGH-6015	ECH	650.804	132.277	4.92	882.724	588.634	1.5
939	BRUCE	SGH-7015	ECH	759.271	154.32	4.92	1029.845	686.739	1.5
940	BRUCE	SGH-8015	ECH	867.738	176.37	4.92	1176.966	784.845	1.5
1438	BRUCE	SGV-1000	VIB	569.1	1.032	25	569.1	4.592	25
1401	FAMBO	HR250	ECH	1.806	0.551	3.281	2.45	2.45	1
1403	FAMBO	HR500	ECH	4.344	1.103	3.937	5.892	4.91	1.2
1404	FAMBO	HR1000	ECH	8.679	2.204	3.937	11.772	9.81	1.2
1405	FAMBO	HR1500	ECH	13.023	3.308	3.937	17.664	14.72	1.2
1406	FAMBO	HR2000	ECH	17.358	4.409	3.937	23.544	19.62	1.2
1407	FAMBO	HR2750	ECH	23.87	6.063	3.937	32.376	26.98	1.2
1408	FAMBO	HR3000	ECH	26.037	6.613	3.937	35.316	29.43	1.2
1409	FAMBO	HR4000	ECH	34.716	8.818	3.937	47.088	39.24	1.2
1410	FAMBO	HR5000	ECH	43.396	11.022	3.937	58.86	49.05	1.2
1411	FAMBO	HR7000	ECH	60.754	15.431	3.937	82.404	68.67	1.2
1412	FAMBO	HR8000	ECH	69.451	17.64	3.937	94.2	78.5	1.2
1413	FAMBO	HR10000	ECH	86.791	22.045	3.937	117.72	98.1	1.2
1402	FAMBO	HR500akk	ECH	3.62	1.103	3.281	4.91	4.91	1
271	MENCK	MH 68	ECH	49.176	7.72	6.37	66.701	34.354	1.942

ID	Hammer Manufacturer	Hammer Model	Hammer Type	Energy/Power (kip-ft)/(kW)	Ram Weight (kips)	Stroke (ft)	Energy/Power (kJ)/(kW)	Ram Weight (kN)	Stroke (m)
272	MENCK	MH 96	ECH	69.426	11.02	6.3	94.167	49.039	1.92
273	MENCK	MH 145	ECH	104.8	16.53	6.34	142.147	73.559	1.932
449	MENCK	MHF3-3	ECH	24.764	7.054	3.51	33.589	31.392	1.07
450	MENCK	MHF3-4	ECH	30.956	8.818	3.51	41.987	39.24	1.07
451	MENCK	MHF3-5	ECH	38.694	11.022	3.51	52.483	49.05	1.07
452	MENCK	MHF3-6	ECH	46.433	13.227	3.51	62.98	58.86	1.07
453	MENCK	MHF3-7	ECH	54.172	15.431	3.51	73.477	68.67	1.07
441	MENCK	MHF5-5	ECH	38.694	11.022	3.51	52.483	49.05	1.07
442	MENCK	MHF5-6	ECH	46.433	13.227	3.51	62.98	58.86	1.07
443	MENCK	MHF5-7	ECH	54.172	15.431	3.51	73.477	68.67	1.07
444	MENCK	MHF5-8	ECH	61.911	17.636	3.51	83.974	78.48	1.07
445	MENCK	MHF5-9	ECH	69.65	19.84	3.51	94.47	88.29	1.07
446	MENCK	MHF5-10	ECH	77.389	22.045	3.51	104.967	98.1	1.07
447	MENCK	MHF5-11	ECH	85.128	24.249	3.51	115.464	107.91	1.07
448	MENCK	MHF5-12	ECH	92.866	26.454	3.51	125.96	117.72	1.07
274	MENCK	MHU 195	ECH	143.738	21.361	6.729	194.96	95.056	2.051
275	MENCK	MHU 220	ECH	162.167	24.838	6.529	219.957	110.531	1.99
276	MENCK	MHU 400	ECH	294.824	51.087	5.771	399.887	227.338	1.759
277	MENCK	MHU 600	ECH	442.281	75.522	5.856	599.892	336.074	1.785
300	MENCK	MBS12500	ECH	1581.829	275.58	5.74	2145.53	1226.331	1.75
456	MENCK	MHF 5-14	ECH	108.344	30.863	3.51	146.954	137.34	1.07
454	MENCK	MHF10-15	ECH	124.734	33.06	3.773	169.185	147.117	1.15
455	MENCK	MHF10-20	ECH	166.275	44.07	3.773	225.528	196.111	1.15

ID	Hammer Manufacturer	Hammer Model	Hammer Type	Energy/Power (kip-ft)/(kW)	Ram Weight (kips)	Stroke (ft)	Energy/Power (kJ)/(kW)	Ram Weight (kN)	Stroke (m)
278	MENCK	MHU 1000	ECH	737.381	126.98	5.807	1000.155	565.059	1.77
270	MENCK	MHU 100C	ECH	73.71	11.1	6.64	99.978	49.396	2.024
475	MENCK	MHU 135T	ECH	110.589	17.987	6.148	149.999	80.042	1.874
473	MENCK	MHU 150S	ECH	110.589	17.987	6.148	149.999	80.042	1.874
279	MENCK	MHU 1700	ECH	1253.241	207.152	6.05	1699.846	921.825	1.844
461	MENCK	MHU 200T	ECH	162.241	26.745	6.066	220.057	119.014	1.849
280	MENCK	MHU 2100	ECH	1548.291	257.177	6.02	2100.04	1144.436	1.835
1321	MENCK	MHU 240U	ECH	221.198	35.729	6.191	300.024	158.995	1.887
460	MENCK	MHU 270T	ECH	221.198	35.729	6.191	300.024	158.995	1.887
281	MENCK	MHU 3000	ECH	2211.896	370.228	5.974	3000.128	1647.517	1.821
459	MENCK	MHU 300S	ECH	221.198	35.729	6.191	300.024	158.995	1.887
1323	MENCK	MHU 360U	ECH	324.365	52.449	6.184	439.955	233.398	1.885
462	MENCK	MHU 400T	ECH	324.365	52.449	6.184	439.955	233.398	1.885
1322	MENCK	MHU 440S	ECH	324.365	52.449	6.184	439.955	233.398	1.885
1325	MENCK	MHU 450U	ECH	404.059	65.958	6.126	548.049	293.513	1.867
463	MENCK	MHU 500T	ECH	405.529	65.958	6.148	550.043	293.513	1.874
1327	MENCK	MHU 540U	ECH	485.169	80.393	6.035	658.064	357.747	1.839
1324	MENCK	MHU 550S	ECH	404.059	65.958	6.126	548.049	293.513	1.867
466	MENCK	MHU 600B	ECH	457.032	65.958	6.929	619.899	293.513	2.112
467	MENCK	MHU 600T	ECH	486.628	80.393	6.053	660.043	357.747	1.845
1329	MENCK	MHU 650U	ECH	588.193	99.931	5.886	797.801	444.692	1.794
1326	MENCK	MHU 660S	ECH	485.169	80.393	6.035	658.064	357.747	1.839

ID	Hammer Manufacturer	Hammer Model	Hammer Type	Energy/Power (kip-ft)/(kW)	Ram Weight (kips)	Stroke (ft)	Energy/Power (kJ)/(kW)	Ram Weight (kN)	Stroke (m)
464	MENCK	MHU 700T	ECH	567.722	92.883	6.112	770.036	413.331	1.863
1328	MENCK	MHU 720T	ECH	588.193	99.931	5.886	797.801	444.692	1.794
476	MENCK	MHU 750T	ECH	604.568	99.931	6.05	820.012	444.692	1.844
468	MENCK	MHU 800S	ECH	604.568	99.931	6.05	820.012	444.692	1.844
1332	MENCK	MHU 810U	ECH	736.482	126.98	5.8	998.934	565.059	1.768
465	MENCK	MHU 840S	ECH	619.223	92.883	6.667	839.889	413.331	2.032
1331	MENCK	MHU 900T	ECH	736.482	126.98	5.8	998.934	565.059	1.768
1330	MENCK	MHU1000S	ECH	736.482	126.98	5.8	998.934	565.059	1.768
477	MENCK	MHU1100T	ECH	899.66	145.705	6.175	1220.262	648.386	1.882
469	MENCK	MHU1200S	ECH	884.84	145.705	6.073	1200.162	648.386	1.851
457	MENCK	MHU135T*	ECH	110.589	17.987	6.148	149.999	80.042	1.874
1336	MENCK	MHU1400B	ECH	1032.075	145.705	7.083	1399.865	648.386	2.159
470	MENCK	MHU1500S	ECH	1106.07	178.944	6.181	1500.229	796.3	1.884
478	MENCK	MHU150S*	ECH	110.589	17.987	6.148	149.999	80.042	1.874
1333	MENCK	MHU1700S	ECH	1272.947	207.152	6.145	1726.575	921.825	1.873
471	MENCK	MHU1700T	ECH	1400.86	227.36	6.161	1900.07	1011.752	1.878
472	MENCK	MHU1900S	ECH	1400.86	227.36	6.161	1900.07	1011.752	1.878
1334	MENCK	MHU2100	ECH	1573.921	257.17	6.12	2134.803	1144.43	1.865

ID	Hammer Manufacturer	Hammer Model	Hammer Type	Energy/Power (kip-ft)/(kW)	Ram Weight (kips)	Stroke (ft)	Energy/Power (kJ)/(kW)	Ram Weight (kN)	Stroke (m)
		S			7			6	
474	MENCK	MHU2700S	ECH	1990.188	318.765	6.243	2699.411	1418.503	1.903
1335	MENCK	MHU3000S	ECH	2216.558	370.228	5.987	3006.45	1647.517	1.825
1337	MENCK	MHU3500S	ECH	2582.428	385.845	6.693	3502.702	1717.011	2.04
479	MENCK	MHU600B*	ECH	457.032	65.958	6.929	619.899	293.513	2.112
282	MENCK	MRBS 500	ECH	45.072	11.02	4.09	61.134	49.039	1.247
283	MENCK	MRBS 750	ECH	67.773	16.53	4.1	91.925	73.559	1.25
285	MENCK	MRBS 850	ECH	93.283	18.96	4.92	126.526	84.372	1.5
286	MENCK	MRBS1100	ECH	123.433	24.25	5.09	167.419	107.913	1.551
287	MENCK	MRBS1502	ECH	135.587	33.07	4.1	183.905	147.161	1.25
288	MENCK	MRBS1800	ECH	189.814	38.58	4.92	257.456	171.681	1.5
289	MENCK	MRBS2500	ECH	262.113	63.93	4.1	355.52	284.489	1.25
290	MENCK	MRBS2502	ECH	225.951	55.11	4.1	306.471	245.24	1.25
291	MENCK	MRBS2504	ECH	225.951	55.11	4.1	306.471	245.24	1.25
292	MENCK	MRBS3000	ECH	325.36	66.13	4.92	441.305	294.278	1.5
293	MENCK	MRBS3900	ECH	513.343	86.86	5.91	696.277	386.527	1.801
294	MENCK	MRBS4600	ECH	498.937	101.41	4.92	676.738	451.275	1.5
295	MENCK	MRBS5000	ECH	542.332	110.23	4.92	735.597	490.524	1.5
296	MENCK	MRBS6000	ECH	759.23	132.27	5.74	1029.789	588.602	1.75
297	MENCK	MRBS7000	ECH	631.4	154	4.1	856.406	685.3	1.25
298	MENCK	MRBS8000	ECH	867.74	176.37	4.92	1176.968	784.846	1.5

ID	Hammer Manufacturer	Hammer Model	Hammer Type	Energy/Power (kip-ft)/(kW)	Ram Weight (kips)	Stroke (ft)	Energy/Power (kJ)/(kW)	Ram Weight (kN)	Stroke (m)
299	MENCK	MRBS8800	ECH	954.529	194.01	4.92	1294.685	863.344	1.5
521	DAWSON	HPH1200	ECH	8.717	2.3	3.79	11.823	10.235	1.155
522	DAWSON	HPH1800	ECH	13.721	3.3	4.158	18.611	14.685	1.267
523	DAWSON	HPH2400	ECH	17.316	4.189	4.134	23.486	18.64	1.26
525	DAWSON	HPH4500	ECH	32.56	7.716	4.22	44.163	34.336	1.286
524	DAWSON	HPH6500	ECH	46.979	10.25	4.583	63.721	45.613	1.397
526	DAWSON	HPH9000	ECH	66.303	10.471	6.332	89.93	46.596	1.93
1601	DELMAG	D 2	OED	1.784	0.494	3.609	2.42	2.2	1.1
1602	DELMAG	D 4	OED	3.603	0.838	4.298	4.886	3.73	1.31
1	DELMAG	D 5	OED	10.505	1.1	9.55	14.249	4.895	2.911
3	DELMAG	D 12	OED	22.605	2.75	8.22	30.661	12.238	2.505
4	DELMAG	D 15	OED	27.093	3.3	8.21	36.748	14.685	2.502
6	DELMAG	D 22	OED	40.606	4.91	8.27	55.076	21.849	2.521
11	DELMAG	D 30	OED	59.73	6.6	9.05	81.015	29.37	2.758
16	DELMAG	D 36	OED	83.82	7.93	10.57	113.69	35.288	3.222
21	DELMAG	D 44	OED	90.155	9.5	9.49	122.283	42.275	2.893
22	DELMAG	D 46	OED	107.078	10.14	10.56	145.237	45.123	3.219
27	DELMAG	D 55	OED	125.004	11.86	10.54	169.551	52.777	3.213
47	DELMAG	D 5-42	OED	10.56	1.1	9.6	14.323	4.895	2.926
36	DELMAG	D 6-32	OED	13.524	1.322	10.23	18.343	5.883	3.118
1603	DELMAG	D 8-12	OED	20.099	1.76	11.42	27.262	7.832	3.481
2	DELMAG	D 8-22	OED	20.099	1.76	11.42	27.262	7.832	3.481
37	DELMAG	D 12-32	OED	31.33	2.82	11.11	42.495	12.549	3.386

ID	Hammer Manufacturer	Hammer Model	Hammer Type	Energy/Power (kip-ft)/(kW)	Ram Weight (kips)	Stroke (ft)	Energy/Power (kJ)/(kW)	Ram Weight (kN)	Stroke (m)
38	DELMAG	D 12-42	OED	33.304	2.82	11.81	45.172	12.549	3.6
1604	DELMAG	D 12-52	OED	33.981	2.82	12.05	46.09	12.549	3.673
39	DELMAG	D 14-42	OED	34.501	3.086	11.18	46.796	13.733	3.408
5	DELMAG	D 16-32	OED	40.198	3.52	11.42	54.523	15.664	3.481
1605	DELMAG	D 16-52	OED	40.198	3.52	11.42	54.523	15.664	3.481
40	DELMAG	D 19-32	OED	42.44	4	10.61	57.564	17.8	3.234
41	DELMAG	D 19-42	OED	43.24	4	10.81	58.649	17.8	3.295
35	DELMAG	D 19-52	OED	43.2	4	10.8	58.595	17.8	3.292
46	DELMAG	D 21-42	OED	55.745	4.63	12.04	75.611	20.604	3.67
7	DELMAG	D 22-02	OED	48.5	4.85	10	65.783	21.582	3.048
8	DELMAG	D 22-13	OED	48.5	4.85	10	65.783	21.582	3.048
9	DELMAG	D 22-23	OED	51.216	4.85	10.56	69.467	21.582	3.219
10	DELMAG	D 25-32	OED	66.34	5.51	12.04	89.981	24.52	3.67
1606	DELMAG	D 25-52	OED	66.34	5.51	12.04	89.981	24.52	3.67
12	DELMAG	D 30-02	OED	66.198	6.6	10.03	89.788	29.37	3.057
13	DELMAG	D 30-13	OED	66.198	6.6	10.03	89.788	29.37	3.057
14	DELMAG	D 30-23	OED	73.788	6.6	11.18	100.083	29.37	3.408
15	DELMAG	D 30-32	OED	75.438	6.6	11.43	102.321	29.37	3.484
1607	DELMAG	D 30-52	OED	75.438	6.6	11.43	102.321	29.37	3.484
17	DELMAG	D 36-02	OED	83.82	7.93	10.57	113.69	35.288	3.222
18	DELMAG	D 36-13	OED	83.82	7.93	10.57	113.69	35.288	3.222
19	DELMAG	D 36-23	OED	88.499	7.93	11.16	120.036	35.288	3.402
20	DELMAG	D 36-32	OED	90.561	7.93	11.42	122.833	35.288	3.481

ID	Hammer Manufacturer	Hammer Model	Hammer Type	Energy/Power (kip-ft)/(kW)	Ram Weight (kips)	Stroke (ft)	Energy/Power (kJ)/(kW)	Ram Weight (kN)	Stroke (m)
23	DELMAG	D 46-02	OED	107.078	10.14	10.56	145.237	45.123	3.219
24	DELMAG	D 46-13	OED	96.533	10.14	9.52	130.933	45.123	2.902
25	DELMAG	D 46-23	OED	107.078	10.14	10.56	145.237	45.123	3.219
26	DELMAG	D 46-32	OED	122.187	10.14	12.05	165.73	45.123	3.673
28	DELMAG	D 62-02	OED	152.446	13.66	11.16	206.771	60.787	3.402
29	DELMAG	D 62-12	OED	152.446	13.66	11.16	206.771	60.787	3.402
30	DELMAG	D 62-22	OED	164.603	13.66	12.05	223.261	60.787	3.673
31	DELMAG	D 80-12	OED	186.243	17.62	10.57	252.613	78.409	3.222
32	DELMAG	D 80-23	OED	212.497	17.62	12.06	288.223	78.409	3.676
33	DELMAG	D100-13	OED	265.675	22.066	12.04	360.35	98.194	3.67
43	DELMAG	D120-42	OED	301.794	26.45	11.41	409.342	117.703	3.478
45	DELMAG	D125-42	OED	313.633	27.56	11.38	425.399	122.642	3.469
1611	DELMAG	D138-32	OED	339.511	30.436	11.155	460.499	135.441	3.4
44	DELMAG	D150-42	OED	377.329	33.07	11.41	511.794	147.161	3.478
48	DELMAG	D160-32	OED	393.453	35.272	11.155	533.664	156.96	3.4
1612	DELMAG	D180-32	OED	442.638	39.681	11.155	600.376	176.58	3.4
42	DELMAG	D200-42	OED	492.044	44.09	11.16	667.389	196.201	3.402
49	DELMAG	D260-32	OED	639.362	57.317	11.155	867.204	255.06	3.4
1613	DELMAG	D300-32	OED	737.727	66.135	11.155	1000.624	294.3	3.4
1614	DELMAG	D400-32	OED	983.637	88.18	11.155	1334.166	392.4	3.4

ID	Hammer Manufacturer	Hammer Model	Hammer Type	Energy/Power (kip-ft)/(kW)	Ram Weight (kips)	Stroke (ft)	Energy/Power (kJ)/(kW)	Ram Weight (kN)	Stroke (m)
850	PILECO	D8-22	OED	18.656	1.76	10.6	25.304	7.832	3.231
851	PILECO	D12-42	OED	29.892	2.82	10.6	40.544	12.549	3.231
852	PILECO	D19-42	OED	42.506	4.01	10.6	57.653	17.845	3.231
853	PILECO	D25-32	OED	58.406	5.51	10.6	79.22	24.52	3.231
854	PILECO	D30-32	OED	70.066	6.61	10.6	95.035	29.415	3.231
855	PILECO	D36-32	OED	84.164	7.94	10.6	114.157	35.333	3.231
856	PILECO	D46-32	OED	107.484	10.14	10.6	145.787	45.123	3.231
857	PILECO	D62-22	OED	161.306	13.67	11.8	218.789	60.832	3.597
858	PILECO	D80-23	OED	197.568	17.64	11.2	267.973	78.498	3.414
859	PILECO	D100-13	OED	246.848	22.04	11.2	334.815	98.078	3.414
860	PILECO	D125-32	OED	308.672	27.56	11.2	418.67	122.642	3.414
863	PILECO	D138-32	OED	340.608	30.411	11.2	461.988	135.331	3.414
866	PILECO	D160-32	OED	395.08	35.275	11.2	535.871	156.974	3.414
864	PILECO	D180-32	OED	444.273	39.667	11.2	602.593	176.519	3.414
861	PILECO	D225-22	OED	555.344	49.584	11.2	753.247	220.65	3.414
862	PILECO	D250-22	OED	617.057	55.094	11.2	836.952	245.17	3.414
865	PILECO	D280-22	OED	688.545	61.726	11.155	933.915	274.68	3.4
867	PILECO	D400-12	OED	810.098	88.15	9.19	1098.785	392.268	2.801
868	PILECO	D600-12	OED	1215.102	132.22	9.19	1648.115	588.379	2.801
869	PILECO	D800-22	OED	1620.197	176.3	9.19	2197.57	784.535	2.801
204	VULCAN	VUL 01	ECH	15	5	3	20.345	22.25	0.914
205	VULCAN	VUL 02	ECH	7.26	3	2.42	9.847	13.35	0.738
206	VULCAN	VUL 06	ECH	19.5	6.5	3	26.449	28.925	0.914

ID	Hammer Manufacturer	Hammer Model	Hammer Type	Energy/Power (kip-ft)/(kW)	Ram Weight (kips)	Stroke (ft)	Energy/Power (kJ)/(kW)	Ram Weight (kN)	Stroke (m)
207	VULCAN	VUL 08	ECH	26	8	3.25	35.265	35.6	0.991
208	VULCAN	VUL 010	ECH	32.5	10	3.25	44.082	44.5	0.991
209	VULCAN	VUL 012	ECH	39	12	3.25	52.898	53.4	0.991
210	VULCAN	VUL 014	ECH	42	14	3	56.967	62.3	0.914
211	VULCAN	VUL 016	ECH	48.75	16.25	3	66.123	72.313	0.914
212	VULCAN	VUL 020	ECH	60	20	3	81.382	89	0.914
213	VULCAN	VUL 030	ECH	90	30	3	122.072	133.5	0.914
214	VULCAN	VUL 040	ECH	120	40	3	162.763	178	0.914
215	VULCAN	VUL 060	ECH	180	60	3	244.145	267	0.914
220	VULCAN	VUL 30C	ECH	7.26	3	2.42	9.847	13.35	0.738
231	VULCAN	VUL 320	ECH	60	20	3	81.382	89	0.914
232	VULCAN	VUL 330	ECH	90	30	3	122.072	133.5	0.914
233	VULCAN	VUL 340	ECH	120	40	3	162.763	178	0.914
234	VULCAN	VUL 360	ECH	180	60	3	244.145	267	0.914
235	VULCAN	VUL 505	ECH	25	5	5	33.909	22.25	1.524
236	VULCAN	VUL 506	ECH	32.5	6.5	5	44.082	28.925	1.524
237	VULCAN	VUL 508	ECH	40	8	5	54.254	35.6	1.524
221	VULCAN	VUL 50C	ECH	15.1	5	3.02	20.481	22.25	0.92
238	VULCAN	VUL 510	ECH	50	10	5	67.818	44.5	1.524
239	VULCAN	VUL 512	ECH	60	12	5	81.382	53.4	1.524
240	VULCAN	VUL 520	ECH	100	20	5	135.636	89	1.524
241	VULCAN	VUL 530	ECH	150	30	5	203.454	133.5	1.524
242	VULCAN	VUL 540	ECH	200.001	40.9	4.89	271.273	182.005	1.49

ID	Hammer Manufacturer	Hammer Model	Hammer Type	Energy/Power (kip-ft)/(kW)	Ram Weight (kips)	Stroke (ft)	Energy/Power (kJ)/(kW)	Ram Weight (kN)	Stroke (m)
243	VULCAN	VUL 560	ECH	300	62.5	4.8	406.908	278.125	1.463
222	VULCAN	VUL 65C	ECH	19.175	6.5	2.95	26.008	28.925	0.899
224	VULCAN	VUL 80C	ECH	24.48	8	3.06	33.204	35.6	0.933
225	VULCAN	VUL 85C	ECH	25.986	8.52	3.05	35.246	37.914	0.93
226	VULCAN	VUL 100C	ECH	32.9	10	3.29	44.624	44.5	1.003
227	VULCAN	VUL 140C	ECH	35.98	14	2.57	48.802	62.3	0.783
228	VULCAN	VUL 200C	ECH	50.2	20	2.51	68.089	89	0.765
245	VULCAN	VUL 3100	ECH	300	100	3	406.908	445	0.914
229	VULCAN	VUL 400C	ECH	113.6	40	2.84	154.082	178	0.866
246	VULCAN	VUL 5100	ECH	500	100	5	678.18	445	1.524
247	VULCAN	VUL 5150	ECH	750	150	5	1017.27	667.5	1.524
230	VULCAN	VUL 600C	ECH	179.16	60	2.986	243.005	267	0.91
248	VULCAN	VUL 6300	ECH	1800	300	6	2441.448	1335	1.829
223	VULCAN	VUL 65CA	ECH	19.565	6.5	3.01	26.537	28.925	0.917
171	CONMACO	C 50	ECH	15	5	3	20.345	22.25	0.914
172	CONMACO	C 65	ECH	19.5	6.5	3	26.449	28.925	0.914
175	CONMACO	C 80	ECH	26	8	3.25	35.265	35.6	0.991
176	CONMACO	C 100	ECH	32.5	10	3.25	44.082	44.5	0.991
177	CONMACO	C 115	ECH	37.375	11.5	3.25	50.694	51.175	0.991
182	CONMACO	C 140	ECH	42	14	3	56.967	62.3	0.914
183	CONMACO	C 160	ECH	48.75	16.25	3	66.123	72.313	0.914
184	CONMACO	C 200	ECH	60	20	3	81.382	89	0.914
185	CONMACO	C 300	ECH	90	30	3	122.072	133.5	0.914

ID	Hammer Manufacturer	Hammer Model	Hammer Type	Energy/Power (kip-ft)/(kW)	Ram Weight (kips)	Stroke (ft)	Energy/Power (kJ)/(kW)	Ram Weight (kN)	Stroke (m)
173	CONMACO	C 550	ECH	25	5	5	33.909	22.25	1.524
174	CONMACO	C 565	ECH	32.5	6.5	5	44.082	28.925	1.524
196	CONMACO	C 1750	ECH	1050	175	6	1424.178	778.75	1.829
192	CONMACO	C 50E5	ECH	25	5	5	33.909	22.25	1.524
186	CONMACO	C 5200	ECH	100	20	5	135.636	89	1.524
187	CONMACO	C 5300	ECH	150	30	5	203.454	133.5	1.524
188	CONMACO	C 5450	ECH	225	45	5	305.181	200.25	1.524
189	CONMACO	C 5700	ECH	350	70	5	474.726	311.5	1.524
193	CONMACO	C 65E5	ECH	32.5	6.5	5	44.082	28.925	1.524
190	CONMACO	C 6850	ECH	510	85	6	691.744	378.25	1.829
178	CONMACO	C 80E5	ECH	40	8	5	54.254	35.6	1.524
179	CONMACO	C 100E5	ECH	50	10	5	67.818	44.5	1.524
180	CONMACO	C 115E5	ECH	57.5	11.5	5	77.991	51.175	1.524
181	CONMACO	C 125E5	ECH	62.5	12.5	5	84.773	55.625	1.524
194	CONMACO	C 200E5	ECH	100	20	5	135.636	89	1.524
195	CONMACO	C 300E5	ECH	150	30	5	203.454	133.5	1.524
191	CONMACO	C 160 **	ECH	51.78	17.26	3	70.232	76.807	0.914
90	HITACHI	HNC65	ECH	56.419	14.33	3.937	76.524	63.77	1.2
91	HITACHI	HNC80	ECH	69.433	17.636	3.937	94.176	78.48	1.2
92	HITACHI	HNC100	ECH	86.791	22.045	3.937	117.72	98.1	1.2
93	HITACHI	HNC125	ECH	108.493	27.557	3.937	147.156	122.63	1.2
481	JUNTTAN	HHK3A	ECH	26.048	6.616	3.937	35.33	29.442	1.2
482	JUNTTAN	HHK4A	ECH	34.73	8.822	3.937	47.107	39.256	1.2

ID	Hammer Manufacturer	Hammer Model	Hammer Type	Energy/Power (kip-ft)/(kW)	Ram Weight (kips)	Stroke (ft)	Energy/Power (kJ)/(kW)	Ram Weight (kN)	Stroke (m)
483	JUNTTAN	HHK5A	ECH	43.413	11.027	3.937	58.884	49.07	1.2
951	JUNTTAN	HHK5S	ECH	54.266	11.027	4.921	73.604	49.07	1.5
484	JUNTTAN	HHK6A	ECH	52.095	13.232	3.937	70.66	58.884	1.2
485	JUNTTAN	HHK7A	ECH	60.754	15.431	3.937	82.404	68.67	1.2
952	JUNTTAN	HHK7S	ECH	75.973	15.438	4.921	103.046	68.697	1.5
491	JUNTTAN	HHK9A	ECH	78.143	19.848	3.937	105.99	88.325	1.2
953	JUNTTAN	HHK9S	ECH	97.679	19.848	4.921	132.488	88.325	1.5
961	JUNTTAN	HHU5A	ECH	54.266	11.027	4.921	73.604	49.07	1.5
962	JUNTTAN	HHU7A	ECH	75.942	15.431	4.921	103.005	68.67	1.5
963	JUNTTAN	HHU9A	ECH	97.64	19.84	4.921	132.435	88.29	1.5
486	JUNTTAN	HHK10A	ECH	86.826	22.054	3.937	117.767	98.139	1.2
949	JUNTTAN	HHK10S	ECH	108.494	22.046	4.921	147.157	98.105	1.5
487	JUNTTAN	HHK12A	ECH	104.191	26.465	3.937	141.32	117.767	1.2
954	JUNTTAN	HHK12S	ECH	130.239	26.465	4.921	176.651	117.767	1.5
488	JUNTTAN	HHK14A	ECH	121.556	30.875	3.937	164.874	137.395	1.2
955	JUNTTAN	HHK14S	ECH	151.945	30.875	4.921	206.092	137.395	1.5
494	JUNTTAN	HHK16A	ECH	138.921	35.286	3.937	188.427	157.023	1.2
956	JUNTTAN	HHK16S	ECH	173.652	35.286	4.921	235.534	157.023	1.5
495	JUNTTAN	HHK18A	ECH	156.286	39.697	3.937	211.981	176.651	1.2
957	JUNTTAN	HHK18S	ECH	195.358	39.697	4.921	264.976	176.651	1.5
496	JUNTTAN	HHK20A	ECH	173.652	44.108	3.937	235.534	196.278	1.2
958	JUNTTAN	HHK20S	ECH	217.065	44.108	4.921	294.418	196.278	1.5
959	JUNTTAN	HHK25S	ECH	271.222	55.112	4.921	367.875	245.25	1.5

ID	Hammer Manufacturer	Hammer Model	Hammer Type	Energy/Power (kip-ft)/(kW)	Ram Weight (kips)	Stroke (ft)	Energy/Power (kJ)/(kW)	Ram Weight (kN)	Stroke (m)
950	JUNTTAN	HHK28S	ECH	303.784	61.729	4.921	412.041	274.694	1.5
960	JUNTTAN	HHK36S	ECH	390.56	79.362	4.921	529.74	353.16	1.5
498	JUNTTAN	HHK3AL	ECH	17.365	6.616	2.625	23.553	29.442	0.8
499	JUNTTAN	HHK4AL	ECH	23.154	8.822	2.625	31.405	39.256	0.8
497	JUNTTAN	HHK4SL	ECH	43.396	8.818	4.921	58.86	39.24	1.5
500	JUNTTAN	HHK5AL	ECH	28.942	11.027	2.625	39.256	49.07	0.8
964	JUNTTAN	HHU12A	ECH	130.187	26.454	4.921	176.58	117.72	1.5
965	JUNTTAN	HHU14A	ECH	151.884	30.863	4.921	206.01	137.34	1.5
966	JUNTTAN	HHU16A	ECH	173.582	35.272	4.921	235.44	156.96	1.5
968	JUNTTAN	SHK100-3	ECH	26.905	6.613	4.068	36.493	29.43	1.24
969	JUNTTAN	SHK100-3	ECH	35.888	8.822	4.068	48.677	39.256	1.24
970	JUNTTAN	SHK100-3	ECH	44.842	11.022	4.068	60.822	49.05	1.24
971	JUNTTAN	SHK100-3	ECH	53.815	13.228	4.068	72.992	58.865	1.24
977	JUNTTAN	SHK100-5	ECH	44.844	11.023	4.068	60.825	49.052	1.24
978	JUNTTAN	SHK100-5	ECH	53.815	13.228	4.068	72.992	58.865	1.24
972	JUNTTAN	SHK110-5	ECH	44.976	11.022	4.08	61.004	49.05	1.244
973	JUNTTAN	SHK110-5	ECH	53.824	13.228	4.069	73.005	58.865	1.24
974	JUNTTAN	SHK110-5	ECH	65.622	15.431	4.253	89.007	68.67	1.296
975	JUNTTAN	SHK110-5	ECH	77.421	17.637	4.39	105.011	78.485	1.338
976	JUNTTAN	SHK110-5	ECH	87.741	19.842	4.422	119.009	88.297	1.348
979	JUNTTAN	SHK110-7	ECH	65.632	15.432	4.253	89.021	68.672	1.296
980	JUNTTAN	SHK110-7	ECH	77.43	17.637	4.39	105.023	78.485	1.338
981	JUNTTAN	SHK110-7	ECH	87.741	19.842	4.422	119.009	88.297	1.348

ID	Hammer Manufacturer	Hammer Model	Hammer Type	Energy/Power (kip-ft)/(kW)	Ram Weight (kips)	Stroke (ft)	Energy/Power (kJ)/(kW)	Ram Weight (kN)	Stroke (m)
900	Mueller	MS16HF	VIB	219	1.16	39.2	219	5.162	39.2
901	Mueller	MS25H2	VIB	218	0.904	28	218	4.023	28
902	Mueller	MS25H3	VIB	218	0.904	28	218	4.023	28
903	Mueller	MS50H2	VIB	419	1.2	27	419	5.34	27
904	Mueller	MS50H3	VIB	419	1.2	27	419	5.34	27
905	Mueller	MS25HHF	VIB	274	0.583	27.3	274	2.595	27.3
906	Mueller	MS50HHF	VIB	562	1.166	27.3	562	5.191	27.3
907	Mueller	MS100HHF	VIB	750	2.333	24.9	750	10.382	24.9
910	Mueller	MS-10HFV	VIB	203	0.387	39.3	203	1.721	39.3
908	Mueller	MS120HHF	VIB	895	2.304	25.6	895	10.252	25.6
911	Mueller	MS-16HFV	VIB	294	0.526	39.2	294	2.343	39.2
909	Mueller	MS200HHF	VIB	837	4.253	22.9	837	18.924	22.9
912	Mueller	MS-24HFV	VIB	720	0.847	39.2	720	3.767	39.2
913	Mueller	MS-32HFV	VIB	551	1.053	39.6	551	4.686	39.6
914	Mueller	MS-48HFV	VIB	823	1.693	39.2	823	7.534	39.2
915	Mueller	MS-62HFV	VIB	735	1.823	35	735	8.112	35
1134	Pilemer	DKH-3U	ECH	26.004	6.6	3.94	35.271	29.37	1.201
1135	Pilemer	DKH 10L	ECH	86.791	22.045	3.937	117.72	98.1	1.2
255	RAYMOND	R 0	ECH	24.375	7.5	3.25	33.061	33.375	0.991
251	RAYMOND	R 1	ECH	15	5	3	20.345	22.25	0.914
252	RAYMOND	R 1S	ECH	19.5	6.5	3	26.449	28.925	0.914
258	RAYMOND	R 2/0	ECH	32.5	10	3.25	44.082	44.5	0.991

ID	Hammer Manufacturer	Hammer Model	Hammer Type	Energy/Power (kip-ft)/(kW)	Ram Weight (kips)	Stroke (ft)	Energy/Power (kJ)/(kW)	Ram Weight (kN)	Stroke (m)
259	RAYMOND	R 3/0	ECH	40.625	12.5	3.25	55.102	55.625	0.991
263	RAYMOND	R 30X	ECH	75	30	2.5	101.727	133.5	0.762
261	RAYMOND	R 4/0	ECH	48.75	15	3.25	66.123	66.75	0.991
265	RAYMOND	R 40X	ECH	100	40	2.5	135.636	178	0.762
262	RAYMOND	R 5/0	ECH	56.875	17.5	3.25	77.143	77.875	0.991
266	RAYMOND	R 60X	ECH	150	60	2.5	203.454	267	0.762
253	RAYMOND	R 65C	ECH	19.5	6.5	3	26.449	28.925	0.914
264	RAYMOND	R 8/0	ECH	81.25	25	3.25	110.204	111.25	0.991
256	RAYMOND	R 80C	ECH	24.48	8	3.06	33.204	35.6	0.933
260	RAYMOND	R 150C	ECH	48.75	15	3.25	66.123	66.75	0.991
254	RAYMOND	R 65CH	ECH	19.5	6.5	3	26.449	28.925	0.914
257	RAYMOND	R 80CH	ECH	24.48	8	3.06	33.204	35.6	0.933
514	UDDCOMB	H2H	ECH	16.618	4.404	3.773	22.54	19.6	1.15
515	UDDCOMB	H3H	ECH	24.882	6.6	3.77	33.749	29.37	1.149
516	UDDCOMB	H4H	ECH	33.176	8.8	3.77	44.999	39.16	1.149
517	UDDCOMB	H5H	ECH	41.47	11	3.77	56.248	48.95	1.149
518	UDDCOMB	H6H	ECH	49.764	13.2	3.77	67.498	58.74	1.149
519	UDDCOMB	H8H	ECH	82.192	17.6	4.67	111.482	78.32	1.423
520	UDDCOMB	H10H	ECH	86.877	22.05	3.94	117.836	98.122	1.201
401	BERMINGH	B23	CED	22.988	2.8	8.21	31.18	12.46	2.502
434	BERMINGH	B-9	OED	21	2	10.5	28.484	8.9	3.2
402	BERMINGH	B200	OED	18	2	9	24.414	8.9	2.743
406	BERMINGH	B-21	OED	53.245	4.63	11.5	72.219	20.604	3.505

ID	Hammer Manufacturer	Hammer Model	Hammer Type	Energy/Power (kip-ft)/(kW)	Ram Weight (kips)	Stroke (ft)	Energy/Power (kJ)/(kW)	Ram Weight (kN)	Stroke (m)
403	BERMINGH	B225	OED	29.25	3	9.75	39.674	13.35	2.972
404	BERMINGH	B300	OED	40.313	3.75	10.75	54.678	16.688	3.277
435	BERMINGH	B-32	OED	81.075	7.05	11.5	109.967	31.373	3.505
405	BERMINGH	B400	OED	53.75	5	10.75	72.904	22.25	3.277
436	BERMINGH	B-64	OED	166.498	14.11	11.8	225.831	62.789	3.597
422	BERMINGH	B2005	OED	18	2	9	24.414	8.9	2.743
414	BERMINGH	B23 5	CED	22.988	2.8	8.21	31.18	12.46	2.502
424	BERMINGH	B2505	OED	35.4	3	11.8	48.015	13.35	3.597
425	BERMINGH	B3005	OED	35.4	3	11.8	48.015	13.35	3.597
416	BERMINGH	B3505	OED	47.2	4	11.8	64.02	17.8	3.597
417	BERMINGH	B4005	OED	59	5	11.8	80.025	22.25	3.597
418	BERMINGH	B4505	OED	77.88	6.6	11.8	105.633	29.37	3.597
419	BERMINGH	B5005	OED	92.04	7.8	11.8	124.839	34.71	3.597
420	BERMINGH	B5505	OED	108.56	9.2	11.8	147.246	40.94	3.597
431	BERMINGH	B6005	OED	160.952	13.64	11.8	218.309	60.698	3.597
433	BERMINGH	B6505	OED	202.86	17.64	11.5	275.151	78.498	3.505
415	BERMINGH	B250 5	OED	26.25	2.5	10.5	35.604	11.125	3.2
410	BERMINGH	B300 M	OED	40.313	3.75	10.75	54.678	16.688	3.277
411	BERMINGH	B400 M	OED	53.75	5	10.75	72.904	22.25	3.277
421	BERMINGH	B550 C	OED	88	11	8	119.36	48.95	2.438
432	BERMINGH	B6505 C	OED	253	22	11.5	343.159	97.9	3.505
412	BERMINGH	B400 4.8	OED	43.2	4.8	9	58.595	21.36	2.743
413	BERMINGH	B400 5.0	OED	45	5	9	61.036	22.25	2.743

ID	Hammer Manufacturer	Hammer Model	Hammer Type	Energy/Power (kip-ft)/(kW)	Ram Weight (kips)	Stroke (ft)	Energy/Power (kJ)/(kW)	Ram Weight (kN)	Stroke (m)
437	BERMINGH	B-6505HD	OED	220.5	22.05	10	299.077	98.122	3.048
1001	DFI-Corp	HHA250-4	ECH	25.181	5.51	4.57	34.154	24.52	1.393
1002	DFI-Corp	HHA300-4	ECH	28.753	6.61	4.35	39	29.415	1.326
1003	DFI-Corp	HHA325-4	ECH	30.358	7.16	4.24	41.177	31.862	1.292
1004	DFI-Corp	HHA350-4	ECH	31.801	7.7	4.13	43.134	34.265	1.259
1005	DFI-Corp	HHA400-6	ECH	51.92	8.8	5.9	70.422	39.16	1.798
1006	DFI-Corp	HHA450-6	ECH	57.04	9.92	5.75	77.367	44.144	1.753
1007	DFI-Corp	HHB500-6	ECH	66.66	11	6.06	90.415	48.95	1.847
1008	DFI-Corp	HHB600-6	ECH	77.88	13.2	5.9	105.633	58.74	1.798
372	FAIRCHLD	F-32	ECH	32.55	10.85	3	44.15	48.283	0.914
371	FAIRCHLD	F-45	ECH	45	15	3	61.036	66.75	0.914
998	HYPOTHET	EX 4	OED	23.375	2.75	8.5	31.705	12.238	2.591
1630	LBFoster	4150	VIB	335	0.534	25	335	2.376	25
1201	Liebherr	H 50/3	ECH	28.974	6.6	4.39	39.299	29.37	1.338
1202	Liebherr	H 50/4	ECH	35.024	8.8	3.98	47.505	39.16	1.213
1203	Liebherr	H 85/5	ECH	43.34	11	3.94	58.785	48.95	1.201
1204	Liebherr	H 85/7	ECH	60.158	15.425	3.9	81.595	68.641	1.189
1205	Liebherr	H 110/7	ECH	60.158	15.425	3.9	81.595	68.641	1.189
1206	Liebherr	H 110/9	ECH	78.011	19.85	3.93	105.81	88.333	1.198
81	LINKBELT	LB 180	CED	8.096	1.73	4.68	10.982	7.699	1.426
82	LINKBELT	LB 312	CED	15.015	3.86	3.89	20.366	17.177	1.186
83	LINKBELT	LB 440	CED	18.2	4	4.55	24.686	17.8	1.387
84	LINKBELT	LB 520	CED	26.313	5.07	5.19	35.69	22.562	1.582

ID	Hammer Manufacturer	Hammer Model	Hammer Type	Energy/Power (kip-ft)/(kW)	Ram Weight (kips)	Stroke (ft)	Energy/Power (kJ)/(kW)	Ram Weight (kN)	Stroke (m)
85	LINKBELT	LB 660	CED	51.627	7.57	6.82	70.025	33.687	2.079
458	MENCK-UW	MHU500T*	ECH	368.741	65.958	5.591	500.146	293.513	1.704
61	MITSUBIS	M 14	OED	25.245	2.97	8.5	34.241	13.217	2.591
63	MITSUBIS	M 23	OED	43.01	5.06	8.5	58.337	22.517	2.591
65	MITSUBIS	M 33	OED	61.71	7.26	8.5	83.701	32.307	2.591
67	MITSUBIS	M 43	OED	80.41	9.46	8.5	109.065	42.097	2.591
62	MITSUBIS	MH 15	OED	28.135	3.31	8.5	38.161	14.729	2.591
64	MITSUBIS	MH 25	OED	46.835	5.51	8.5	63.525	24.52	2.591
66	MITSUBIS	MH 35	OED	65.62	7.72	8.5	89.004	34.354	2.591
68	MITSUBIS	MH 45	OED	85.425	10.05	8.5	115.867	44.723	2.591
70	MITSUBIS	MH 72B	OED	135.15	15.9	8.5	183.312	70.755	2.591
71	MITSUBIS	MH 80B	OED	149.6	17.6	8.5	202.911	78.32	2.591
656	Pilemast	24-750	ECH	1.5	0.75	2	2.035	3.338	0.61
657	Pilemast	24-900	ECH	1.8	0.9	2	2.441	4.005	0.61
658	Pilemast	24-2000	ECH	4	2	2	5.425	8.9	0.61
659	Pilemast	24-2500	ECH	5	2.5	2	6.782	11.125	0.61
660	Pilemast	36-3000	ECH	9	3	3	12.207	13.35	0.914
661	Pilemast	36-5000	ECH	15	5	3	20.345	22.25	0.914
650	Twinwood	V20B	ECH	35.584	9.038	3.937	48.265	40.221	1.2
651	Twinwood	V100D	ECH	87.659	22.265	3.937	118.897	99.081	1.2
652	Twinwood	V160B	ECH	140.582	35.708	3.937	190.68	158.9	1.2
653	Twinwood	V400A	ECH	263.841	67.016	3.937	357.864	298.22	1.2

Appendix D

A comparison between the collected field measurments and the theortical expriments of PPV are plotted in the following graph, also the out put of the numerical modeling by Plaxis in this thesis is included in the comparison.

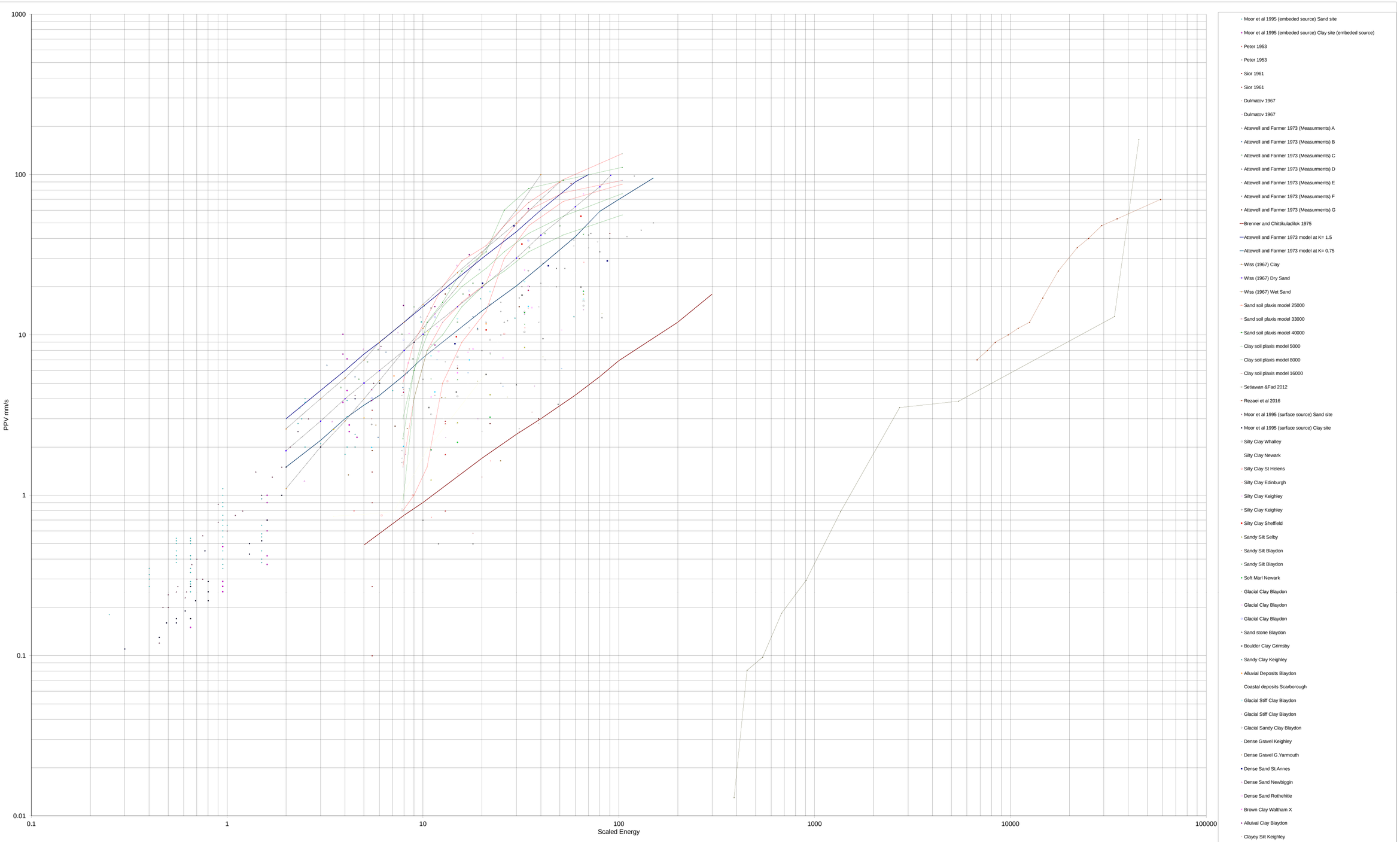

LIST OF PUBLICATIONS

LIST OF PUBLICATIONS

Marawan, Sh., Farouk, A. and Ramadan, M., (2016) "The Effect of Pile Driving on Soil and Adjacent Structure Response - Numerical Study" The 9th Alexandria International Conference Of Structural and Geotechnical Engineering 2016, December 19th-21st.

Marawan, Sh., Farouk, A. and Ramadan, M., (2017). "Influence of Pile Driving and Dynamic Compaction Earthborn Vibration on Adjacent Soil Response" The 17th International Conference on Advances in Structural and Geotechnical Engineering. March 27-30, 2017- Hurghada, Red Sea, Egypt.

Further Publications

Marawan, Sh., Farouk, A. and Ramadan, M., (2019). "Control construction vibration induced structural damage using wave barriers" The 19th International Conference on Advances in Structural and Geotechnical Engineering. March 25-28, 2019- Hurghada, Red Sea, Egypt.